Electronic Thesis and Dissertation Repository

9-16-2016 12:00 AM

Numerical Studies for Improving Fracture Toughness Resistance Curve Testing Using Single-Edge (Notched) Tension Specimens

Yifan Huang
The University of Western Ontario

Supervisor
Dr. Wenxing Zhou
The University of Western Ontario

Graduate Program in Civil and Environmental Engineering
A thesis submitted in partial fulfillment of the requirements for the degree in Doctor of Philosophy
© Yifan Huang 2016

Abstract

The fracture toughness resistance curve, i.e. the *J*-integral resistance curve (*J-R* curve) or the crack tip opening displacement resistance (*CTOD-R*) curves, is widely used in the integrity assessment and strain-based design of energy pipelines with respect to planar defects (i.e. cracks). This thesis deals with issues related to the experimental determination of *J*(*CTOD*)-R curves using the newly-developed single-edge (notched) tension (SE(T)) specimens. In the first study, the plastic geometry factor, i.e. the η_{pl} factor, used to evaluate *J* in a *J-R* curve test based on an SE(T) specimen is developed based on three-dimensional (3D) finite element analysis (FEA). In the second study, 3D FEA is carried out on SE(T) specimens to develop the plastic constraint factor, i.e. the *m* factor, used to evaluate *CTOD* from *J*. The third study reported in this thesis focuses on the compliance equation, which relates the crack length and specimen's compliance (i.e. inverse of stiffness) in the *J*(*CTOD*)-R curves testing. Three-dimensional FEA of clamped SE(T) specimens is performed to examine the accuracy of the crack mouth opening displacement (*CMOD*) compliance equations reported in the literature. In the fourth study, the impact of the crack front curvature on the *J-R* curve measured from the SE(T) specimen is investigated through systematic elastic-plastic 3D FEA of SE(T) specimens containing both straight and curved crack fronts. The last study reported in this thesis is focused on developing the effective thickness that takes accounts for the side groove effects on the estimations of the stress intensity factor (*K*) and *J* for SE(T) specimens. The outcomes of these studies will facilitate and improve the evaluation of *J*(*CTOD*)-R curves using side-grooved SE(T) specimens.

Keywords

Pipeline, Fracture toughness, *J*-integral, Crack tip opening displacement (*CTOD*), Finite element analyses, SE(T) specimen, plastic geometry factor, plastic constraint factor, compliance equation, curved crack front, side groove.

Co-Authorship Statement

The materials presented in Chapters 2 to 6 of this thesis have been published in five peer-reviewed journal papers, respectively. The permission to reproduce the published work in this thesis has been granted by the copyright holders and included at the end of this thesis.

A version of Chapter 2, co-authored by **Yifan Huang** and Wenxing Zhou has been published in *Engineering Fracture Mechanics*, 2014, 132: 120-135. Copyright Elsevier, 1600 JFK Boulevard, Suite 1800, Philadelphia, PA 19103-2899
Link: http://www.sciencedirect.com/science/article/pii/S0013794414003580

A version of Chapter 3, co-authored by **Yifan Huang** and Wenxing Zhou has been published in *Engineering Fracture Mechanics*, 2014, 131: 643-655. Copyright Elsevier, 1600 JFK Boulevard, Suite 1800, Philadelphia, PA 19103-2899
Link: http://www.sciencedirect.com/science/article/pii/S0013794414003294

A version of Chapter 4, co-authored by **Yifan Huang** and Wenxing Zhou has been published in *Fatigue and Fracture of Engineering Materials and Structures*, 2015, 38: 1137-1154. Copyright John Wiley & Sons Ltd, Southern Gate, Chichester, West Sussex, PO19 8SQ UK.
Link: http://onlinelibrary.wiley.com/doi/10.1111/ffe.12293/abstract

A version of Chapter 5, co-authored by **Yifan Huang** and Wenxing Zhou has been published in *International Journal of Pressure Vessels and Piping*, 2015, 134: 112-127. Copyright Elsevier, 1600 JFK Boulevard, Suite 1800, Philadelphia, PA 19103-2899
Link: http://www.sciencedirect.com/science/article/pii/S0308016115000538

A version of Chapter 6, co-authored by **Yifan Huang** and Wenxing Zhou has been published in *ASTM Journal of Testing and Evaluation*, DOI: 10.1520/JTE20150274. Reproduce with permission, from the *Journal of Testing and Evaluation*, copyright ASTM International, 100 Barr Harbor Drive, West Conshohocken, PA 19428.
Link: http://dx.doi.org/10.1520/JTE20150274

Dedication

To my parents, grandparents and my wife

Acknowledgments

My deepest gratitude goes first and foremost to Dr. Wenxing Zhou, my supervisor as well as my career mentor, for his patient guidance, understanding, encouragement, and most importantly for continuously supporting me with his profound insight throughout this study. He has walked me through all the stages of my graduate study. Without his consistent and illuminating instruction, this thesis could not have reached its present form. It has been a great privilege and joy of being a member of his research group and studying under his guidance and supervision.

I would also like to thank Dr. Ashraf A. El Damatty, Dr. Tim A. Newson, Dr. Liying Jiang and Dr. Xin Wang for being my examiners and for their constructive advice to this thesis. I would also express my gratitude to Dr. Guowu Shen, previous senior research scientist at CANMET-MTL and Adjunct Professor in the Department of Civil and Environmental Engineering at Western, for his valuable comments and suggestions in my master study. Assistance from Mr. Jie Liang at CANMET-MTL is very much appreciated.

My special thanks to all my colleagues and alumni in our research group, for making my graduate life so colorful and also for their encouragement and assistances. Financial support provided by TransCanada and the Natural Sciences and Engineering Research Council of Canada (NSERC) and by the Faculty of Engineering at Western University is gratefully acknowledged.

Growing up, I am grateful for the selfless love and limitless education provided by my parents and grandparents. My hearty thanks would also go to my wife for her love, encouragement and support throughout my PhD program.

Table of Contents

List of Tables

List of Figures

List of Abbreviations and Symbols

Abbreviations

ASTM	American Society for Testing and Materials
BSI	British Standard Institution
CEPA	Canadian Energy Pipeline Association
CMOD	Crack mouth opening displacement
C(T)	Compact tension
CTOD	Crack tip opening displacement
EPFM	Elastic-plastic fracture mechanics
FEA	Finite element analyses
HRR	Hutchinson-Rice-Rosengren
LEFM	Linear-elastic fracture mechanics
LLD	Load line displacement
LSY	Large scale yielding
NEB	National Energy Board
PS	Plane-sided
R-curve	Resistance curve
SBD	Strain-based design
SE(B)	Single-edge bend
SE(4PB)	Single-edge four-point bend
SE(T)	Single-edge tension
SSY	Small scale yielding
SG	Side-grooved
UC	Unloading compliance
2D	Two dimensional
3D	Three dimensional

Symbols

CHAPTER 1

a	crack length
B	thickness of the specimen
B_N	net thickness of the specimen
ds	the length increment along the contour
E	elastic (Young's) modulus
E_{2D}	elastic modulus in two-dimensional analysis
f_{ij}	dimensionless function of θ
G	energy release rate (energy/area or force/length)
H	daylight length (distance between grips)
I_n	integration constant that depends on n
J	J-integral, nonlinear energy release rate
K	stress intensity factor
K_C	critical stress intensity factor
K_{IC}	fracture toughness
$m_{(SSY)}$	dimensionless constraint parameter for SSY condition
n	strain hardening exponent
n_j	the component of the unit normal vector to Γ
r	coordinates in the polar coordinate system near the crack tip
r_p	size of the plastic zone ahead of the crack tip
S	the span of the specimen
T_i	traction vectors
u_i	components of the displacement
W	the width of the specimen
w	strain energy density
α	coefficient in the Ramberg-Osgood stress-strain relationship
Γ	arbitrary counterclockwise contour around the crack tip
δ	crack tip opening displacement
δ_{ij}	Kronecker delta

ε_0	reference strain, $\varepsilon_0 = \sigma_{YS}/E$
ε_{ij}	total strain tensor
ε_{ij}^{pl}	plastic strain tensor
$\tilde{\varepsilon}_{ij}$	dimensionless functions of n, θ in the HRR solution
θ	coordinates in the polar coordinate system near the crack tip
ν	Poisson's ratio
σ_{ij}	stress tensor
σ_0	reference stress
σ_{YS}	yield strength
$\tilde{\sigma}_{ij}$	dimensionless functions of n, θ in the HRR solution

CHAPTER 2

A	area under the load versus displacement curve
A_{el}	elastic component of A
A_{pl}	plastic component of A
$\bar{A}_{pl}$	non-dimensionalized A_{pl}, $\bar{A}_{pl} = A_{pl}/b^2 B_N \sigma_{YS}$
A_{pl}^{CMOD}	plastic area under the P-$CMOD$ curve
A_{pl}^{LLD}	plastic area under the P-LLD curve
a	crack length
B	thickness of the specimen
B_N	net thickness of the specimen
b	length of the uncracked ligament
C_0	initial compliance
E	elastic (Young's) modulus
e_{ac}	sum of the relative errors
e_J	relative error of J_η, $e_J = (J_\eta - J_{ave})/J_{ave}$
F	non-dimensional stress intensity factor
H	daylight length (distance between grips)
J	J-integral, nonlinear energy release rate

J_2 second invariant of the deviatoric stress tensor

J_{ave} the average J value along the crack front

J_η the estimated J value based on the given η_{pl}

J_{el} elastic component of J

J_{pl} plastic component of J

$\bar{J}_{pl}$ non-dimensionalized J_{pl}, $\bar{J}_{pl} = J_{pl}/b\sigma_{YS}$

K stress intensity factor

M_{ij} fitting coefficients of Eq. (2.28)

M_Δ, M_V load separation functions in Eqs. (2.10) and (2.12)

m_i coefficients of Eq. (2.15)

N_{ij} fitting coefficients of Eq. (2.29)

N_Δ, N_V load separation functions in Eqs. (2.10) and (2.12)

n_i coefficients of Eq. (2.15)

n strain hardening exponent

P applied load

P_Y limit load for SE(T) specimen, $P_Y = B_N b \sigma_Y$

t_i fitting coefficients of Eq. (2.22b)

V crack mouth opening displacement

V_{el} the elastic component of $CMOD$

V_{pl} the plastic component of $CMOD$

W the width of the specimen

γ_{pl} plastic geometry factor used to calculate J_{pl} for a growing crack

Δ load-line displacement

Δ_{el} the elastic component of LLD

Δ_{pl} the plastic component of LLD

ε_0 reference strain, $\varepsilon_0 = \sigma_{YS}/E$

ε_u true strain corresponding to σ_{UTS}

η_{pl} plastic geometry factor used to calculate plastic component of J

η_{pl}^{LLD} LLD- based η_{pl}

η_{pl}^{CMOD} $CMOD$- based η_{pl}

ν	Poisson's ratio
ρ_0	radius of the blunt crack tip in FEA model
σ_Y	flow stress
σ_{YS}	yield strength of the material
σ_{UTS}	ultimate tensile strength of the material
ξ_i	fitting coefficients of Eq. (2.17)
ϕ_i	fitting coefficients of Eq. (2.16)
ψ_i	fitting coefficients of Eq. (2.18)

CHAPTER 3

a	crack length
B	thickness of the specimen
B_N	net thickness of the specimen
E	elastic (Young's) modulus
e_δ	prediction error of *CTOD*
H	daylight length (distance between grips)
J	*J*-integral, nonlinear energy release rate
J_2	second invariant of the deviatoric stress tensor
J_{ave}	the average *J* value along the crack front
J_{el}	elastic component of *J*
J_{pl}	plastic component of *J*
M_i	fitting coefficients of Eq. (3.8)
$m, m_{(i)}$	plastic constraint factor
N, n	strain hardening exponent
P	applied load
P_Y	limit load, $P_Y = B_N b \sigma_Y$
p_{ij}	fitting coefficients of Eq. (3.9)
Q_i	fitting coefficients of Eq. (3.8)
q_{ij}	fitting coefficients of Eq. (3.9)
V	crack mouth opening displacement

W	the width of the specimen
λ_0	fitting coefficients of Eq. (3.9)
ε_0	reference strain, $\varepsilon_0 = \sigma_{YS}/E$
ε_u	true strain corresponding to σ_{UTS}
δ	crack tip opening displacement
δ_{90}	the *CTOD* value estimated in the FEA based on the 90° intercept method
δ_{est}	the estimated *CTOD* value based on the given m factor
δ_{el}	elastic component of *CTOD*
δ_{pl}	plastic component of *CTOD*
η_J, η_δ	plastic geometry factor used to calculate J_{pl} and δ_{pl}
ν	Poisson's ratio
ρ_0	radius of the blunt crack tip in FEA model
σ_Y	flow stress
σ_{YS}	yield strength of the material
σ_{UTS}	ultimate tensile strength of the material

CHAPTER 4

a	crack length
B	thickness of the specimen
BCE_{2D}	normalized compliance
$B_{e(1)}$	effective thickness for normalized compliance
B_N	net thickness of the specimen
C	elastic compliance
E, E'	elastic modulus for plane stress and plane strain analysis
E_{2D}	elastic modulus in two-dimensional analysis
E_e	effective elastic modulus
e_1, e_2	prediction error of crack length and compliance
H	daylight length (distance between grips)
J	*J*-integral, nonlinear energy release rate
P	applied load

R_i	fitting coefficients in Eq. (4.17)
r_{sg}	root radius of the side groove
u	non-dimensional factor, $u = 1/(1+\sqrt{BCE_{2D}})$
V	crack mouth opening displacement
V_{el}	elastic and plastic component of $CMOD$
V_{pl}	elastic and plastic component of $CMOD$
W	the width of the specimen
γ	non-dimensional factor, $\gamma = (a/W)^{1/(1+\sqrt{B/W})}$
ν	Poisson's ratio
$\rho_{(a/W)}$	3D crack length modification factor
$\rho_{(BCE)}$	3D compliance modification factor
ω	non-dimensional factor, $\omega = 1/(1+\sqrt{WCE})$

CHAPTER 5

a	crack length
a_{ave}	average crack length over the specimen thickness
a_{ave9}	average crack lengths based on the nine-point measurement
a_{max7}, a_{min7}	maximum and minimum values of crack lengths measured among the inner seven points along the specimens thickness
a_{max9}, a_{min9}	maximum and minimum values of crack lengths measured among the nine points along the specimens thickness
$a_{z=0}$, $a_{z=\pm B/2}$	crack lengths at the mid-plane and surfaces of the specimen
B	thickness of the specimen
C_0, C_i	compliances of the undeformed and deformed specimens
E	elastic (Young's) modulus
e_C	difference between compliances estimated from specimens with straight and curved crack fronts
$e_{J(\lambda)}$	difference between J estimated from specimens with straight and curved crack fronts
e_F	prediction error of F_r

F_r	compliance rotation correction factor
H	daylight length (distance between grips)
h	applied displacement on clamped surface in FEA
J	J-integral, nonlinear energy release rate
J_2	second invariant of the deviatoric stress tensor
J_{ave}	average J evaluated over the crack front.
n	strain hardening exponent
P	applied load
p	shape parameter used in Eq. (5.8)
P_Y	limit load, $P_Y = B(W - a_{ave})(\sigma_{YS} + \sigma_{UTS})/2$
q_1, q_2	coefficients used to convert a_{ave} and λ to a_{ave9} and κ, respectively
V	crack mouth opening displacement
W	the width of the specimen
α	coefficient in the Ramberg-Osgood stress-strain relationship
β	parameter used to characterize the crack front curvature
β_7, β_9	curvature parameters based on the nine points measurement: $\beta_9 = (a_{max9} - a_{min9})/W$; $\beta_7 = (a_{max7} - a_{min7})/W$
Λ	distance between the measured end point and the specimen side surface.
λ	parameter used to characterize the crack front curvature
λ_7, λ_9	Curvature parameters based on the nine points measurement: $\lambda_7 = \text{Max}[a_{max7} - a_{ave9}, a_{ave9} - a_{min7}]/W$; $\lambda_9 = \text{Max}[a_{max9} - a_{ave9}, a_{ave9} - a_{min9}]/W$ (subscripts "(BS)" and "(ASTM)" denote the measurement methods specified in the corresponding standards).
ε_0	yield strain, $\varepsilon_0 = \sigma_{YS}/E$
κ	standard-specific curvature parameter
ρ_0	radius of the blunt crack tip in FEA model
σ_Y	flow stress
σ_{YS}	yield strength of the material
σ_{UTS}	ultimate tensile strength of the material
ν	Poisson's ratio

CHAPTER 6

A_{pl} plastic area under the load versus displacement curve

a crack length

B gross thickness of the specimen

$B_{e(i)}$ effective thickness

B_N net thickness of the specimen

C elastic compliance

C_N normalized compliance, $C_N = BCE$

d_{sg} depth of the side groove on each side

E elastic (Young's) modulus

e_J prediction error of estimated J based on given η_{pl}

e_K prediction error of estimated K based on given F

e_ψ prediction error of estimated $\psi_{(3)}$

F non-dimensional stress intensity factor

H daylight length (distance between grips)

h applied displacement on clamped surface in FEA

J nonlinear energy release rate

J_2 second invariant of the deviatoric stress tensor

J_{ave} the average J value along the crack front

J_{el} elastic component of J

J_{pl} plastic component of J

$J_{loc(i)}$ the local J value at the ith layer

J_{mid} the local J value in the mid-plane

J_η the estimated J value based on the given η_{pl}

J_ψ plastic component of J estimated from Eq. (6.10b) based on a given $\psi_{(3)}$

K stress intensity factor

K_{ave} the average K value along the crack front

K_F the estimated K value based on the given $F(a/W)$

n strain hardening exponent

P applied concentrated force

P_Y limit load for SE(T) specimen, $P_Y = B_N(W - a)\sigma_Y$

r_{sg}	root radius of the side groove
V	crack mouth opening displacement
W	specimen width
ε_0	reference strain, $\varepsilon_0 = \sigma_{YS}/E$
ε_u	true strain corresponding to σ_{UTS}
η_{pl}^{CMOD}	*CMOD*- based plastic geometry factor used to calculate J_{pl}
θ_{sg}	side groove machined angle
σ_Y	flow stress
σ_{YS}	yield strength of the material
σ_{UTS}	ultimate tensile strength of the material
μ	coefficient for $B_{e(3)}$ in Eqs. (6.4) and (6.7c)
ν	Poisson's ratio
τ	coefficient for $B_{e(2)}$ in Eqs. (6.2) and (6.7a)
$\psi_{(i)}$	thickness correction factor
χ	ratio between the net and gross specimen thicknesses

Chapter 1 Introduction

1.1 Background

Pipelines are an effective and safe means to transport large quantities of hydrocarbons over a long distance (PHMSA 2012). According to the Canadian Energy Pipeline Association (CEPA), 97% of Canadian natural gas and crude oil production are transported by transmission pipelines. It is reported that over \$134 billion worth of energy products were shipped through the 73,000 km long pipelines regulated by the National Energy Board (NEB) of Canada at an estimated transportation cost of \$7.1 billion in 2013 (NEB 2014).

Energy pipelines may contain planar defects, i.e. cracks, in the pipe base metal and weldments due to various causes such as stress corrosion cracking, fatigue and the welding process. The fracture toughness resistance curve (*R*-curve) of pipeline steels is a key input to the structural integrity assessment and strain-based design of pipelines with respect to cracks (Fairchild et al. 2012). The *R*-curve is generally represented by either the *J*-integral resistance curve (*J-R* curve) or the crack tip opening displacement (*CTOD*) resistance curve (*CTOD-R* curve) (Anderson, 2005). It follows that the accuracy of the experimentally measured *R*-curve directly influences the accuracy of the design and assessment of pipelines.

The *R*-curve is typically determined from small-scale test specimens cut from the pipe, such as the single-edge notched bend (SE(B) or SENB) and compact tension (C(T)) specimens, which have been standardized in standards such as ASTM E1820-13 (ASTM, 2013) and BS7448 (BSI, 1997). Previous studies (e.g. Zhu et al, 2005; Shen and Tyson, 2009) reveal that using *R*-curves evaluated from the standard deeply-cracked SE(B) and C(T) specimens generally leads to conservative outcomes in the design and assessment of pipelines containing surface cracks. Over the last decade, the use of the clamped single-edge notched tension (SE(T) or SENT) specimen, which was recently standardized in BS 8571 (BSI, 2014), to determine the *R*-curve has gained significant research interests (Cravero and Ruggieri, 2007; Ruggieri, 2012; Wang et al, 2012, 2013) in the energy pipeline industry. This is because the crack-tip stress and strain fields of the SE(T)

specimen are more relevant to a full-scale pipe containing surface cracks under internal pressure and/or longitudinal tension than the conventional standard SE(B) and C(T) specimens (Chiesa et al., 2001; Tang et al., 2010; Wang et al, 2011); therefore, the *R*-curve determined from the SE(T) specimen can lead to more accurate design and assessment of pipelines with respect to cracks. The objective of the study reported in this thesis is to address several issues related to the experimental determination of the *R*-curve using the SE(T) specimens and to improve the current SE(T) test method. To this end, some basic concepts of fracture mechanics are briefly reviewed first in Section 1.2.

1.2   Fundamentals of Fracture Mechanics

1.2.1 Linear Elastic Fracture Mechanics

Fracture mechanics consists of two main branches: the linear elastic fracture mechanics (LEFM) and the elastic plastic fracture mechanics (EPFM) (Anderson, 2005). The former attempts to describe the fracture behavior of a material when the plastic deformation is confined to a small region surrounding the crack tip, known as the small scale yielding (SSY) condition. On the other hand, EPFM applies to the large scale yielding (LSY) condition where significant plasticity in the vicinity of the crack tip is considered.

In fracture mechanics, there are three typical loading modes based on the loading position and direction with respect to the crack (see Fig. 1.1), namely the opening mode (mode I), the in-plane shearing mode (mode II), and the out-of-plane shearing mode (mode III) (Anderson, 2005). Mixed mode loading arises if any two or three of these modes take place concurrently. This thesis is focused on the Mode I loading because it is the most critical fracture mode for ductile metals. All the discussions thereafter are with respected to the Mode I loading.

Consider an isotropic linear elastic body containing a crack as illustrated in Fig. 1.2. Define a polar coordinate system with the origin located at the crack tip. The stress field at the crack tip can be written as (Westergaard, 1939; Irwin, 1957; Williams, 1957):

$$\lim_{r \to 0} \sigma_{ij} = \left(\frac{K}{\sqrt{2\pi r}} \right) f_{ij}(\theta) \tag{1.1}$$

where σ_{ij}[1] is the stress tensor; r and θ are coordinates defined in Fig. 1.2; f_{ij} is a dimensionless function of θ, and K is the so-called stress intensity factor in the unit of force/area×(length)$^{0.5}$. Equation (1.1) describes a stress singularity at the crack tip, because σ_{ij} approaches infinity as $r \to 0$. The stress intensity factor completely defines the amplitude of the stress singularity; that is, the stresses, strains and displacements near the crack tip can be completely determined given K (Hutchinson, 1983; Anderson, 2005). This single-parameter characterization by K strictly relies on the satisfaction of the SSY condition, which requires the zone of plastic deformation to be contained well within the singularity fields (Hutchinson, 1983). The size of the plastic zone ahead of the crack tip, r_p, can be approximately calculated using the following equation (Hutchinson, 1983):

$$r_p = \begin{cases} \dfrac{1}{3\pi} \left(\dfrac{K}{\sigma_{YS}} \right)^2 & (\text{plane-strain}) \\[3mm] \dfrac{1}{\pi} \left(\dfrac{K}{\sigma_{YS}} \right)^2 & (\text{plane-stress}) \end{cases} \tag{1.2}$$

where σ_{YS} is the yield strength. The ASTM standard for experimentally determining the linear elastic plane-strain fracture toughness of metallic materials, ASTM E399 (ASTM, 2012), requires the crack length and uncracked ligament of the test specimen to be no less than $25r_p$ at the point of fracture to satisfy SSY. Generally speaking, SSY is met if the applied load is less than half the limit load at which plastic yielding extends throughout the uncracked ligament (Hutchinson, 1983). Under SSY, the energy release rate G, defined as the rate of decrease in the potential energy with a unit increase in the crack area (Irwin, 1957), can be related to the stress intensity factor K as follows:

---

[1] In this thesis, only $i, j = 1, 2,$ or 3 are the subscripts of tensors. All symbols with other subscripts denote scalars.

$$G = \frac{K^2}{E_{2D}} \tag{1.3}$$

where E_{2D} is the elastic modulus in two-dimensional analysis and is defined as

$$E_{2D} = \begin{cases} E & \text{(plane-stress)} \\ E' = \dfrac{E}{(1-v^2)} & \text{(plane-strain)} \end{cases} \tag{1.4}$$

with E and v being Young's modulus and Poisson's ratio, respectively.

For a given material at a given temperature, there exists a critical stress intensity factor, K_c, associated with the onset of crack growth under monotonic loading (Hutchinson, 1983). Generally for mode I loading, K_c decreases as the thickness of the cracked body increases (Anderson, 2005). In particular, the critical stress intensity factor in a mode I, plane-strain condition is called the fracture toughness of the material at the given temperature and denoted by K_{Ic}. K_{Ic} is expected to be a material property (Broek, 1986). To ensure the plane-strain condition in the fracture toughness test, ASTM E399 (ASTM, 2012) also requires the thickness of the test specimen to be at least $25r_p$.

For highly brittle materials, cracks will run dynamically once K reaches K_{Ic}, and K_{Ic} remains constant during the crack growth. For more ductile materials, however, more energy is required to extend the crack after the onset of crack growth, due to the energy dissipation in the plastic zone at the crack tip (Anderson, 2005); that is, the fracture toughness increases as the crack grows. The relationship between the fracture toughness and crack extension Δa under stable quasi-static growth conditions is defined as the fracture toughness resistance curve (Hutchinson, 1983; Anderson, 2005).

1.2.2 Elastic Plastic Fracture Mechanics

Linear elastic fracture mechanics (LEFM) loses validity when the fracture processes are accompanied by significant plastic deformation at the crack tip (Anderson, 2005). As a rough approximation, the application of LEFM becomes questionable if the applied load is greater than one half of the load at which full plastic yielding occurs (Hutchison, 1983).

To characterize the fracture behavior of ductile materials with medium-to-high toughness, elastic plastic fracture mechanics (EPFM) is required.

Before further discussions of the elastic plastic fracture mechanics, it is necessary to introduce some fundamentals of the theory of plasticity. There are two main theories of plasticity based on two different constitutive relations. The incremental (or flow) theory of plasticity employs the formulations relating increments of stress and strain, whereas the deformation theory of plasticity employs the formulations relating the total stress and strain. The incremental theory of plasticity is loading-path-dependent, whereas the deformation theory of plasticity is loading-path-independent. Under the monotonic and proportional loading condition, the deformation theory of plasticity is equivalent to the incremental theory of plasticity. Note that the deformation theory of plasticity is equivalent to nonlinear elasticity provided that no unloading occurs.

The *J*-integral proposed by Rice (1968) and crack tip opening displacement (*CTOD*) proposed by Wells (1961) are the two most important concepts in EPFM (Anderson, 2005). Both parameters describe the mechanical behaviors of the elastic-plastic materials near the crack-tip. Each of them can serve as a measure of material's toughness and therefore can be used to set up fracture criteria. Consider a two-dimensional cracked body (see Fig. 1.3) characterized by the deformation theory of plasticity (i.e. small strain kinematics and nonlinear elastic constitutive model) with an arbitrary counterclockwise path (Γ) around the crack tip. The *J*-integral or *J* is defined as

$$J = \int_{\Gamma} \left(w \, dy - T_i \cdot \frac{\partial u_i}{\partial x} \, ds \right) \tag{1.5}$$

where u_i and T_i are components of the displacement and traction vectors, respectively ($i = 1, 2$ or 3); w is the strain energy density, and ds is the length increment along the contour Γ. Note that the unit of *J* is energy/area or equivalently force/length. The strain energy density w and traction T_i are given by (Anderson, 2005):

$$w = w(x, y) = w\left(\varepsilon_{ij}\right) = \int_0^{\varepsilon_{ij}} \sigma_{ij} d\varepsilon_{ij} \tag{1.6}$$

$$T_i = \sigma_{ij} n_j \qquad (1.7)$$

where ε_{ij} ($i, j = 1, 2,$ or 3) is the strain tensor, and n_j is the component of the unit normal vector to Γ. Rice (1968) showed that the value of J is independent of the integration path, i.e. Γ, around the crack tip. Therefore, J is a path-independent integral. It can be further shown (Rice, 1968; Anderson, 2005) that J is also equivalent to the energy release rate for the nonlinear elastic cracked body, and reduces to G for a linear elastic cracked body. From this point, J is also known as the nonlinear energy release rate.

Similar to K, J is also an intensity parameter characterizing the stress state near the crack tip (Anderson, 2005). Consider a two-dimensional (i.e. plane-strain or plane-stress) cracked body characterized by the deformation plasticity and a Ramberg-Osgood stress-strain relationship as follows:

$$\frac{\varepsilon}{\varepsilon_0} = \frac{\sigma}{\sigma_0} + \alpha \left(\frac{\sigma}{\sigma_0} \right)^n \qquad (1.8)$$

where σ_0 is the reference stress and typically set equal to the yield strength; $\varepsilon_0 = \sigma_0/E$, and α and n are parameters of the Ramberg-Osgood relationship with n commonly known as the strain hardening exponent. Hutchinson (1968) as well as Rice and Rosengren (1968) independently showed that at distances close to the crack tip, where the elastic strain is negligible compared with the plastic strain, the stresses and strains are related to J through the following equations:

$$\sigma_{ij} = \sigma_0 \left(\frac{J}{\alpha \sigma_0 \varepsilon_0 I_n r} \right)^{\frac{1}{n+1}} \tilde{\sigma}_{ij}(\theta, n) \qquad (1.9)$$

$$\varepsilon_{ij} = \frac{\alpha \sigma_0}{E} \left(\frac{J}{\alpha \sigma_0 \varepsilon_0 I_n r} \right)^{\frac{n}{n+1}} \tilde{\varepsilon}_{ij}(\theta, n) \qquad (1.10)$$

where I_n is an integration constant that depends on n, and $\tilde{\sigma}_{ij}$ and $\tilde{\varepsilon}_{ij}$ are dimensionless functions of n, θ, and stress state (plane-strain or plane-stress). Equations (1.9) and (1.10) are known as the HRR solutions (singularity) (Anderson, 2005). Therefore, J provides a

single-parameter characterization of the crack-tip fields in EPFM, just as *K* provides a single-parameter characterization of the crack-tip fields in LEFM.

Several important points about *J* and HRR solutions are worth emphasizing. First, the *J*-integral as originally proposed by Rice (1968) is applicable to two-dimensional (2D) configurations. Further research has extended the *J* concept to three-dimensional (3D) configurations (Anderson, 2005; Shih et al. 1986), where *J* is considered as a local value that varies along the crack front. However, *J* in a 3D configuration has no direct relationship with the near-tip stress and strain fields, but is simply a characterizing parameter that quantifies the severity of the crack-tip fields (Nikishkov and Atluri, 1987). Second, *J* is path-independent only for materials characterized by deformation plasticity (i.e. nonlinear elastic). *J* is path-dependent for materials characterized by incremental plasticity. However, as long as the loading is proportional everywhere in the cracked body (Anderson, 2005), the deformation plasticity is equivalent to the incremental plasticity. Finally, the HRR solutions are only applicable at locations near the crack tip, where the elastic strains are negligible and the singularity terms in Eqs. (1.9) and (1.10) dominate. At locations immediately ahead of the crack tip, however, the HRR solutions are invalid because they do not account for the finite geometry change (i.e. large strain) at the crack tip (Anderson, 2005).

The crack tip opening displacement (*CTOD*) proposed by Wells (1961) is another parameter describing crack-tip conditions for elastic-plastic materials. It is found that for materials with high toughness, the initial sharp crack tip is firstly blunted due to high degree of plastic deformation before subsequent ductile tearing, as shown in Fig. 1.4 (a). At present, there are two widely used definitions of *CTOD*, namely the displacement at the original crack tip and the 90 degree intercept definition, as illustrated in Figs. 1.4 (a) and (b), respectively. The first one was originally proposed by Wells (1961), and the second definition was suggested by Rice (1968) and Shih (1981) and commonly used for the *CTOD* evaluation in the finite element analysis. If a semicircle (blunt) crack tip is assumed, these two definitions are essentially equivalent. Within the limit of the SSY condition, the value of *CTOD* (δ) can be related to *K* or *G* (Irwin, 1961; Burdekin and Stone, 1966):

$$\delta = \frac{K^2}{m_{(SSY)}E_{2D}\sigma_0} = \frac{G}{m_{(SSY)}\sigma_0} \qquad (1.11)$$

where $m_{(SSY)}$ is a dimensionless constraint parameter that is approximately unity for the plane stress condition and 2 for the plane strain condition (Hollstein and Blauel, 1977). For linear elastic conditions, J is equivalent to the energy release rate G, and Eq. (1.11) demonstrate the equivalence of the fracture parameters (K, G, J and $CTOD$) in the limit of linear elastic conditions. Based on the displacements at the crack tip obtained from the HRR solutions and the elastic-plastic finite element analyses, Shih (1981) further proved that $CTOD$ is linearly related to J well beyond the validity limits of LEFM, and therefore $CTOD$ and J can be considered as equivalent fracture toughness parameters in EPFM. A great deal of efforts have been made to investigate the J-$CTOD$ relationship under SSY and LSY conditions for different specimen configurations through finite element analyses (Kirk and Wang, 1995; Wang et al., 1997; Panontin et al., 2000; Shen and Tyson, 2009; Ruggieri, 2012).

1.2.3 Fracture Toughness Resistance Curve for Elastic-plastic Materials

Because J and $CTOD$ are considered characterizing parameters for the crack-tip fields, it is natural to experimentally determine the fracture toughness of the material as the critical values of J and $CTOD$ at the onset of crack growth, which are known as J_{Ic} and δ_{Ic}. In addition, J can also be considered as an intensity measure even with a small amount of crack growth, as long as the conditions for the so-called J-controlled crack growth are satisfied (Hutchinson, 1983). These conditions essentially limit the amount of crack growth such that the elastic unloading and nonproportional loading near the crack tip associated with the crack growth are well contained within the region where the deformation plasticity on which the J-integral is based is still applicable. Based on this argument, tests can be carried out to develop J versus (small amounts of) crack extension Δa for ductile material, known as the J-Resistance curve or J-R curve (Hutchinson, 1983; Anderson, 2005). Equivalently, the $CTOD$ resistance curve ($CTOD$-R curve) can also be obtained from the tests. The $J(CTOD)$-R curve is a generalization of the K-based resistance curve (K-R curve), as the latter is only applicable under the small scale yielding condition.

For ductile materials, *J* and *CTOD* always increase with small amounts of crack advance; therefore, the *J*(*CTOD*)-*R* curve has significant practical implications for structures that are made of ductile materials and can tolerate certain amount of crack growth, because significant additional load carrying capacity can be achieved with the application of the *J*(*CTOD*)-*R* curve. In this thesis, the fracture toughness resistance curve (*R*-curves) is referred to the *J*(*CTOD*)-*R* curve.

In the pipeline industry, the *R*-curve tests are commonly conducted on small-scale specimens such as SE(B), C(T) and SE(T) specimens cut from the pipe. The evaluation of the load versus load line displacement (*P-LLD*) curve or load versus crack mouth opening displacement (*P-CMOD*) curve is key to the experimental evaluation of the *R*-curve for these specimens. Figures 1.5(a) through 1.5(d) show schematics of the plane-sided and side-grooved SE(B), C(T) and SE(T) specimens as well as the corresponding *LLD* and *CMOD*, where dimensions *B*, B_N, *S*, *W*, *H*, and *a* denote the specimen thickness, net thickness, specimen span, width, distance between grips and crack length, respectively. Note that the side-grooved specimen is often used in the *R* curve test to promote a straight crack front during the crack growth process (Anderson, 2005).

1.3   Objectives and Research Significance

1.3.1 Investigation of Plastic Geometry Factors

The objective of the study reported in Chapter 2 of this thesis was to carry out a systematic investigation of the plastic geometry factors for SE(T) specimens using three-dimensional (3D) finite element analyses (FEA). Both plane-sided and side-grooved SE(T) specimens with a wide range of the crack depth-over-specimen width ratios (*a/W*) and specimen thickness-over-width ratios (*B/W*) were analyzed. The load line displacement (*LLD*)- and crack mouth opening displacement (*CMOD*)-based η_{pl} corresponding to the average *J* value over the crack front were evaluated. The impact of *a/W*, *B/W* and the strain hardening characteristics on the η_{pl} factor were also investigated. The research outcome will improve the accuracy of the *J-R* curve obtained from the experiment and facilitate the evaluation of *J-R* curves using SE(T) specimens.

1.3.2   Investigation of *J-CTOD* Relationship for Clamped SE(T) Specimens

The study reported in Chapter 3 was aimed at developing a more accurate expression of the *m* factor that relates *J* and *CTOD* based on 3D FEA of clamped SE(T) specimen. The analysis covered both plane-sided and side-grooved specimens with a range of specimen configurations (a/W = 0.2 to 0.7 and B/W = 1 and 2) and strain hardening exponents (n =5, 8.5, 10, 15 and 20). Based on the analysis results, a new empirical *m*-factor equation is proposed as a function of a/W, B/W, the yield-to-tensile strength ratio and loading level. The proposed *m*-factor equation will improve the accuracy of the *CTOD-R* curve experimentally obtained from SE(T) specimens.

1.3.3   Investigation of Compliance Equations

The study reported in Chapter 4 focused on the compliance equation, which relates the crack length and specimen's compliance (i.e. inverse of stiffness) in the *R*-curve testing. Three-dimensional FEA of clamped SE(T) specimens is performed to examine the accuracy of the *CMOD* compliance equations reported in the literature. The analysis covered both plane-sided and side-grooved specimens with a wide range of specimen configurations including nine relative crack lengths (a/W) ranging from 0.1 to 0.9, and seven relative thicknesses (B/W) ranging from 0.25 to 4. Based on the FEA results, the crack length/compliance modification factors ($\rho_{(a/W)}$ and $\rho_{(BCE)}$) are developed to improve the accuracy of the compliance equations. The results of this study can improve the accuracy of the experimentally determined *J-* and *CTOD-R* curves using the single-specimen technique and SE(T) specimens.

1.3.4   Investigation of Effects of Crack Front Curvature for the *J-R* Curve Testing

As specified in the *J-R* curve test standards, all machine-notched specimens need to be fatigue pre-cracked to simulate natural cracks before the *J-R* curve testing. The fatigue pre-cracking often introduces curved as opposed to straight crack fronts. The study reported in Chapter 5 investigated the impact of the crack front curvature on the

compliance, compliance rotation correction factor and values of the J-integral for the SE(T) specimen. Based on the analysis results, new crack front straightness criteria that are in most cases less stringent than the existing criteria specified in relevant test standards are recommended. The suggested criteria can potentially lead to cost savings by reducing the specimen rejection rate.

1.3.5 Investigation of Effective Thickness of Side-grooved Clamped SE(T) Specimens for *J-R* Curve Testing

In the study reported in Chapter 6, 3D FEA are performed on clamped SE(T) specimens to investigate the effective thickness used in the calculations of the stress intensity factor (K) and plastic eta factor-based J-integral. The SE(T) specimens with six relative crack lengths (a/W ratios from 0.2 to 0.7), one relative thickness ($B/W = 1$) and eleven depths of side groove (i.e. $B_N/B = 1$, 0.94, 0.92, 0.9, 0.88, 0.86, 0.85, 0.84, 0.82, 0.8 and 0.75) are considered in the analyses. Based on the FEA results, new effective thickness expressions and values for K and J estimations for side-grooved SE(T) specimens are proposed and validated. The research outcome will facilitate the evaluation of *J-R* curves using the side-grooved SE(T) specimens.

1.4   Thesis Format

This thesis is prepared in an integrated-article format as specified by the School of Graduate and Postdoctoral Studies at the University of Western Ontario and consists of seven chapters. Chapter 1 is the introduction of the entire thesis where a brief review of fundamentals of LEFM and EPFM is presented. Chapters 2 through 6 form the main body of the thesis, each of which addresses an individual topic and is presented as a stand-alone manuscript without any abstract, but with its own references. Finally, a summary of the study, main conclusions of the thesis and recommendations for future study are included in Chapter 7.

References

Anderson, T. L. (2005). *Fracture Mechanics—Fundamentals and Applications, Third edition*. CRC Press, Boca Raton.

ASTM (2012). *ASTM E399-12*: *Standard Test Method for Linear-Elastic Plane-Strain Fracture Toughness K_{Ic} of Metallic Materials*. America Society of Testing and Materials International, West Conshohocken, PA.

ASTM (2013). *ASTM E1820-13: Standard Test Method for Measurement of Fracture Toughness*. America Society of Testing and Materials International, West Conshohocken, PA.

BSI (1997). *BS 7448 Part IV: Method for determination of fracture resistance curves and initiation values for stable crack extension in metallic materials*. British Standard Institution, London.

BSI (2014). *BS 8571 Part IV: Method of Test for Determination of Fracture Toughness in Metallic Materials Using Single Edge Notched Tension (SENT) Specimens*. British Standard Institution, London.

Burdekin, F. M. and Stone, D. E. W. (1966). The Crack Opening Displacement Approach to Fracture Mechanics in Yielding Materials. *The Journal of Strain Analysis for Engineering Design*, 1(2):145-153.

Broek D. (1986). *Elementary Engineering Fracture Mechanics*, Fourth edition. Kluwer Academic Publishers, Dordrecht, The Netherlands.

Chiesa M, Nyhus B, Skallerud B, Thaulow C. (2001). Efficient fracture assessment of pipelines. A constraint-corrected SENT specimen approach. *Engineering Fracture Mechanics*, 68:527–547.

Clarke, G. A., Andrews, W. R., Paris, P. C., Schmidt, D. W. (1976). Single Specimen Tests for JIc Determination. *Mechanics of Crack Growth*, ASTM STP 590, American Society for Testing and Materials, Philadelphia, 27-42.

Cravero, S. and Ruggieri, C. (2007). Estimation Procedure of J Resistance Curves for SE (T) Fracture Specimens Using Unloading Compliance. *Engineering Fracture Mechanics*, 74(17):2735-2757.

Fairchild, D. P., Kibey, S. A., Tang, H., Krishnan, V. R., Wang, X., Macia, M. L., and Cheng, W. (2012). Continued Advancements Regarding Capacity Prediction of Strain-based Pipelines. *Proceedings of 9th International Pipeline Conference (IPC2012)*, Calgary, Alberta, Canada, September 24–28.

Hollstein, T. and Blauel, J. G. (1977). On the Relation of the Crack Opening Displacement to the J-integral, *International Journal of Fracture*, 13:385-390.

Hutchinson, J. W. (1968). Singular Behavior at the End of a Tensile Crack in a Hardening Material. *Journal of the Mechanics of Physics and Solids*, 16:13-31.

Hutchinson, J. W. (1983). Fundamentals of the Phenomenological Theory of Nonlinear Fracture Mechanics. *Journal of Applied Mechanics*, 50:1042-1051.

Irwin, G. R. (1957). Analysis of Stresses and Strains Near the End of a Crack Traversing a Plate. *Journal of Applied Mechincs*, 24:361-364.

Irwin, G. R. (1961). Plastic zone near a crack and fracture toughness. *Sagamore Research Conference Proceedings*, 63-78.

Kirk, M. T. and Wang, Y. Y. (1995). Wide Range CTOD Estimation Formulae for SE(B) Specimens. *Fatigue and Fracture Mechanics, ASTM STP 1256*, American Society for Testing and Materials, 26:126-141.

National Energy Board (NEB), (2014). *Canadian Pipeline Transportation System - Energy Market Assessment*, National Energy Board, Canada.

Nikishkov, G. P. and Atluri, S. N. (1987). Calculation of Fracture Mechanics Parameters for an Arbitrary Three-dimensional Crack, by the 'Equivalent Domain Integral' Method. *International Journal for Numerical Methods in Engineering*, 24(9):1801-1821.

Panontin, T. L., Makino, A. and Williams, J. F. (2000). Crack Tip Opening Displacement Estimation Formulae for C(T) Specimens. *Engineering Fracture Mechanics*, 67:293-301.

PHMSA, (2012). Pipeline Incidents and Mileage Reports, March 2012. Pipeline & Hazardous Materials Safety Administration; http://primis.phmsa.dot.gov/comm/reports/safety/PSI.html.

Rice, J. R. (1968). A Path Independent Integral and the Approximate Analysis of Strain Concentration by Notches and Cracks. *Journal of Applied Mechanics*, 35:379-386.

Rice, J. R. and Rosengren, G. F. (1968). Plane Strain Deformation Near a Crack Tip in a Power Law Hardening Material. *Journal of the Mechanics of Physics and Solids*, 16:1-12.

Ruggieri, C. (2012). Further Results in J and CTOD Estimation Procedures for SE (T) Fracture Specimens–Part I: Homogeneous Materials. *Engineering Fracture Mechanics*, 79:245-265.

Shen, G., and Tyson, W. R. (2009). Evaluation of CTOD from J-integral for SE(T) Specimens. *Pipeline Technology Conference*, Ostend, Belgium, October 12-14.

Shih, C. F. (1981). Relationships between the J-integral and the Crack Opening Displacement for Stationary and Extending Cracks. *Journal of the Mechanics and Physics of Solids*, 29(4):305-326.

Shih, C. F, Moran, B. and Nakamura, T. (1986). Energy Release Rate along a Three-dimensional Crack Front in a Thermally Stressed Body. *International Journal of Fracture*. 30:79-102.

Tang, H., Macia, M., Minnaar, K., Gioielli, P., Kibey, S., and Fairchild, D. (2010). Development of the SENT Test for Strain-Based Design of Welded Pipelines. *Proceedings of 8th International Pipeline Conference (IPC2010)*, Calgary, Alberta, Canada, September 27–October 1.

Wang, E., Zhou, W., Shen, G., and Duan, D. (2012). An Experimental Study on J(CTOD)-R Curves of Single Edge Tension Specimens for X80 Steel. *International Pipeline*

Conference (IPC2012), Calgary, Alberta, Canada, September 24–28, Paper Number: IPC2012-90323.

Wang, E., Zhou, W. and Shen, G. (2013) Three-dimensional finite element analysis of crack-tip fields of clamped single-edge tension specimens – Part I: Crack-tip stress fields. *Engineering Fracture Mechanics*, 116:122–143.

Wang, Y. Y., Reemsnyder, H. S. and Kirk, M. T. (1997). Inference Equations for Fracture Toughness Testing: Numerical Analysis and Experimental Verification. *Fatigue and Fracture Mechanics, ASTM STP 1321*, American Society for Testing and Materials, 28:469-484.

Wang, Y., Liu, M. and Song, Y. (2011). Second generation models for strain-based design. 3801 Kirby Drive, Suite 520, Houston, Texas, US 77098: Center for Reliable Energy Systems.

Wells, A. A. (1961). Unstable Crack Propagation in Metals, Cleavage and Fast Fracture. *Proceedings of the Crack Propagation Symposium*, Cranfield, UK, 1:84.

Westergaard, H. M. (1939). Bearing Pressures and Cracks. *Journal of Applied Mechanics*, 6:49-53.

Williams, M. L. (1957). On the Stress Distribution at the Base of a Stationary Crack. *Journal of Applied Mechincs*, 24:109-114.

Zhu, X. K., Leis, B. N. and Joyce, J. A. (2005). Constraint Corrected *J-R* Curves and Its Application to Fracture Assessment for X80 Pipelines. *Journal of ASTM International*, 3(6):1-17.

(a) Mode I: opening mode **(b) Mode II: in-plane shearing mode** **(c) Mode III: out-of-plane shearing mode**
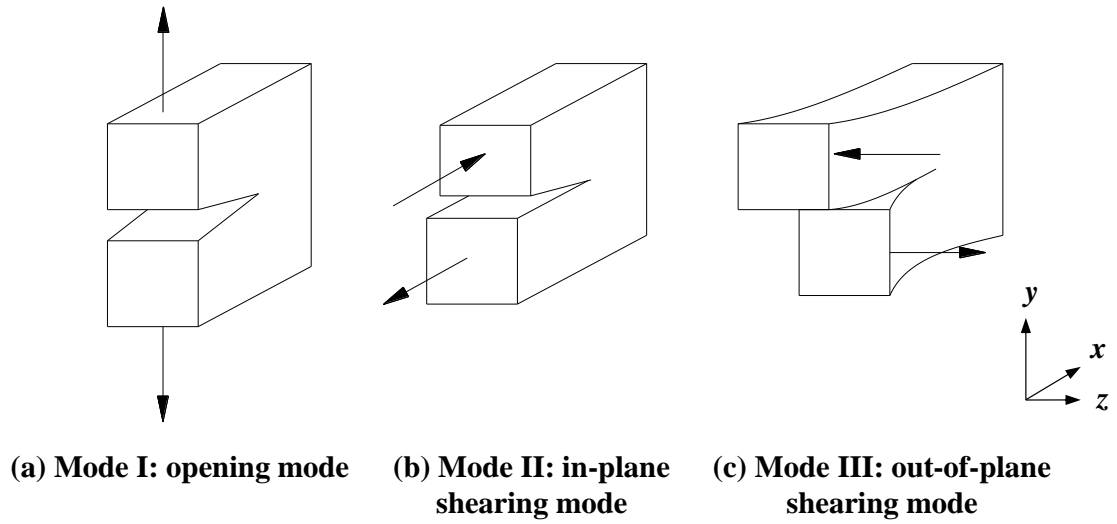
Figure 1.1: Three typical loading modes in fracture mechanics
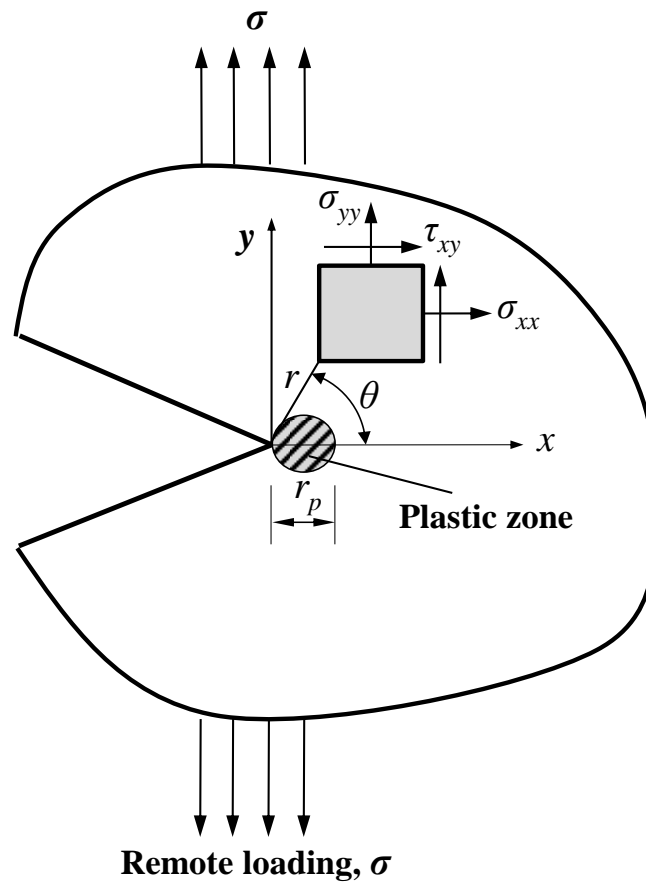
Figure 1.2: Stress field near the crack tip
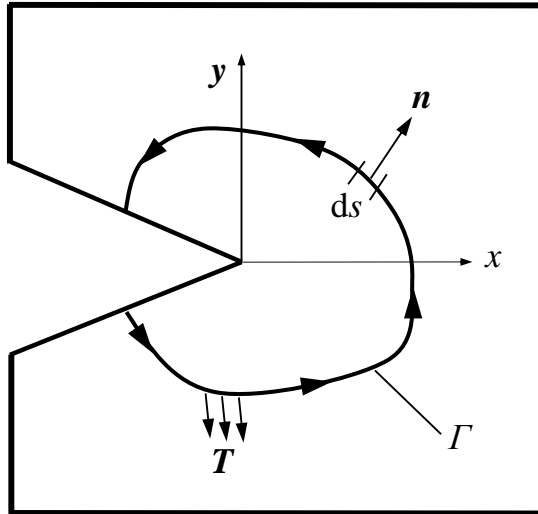
Figure 1.3: Schematic of *J*-integral
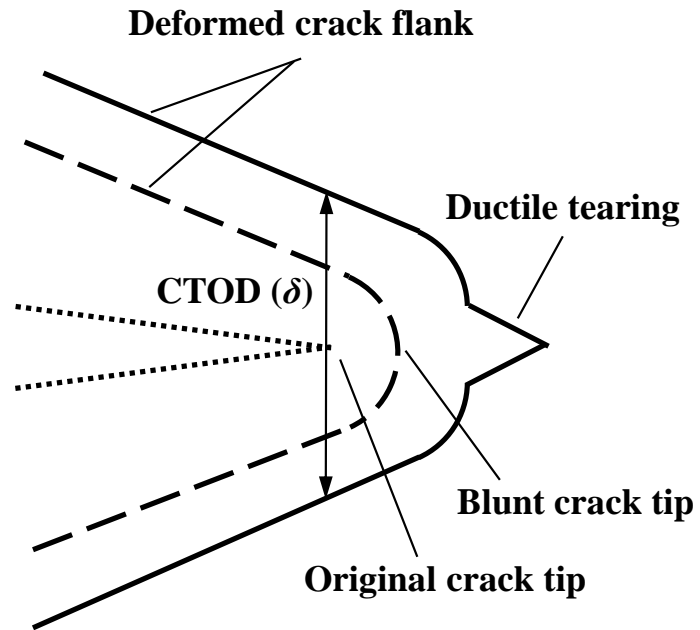
(a) Displacement at the original crack tip
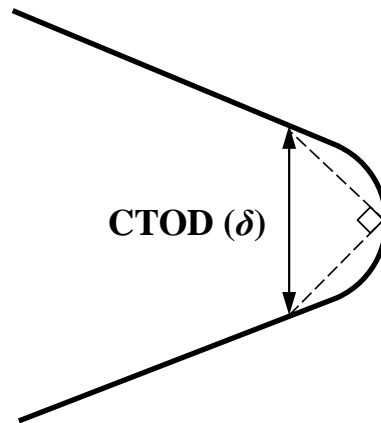
(b) Displacement at the intersection of a 90 degree vertex with the crack flanks

Figure 1.4: Schematically illustration of *CTOD* definitions
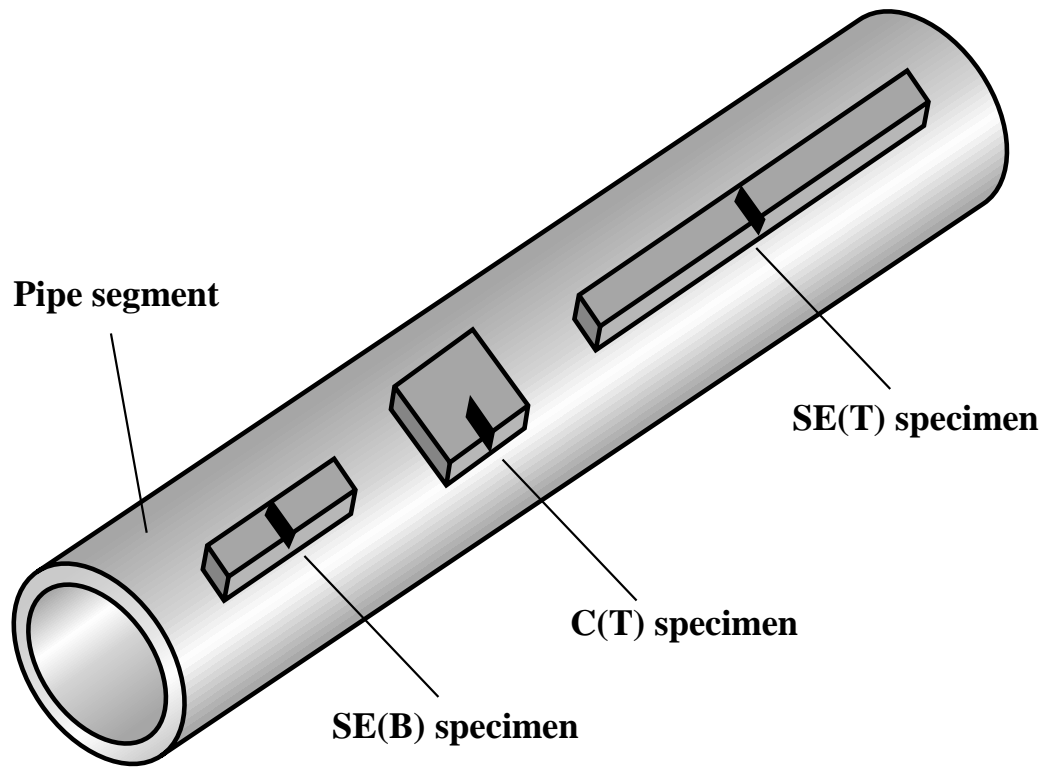
(a) Small-scale specimens cut from the pipe
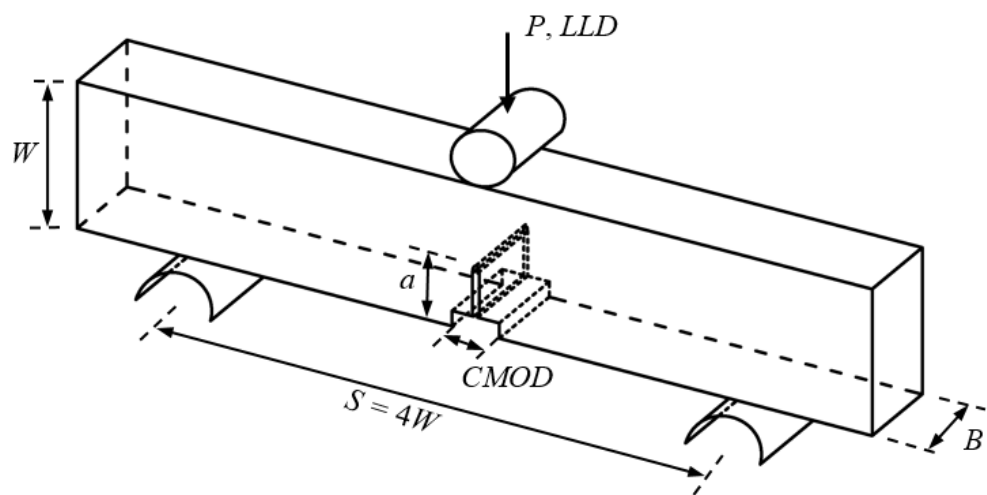
(b) Plane-sided three-point single-edge bend (SE(B)) specimen
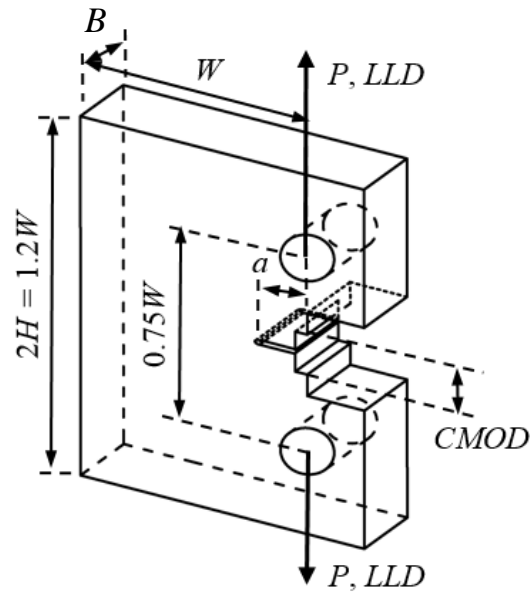
(c) Plane-sided compact tension (C(T)) specimen
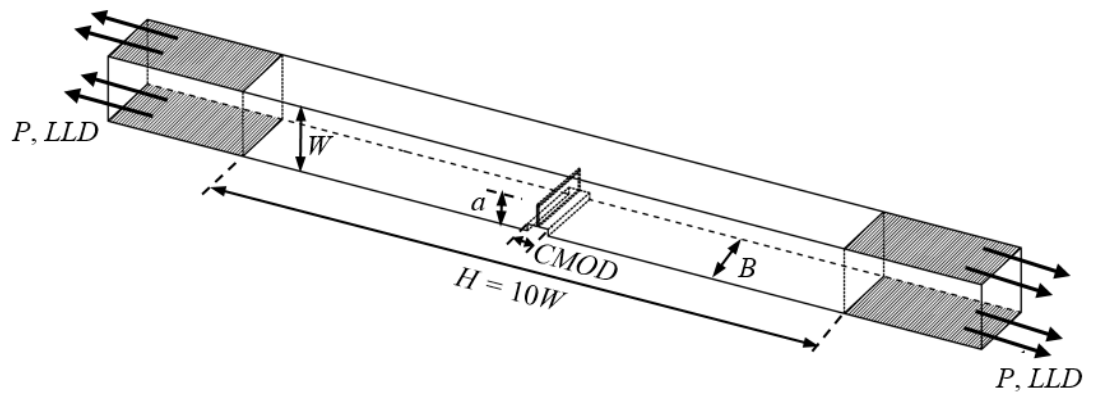
(d) Plane-sided clamped single-edge tension (SE(T)) specimen
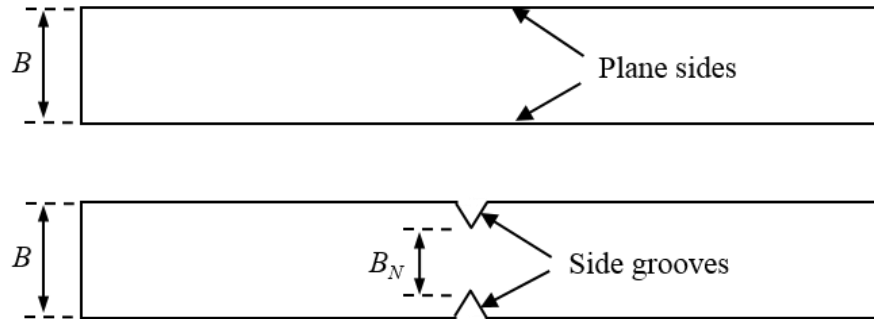
(e) Schematic of side grooves

Figure 1.5: Schematic of small-scale specimens cut from the pipe

Chapter 2 Evaluation of Plastic Geometry Factors for SE(T) Specimens Based on Three-dimensional Finite Element Analysis

2.1 Background and Objective

2.1.1 Estimation of *J* Using Plastic Geometry Factors

As an important input in the structural integrity assessment of steel structures such as pressure vessels and energy pipelines, the fracture toughness resistance curve, i.e. *J*-integral resistance (*J-R*) curve, is generally obtained from the small-scale fracture test specimens such as the single-edge bend (SE(B)) and compact tension (C(T)) specimens. The test procedures for such specimens have been standardized in standards such as ASTM E1820-11E2 (ASTM, 2013) and BS7448-97 (BSI, 1997). This section briefly describes the development of the experimental estimation methods of *J*-integral (*J*).

Begley and Landes (1972) were among the first to evaluate *J* experimentally based on its interpretation as the energy release rate:

$$J = -\frac{dU}{Bda} \tag{2.1}$$

where *U* denotes the strain energy; *a* and *B* are the crack length and specimen thickness, respectively. This method requires testing multiple specimens with different crack lengths, which can be costly and time consuming. Subsequent work by Rice et al. (1973) introduced a more convenient way to evaluate *J* from a single test specimen. *J* can be evaluated in either a load controlled (Eq. 2.2) or displacement controlled (Eq. 2.3) condition as follows (see Fig. 2.1):

$$J = \frac{1}{B}\int_0^P \frac{\partial \Delta}{\partial a}dP \tag{2.2}$$

or

$$J = -\frac{1}{B}\int_0^\Delta \frac{\partial P}{\partial a}d\Delta \tag{2.3}$$

where P denotes the applied load, and Δ is the load-line displacement (*LLD*). Figure 2.2 shows a typical load vs. displacement curve in the fracture toughness test. The total area under the loading path, A, is defined as the work done by the external force during the test. As indicated in Fig. 2.2, A can be separated by an elastic unloading path into an elastic component, A_{el}, and a plastic component, A_{pl}, i.e. $A = A_{el} + A_{pl}$. Similarly, this unloading path separates Δ into an elastic component, Δ_{el}, and a plastic component, Δ_{pl}, i.e. $\Delta = \Delta_{el} + \Delta_{pl}$, and Eq. (2.3) can be accordingly rewritten as

$$J = -\frac{1}{B}\int_0^{\Delta_{el}} \frac{\partial P}{\partial a} d\Delta_{el} - \frac{1}{B}\int_0^{\Delta_{pl}} \frac{\partial P}{\partial a} d\Delta_{pl} = J_{el} + J_{pl} \qquad (2.4)$$

where J_{el} and J_{pl} are the elastic and plastic components of J, respectively. J_{el} can be determined from the stress intensity factor K (Anderson, 2005):

$$J_{el} = \frac{K^2(1-v^2)}{E} \qquad (2.5)$$

where E and v are Young's modulus and Poisson's ratio respectively. The solutions for K have been well documented (e.g. Tada, 2000). Sumpter and Turner (1976) introduced a dimensionless plastic geometry factor, η_{pl}^{LLD}, to relate J_{pl} to the plastic area under the load (P) versus load-line displacement (*LLD*) curve, A_{pl}^{LLD}:

$$J_{pl} = \frac{\eta_{pl}^{LLD}}{bB}\int_0^{\Delta_{pl}} P d\Delta_{pl} = \frac{\eta_{pl}^{LLD} A_{pl}^{LLD}}{bB} \qquad (2.6)$$

where b is the length of the remaining ligament, $b = W - a$. Alternatively, J_{pl} can be evaluated from the crack mouth opening displacement (*CMOD* or V) as opposed to *LLD* (Kirk and Dodds, 1993); therefore,

$$J_{pl} = -\frac{1}{B}\int_0^{V_{pl}} \frac{\partial P}{\partial a} dV_{pl} \qquad (2.7)$$

or

$$J_{pl} = \frac{\eta_{pl}^{CMOD}}{bB} \int_0^{V_{pl}} P dV_{pl} = \frac{\eta_{pl}^{CMOD} A_{pl}^{CMOD}}{bB} \tag{2.8}$$

where V_{pl} is the plastic component of *CMOD*, A_{pl}^{CMOD} represents the plastic area under the load versus *CMOD* curve (see Fig. 2.2), and η_{pl}^{CMOD} denotes the *CMOD*-based plastic geometry factor. Equations (2.6) and (2.8) are prescribed in the testing standards (ASTM, 2013; BSI, 1997) as the *J* calculations for basic test method. Note that these two equations are limited to stationary cracks and therefore used to determine either the critical *J* (J_{IC}) by testing a single specimen, or the *J-R* curve by testing multiple specimens. For the determination of the *J-R* curve using the single-specimen testing method, another plastic geometry factor, γ_{pl}, is needed to make the crack growth correction in the eta factor-based evaluation of *J* (Ernst et al., 1981) as described in Appendix A. Parameters η_{pl} (i.e., η_{pl}^{LLD} and η_{pl}^{CMOD}) and γ_{pl} are key parameters to the experimental evaluation of the *J*-integral.

2.1.2 Development and Evaluation of η_{pl} Factor

This section briefly describes evaluation methods for the η_{pl} factors. Combining the second term of Eqs. (2.4) and (2.6) (or Eqs. (2.7) and (2.8)), η_{pl}^{LLD} and η_{pl}^{CMOD} are expressed as follows:

$$\begin{cases} \eta_{pl}^{LLD} = \dfrac{-b\int_0^{\Delta_{pl}} \dfrac{\partial P}{\partial a} d\Delta_{pl}}{\int_0^{\Delta_{pl}} P d\Delta_{pl}} & \text{(a)} \\[4ex] \eta_{pl}^{CMOD} = \dfrac{-b\int_0^{V_{pl}} \dfrac{\partial P}{\partial a} dV_{pl}}{\int_0^{V_{pl}} P dV_{pl}} & \text{(b)} \end{cases} \tag{2.9}$$

If the load *P* can be separated into a function of *a/W* and a function of Δ_{pl}/W, denoted as $M_\Delta(a/W)$ and $N_\Delta(\Delta_{pl}/W)$:

$$P\left(\frac{a}{W}, \frac{\Delta_{pl}}{W}\right) = M_\Delta\left(\frac{a}{W}\right) \cdot N_\Delta\left(\frac{\Delta_{pl}}{W}\right) \tag{2.10}$$

Then Eq. (2.9a) can be further rewritten as:

$$
\eta_{pl}^{LLD} = \frac{-b \int_0^{\Delta_{pl}} \left\{ \dfrac{\partial \left[M_\Delta \left(a/W \right) \cdot N_\Delta \left(\Delta_{pl}/W \right) \right]}{\partial a} \right\} d\Delta_{pl}}{\int_0^{\Delta_{pl}} \left[M_\Delta \left(a/W \right) \cdot N_\Delta \left(\Delta_{pl}/W \right) \right] d\Delta_{pl}}
$$
$$
= \left(\frac{a}{W} - 1 \right) \frac{\partial M_\Delta \left(a/W \right)}{\partial \left(a/W \right)} \frac{1}{M_\Delta \left(a/W \right)}
$$

$$(2.11)$$

The same approach can be used to evaluate η_{pl}^{CMOD} if P can be separated into a function of a/W and a function of V_{pl}/W, denoted as $M_V(a/W)$ and $N_V(V_{pl}/W)$:

$$
P\left(\frac{a}{W}, \frac{V_{pl}}{W} \right) = M_V\left(\frac{a}{W} \right) \cdot N_V\left(\frac{V_{pl}}{W} \right)
$$

$$(2.12)$$

and η_{pl}^{CMOD} is expressed as:

$$
\eta_{pl}^{CMOD} = \left(\frac{a}{W} - 1 \right) \frac{\partial M_V \left(a/W \right)}{\partial \left(a/W \right)} \frac{1}{M_V \left(a/W \right)}
$$

$$(2.13)$$

The evaluation of $\eta_{pl}^{LLD}(\eta_{pl}^{CMOD})$ from Eqs. (2.10) through (2.13) is based on analytical procedures and is known as the load separation analysis method (Sumpter and Turner, 1976; Paris et al., 1980). In these cases, $\eta_{pl}^{LLD}(\eta_{pl}^{CMOD})$ only depends on a/W and is therefore referred to as "the geometry factor". The existence of Eq. (2.10) (or Eq. (2.12)) is the basis to develop $\eta_{pl}^{LLD}(a/W)$ (or $\eta_{pl}^{CMOD}(a/W)$). Equations (2.10) and (2.12) are generally satisfied for cracked body composed by elastic-perfectly plastic materials. For hardening materials, $\eta_{pl}^{LLD}(\eta_{pl}^{CMOD})$ factor may depend on the strain hardening exponent (n) in addition to a/W.

Paris et al. (1980) suggested that η_{pl}^{LLD} that is independent of the loading and n exists for deeply-cracked bending and tension specimens of power-law hardening materials with $n \geq$ 10. Particularly, for many cracked body geometries, Eqs. (2.10) and (2.12) exist when the load is greater or equal to the limit load (P_Y). Therefore the estimation of $\eta_{pl}^{LLD}(\eta_{pl}^{CMOD})$ can also be converted to the limit load analysis. The limit loads for a variety of specimen

configurations have been well documented (Green and Hundy, 1956; Joch et al., 1993; Kanninen and Popelar, 1985; Miller, 1988; Khan and Ghosh, 2007).

For a given specimen at a given loading level, the values of η_{pl}^{LLD} and η_{pl}^{CMOD} can also be calculated from A_{pl}^{LLD} and A_{pl}^{CMOD} and corresponding J_{pl} by rearranging Eqs. (2.6) and (2.8) as follows:

$$
\begin{cases}
\eta_{pl}^{LLD} = \dfrac{J_{pl}bB}{A_{pl}^{LLD}} & \text{(a)} \\[4mm]
\eta_{pl}^{CMOD} = \dfrac{J_{pl}bB}{A_{pl}^{CMOD}} & \text{(b)}
\end{cases}
\tag{2.14}
$$

Note that Eq. (2.14) is theoretically equivalent to Eq. (2.9). Note also that for side-grooved specimens, the specimen thickness B in Eqs. (2.6), (2.7), (2.8) and (2.14) is replaced by the net thickness, B_N. The evaluation of η_{pl}^{LLD} (η_{pl}^{CMOD}) using Eq. (2.14) is known as the plastic work anaysis method (Ruggieri, 2012) and usually carried out with the aid of finite element analyses (FEA). To facilitate the experimental evaluation of J, a single value of η_{pl}^{LLD} or η_{pl}^{CMOD} is commonly determined from the regression analysis of a set of A_{pl}-J_{pl} data corresponding to a certain range of loading levels (Kirk and Dodds, 1993; Ruggieri, 2012; Kim and Budden, 2001; Kim and Schwalbe, 2012; Huang et al., 2013) (i.e., to make η_{pl} factors independent of the loading). Generally speaking, using the plastic work analysis is more advantageous than using the load separation analysis to determine η_{pl}^{LLD} (η_{pl}^{CMOD}) if P cannot be easily separated into the two functions as shown in Eqs. (2.10) and (2.12). The evaluation of η_{pl} for the SE(B) and C(T) specimens based on two-dimensional (2D) and three-dimensional (3D) FEA has been well reported in the literature (e.g. Kirk and Dodds, 1993; Kim and Schwalbe, 2001; Huang et al., 2013; Kim et al., 2004; Zhu et al., 2008; Kulka and Sherry, 2012). The evaluation of η_{pl} using the plastic work analysis for the SE(T) specimens is the focus of the study reported in this chapter.

2.1.3 Literature Review of Plastic Geometry Factors for SE(T) Specimen

Det Norske Veritas (DNV) (2006) developed the following 5th-order polynomial equation to evaluate η_{pl}^{CMOD} as a function of a/W and B/W based on the results of 3D FEA:

$$\eta_{pl}^{CMOD} = 0.85 \sum_{i=0}^{5} \left\{ \left(m_i \exp\left(-\frac{B}{W} \right) + n_i \right) \right\} \left(\frac{a}{W} \right)^i \tag{2.15}$$

where the factor 0.85 is included to account for the weak influence of work hardening and weld metal mismatch on η_{pl}^{CMOD}, and regression coefficients m_i and n_i ($i = 0, 1, ..., 5$) are listed in Table 2.1(a). Equation (2.15) is specified to be applicable for clamped plane-sided specimens with $0.2 \leq a/W \leq 0.5$, $1 \leq B/W \leq 5$ and $H/W = 10$. Note that Eq. (2.15) is independent of the strain hardening exponent (n). Note also that no equation for the η_{pl}^{LLD} factor for the side-grooved SE(T) specimen has been recommended by DNV.

By carrying out 2D plane-strain FEA, Shen and his co-workers (Shen et al., 2008, 2009) obtained values of η_{pl}^{LLD} and η_{pl}^{CMOD} for clamped SE(T) specimens with $0.1 \leq a/W \leq 0.7$ and $H/W = 10$. They observed that η_{pl}^{CMOD} is insensitive to n for $5 \leq n \leq 20$ and $a/W \leq 0.5$, and that η_{pl}^{LLD} is insensitive to n for $15 \leq n \leq 20$. Based on these observations, they proposed a 10th-order polynomial to evaluate η_{pl}^{LLD} or η_{pl}^{CMOD} as follows:

$$\eta_{pl}^{LLD} \left(\eta_{pl}^{CMOD} \right) = \sum_{i=0}^{10} \phi_i \left(\frac{a}{W} \right)^i \tag{2.16}$$

where two sets of regression coefficients ϕ_i ($i = 0, 1, ..., 10$), one for η_{pl}^{LLD} and the other for η_{pl}^{CMOD}, are developed based on the FEA results corresponding to $15 \leq n \leq 20$ and $5 \leq n \leq 20$, respectively, and listed in Table 2.1(b). It is indicated by Shen et al. (2008, 2009) that η_{pl}^{LLD} obtained from Eq. (2.16) be only used to evaluate the crack growth correction factor, γ_{pl}, but unsuitable for evaluating the experimental J through Eq. (2.6). By carrying out 3D FEA of the plane-sided clamped SE(T) specimen of Grade X100 steel (API, 2012) with $a/W = 0.34$ and $B/W = 2$, Pisarski (2010) reported that the errors of J values evaluated using η_{pl}^{CMOD} determined from Eqs. (2.15) and (2.16) are less than 3%.

Ruggieri (2012) carried out 2D plane-strain FEA and evaluated η_{pl}^{LLD} and η_{pl}^{CMOD} for clamped SE(T) specimens with $0.2 \leq a/W \leq 0.7$, and $H/W = 6$ and 10. Three pairs of 5th-order polynomials for η_{pl}^{LLD} and η_{pl}^{CMOD} for specimens with $n = 5$, 10 and 20, respectively, were proposed:

$$\eta_{pl}^{LLD}\left(\eta_{pl}^{CMOD}\right) = \sum_{i=0}^{5} \xi_i \left(\frac{a}{W}\right)^i \tag{2.17}$$

where coefficients ξ_i ($i = 0, 1, ..., 5$) for η_{pl}^{LLD} or η_{pl}^{CMOD} corresponding to $n = 5$, 10, and 20 are listed in Table 2.1(c). Ruggieri (2012) further carried out 3D FEA of clamped SE(T) specimens with $a/W = 0.1$ to 0.7, $B/W = 0.5$ and 2, and $n = 5$ and 20 to evaluate η_{pl}^{CMOD} values. He reported that values of η_{pl}^{CMOD} determined in Eq. (2.17) are generally similar to those obtained in 3D FEA. However, the η_{pl}^{LLD} values obtained from Eq. (2.17) have not been verified by 3D FEA. Furthermore, it is unclear how Eq. (2.17) can be applied to specimens with n values other than 5, 10 or 20.

More recently, Mathias et al. (2013) proposed the following expression for η_{pl}^{LLD} and η_{pl}^{CMOD} by summarizing the results reported by Ruggieri (2012) and Cravero and Ruggieri (2007):

$$\eta_{pl}^{LLD}\left(\eta_{pl}^{CMOD}\right) = \sum_{i=0}^{5} \psi_i \left(\frac{a}{W}\right)^i \tag{2.18}$$

where coefficients ψ_i ($i = 0, 1, ..., 5$) are listed in Table 2.1(d). Equation (2.18) is more concise than Eq. (2.17) in that the former is independent of the strain hardening exponent; however, the adequacy of Eq. (2.18) has not been investigated. Note that the adequacy of Eqs. (2.15) through (2.18) has not been investigated for side-grooved SE(T) specimens.

2.1.4 Objective and Approach

Although various equations of η_{pl} for the SE(T) specimen have been reported in the aforementioned studies, there is a lack of a systematic study that develops η_{pl} equations for both plane-sided and side-grooved SE(T) specimens with wide ranges of a/W, B/W, and n.

Such a study is valuable in that it provides appropriate η_{pl} factor to obtain the most accurate J evaluated in the J-R curve test and facilitates the standardization of the testing procedure for the SE(T) specimen. To this end, the objective of the study reported in this chapter was to carry out a systematic investigation of the η_{pl} factors for SE(T) specimens. The focus of the study is the clamped SE(T) specimen with H/W = 10 because the crack-tip stress fields of such a specimen correspond closely to those of the full-scale pipes containing circumferential cracks (Shen et al., 2008), which are of primary concern to the design and structural integrity assessment of pipelines. Extensive 3D finite element analyses of both plane-sided and side-grooved clamped SE(T) specimens with six crack lengths (a/W= 0.2, 0.3, 0.4, 0.5, 0.6 and 0.7), two thickness-to-width ratios (B/W = 1 and 2), and five strain hardening exponents (n = 5, 8.5, 10, 15 and 20) are carried out. For each of the specimens, the J values obtained from the virtual crack extension method as implemented in FEA were used to evaluate the corresponding η_{pl}^{LLD} or η_{pl}^{CMOD}. Based on the results of the investigation, a set of new equations for the eta factor are proposed and recommendations are provided as to the adequacy of the proposed η_{pl} equations.

The organization of this chapter is as follows. Section 2.2 describes the configurations of the FE models, material properties and computational procedures. Section 2.3 discusses the impact of specimen configurations and material hardening properties on eta. New η_{pl} equations are developed and verified in Section 2.4, followed by conclusions in Section 2.5.

2.2   Numerical Analysis

2.2.1   Finite Element Model

Three-dimensional models of both plane-sided (PS) and side-grooved (SG) SE(T) specimens with clamped ends were prepared for FEA. The analysis matrix includes specimens with six different a/W ratios (a/W = 0.2, 0.3, 0.4, 0.5, 0.6 and 0.7) and two B/W ratios (B/W = 1 and 2). Stationary cracks were assumed in the analysis. For side-grooved specimens, a side groove depth of 7.5%B at each side of the specimen was adopted based on the recommendation by Shen et al. (2010). All the specimens included in the analysis

matrix have the same width ($W = 20$ mm) and daylight length ($H/W = 10$). A typical side-grooved FE model with $a/W = 0.5$ and $B/W = 1$ is schematically shown in Fig. 2.3(a) together with the fixation and loading conditions.

The FEA code ADINA® (ADINA, 2012) was employed to analyze all the models. Because of symmetry, only one quarter of the specimen with appropriate constraints imposed on the remaining ligament was modelled. A typical quarter-symmetric 3D model has 10 layers over the half net thickness ($B_N/2$). For the side-grooved model, the depth of the side groove (i.e. $(B - B_N)/2$) was divided into 8 layers. The thickness of each layer was arranged such that the corresponding mesh density increases from the center plane to the free surface (or root of the side groove) to capture the high stress gradients at these locations. The total number of elements is approximately 12,000 in a typical plane-sided specimen, and 21,000 in a typical side-grooved specimen. For simplicity, the side groove was modelled in the present study as a sharp V-notch with an opening angle of 45° as schematically shown in Fig. 2.3(b). The 8-node 3D brick elements with 2×2×2 integration were used; the accuracy of using such elements to calculate J has been shown to be adequate (Kulka and Sherry, 2012). Convergence studies on mesh density were conducted by increasing the number of the layers along the half net tthickness from 10 to 17. Good convergence of the output J was observed.

The large-displacement large (finite)-strain formulation was employed in FEA as it can more accurately simulate the deformed configuration of the specimen. This is a key difference between the FE model developed in the present study and those employed in the previous studies described in Section 2.1.3, all of which employed the small-strain formulation. The large-strain analysis employs the finite strain tensor, whereas the small-strain analysis employs the infinitesimal strain tensor and neglects the second and higher order terms of the displacement gradients (Mase, 1970). The use of the small-displacement formulation basically ignores the difference between the spatial and material coordinate systems, whereas the large-displacement formulation takes this difference into account and the Lagrangian coordinate system was selected in this study (ADINA, 2012). To simulate the crack tip blunting and facilitate convergence of the finite strain analysis, a blunt crack tip with a radius (ρ_0) of 2.5 µm (see Fig. 2.3(c)) was incorporated in the FE model (Dodds,

2009). Cravero and Ruggieri (2005) reported that such a mesh design is adequate for accurately evaluating the crack-tip stress and strain fields as well as *J* values. The blunt crack tip was also prepared through the thickness of the side groove (see Fig. 2.3(d)) to reduce the impact of the singularity caused by the sharp V-notch groove. All of the FE models have 45 focused annular rings around the crack tip with 16 elements in each ring. The minimum in-plane dimension of the 1st ring is about $0.1\rho_0$ (Graba and Galkiewicz, 2007; Qian and Dodds, 2006), whereas the corresponding in-plane dimension of the elements in the 45th ring is about 2,000 times that of the element in the 1st ring (Dodds, 2009). The results of convergence studies on blunt tip radius and mesh density show good convergence in the elastic-plastic analyses.

2.2.2 Material Model

In ADINA, the large-displacement large-strain formulation requires input of the Cauchy (true) stress-logarithmic (true) strain relationship (ADINA, 2012). The von Mises yield criterion and isotropic hardening rule were adopted in the analysis. The von Mises yield criterion states that yielding is dependent on the second invariant of the deviatoric stress tensor, J_2. An elastic-plastic constitutive model with the J_2 incremental theory of plasticity (ADINA, 2012) was adopted in the analysis. The true stress (σ) and true strain (ε) relationship of the material is characterized as follows:

$$\frac{\varepsilon}{\varepsilon_0} = \begin{cases} \dfrac{\sigma}{\sigma_{YS}} & , \varepsilon \leq \varepsilon_0 \\ \left(\dfrac{\sigma}{\sigma_{YS}}\right)^n & , \varepsilon > \varepsilon_0 \end{cases} \tag{2.19}$$

where σ_{YS} is the yield strength, and ε_0 ($\varepsilon_0 = \sigma_{YS}/E$) denotes the yield strain. The yield strength, elastic modulus and Poisson's ratio were assumed to be 510 MPa, 200 GPa and 0.3, respectively. Five different strain hardening exponents were considered (i.e. $n = 5$, 8.5, 10, 15 and 20). The flow stress (σ_Y) that was used to determine the limit load ($P_Y = B_N b \sigma_Y$) (Shen et al., 2008, 2009) for the SE(T) specimen was calculated as ($\sigma_{YS} + \sigma_{UTS}$)/2.

The quantity σ_{UTS} is the ultimate tensile strength and can be estimated from the following equation (Wang et al., 2013):

$$\sigma_{UTS} = \frac{E^{1/n} \sigma_{YS}^{(n-1)/n} \varepsilon_u^{1/n}}{\exp(\varepsilon_u)} \tag{2.20}$$

where ε_u is the (true) strain corresponding to σ_{UTS} and assumed to equal $1/n$ (Dieter, 1986). For $\sigma_{YS} = 510$ MPa and $E = 200$ GPa, σ_{UTS} is about 999, 712, 666, 593, and 563 MPa ($\sigma_{YS}/\sigma_{UTS} = 0.511, 0.717, 0.766, 0.860$ and 0.906) corresponding to $n = 5, 8.5, 10, 15$ and 20, respectively.

2.2.3 Computational Procedure

The load was applied based on the displacement control condition. Uniform displacements were applied on two lateral surfaces that are considered as the clamped surfaces with a length of $2W$ (see Fig. 2.3(a)). The final applied displacement corresponding to $P/P_Y = 1.25 - 1.3$ was reached in about 5,000 steps in each simulation. The sparse matrix solver was selected for its high efficiency in numerical analysis (ADINA, 2012). The full Newton-Raphson iteration method was adopted to find the solution of nonlinear equations with the maximum number of iterations for each step being 50. The displacement convergence criterion was selected, in which the displacement tolerance equaled 0.0001 corresponding to a reference displacement of 1 mm (ADINA, 2012). At a given loading step, the values of J in each of the 10 layers along the thickness direction, i.e. the local J values, denoted by $J_{loc}^1, J_{loc}^2, \ldots J_{loc}^{10}$, were calculated using the virtual crack extension method implemented in ADINA (Anderson, 2005; ADINA, 2012). A brief description of this method is included in Appendix B. Note that the local J value at the mid-plane, J_{mid}, equals J_{loc}^0. Let z_i denote the distance between the end of the ith layer and mid-plane (i.e. $z_0 = 0$) as shown in Fig. 2.4. The weighted average J value over the entire crack front, J_{ave}, is then calculated as follows based on the trapezoidal rule:

$$J_{ave} = \frac{1}{\left[\dfrac{B_N}{2} - \dfrac{(z_{10} - z_9)}{2}\right]} \left[\sum_{i=0}^{8} \frac{(z_{i+1} - z_i)\left(J_{loc}^i + J_{loc}^{i+1}\right)}{2} + \frac{(z_{10} - z_9)J_{loc}^9}{2}\right] \qquad (2.21)$$

Note that the local J value at the specimen free surface, i.e. J_{loc}^{10}, cannot be accurately evaluated from FEA and that the width of the 10th layer is relatively small: $(z_{10} - z_9)/(B/2)$ = 0.02. Therefore, the 10th trapezoid is approximated by a rectangle with its area equal to $[J_{loc}^9(z_{10} - z_9)]/2$. To ensure the path-independence of the calculated J values, the two outermost semicircular rings surrounding the crack tip were used to define the virtual shifts. For a representative PS specimen with $a/W = 0.5$, $B/W = 1$ and $n = 10$, the difference between J_{ave} corresponding to the 20th and 45th ring is about 6.5%, and the difference between J_{ave} corresponding to the 40th and 45th rings is about 1.3% at the loading level of $P/P_Y = 1.3$. In this study, J_{ave} as opposed to the local J values was used to evaluate the eta factors because the eta factors specified in testing standards (ASTM, 2013; BSI, 1997) are typically corresponding to J_{ave}.

Evaluation of η_{pl} requires computation of J_{pl} and the load-displacement response. At a given loading level (i.e. P/P_Y), J_{pl} is calculated as the difference between J_{ave} and J_{el} as indicated in Eqs. (2.4) and (2.5). The stress intensity factor defined by Eq. (2.22) is employed to estimate J_{el}:

$$\begin{cases} K = \dfrac{P}{B\sqrt{W}} F\left(\dfrac{a}{W}\right) & \text{(a)} \\[4mm] F\left(\dfrac{a}{W}\right) = \sqrt{\dfrac{\pi a}{W}} \sum_{i=1}^{12} t_i \left(\dfrac{a}{W}\right)^{i-1} & \text{(b)} \end{cases} \qquad (2.22)$$

In the present study, the non-dimensional function $F(a/W)$ proposed by Shen et al. (2008, 2009) as shown in Eq. (2.22b) is adopted, where coefficients t_i ($i = 1, 2, ..., 12$) are listed in Table 2.2. Note that for side-grooved specimens, the specimen thickness, B, in Eq. (2.22a) should be replaced by $(BB_N)^{1/2}$ (ASTM, 2013; BSI, 1997). To verify the accuracy of Eq. (2.22b), Eq. (2.22b) is compared with $F(a/W)$ solutions proposed by Ahmad et al. (1991), John and Rigling (J&R) (1998) (for $H/W = 10$) and Cravero and Ruggieri (C&R) (2007). The first one is an analytical solution and has been recommended in DNV-RP-

F108 (2006), whereas the latter two were developed based on results of 2D plane-stress and plane-strain FEA. The comparison is shown in Fig. 2.5. The figure indicates that Eq. (2.22b) is practically identical to J&R's and C&R's solutions. Furthermore, Eq. (2.22b) and J&R's and C&R's solutions are essentially the same as Ahmad et al.'s solution for a/W ≤ 0.6. On the other hand, there exists an unreasonable kink at $a/W > 0.6$ in Ahmad et al.'s solution, which has also been pointed out by Shen et al. (2008). Given that Eq. (2.22b) agrees very well with solutions from three independent studies, the accuracy of this equation is considered adequate.

The plastic work A_{pl}^{LLD} and A_{pl}^{CMOD} in Eqs. (2.6), (2.8) and (2.14) are calculated as follows, which is consistent with Fig. 2.2:

$$A_{pl} = A - A_{el} = A - \frac{P^2 C_0}{2} \tag{2.23}$$

where C_0 is the compliance (i.e. inverse of the slope of the unloading path as shown in Fig. 2.2) determined at the initial loading steps. In establishing the load-displacement curves, $CMOD$ was determined at the crack mouth at the mid-thickness (i.e. symmetric plane) of the specimen. LLD should ideally be determined at the end (clamped) surface of the specimen; however, it is observed that the difference between the displacement of the end surface and remotely applied displacement differ by less than 0.3%. To reduce the data processing time, LLD was taken as the remotely applied displacement.

Ruggieri (2012) introduced the following equation to express η_{pl} based on Eq. (2.14):

$$\eta_{pl} = \frac{J_{pl} b B_N}{A_{pl}} = \frac{\left(\dfrac{J_{pl}}{b \sigma_{YS}}\right)}{\left(\dfrac{A_{pl}}{b^2 B_N \sigma_{YS}}\right)} = \frac{\overline{J}_{pl}}{\overline{A}_{pl}} \tag{2.24}$$

where $\overline{J}_{pl}$ and $\overline{A}_{pl}$ are the normalized J_{pl} and A_{pl}, respectively. The η_{pl} factor at a given loading level can be computed using Eq. (2.24) based on the corresponding $\overline{J}_{pl}$ and $\overline{A}_{pl}$.

For a given specimen, a single value of η_{pl}^{LLD} or η_{pl}^{CMOD} is commonly determined from the regression analysis of a set of data within a certain range of loading levels. In general, the lower bound of the loading range is set to be the limit load (P_Y), because η_{pl}^{LLD} and η_{pl}^{CMOD} at $P \geq P_Y$ are typically independent of the loading level (Sumpter and Turner, 1976). In the present study, the upper bound of the loading range was set to be approximately 1.25P_Y, which corresponds to typical maximum loading level in the SE(T) test (Shen et al., 2009; Mathias et al., 2013; Dodds and Read, 1990; Pussegoda, 2013). The values of η_{pl}^{LLD} and η_{pl}^{CMOD} were evaluated by minimizing the sum of relative errors of estimated J_{ave} values within the considered loading range:

$$e_{ac} = \sum_P |e_J| = \sum_P \left| \frac{J_\eta - J_{ave}}{J_{ave}} \right| \tag{2.25}$$

where e_{ac} is the sum of the relative errors; J_η is the J value estimated from Eqs. (2.4) – (2.6), (2.8) and (2.22) corresponding to a given η_{pl}, and $e_J = (J_\eta - J_{ave})/J_{ave}$ denotes the relative error of J_η at a given loading level. It is worth noting that η_{pl}^{LLD} and η_{pl}^{CMOD} determined from Eq. (2.25) can account for more contributions from data at relatively low loading levels than those determined by minimizing the sum of the absolute errors associated with J_η (e.g. $(J_\eta - J_{ave})^2$) (Huang et al., 2013).

2.3 Results and Discussions

2.3.1 Evaluated η_{pl} Factors

Figures 2.6(a) and 2.6(b) depict $\bar{J}_{pl}$ with respect to *LLD*-based and *CMOD*-based $\bar{A}_{pl}$, respectively, for PS specimens with $a/W = 0.2$ to 0.7, $n = 10$, and $B/W = 1$. At a given loading level (e.g. $\bar{A}_{pl}$), η_{pl} can be evaluated as the ratio of the corresponding vertical and horizontal coordinates in the figures. Figure 2.6(a) indicates that the slope of the $\bar{J}_{pl}$ vs. *LLD*-based $\bar{A}_{pl}$ line for a given a/W ratio decreases as the loading level increases from zero to P_Y; however, the slope of the line is more or less constant for $P > P_Y$. This implies that η_{pl}^{LLD} (for $n = 10$ and $B/W = 1$) is dependent on the loading level for $P \leq P_Y$, but

approximately independent of the loading level for $P > P_Y$. On the other hand, the slope of the $\bar{J}_{pl}$ vs. *CMOD*-based $\bar{A}_{pl}$ line corresponding to a given *a/W* ratio remains approximately constant for the entire loading range, which suggests that η_{pl}^{CMOD} (for $n = 10$ and $B/W = 1$) is independent of the loading level. The above observations are consistent with those reported in the literature (e.g. Ruggieri, 2012; Cravero and Ruggieri, 2007).

For a given specimen, η_{pl}^{LLD} and η_{pl}^{CMOD} were determined by minimizing e_{ac} as defined in Eq. (2.25) for the loading range between P_Y and $1.25P_Y$. The evaluated η_{pl}^{LLD} and η_{pl}^{CMOD} for all the specimens considered are listed in Table 2.3. Figures (2.7) and (2.8) show η_{pl}^{LLD} and η_{pl}^{CMOD} values plotted against *a/W* for both PS and SG specimens with different *B/W* ratios and *n* values. Discussions of the impacts of *a/W*, *B/W*, side-grooving and the strain hardening exponent on η_{pl} are presented in Sections 2.3.2 to 2.3.4.

2.3.2 Impact of *a/W*

Figures (2.7) and (2.8) indicate that both η_{pl}^{LLD} and η_{pl}^{CMOD} strongly depend on the *a/W* ratio. Figures 2.7(a) through 2.7(d) show that η_{pl}^{LLD} increases as *a/W* increases until *a/W* reaches 0.4 – 0.5, after which η_{pl}^{LLD} decreases as *a/W* further increases. Figures 2.8(a) through 2.8(d) show that η_{pl}^{CMOD} in general decreases as *a/W* increases. Similar variations of η_{pl}^{LLD} and η_{pl}^{CMOD} with respect to *a/W* are also reported in (Ruggieri, 2012; Kim and Schwalbe, 2001; Huang et al., 2013; Kim and Budden, 2001; Paris et al., 1980; Kim et al., 2004; Zhu et al., 2008; Cravero and Ruggieri, 2007; Shen et al., 2008, 2009; Mathias et al., 2013). For comparisons, expressions for η_{pl}^{LLD} and η_{pl}^{CMOD} developed by DNV (Eq. (2.15)), Shen et al. (Eq. (2.16)), Ruggieri (Eq. (2.17)) and Mathias et al. (Eq. (2.18)) are also plotted in Figs. (2.7) and (2.8). It is observed that the values of η_{pl}^{LLD} corresponding to PS specimens with $a/W \geq 0.4$ and η_{pl}^{CMOD} corresponding to PS specimens with $0.2 \leq a/W \leq 0.7$ obtained from the present study agree well with those evaluated from Eqs. (2.15) – (2.17). On the other hand, the values of η_{pl}^{LLD} obtained from the present study for PS specimens with $a/W < 0.4$ are generally lower than those from Eqs. (2.15) – (2.17). This may be partly attributed to the use of large-strain formulation in the present FEA as opposed to the small-

strain formulation adopted in the previous studies, and values of η_{pl}^{LLD} corresponding to shallow-cracked PS specimens is sensitive to the formulation adopted in the FEA.

2.3.3 Impact of *B/W* and Side Grooving

The results given in Tables 2.3(a) and 2.3(b) suggest that the *B/W* ratio in general has a small impact on η_{pl}^{LLD} and η_{pl}^{CMOD} as the difference between η_{pl}^{LLD} (η_{pl}^{CMOD}) values corresponding to different *B/W* ratios is less than 6% (10%), except for η_{pl}^{LLD} for PS specimens with *a/W* = 0.2. For such specimens, η_{pl}^{LLD} decreases by 12% - 28% as *B/W* increases from 1 to 2 for different *n* values. On the other hand, the side grooving has a relatively large impact on η_{pl}: For given *a/W*, *B/W* and *n*, the value of $\eta_{pl}^{LLD}(\eta_{pl}^{CMOD})$ corresponding to the SG specimen is always greater than that corresponding to the PS specimen. In particular, the values of η_{pl}^{LLD} corresponding to SG specimens are markedly higher than those corresponding to PS specimens for *a/W* ≤ 0.5 and *n* ≥ 10. This can be explained by the fact that the distribution of the local *J* over the crack front in an SG specimen is more uniform than that in the corresponding PS specimen for a given loading level (Wang et al., 2013); as a result, the average *J* corresponding to the SG specimen is higher than that corresponding to the PS specimen for the same loading level, leading to a higher eta factor for the SG specimen.

2.3.4 Impact of Strain Hardening Exponent

The results in Tables 2.3(a) and 2.3(b) indicate that for a given specimen configuration, η_{pl}^{LLD} generally increases with *n*, whereas η_{pl}^{CMOD} generally decreases (increases) as *n* increases for specimen with *a/W* < 0.5 (*a/W* ≥ 0.5). It is also observed that *n* has a pronounced impact on η_{pl}^{LLD}, but a relatively small impact on η_{pl}^{CMOD}. For example, the values of η_{pl}^{LLD} corresponding to *n* = 5 and *n* = 20 differ by as much as 210% for *a/W* = 0.2 and *B/W* = 1, whereas this difference for η_{pl}^{CMOD} is around 10%. Figures (2.7) and (2.8) suggest that the η_{pl} factors for SG specimens are somewhat more sensitive to *n* than those for the PS specimens.

2.4 Development of New Expressions for η_{pl}

2.4.1 Expressions for Evaluated η_{pl} Factors

To facilitate the experimental evaluation of J using clamped SE(T) specimens, for a given B/W ratio, the following polynomial equation was proposed to express η_{pl} as a function of a/W based on the values of η_{pl}^{LLD} and η_{pl}^{CMOD} shown in Tables 2.3(a) and 2.3(b):

$$\eta_{pl}^{LLD} = \sum_{i=0}^{3} p_i \left(\frac{a}{W} \right)^i \tag{2.26}$$

$$\eta_{pl}^{CMOD} = \sum_{i=0}^{2} q_i \left(\frac{a}{W} \right)^i \tag{2.27}$$

where p_i and q_i are fitting coefficients. To take into account the impact of the strain hardening exponent on the eta factor, p_i and q_i were further proposed to be polynomial functions of σ_{YS}/σ_{UTS} as follows:

$$p_i = \sum_{j=0}^{3} M_{ij} \left(\frac{\sigma_{YS}}{\sigma_{UTS}} \right)^j \tag{2.28}$$

$$q_i = \sum_{j=0}^{3} N_{ij} \left(\frac{\sigma_{YS}}{\sigma_{UTS}} \right)^j \tag{2.29}$$

where the fitting coefficients M_{ij} and N_{ij} are listed in Tables 2.4 and 2.5. Therefore, the advantage of the proposed η_{pl}^{LLD} and η_{pl}^{CMOD} equations is that the key influencing factors (i.e. a/W, B/W and n) are all explicitly taken into consideration.

Figures 2.9(a) through 2.9(d) depict Eqs (2.26) and (2.27) for both PS and SG specimens with a representative $n = 10$. Equations (2.15) – (2.18) were also plotted in the figures for comparison. Figures 2.9(a) and 2.9(b) indicate that the η_{pl}^{LLD} values evaluated from Eq. (2.26) are close to those given by Eqs. (2.16) – (2.18) for the PS specimens with $a/W \geq 0.4$, but are smaller than those given by Eqs. (2.16) – (2.18) for the PS specimens with $a/W <$ 0.4. On the other hand, the η_{pl}^{LLD} values evaluated from Eq. (2.26) are generally larger than

those given by Eqs. (2.16) – (2.18) for the SG specimens. Figure 2.9(c) indicates that the η_{pl}^{CMOD} values evaluated from Eq. (2.27) agree well those given by Eq. (2.16) for SG specimens with $B/W = 1$ and $a/W = 0.2 - 0.6$, and Figure 2.9(d) indicates that the η_{pl}^{CMOD} values obtained from Eq. (2.27) are similar to those given by Eqs. (2.17) and (2.18) for PS specimens with $B/W = 2$ and $a/W = 0.2 - 0.7$. The implications of the proposed η_{pl} equations for the J evaluation are discussed in Section 2.4.2. For a propagating crack, another geometry factor, γ_{pl}, can be evaluated by substituting Eq. (2.26) into Eq. (A.2):

$$
\begin{aligned}
\gamma_{pl}^{LLD} = \gamma_{pl}^{CMOD} &= \eta_{pl}^{LLD} - 1 - \frac{\left(\dfrac{b}{W}\right)}{\eta_{pl}^{LLD}} \frac{\partial \eta_{pl}^{LLD}}{\partial \left(\dfrac{a}{W}\right)} \\
&= \sum_{i=0}^{3} p_i \left(\frac{a}{W}\right)^i - 1 - \frac{\left(\dfrac{b}{W}\right)}{\displaystyle\sum_{i=0}^{3} p_i \left(\frac{a}{W}\right)^i} \left[\sum_{i=1}^{3} i p_i \left(\frac{a}{W}\right)^{i-1} \right]
\end{aligned}
\tag{2.30}
$$

2.4.2 Adequacy of New Expressions for η_{pl} in J Evaluation

To investigate the adequacy of η_{pl}^{LLD} and η_{pl}^{CMOD} determined from Eqs. (2.26) and (2.27) respectively, J_η values estimated through the use of Eqs. (2.4) - (2.6), (2.8), (2.22), (2.26) and (2.27) were compared with the corresponding J_{ave} values obtained from FEA. For comparisons, η_{pl}^{LLD} and η_{pl}^{CMOD} evaluated from Eqs. (2.15) and (2.16) were also used to compute J_η. These two equations were selected because the K solution for evaluating J_{el} associated with Eq. (2.16) is the same as the K solution adopted in the present study (i.e. Eq. (2.22b)), and the K solution associated with Eq. (2.15) is nearly identical to Eq. (2.22) (up to $a/W = 0.6$). Therefore, the comparison is not impacted by the choice of the K solution. The prediction error of J_η, e_J, as defined in Eq. (2.25) was calculated to evaluate the accuracy of the above-mentioned η_{pl} factor equations. Figures (2.10) and (2.11) depict LLD- and $CMOD$-based e_J, respectively, as a function of the loading level characterized by P/P_Y for the PS and SG specimens with $B/W = 1$ and 2, $a/W = 0.5$, and $n = 10$. Only values of e_J corresponding to $0.8 \leq P/P_Y \leq 1.25$ (or J_{ave} approximately between 100 and 400 kN/m)

are shown in these figures because the elastic component of J_η is significant (can be more than 50% of the total J_η) for $P/P_Y < 0.8$, and $P = 1.25P_Y$ is typically the maximum loading level in the SE(T)-based $J\text{-}R$ curve test (Shen et al., 2009; Mathias et al., 2013; Dodds and Read, 1990; Pussegoda et al., 2013).

Figures (2.10) and (2.11) indicate that Eqs. (2.15), (2.16), (2.26) and (2.27) generally lead to underestimated J values (i.e. $e_J < 0$) for $0.8 \leq P/P_Y \leq 1.2$, but overestimated J values (i.e. $e_J > 0$) for $P > 1.2P_Y$, for PS and SG specimens with $a/W = 0.5$ and $n = 10$. For a given specimen configuration, η_{pl}^{CMOD} leads to more accurate predictions of J than η_{pl}^{LLD}. The variations of e_J within the considered loading levels for specimens with other a/W ratios and n values generally follow the same trend but are not presented here to save space. Tables 2.6 and 2.7 summarize the maximum values of $|e_J|$ for $0.8 \leq P/P_Y \leq 1.25$ associated with Eqs. (2.15), (2.16), (2.26) and (2.27) for all the analysis cases considered. The results in these tables indicate that η_{pl}^{LLD} evaluated from Eqs. (2.16) and (2.26) may lead to large errors in J ($|e_J|$ ranging from 10% - 304%) for shallow-cracked specimens with $a/W \leq 0.3$, whereas η_{pl}^{CMOD} evaluated from Eqs. (2.15), (2.16) and (2.27) generally lead to accurate predictions of J with $|e_J|$ less than 20% for all the analysis cases considered. Furthermore, $|e_J|$ for the SG specimen is smaller than that for the corresponding PS specimen because the crack-tip stress state in SG specimens is closer to the plane-strain condition and the error in J_{el} evalauted from Eq. (2.5) is smaller for the SG specimen than the PS specimen. For most of the analysis cases considered, the η_{pl} equations proposed in the present study lead to markedly more accurate predictions of J than Eqs. (2.15) and (2.16). The maximum $|e_J|$ corresponding to the proposed η_{pl}^{CMOD} equation (Eq. (2.27)) is 9% for both the PS and SG specimens with $0.2 \leq a/W \leq 0.7$. The maximum $|e_J|$ corresponding to the proposed η_{pl}^{LLD} equation (Eq. (2.26)) for specimens with $a/W \leq 0.3$ is 45%. For specimens with $a/W > 0.3$, Eq. (2.26) leads to maximum $|e_J|$ of 19% and 13% for PS and SG specimens, respectively. Based on the results in Tables 2.6 and 2.7, we provide the following recommendations as to the adequacy and applicability of Eqs. (2.26) and (2.27).

(1) The use of η_{pl}^{CMOD} (Eq. (2.27)) is preferred than the use of η_{pl}^{LLD} (Eq. (2.26)) for evaluating J values for the clamped SE(T) specimen regardless of the specimen configuration and material hardening property.

(2) For shallow-cracked clamped SE(T) specimens with $a/W \leq 0.3$, the use of η_{pl}^{LLD} to evaluate J is not recommended because the evaluated J values can be associated with large errors.

2.5 Conclusions

Systematic three-dimensional finite element analyses with the large-displacement/finite-strain formulation have been performed on clamped SE(T) specimens to evaluate the plastic eta factor (η_{pl}) for such specimens. Both plane-sided and side-grooved SE(T) specimens with a wide range of configurations (a/W = 0.2 to 0.7 with an increment of 0.1, and B/W = 1 and 2) and strain hardening exponents (n = 5, 8.5, 10, 15 and 20) were considered in the analyses. A side groove depth of 7.5%B on each side was included in the SG specimens. A set of expressions for both *LLD*- and *CMOD*-based η_{pl} were proposed as functions of a/W, B/W, and the yield-to-tensile strength ratio. The adequacy of the proposed η_{pl} equations was examined by comparing the corresponding η_{pl}-based J values with J_{ave} evaluated from FEA for P/P_Y levels ranging from 0.8 to 1.25.

The analysis results suggest that η_{pl}^{CMOD} leads to more accurately predicted J_{ave} values than η_{pl}^{LLD} for all the specimens considered. The η_{pl}^{CMOD} and η_{pl}^{LLD} equations proposed in this study lead to markedly more accurate predictions of J_{ave} values than those developed by DNV and Shen et al. for most of the analysis cases considered. The maximum error associated with the J_{ave}values predicted based on the proposed η_{pl}^{CMOD} equation is 9% for both the PS and SG specimens with $0.2 \leq a/W \leq 0.7$ and loading levels between 0.8 and 1.25P_Y. For specimens with $a/W > 0.3$, the maximum errors associated with the J_{ave}values predicted based on the proposed η_{pl}^{LLD} equation are 19% and 13% for PS and SG specimens, respectively. However, none of the η_{pl}^{LLD} equations considered in this study is able to

predict J_{ave} with reasonable accuracies for specimens with $a/W \leq 0.3$; therefore, η_{pl}^{CMOD} as opposed to η_{pl}^{LLD} is recommended for the J evaluation for such specimens.

References

ADINA. (2012). Theory and Modeling Guide, ADINA R. & D. Inc., Watertown, USA.

Ahmad, J., Papaspyropoulos, V. and Hopper, A. T. (1991). Elastic-plastic analysis of edge-notched panels subjected to fixed grip loading. *Engineering fracture mechanics*, 38(4):283-294.

Anderson, T. L. (2005). *Fracture Mechanics—Fundamentals and Applications, Third edition*. CRC Press, Boca Raton.

API. (2012). *API Specification 5L: Specification for Line Pipe*, Ed. 45, American Petroleum Institute, Washington, D.C.

ASTM (2013). *ASTM E1820-13: Standard Test Method for Measurement of Fracture Toughness*. America Society of Testing and Materials International, West Conshohocken, PA.

Begley, J. A. and Landes, J. D. (1972). The *J*-integral as a Fracture Criterion. *Fracture Mechanics*, *ASTM STP 514*, ASTM International, West Conshohocken, PA; 515:1-23.

BSI (1997). *BS 7448-4: Method for determination of fracture resistance curves and initiation values for stable crack extension in metallic materials,* British Standard Institution, London.

Cravero, S. and Ruggieri, C. (2005). Correlation of fracture behavior in high pressure pipelines with axial flaws using constraint designed test specimens - Part I: Plane-strain analyses. *Engineering Fracture Mechanics*, 72:1344-1360.

Cravero, S. and Ruggieri, C. (2007). Estimation Procedure of J Resistance Curves for SE (T) Fracture Specimens Using Unloading Compliance. *Engineering Fracture Mechanics*, 74(17):2735-2757.

Det Norske Veritas. (2006). Fracture control for pipeline installation methods introducing cyclic plastic strain. DNV-RP-F108. Norway: DNV.

Dodds, R, H. and Read, D. (1990). Experimental and numerical studies of the *J*-integral for a surface flaw. *International Journal of Fracture*, 43:47-67.

Dodds, R. H. (2009). WARP3D: Notes on solution & convergence parameters for a shallow-notch SE(B) model.

Dieter, G. E. (1986). Mechanical metallurgy: McGraw-Hill.

Ernst, H. A., Paris, P. C. and Landes, J. D. (1981). Estimation on *J*-integral and tearing modulus *T* from a single specimen test record. *Fracture mechanics: Thirteenth conference*, ASTM STP 743. Baltimore, MD: American Society for Testing and Materials; p. 476-502.

Graba, M. and Galkiewicz, J. (2007). Influence of the crack tip model on results of the finite element method. *Journal of Theoretical and Applied Mechanics*, 45:225-237.

Green, A. P. and Hundy, B. B. (1956). Initial Plastic Yielding in Notch Bend Tests. *Journal of the Mechanics and Physics of Solids*, 4(2):128-144.

Huang, Y., Zhou, W. and Yan, Z. (2013). Evaluation of plastic geometry factor for SE(B) specimens based on three-dimensional finite element analyses. *International Journal of Pressure Vessels and Piping*, 123:99-110.

Joch, J., Ainsworth, R. A. and Hyde, T. H. (1993). Limit Load and *J*-estimates for Idealised Problems of Deeply Cracked Welded Joints in Plane‐Strain Bending and Tension. *Fatigue & Fracture of Engineering Materials & Structures*, 16(10):1061-1079.

John, R. and Rigling, B. (1998). Effect of height to width ratio on *K* and *CMOD* solutions for a single edge cracked geometry with clamped ends. *Engineering fracture mechanics*, 60(2):147-156.

Kanninen, M. F. and Popelar, C. H. (1985). *Advanced Fracture Mechanics*, Oxford University Press, New York.

Khan, I. A. and Ghosh, A. K. (2007). A Modified Upper Bound Approach to Limit Analysis for Plane Strain Deeply Cracked Specimens. *International Journal of Solids and Structures*, 44(10):3114-3135.

Kim, Y. J. and Budden, P. (2001). Plastic η factor solutions of homogeneous and bi‐material SE(T) specimens for toughness and creep crack growth testing. *Fatigue and Fracture of Engineering Materials and Structures*, 24:751-760.

Kim, Y. J., Kim, J. S. and Cho, S. M. (2004). 3-D constraint effects on *J* testing and crack tip constraint in M(T), SE(B), SE(T) and C(T) specimens: numerical study. *Engineering Fracture Mechanics*, 71:1203-1218.

Kim, Y. J. and Schwalbe, K. H. (2001). On the sensitivity of *J* estimation to materials' stress-strain curves in fracture toughness testing using the finite element method. *Journal of Testing and Evaluation*, 29:18-30.

Kirk, M. T. and Dodds, R. H. (1993). J and CTOD estimation equations for shallow cracks in single edge notch bend specimens. *Journal of Testing and Evaluation*, 21:228-238.

Kulka, R. and Sherry, A. (2012). Fracture toughness evaluation in C(T) specimens with reduced out-of-plane constraint. *ASME Pressure Vessels and Piping Conference*: American Society of Mechanical Engineers. p. 877-885.

Mase, G. E. (1970). *Schaum's Outline of Continuum Mechanics*. McGraw-Hill.

Mathias, L. L., Sarzosa, D. F. and Ruggieri, C. (2013). Effects of specimen geometry and loading mode on crack growth resistance curves of a high-strength pipeline girth weld. *International Journal of Pressure Vessels and Piping*, 111:106-119.

Miller, A. G. (1988). Review of Limit Loads of Structures Containing Defects. *International Journal of Pressure Vessels and Piping*, 32:197-327.

Paris, P. C., Ernst, H. and Turner, C. (1980). A *J*-lntegral approach to development of η-factors. *American Society for Testing and Materials Special Technical Publication*, 338-351.

Pisarski, H. G. (2010). Determination of pipe girth weld fracture toughness using SENT specimens. *The 8th International Pipeline Conference*: American Society of Mechanical Engineers. p. 217-24.

Pussegoda, L. N., Tiku, S., Tyson, W. R., Park, D-Y., Gianetto, J. A., Shen, G. and Pisarski, H.G. (2013). Comparison of resistance curves from multi-specimen and single-specimen SENT Tests. *Proceedings of Twenty-third International Offshore and Polar Engineering Conference*. Anchorage, Alaska, USA: The International Society of Offshore and Polar Engineers (ISOPE); p. 482-8.

Qian, X. and Dodds, R. H. (2006). WARP3D: Effect of mesh refinement on the crack-tip stress field for SSY models.

Rice, J. R., Paris, P. C., Merkle, J. G. (1973). Some Further Results of *J*-integral Analysis and Estimates. *Progress in flaws growth and fracture toughness testing*, *ASTM STP 536*. ASTM; 231-45.

Ruggieri, C. (2012). Further Results in J and CTOD Estimation Procedures for SE(T) Fracture Specimens–Part I: Homogeneous Materials. *Engineering Fracture Mechanics*, 79:245-265.

Shen, G., Gianetto, J. A, and Tyson, W. R. (2008). Report 2008-18(TR): Development of procedure for low-constraint toughness testing using a single-specimen technique. Ottawa, Canada: CANMET-MTL.

Shen, G., Gianetto, J. A, and Tyson, W. R. (2009). Measurement of *J-R* Curves using single-specimen technique on clamped SE(T) specimens. *Proceedings of the Nineteenth*

International Offshore and Polar Engineering Conference. Osaka, Japan: The International Society of Offshore and Polar Engineers; p. 92-99.

Shen, G., Tyson, W. R., Gianetto, J. A. and Park, D-Y. (2010). Effect of side grooves on compliance, *J*-Integral and constraint of a clamped SE(T) specimen. *ASME Conference Proceedings*. 81-89.

Sumpter, J. D. G. and Turner, C. E. (1976). Method for Laboratory Determination of Jc (Contour Integral for Fracture Analysis). *Cracks and Fracture, ASTM STP 601*, ASTM, West Conshohocken, PA; 3-18.

Tada, H., Paris, P. C. and Irwin, G. R. (2000).*The Stress Analysis of Cracks Handbook*, Third edition. ASME Press, New York.

Wang, E., Zhou, W. and Shen, G. (2013). Three-dimensional finite element analysis of crack-tip fields of clamped single-edge tension specimens – Part I: Crack-tip stress fields. *Engineering Fracture Mechanics*, 116:122-143.

Zhu, X. K., Leis, B. N., and Joyce, J. A. (2008). Experimental estimation of *J-R* curves from load-*CMOD* record for SE(B) specimens. *Journal of ASTM International*, 5:66-86.

Table 2.1: Summary of coefficients of Eqs. (2.15) – (2.18) for η_{pl}.

(a) Equations (2.15)

	$i = 5$	$i = 4$	$i = 3$	$i = 2$	$i = 1$	$i = 0$
m_i	196.719	-493.511	463.503	-201.862	39.413	-2.064
n_i	-64.642	138.837	-106.207	34.532	-4.525	1.039

(b) Equations (2.16)

	$i = 10$	$i = 9$	$i = 8$	$i = 7$	$i = 6$	$i = 5$
LLD-based ϕ_i	14.187	5.397	-4.447	-12.202	-12.756	-1.273
	$i = 4$	$i = 3$	$i = 2$	$i = 1$	$i = 0$	
	18.399	18.644	-35.440	15.190	-0.880	
$CMOD$-based ϕ_i	$i = 10$	$i = 9$	$i = 8$	$i = 7$	$i = 6$	$i = 5$
	-110.770	43.306	101.401	38.487	-77.984	-73.116
	$i = 4$	$i = 3$	$i = 2$	$i = 1$	$i = 0$	
	109.225	-48.572	9.519	-1.089	1.000	

(c) Equations (2.17)

	n	$i = 5$	$i = 4$	$i = 3$	$i = 2$	$i = 1$	$i = 0$
LLD-based ξ_i	5	-320.4615	751.1830	-664.9214	266.7557	-44.8018	2.8802
	10	128.2564	-289.9382	262.9431	-124.8165	31.1679	-2.0530
	20	84.2051	-175.5082	142.2847	-61.6162	14.4939	-0.1600
$CMOD$-based ξ_i	5	-12.6667	41.7774	-47.7238	23.2332	-5.4920	1.4324
	10	-1.1282	16.4779	-23.5153	10.9659	-2.3047	1.0823
	20	61.2821	-131.9872	108.4318	-43.2838	7.7140	0.4023

(d) Equations (2.18)

	$i = 5$	$i = 4$	$i = 3$	$i = 2$	$i = 1$	$i = 0$
LLD- based ψ_i	-44.875	87.697	-47.963	-4.584	9.336	-0.623
CMOD- based ψ_i	-3.083	15.295	-18.269	7.808	-1.767	1.067

Table 2.2: Coefficients of Eq. (2.22b) for *F*.

	$i = 12$	$i = 11$	$i = 10$	$i = 9$	$i = 8$	$i = 7$
t_i	19.465	18.574	-52.322	-6.607	51.215	-36.137
	$i = 6$	$i = 5$	$i = 4$	$i = 3$	$i = 2$	$i = 1$
	-41.397	100.462	-69.051	23.886	-2.133	1.197

Table 2.3: The η_{pl} factors obtained from FEA for specimens with various configurations and strain-hardening exponents.

(a) η_{pl} for specimens with $B/W = 1$

	n	a/W											
		0.2		0.3		0.4		0.5		0.6		0.7	
		η_{LLD}	η_{CMOD}	η_{LLD}	η_{CMOD}	η_{LLD}	η_{CMOD}	η_{LLD}	η_{CMOD}	η_{LLD}	η_{CMOD}	η_{LLD}	η_{CMOD}
Plane-sided	5	0.26	0.92	0.58	0.85	0.95	0.79	0.93	0.71	0.83	0.59	0.72	0.5
	8.5	0.38	0.87	0.94	0.81	1.03	0.78	1.02	0.71	0.91	0.61	0.8	0.53
	10	0.44	0.86	0.96	0.82	1.04	0.77	1.03	0.72	0.92	0.61	0.81	0.53
	15	0.69	0.85	0.99	0.81	1.04	0.77	1.05	0.72	0.94	0.62	0.82	0.54
	20	0.81	0.83	0.98	0.8	1.01	0.76	1.03	0.72	0.94	0.62	0.83	0.54
Side-grooved	5	0.34	0.92	0.89	0.85	1.08	0.8	1.08	0.73	0.96	0.62	0.81	0.52
	8.5	0.93	0.9	1.29	0.88	1.35	0.83	1.27	0.77	1.1	0.66	0.88	0.54
	10	1.08	0.91	1.39	0.89	1.42	0.85	1.31	0.77	1.11	0.66	0.9	0.54
	15	1.31	0.95	1.52	0.91	1.52	0.87	1.36	0.79	1.14	0.67	0.91	0.55
	20	1.44	0.98	1.62	0.93	1.54	0.87	1.37	0.79	1.15	0.67	0.92	0.55

(b) η_{pl} for specimens with $B/W = 2$

	n	a/W											
		0.2		0.3		0.4		0.5		0.6		0.7	
		η_{LLD}	η_{CMOD}	η_{LLD}	η_{CMOD}	η_{LLD}	η_{CMOD}	η_{LLD}	η_{CMOD}	η_{LLD}	η_{CMOD}	η_{LLD}	η_{CMOD}
Plane-sided	5	0.22	0.93	0.51	0.88	0.93	0.81	0.96	0.73	0.85	0.6	0.73	0.5
	8.5	0.3	0.89	0.9	0.85	1.06	0.81	1.06	0.73	0.93	0.61	0.81	0.53
	10	0.34	0.88	0.95	0.85	1.08	0.81	1.09	0.74	0.96	0.62	0.83	0.53
	15	0.5	0.87	1.01	0.84	1.11	0.8	1.12	0.74	0.98	0.62	0.84	0.53
	20	0.6	0.85	1.01	0.84	1.11	0.8	1.12	0.74	0.99	0.63	0.85	0.54
Side-grooved	5	0.3	0.95	0.83	0.89	1.1	0.84	1.12	0.76	1	0.65	0.83	0.54
	8.5	0.8	0.93	1.29	0.91	1.4	0.88	1.33	0.81	1.14	0.69	0.9	0.56
	10	0.98	0.92	1.4	0.93	1.44	0.89	1.36	0.82	1.15	0.69	0.91	0.56
	15	1.27	0.94	1.54	0.95	1.54	0.91	1.4	0.83	1.18	0.69	0.93	0.56
	20	1.34	0.98	1.58	0.98	1.6	0.92	1.41	0.83	1.19	0.7	0.92	0.57

Table 2.4: Coefficients M_{ij} in Eq. (2.28).

| | | $B/W = 1$ | | | | $B/W = 2$ | | | |
		$j = 3$	$j = 2$	$j = 1$	$j = 0$	$j = 3$	$j = 2$	$j = 1$	$j = 0$
Plane-sided	$i = 3$	528.840	-1589.663	1428.230	-379.643	-87.313	-190.103	433.807	-159.729
	$i = 2$	-634.869	2038.619	-1888.257	502.526	199.494	121.911	-518.671	198.286
	$i = 1$	221.543	-789.313	761.096	-201.946	-129.052	27.746	172.821	-70.266
	$i = 0$	-23.045	93.004	-92.427	24.722	22.430	-14.585	-14.226	6.992
Side-grooved	$i = 3$	-253.395	569.934	-427.915	120.453	803.107	-1823.304	1342.474	-304.138
	$i = 2$	437.980	-968.471	721.007	-205.147	-1442.261	3252.887	-2373.697	529.551
	$i = 1$	-230.447	503.325	-377.091	109.734	824.519	-1846.804	1331.880	-292.147
	$i = 0$	34.835	-76.304	60.148	-17.549	-147.141	326.224	-230.353	50.164

Table 2.5: Coefficients N_{ij} in Eq. (2.29).

| | | $B/W = 1$ | | | | $B/W = 2$ | | | |
		$j = 3$	$j = 2$	$j = 1$	$j = 0$	$j = 3$	$j = 2$	$j = 1$	$j = 0$
	$i = 2$	19.164	-42.000	29.053	-6.982	3.693	-10.995	8.889	-3.027
Plane-sided	$i = 1$	-10.250	22.285	-14.340	2.533	0.196	2.192	-1.930	0.284
	$i = 0$	-1.282	2.815	-2.474	1.708	-1.671	3.089	-2.252	1.555
	$i = 2$	25.040	-42.248	20.037	-3.196	51.818	-101.542	61.517	-12.686
Side-grooved	$i = 1$	-23.177	36.942	-15.685	1.261	-54.803	106.394	-64.095	12.230
	$i = 0$	4.645	-6.629	2.244	0.946	13.948	-26.896	16.344	-2.196

Table 2.6: Maximum absolute values of e_J corresponding to the *LLD*-based η_{pl} over $P/P_Y = 0.8 - 1.25$.

(a) Plane-sided specimens

	a/W	**B/W = 1**						**B/W = 2**					
		0.2	0.3	0.4	0.5	0.6	0.7	0.2	0.3	0.4	0.5	0.6	0.7
n = 5	Eq. (2.16)	247.0%	104.8%	20.8%	12.3%	11.1%	11.9%	304.4%	130.9%	23.4%	11.9%	9.4%	10.8%
	Eq. (2.26)	21.7%	23.6%	14.6%	9.2%	6.7%	4.7%	23.3%	28.7%	15.9%	9.9%	8.2%	4.8%
n = 8.5	Eq. (2.16)	158.8%	27.7%	15.4%	13.6%	6.5%	5.5%	220.2%	36.8%	13.8%	13.2%	6.7%	4.5%
	Eq. (2.26)	45.3%	22.3%	14.7%	12.1%	6.7%	3.0%	45.4%	20.5%	13.4%	11.0%	5.9%	3.0%
n = 10	Eq. (2.16)	128.7%	24.1%	15.6%	13.8%	6.7%	4.7%	190.6%	25.7%	14.1%	13.4%	6.9%	4.4%
	Eq. (2.26)	41.1%	22.2%	15.3%	12.0%	6.5%	3.0%	43.4%	19.7%	13.3%	10.7%	5.9%	2.9%
n = 15	Eq. (2.16)	50.9%	20.8%	16.1%	14.2%	7.1%	4.3%	105.3%	18.5%	14.7%	13.9%	7.3%	4.7%
	Eq. (2.26)	30.6%	22.1%	17.3%	13.0%	6.0%	3.2%	35.7%	18.8%	13.6%	10.8%	5.3%	2.9%
n = 20	Eq. (2.16)	26.1%	21.8%	17.3%	14.4%	7.3%	4.6%	77.8%	18.2%	14.9%	14.2%	7.5%	4.7%
	Eq. (2.26)	25.7%	22.4%	18.6%	14.1%	6.1%	3.0%	30.9%	18.7%	14.1%	11.1%	5.1%	3.2%

(b) Side-grooved specimens

	a/W	B/W = 1						B/W = 2					
		0.2	0.3	0.4	0.5	0.6	0.7	0.2	0.3	0.4	0.5	0.6	0.7
$n = 5$	Eq. (2.16)	179.0%	39.8%	14.5%	12.9%	8.4%	4.5%	212.4%	50.7%	14.5%	13.8%	9.5%	4.4%
	Eq. (2.26)	40.6%	20.0%	12.5%	9.2%	5.9%	2.6%	39.9%	20.3%	13.1%	9.2%	5.7%	2.9%
$n = 8.5$	Eq. (2.16)	20.1%	16.4%	15.8%	14.0%	9.3%	4.8%	33.1%	15.4%	15.8%	14.9%	10.4%	5.4%
	Eq. (2.26)	19.7%	12.6%	9.2%	6.8%	4.2%	2.2%	21.3%	12.1%	8.5%	6.4%	4.3%	2.5%
$n = 10$	Eq. (2.16)	20.7%	16.8%	16.1%	14.2%	9.5%	4.8%	18.3%	15.6%	16.0%	15.2%	10.5%	5.5%
	Eq. (2.26)	15.8%	11.6%	8.7%	6.2%	4.0%	2.3%	16.1%	10.2%	8.2%	6.1%	4.2%	2.5%
$n = 15$	Eq. (2.16)	22.2%	17.4%	16.5%	14.6%	9.8%	5.0%	19.3%	16.2%	16.5%	15.6%	10.9%	5.7%
	Eq. (2.26)	12.3%	9.9%	8.4%	5.7%	4.1%	2.3%	13.1%	8.8%	7.0%	5.7%	4.2%	2.5%
$n = 20$	Eq. (2.16)	22.5%	17.7%	16.7%	14.8%	10.0%	5.1%	19.8%	16.5%	16.7%	15.7%	11.0%	5.8%
	Eq. (2.26)	10.9%	9.1%	7.7%	5.8%	3.9%	2.4%	10.1%	7.8%	6.5%	5.4%	3.8%	2.9%

Table 2.7: Maximum absolute values of e_J corresponding to the *CMOD*-based η_{pl} over $P/P_Y = 0.8 - 1.25$.

(a) Plane-sided specimens

		B/W = 1						B/W = 2					
	a/W	0.2	0.3	0.4	0.5	0.6	0.7	0.2	0.3	0.4	0.5	0.6	0.7
	Eq. (2.15)	5.4%	10.7%	8.8%	12.3%			10.1%	5.8%	6.1%	4.9%		
n = 5	Eq. (2.16)	2.7%	4.7%	6.0%	7.3%	8.7%	15.1%	1.9%	3.3%	3.3%	4.7%	7.8%	15.3%
	Eq. (2.27)	0.7%	1.6%	1.9%	2.7%	2.0%	1.2%	0.8%	1.1%	1.7%	2.7%	2.6%	1.8%
	Eq. (2.15)	12.6%	17.5%	11.5%	11.7%			7.8%	6.7%	7.1%	6.0%		
n = 8.5	Eq. (2.16)	7.9%	11.1%	8.5%	6.8%	6.2%	10.3%	4.9%	4.9%	5.1%	4.7%	5.9%	10.7%
	Eq. (2.27)	3.5%	6.6%	4.9%	4.6%	1.8%	0.5%	2.0%	3.1%	4.3%	4.3%	2.8%	1.2%
	Eq. (2.15)	14.6%	15.3%	11.8%	11.5%			7.9%	6.9%	7.3%	6.1%		
n = 10	Eq. (2.16)	9.8%	9.0%	8.8%	6.6%	5.6%	9.6%	6.0%	5.1%	5.2%	4.8%	5.4%	10.0%
	Eq. (2.27)	5.1%	5.2%	5.3%	4.5%	1.7%	0.8%	3.8%	4.1%	4.8%	4.3%	2.8%	1.2%
	Eq. (2.15)	16.5%	17.5%	12.9%	11.1%			8.1%	7.2%	7.5%	6.2%		
n = 15	Eq. (2.16)	11.6%	11.1%	9.9%	6.3%	4.5%	8.8%	7.8%	6.0%	5.6%	4.9%	4.6%	9.2%
	Eq. (2.27)	8.0%	7.1%	6.3%	4.9%	1.2%	1.0%	5.9%	5.8%	5.7%	4.7%	2.7%	1.3%
	Eq. (2.15)	20.4%	19.2%	14.1%	11.2%			8.3%	7.3%	7.7%	6.3%		
n = 20	Eq. (2.16)	15.3%	12.6%	11.0%	6.3%	3.9%	8.5%	10.7%	7.2%	6.3%	5.0%	4.3%	9.0%
	Eq. (2.27)	9.1%	8.0%	6.9%	5.3%	0.8%	1.0%	7.0%	6.5%	6.2%	4.9%	2.6%	1.5%

(b) Side-grooved specimens

	a/W	B/W = 1						B/W = 2					
		0.2	0.3	0.4	0.5	0.6	0.7	0.2	0.3	0.4	0.5	0.6	0.7
	Eq. (2.15)	5.4%	9.0%	7.7%	9.0%			11.1%	8.4%	8.7%	7.5%		
n = 5	Eq. (2.16)	6.5%	5.7%	5.3%	4.8%	4.6%	10.1%	7.4%	6.7%	6.7%	6.0%	3.7%	8.8%
	Eq. (2.27)	0.9%	2.1%	3.5%	3.8%	1.8%	0.6%	0.9%	1.5%	3.6%	4.0%	2.1%	0.9%
	Eq. (2.15)	7.0%	7.8%	6.0%	5.3%			11.2%	9.4%	9.5%	8.2%		
n = 8.5	Eq. (2.16)	7.8%	6.7%	6.6%	5.8%	3.6%	7.4%	9.2%	7.9%	7.8%	7.1%	4.8%	6.3%
	Eq. (2.27)	7.1%	5.7%	4.6%	3.8%	1.7%	1.4%	6.8%	5.0%	4.5%	3.8%	1.9%	1.6%
	Eq. (2.15)	7.0%	6.7%	6.1%	4.8%			11.4%	9.6%	9.6%	8.3%		
n = 10	Eq. (2.16)	7.8%	6.9%	6.8%	6.0%	3.8%	7.0%	9.4%	8.0%	7.9%	7.2%	4.9%	6.1%
	Eq. (2.27)	7.4%	6.1%	4.9%	3.6%	1.8%	1.6%	7.8%	5.7%	4.9%	3.5%	2.0%	1.8%
	Eq. (2.15)	7.1%	5.7%	6.3%	5.0%			11.7%	9.9%	9.8%	8.4%		
n = 15	Eq. (2.16)	8.0%	7.0%	6.9%	6.2%	4.0%	6.6%	9.5%	8.3%	8.1%	7.3%	5.1%	5.6%
	Eq. (2.27)	7.1%	5.6%	4.9%	3.6%	2.0%	1.7%	8.5%	5.9%	4.8%	3.4%	2.4%	2.0%
	Eq. (2.15)	7.5%	5.9%	6.4%	5.2%			11.9%	10.0%	10.0%	8.5%		
n = 20	Eq. (2.16)	8.4%	7.2%	7.0%	6.3%	4.2%	6.4%	9.6%	8.3%	8.2%	7.4%	5.2%	5.7%
	Eq. (2.27)	7.0%	5.6%	4.9%	3.8%	1.9%	1.8%	8.2%	5.8%	4.8%	3.4%	2.4%	2.2%
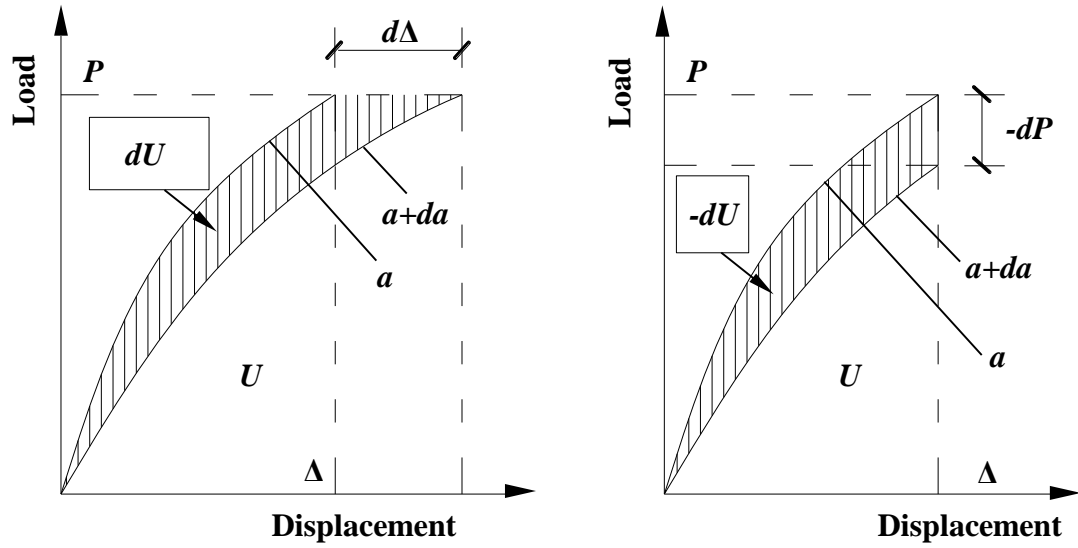
Figure 2.1. Determination of the potential energy
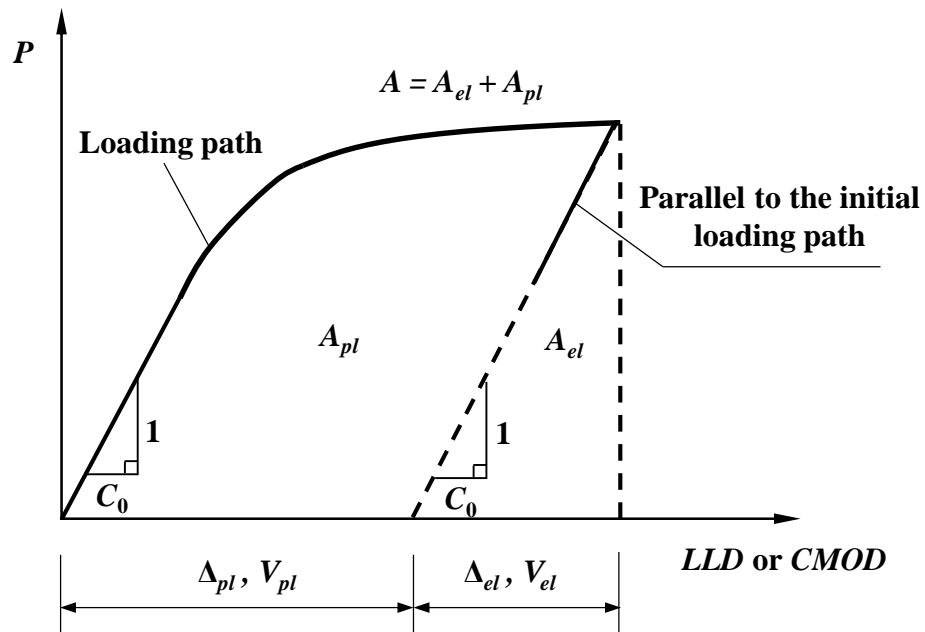
Figure 2.2. Determination of the plastic area under the load-displacement curve

(a) Configuration of a typical side-grooved FE model with *a/W* = **0.5 and** *B/W* = **1**

(b) Configuration of the side groove **(c) Mesh around the blunt crack tip** **(d) Mesh around the root of the side groove**
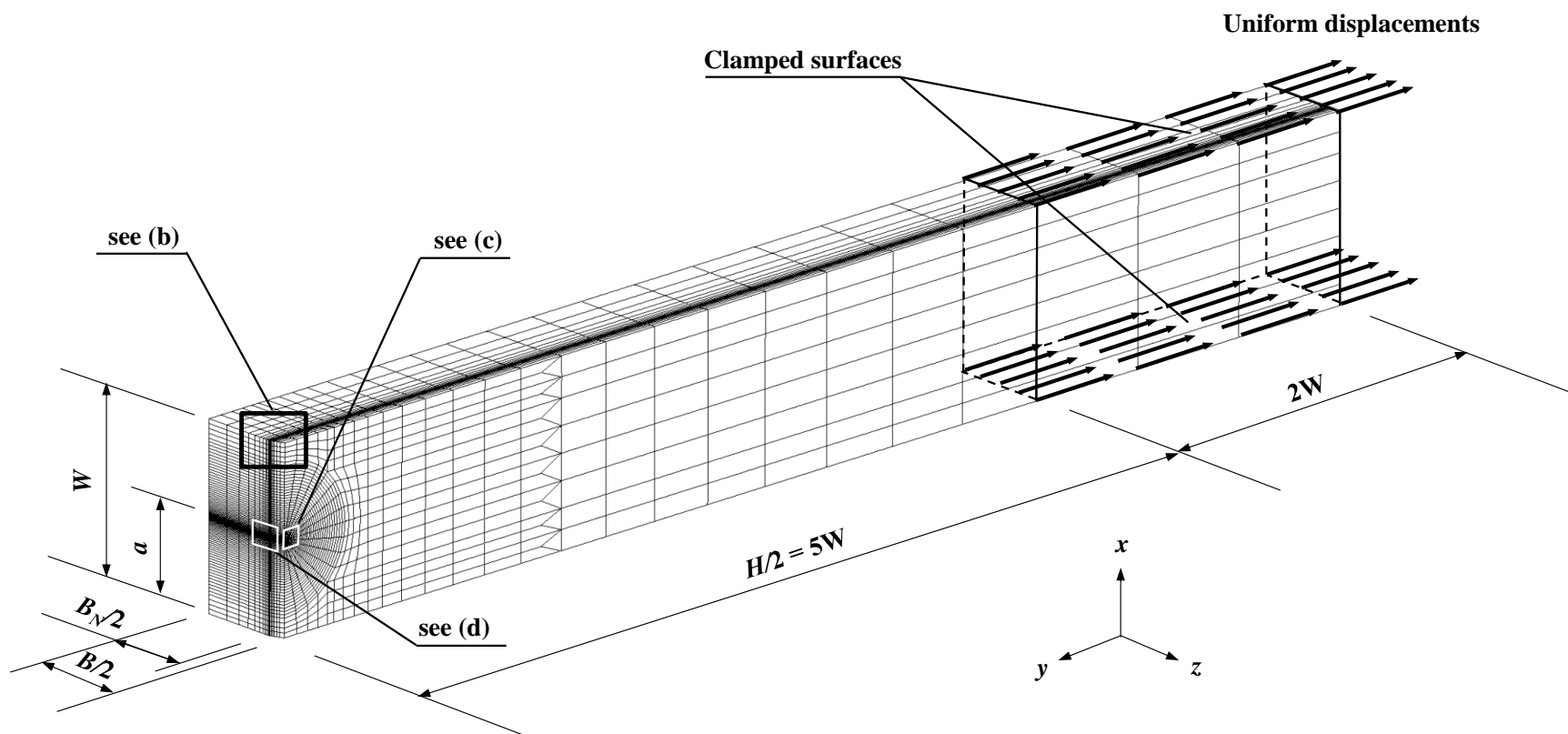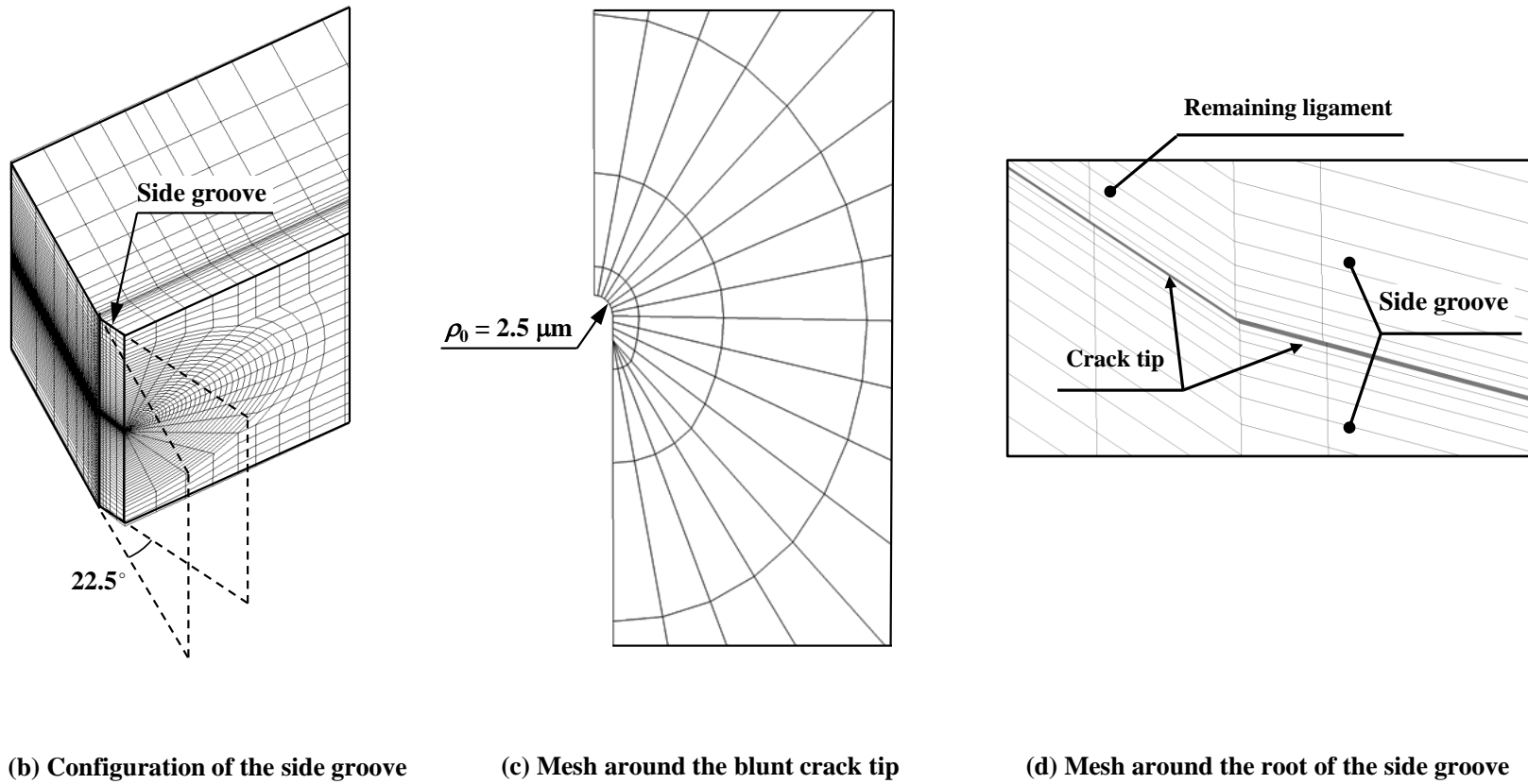
Figure 2.3. Configuration of a typical finite element model with a blunt crack tip
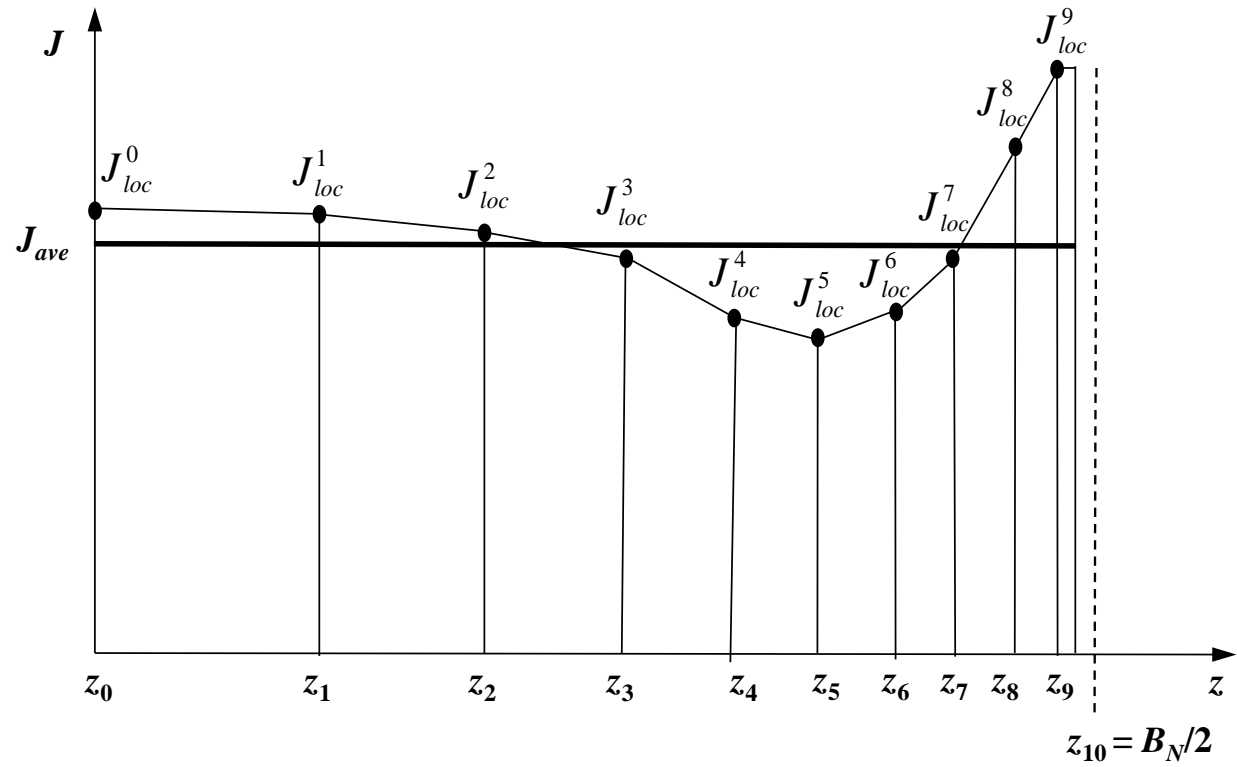
Figure 2.4. Schematic of the calculation of the weighted average J along the crack front
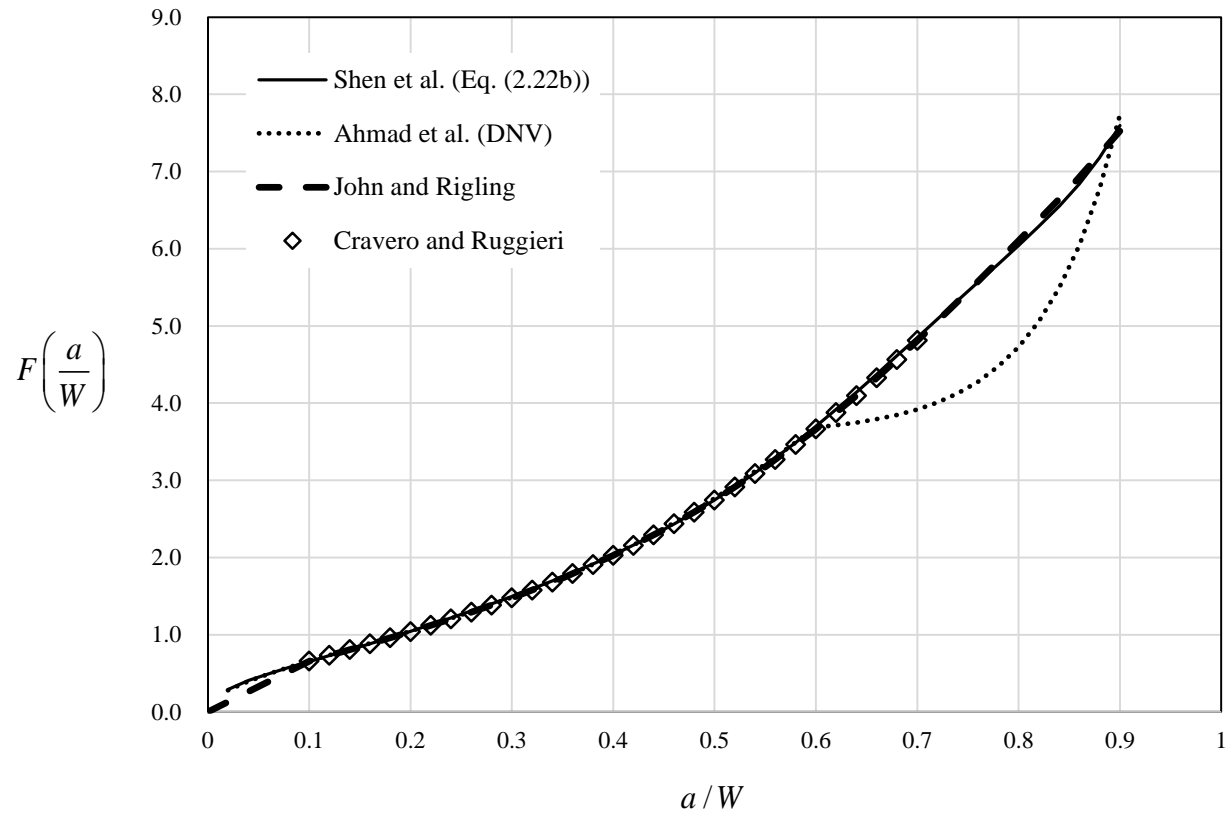
Figure 2.5. Comparisions of different $F(a/W)$ solutions for SE(T) specimen with $H/W = 10$
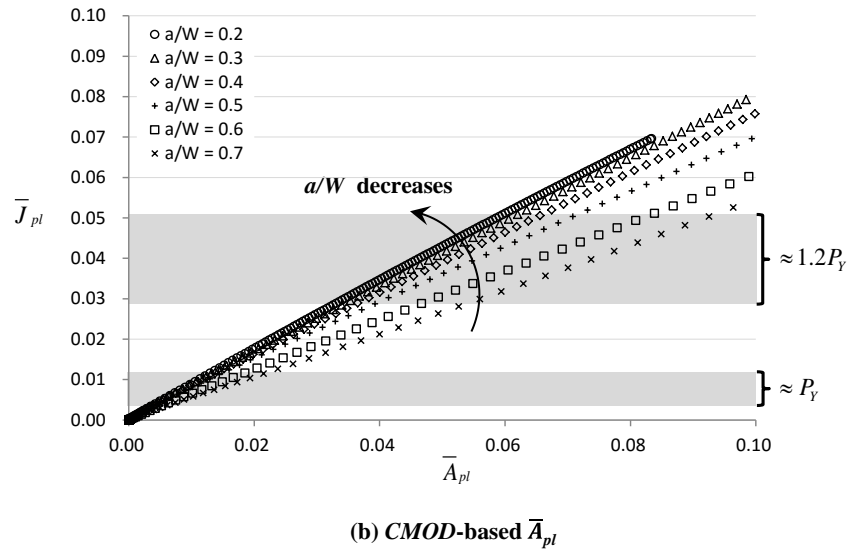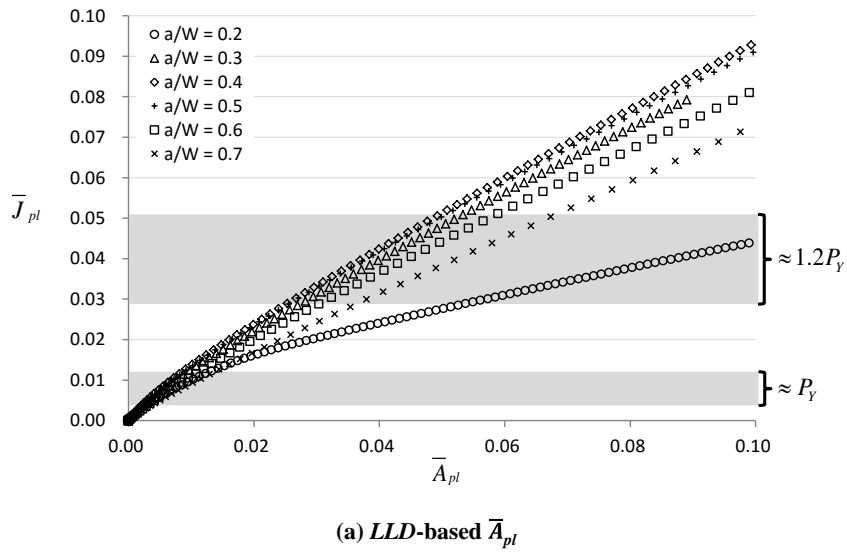
Figure 2.6. Comparisons of $\bar{J}_{pl} - \bar{A}_{pl}$ relationship for specimens with various *a/W* ratios, $n = 10$ and *B/W = 1*
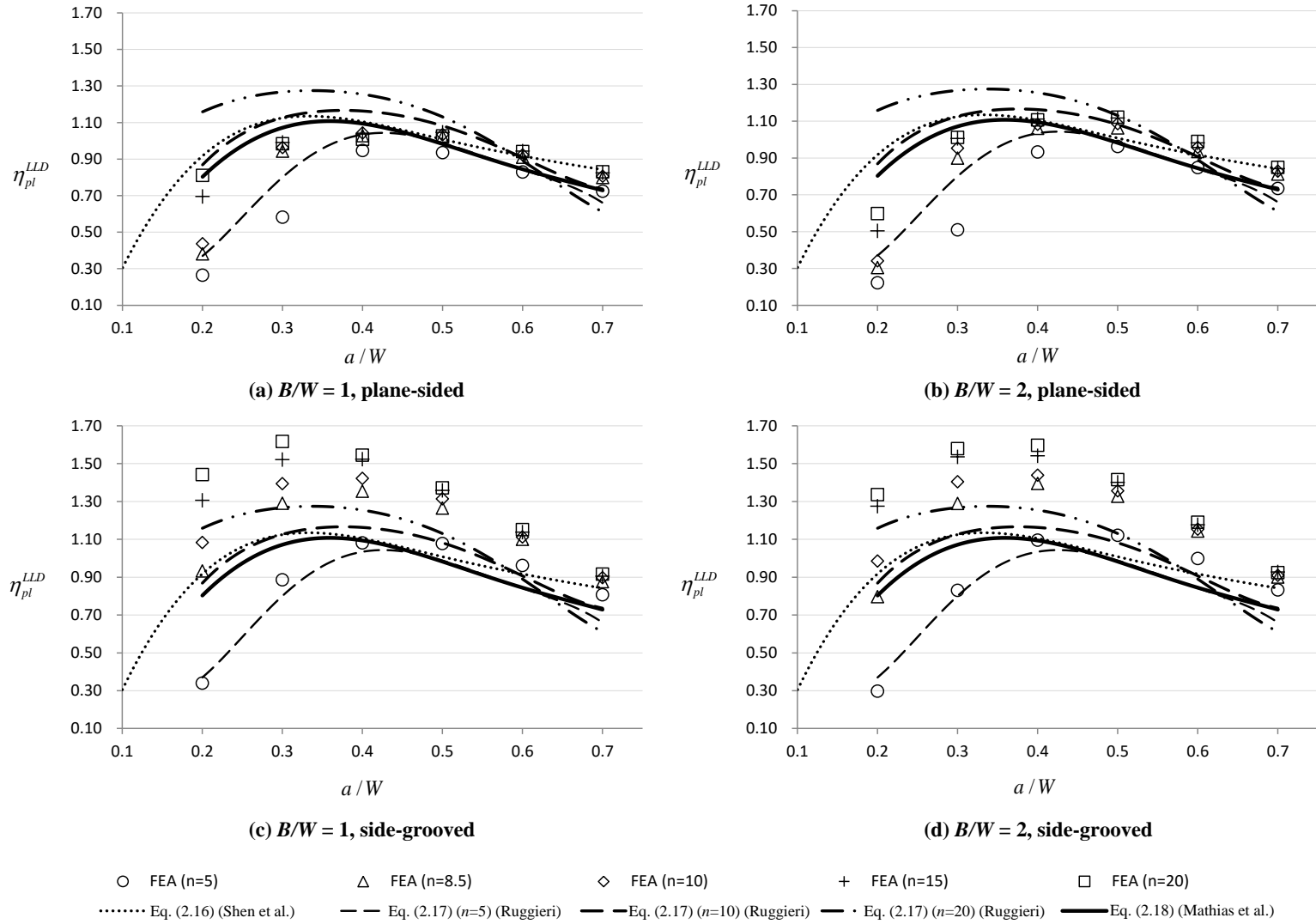
Figure 2.7. Variation of *LLD*-based η_{pl} with *a/W*
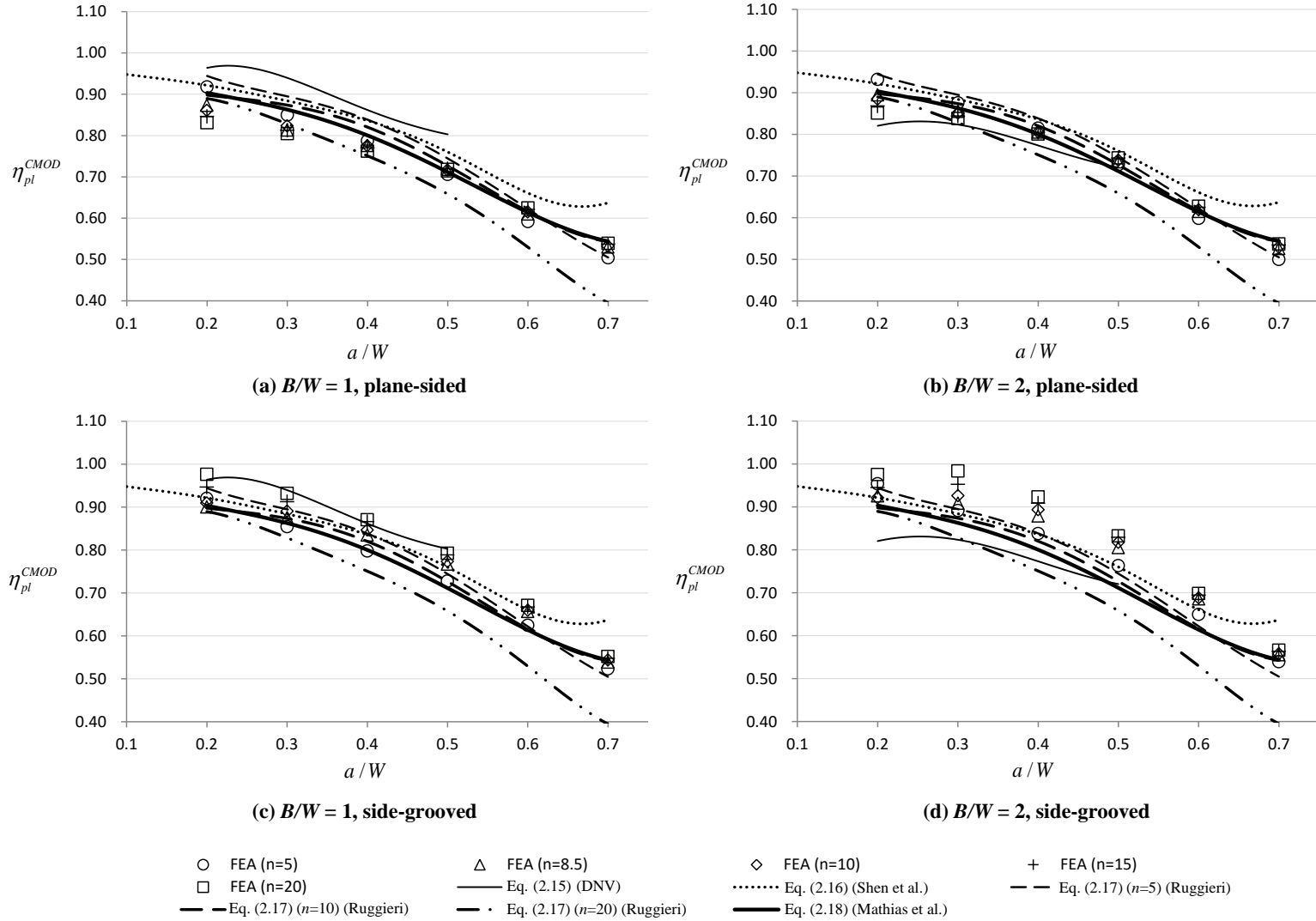
Figure 2.8. Variation of *CMOD*-based η_{pl} with *a/W*
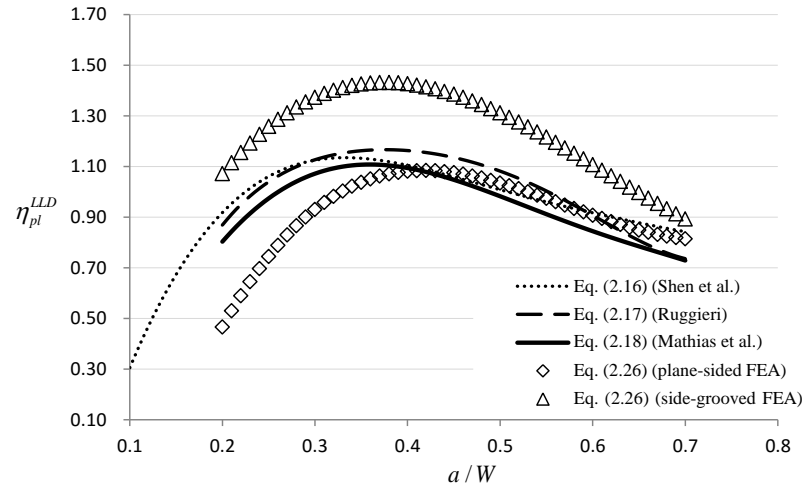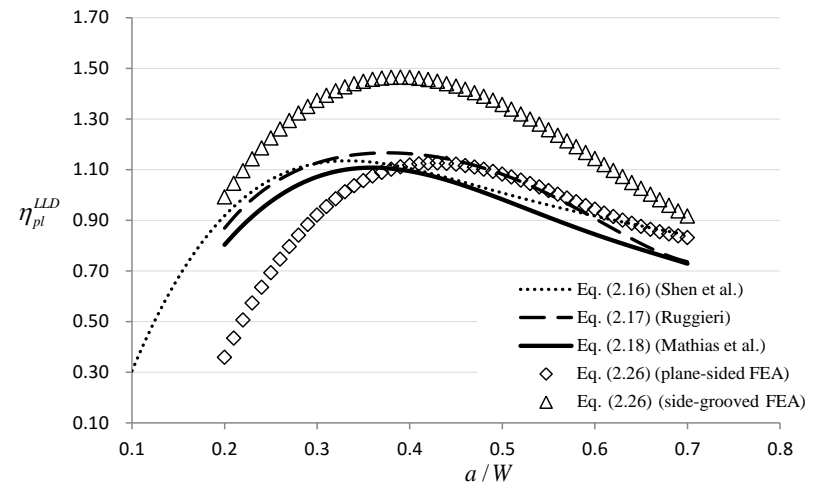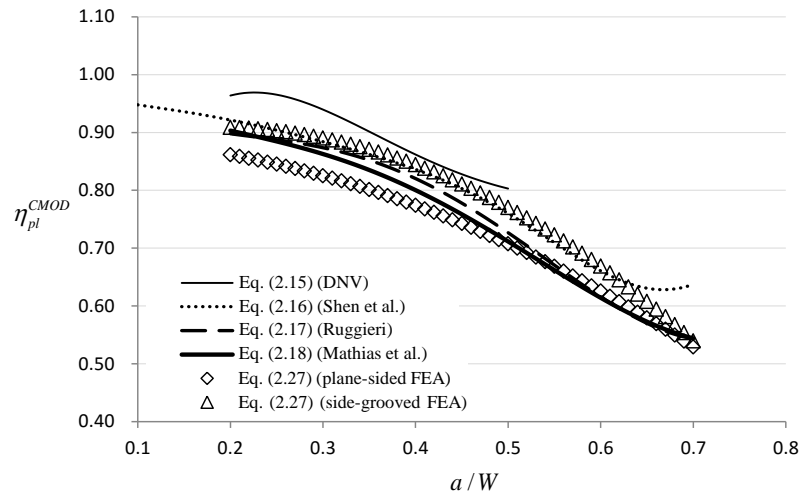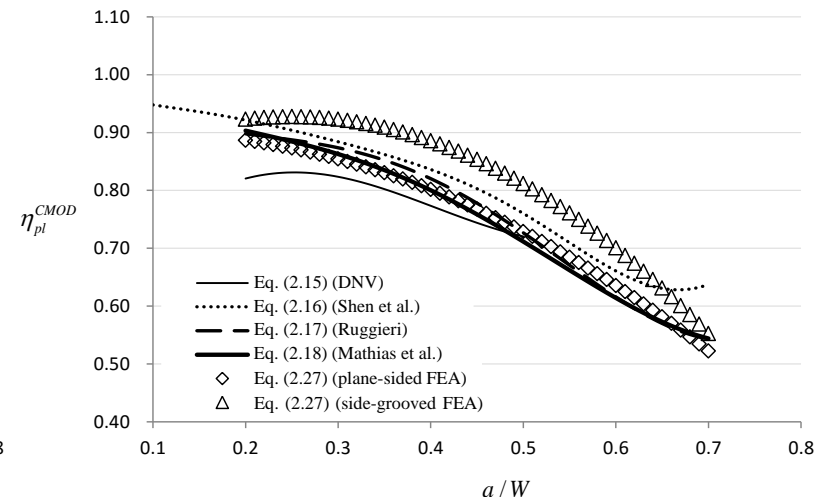
Figure 2.9. Variation of proposed η_{pl} with a/W (Eqs. (2.26) and (2.27)) for $n = 10$ materials

(a) $B/W = 1$, **PS**

(b) $B/W = 2$, **PS**

(c) $B/W = 1$, **SG**

(d) $B/W = 2$, **SG**
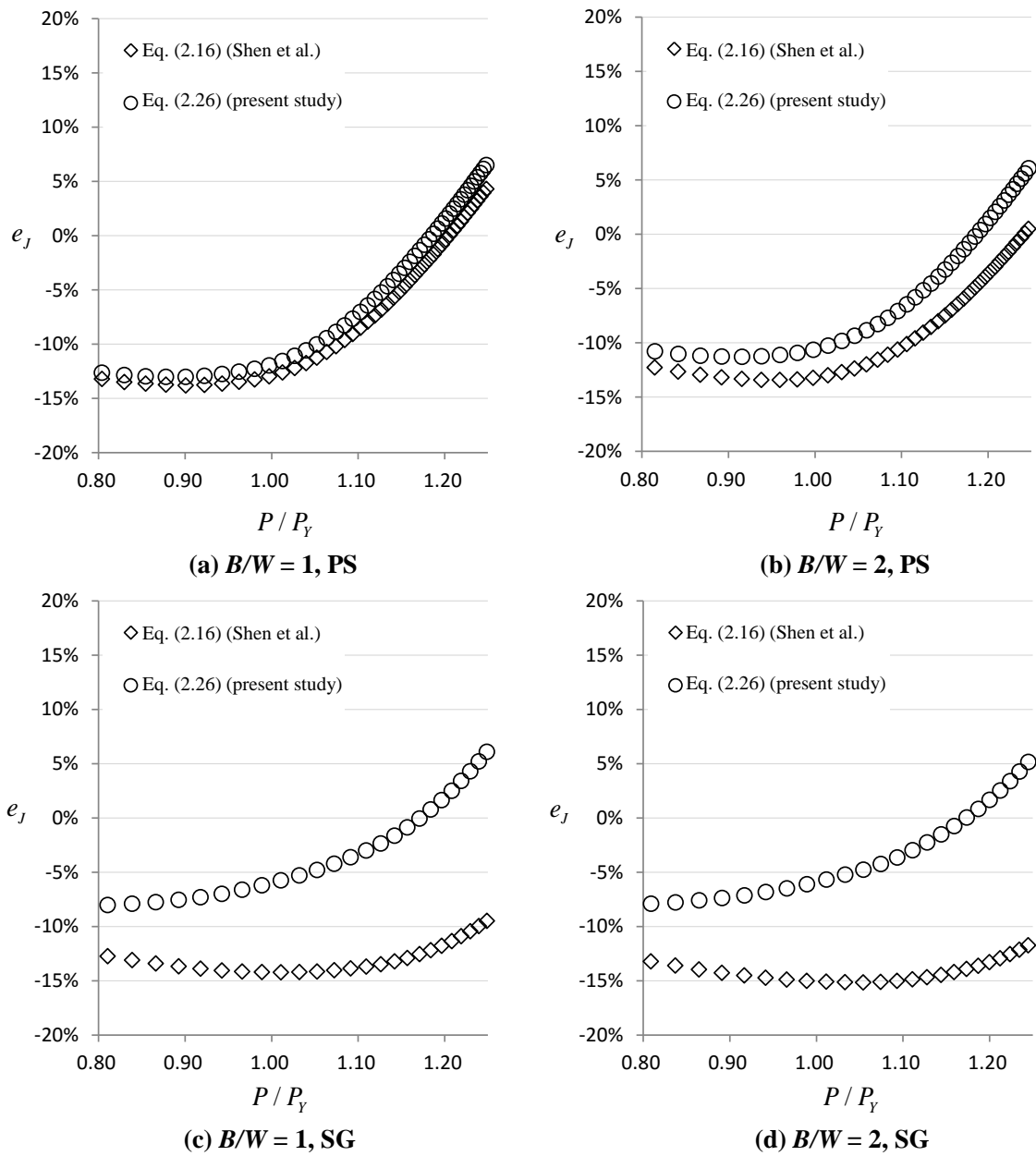
Figure 2.10. Errors in J values evaluated from the *LLD*-based η_{pl} for the specimens with $a/W = 0.5$ and $n = 10$
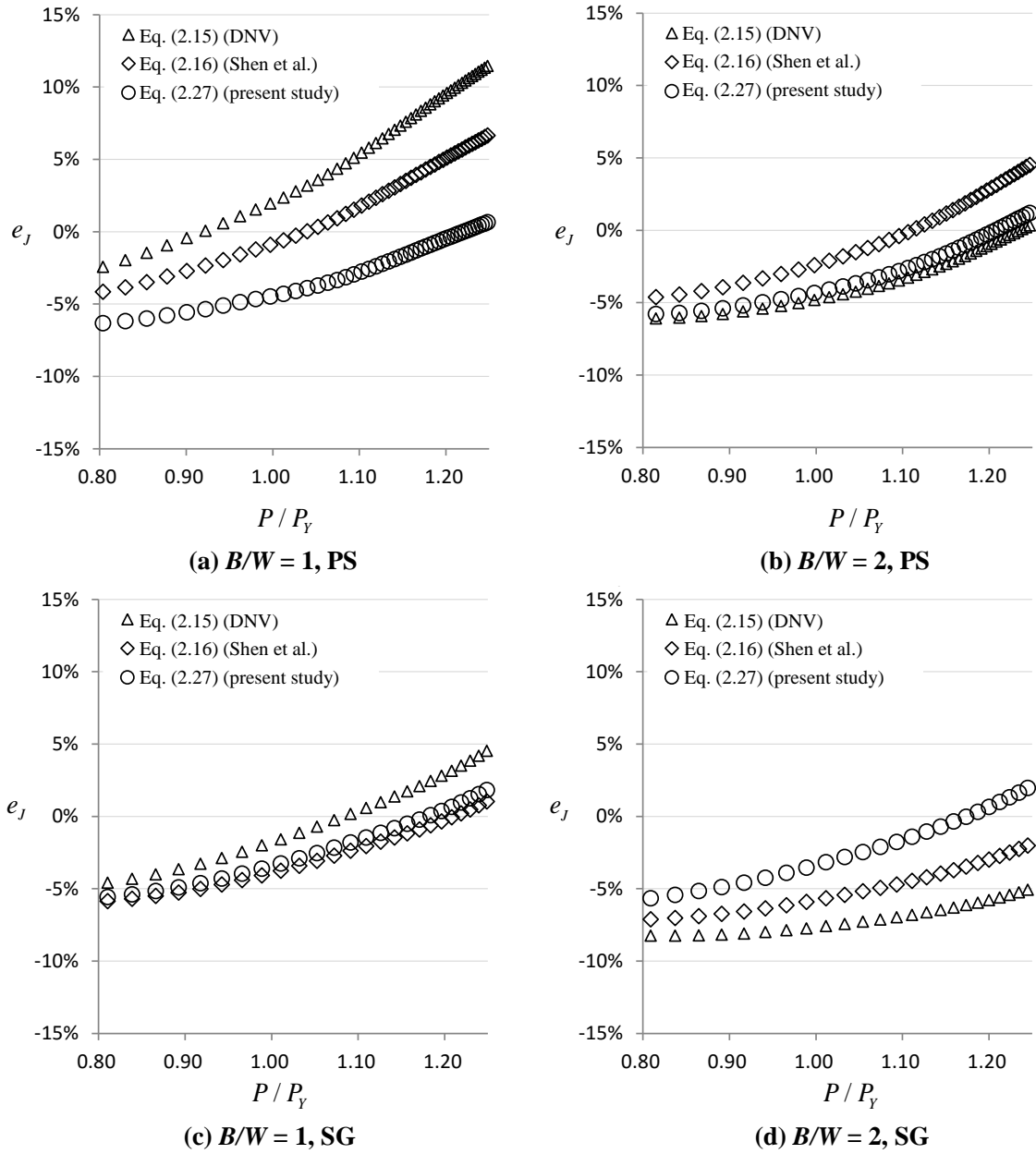
Figure 2.11. Error in *J* values evaluated from the *CMOD*-based η_{pl} for the specimens with $a/W = 0.5$ and $n = 10$

Chapter 3 *J-CTOD* Relationship for Clamped SE(T) Specimens Based on Three-dimensional Finite Element Analyses

3.1 Background and Objective

3.1.1 Estimation of *CTOD* Using Plastic Constraint *m* Factor

The crack tip opening displacement (*CTOD*) is a widely used parameter for characterizing the material fracture toughness meanwhile accommodates crack-tip plasticity. In the integrity assessment of flawed structures, *CTOD* is a design parameter to determine the allowable crack sizes in welded structures (Burdekin and Dawes, 1971; BSI, 2005). In the strain-based design of energy pipelines, the crack driving force as well as the tensile strain capacity is often defined in terms of *CTOD* (Tang et al., 2010; Wang et al., 2011; Fairchild et al., 2012).

There are currently two main approaches to determine *CTOD* experimentally from small-scale specimens. The first approach is based on a plastic hinge model assuming two halves of the specimen rotate rigidly about a rotational center (i.e. plastic hinge) during tests. *CTOD* can be determined directly from the measured crack mouth opening displacement (*CMOD*) through a geometric relationship. This approach is specified in BS 7448 (BSI, 1997) and ISO 12135 (ISO, 2002) for single-edge bend (SE(B)) and compact tension (C(T)) specimens and is suggested in BS 8571 (BSI, 2014) for single-edge tension (SE(T)) specimens.

The second approach relies on the fact that *CTOD* can be uniquely related to the *J*-integral (*J*) (Shih, 1981; Anderson, 2005) and the following equation is widely accepted (Irwin, 1961; Shih, 1981):

$$\delta = \frac{J}{m_{(1)}\sigma_{YS}}$$

(3.1)

where δ and σ_{YS} denote the *CTOD* and material yield strength, respectively; m is the plastic constraint factor, and its subscript (k) (k = 1, 2 or 3) denotes the specific equation (i.e. Eq. (3.k)) for which $m_{(k)}$ is applicable. The value of J can be evaluated from the experimentally measured load-displacement curve through a plastic geometry factor, η_{pl} (see Section 2.1.1). A great deal of effort (e.g. Irwin, 1961; Shih, 1981; Kirk and Dodds, 1993; Kirk and Wang 1995) has been made to quantify the m factor. Early studies by Irwin (1961) showed that m equals 1 and 2 for the plane stress and plane strain conditions, respectively, based on the linear elastic fracture mechanics analysis of the energy release rate. For hardening materials, Shih (1981) reported that within the region dominated by the Hutchinson–Rice–Rosengren (HRR) singularity (Hutchinson, 1968; Rice and Rosengren, 1968), the m factor in Eq. (3.1) (denoted as $1/d_n$ in his study) only depends on material deformation properties (e.g. the Ramberg-Osgood strain hardening exponent, n) under the small-scale yielding (SSY) condition.

Kirk and Dodds (1993) and Kirk and Wang (1995) proposed the following *CTOD-J* equation for the SE(B) specimen, which is the same as Eq. (3.1) except that σ_{YS} is replaced by the flow stress, σ_Y:

$$\delta = \frac{J}{m_{(2)}\sigma_Y} \tag{3.2}$$

where $\sigma_Y = (\sigma_{YS} + \sigma_{UTS})/2$, and σ_{UTS} is the ultimate tensile strength. Based on the results of two-dimensional plane-strain (simply denoted as 2D hereafter) finite element analyses (FEA), these researchers found that the m factor is a function of the relative crack length (a/W) in addition to n. An empirical equation of the m factor was developed by them and adopted in ASTM E1290-02 (2002), which was later superseded by ASTM E1820. The current edition of E1820, ASTM E1820-13 (2013) formulates the m factor as a function of a/W and σ_{YS}/σ_{UTS} for deeply-cracked (i.e. $a/W \geqslant 0.45$) SE(B) and C(T) specimens.

Compared with Eqs. (3.1) and (3.2), an alternative *CTOD-J* relationship is to evaluate the elastic and plastic components of *CTOD* (i.e. δ_{el} and δ_{pl}, respectively) separately as follows:

$$\delta = \delta_{el} + \delta_{pl} = \frac{J_{el}}{m_{SSY}\sigma_{YS}} + \frac{J_{pl}}{m_{(3)}\sigma_{YS}} \tag{3.3}$$

where m_{SSY} denotes the m factor under the SSY condition and is usually assigned a value of 2 (e.g. in the BS7448 standard (BSI, 1997)), and J_{el} and J_{pl} are the elastic and plastic components of J, respectively. The evaluation of J_{el} and J_{pl} is well documented in the literature (e.g. ASTM, 2013; BSI, 1997) and has been discussed in Section 2.1.1. It is observed that Eq. (3.3) is approximately equivalent to Eq. (3.1) with $m_{(1)} = m_{SSY} = 2$ for low loading levels ($\delta_{pl}/\delta_{el} \approx 0$) and $m_{(1)} = m_{(3)}$ for high loadings levels ($\delta_{el}/\delta_{pl} \approx 0$).

Over the last decade, the use of the non-standard single-edge tension (SE(T)) specimen to determine the resistance (R) curve has gained much attention in the energy pipeline industry largely as a result of the development of the strain-based design (Tang et al., 2010; Wang et al., 2011; Wang et al., 2013). The crack-tip stress and strain fields of the SE(T) specimen are more relevant to the full-scale pipe containing surface cracks under internal pressure and/or longitudinal tension than the conventional standard SE(B) and C(T) specimens (Wang et al., 2013; Chiesa et al., 2001; Shen et al., 2008). Shen and Tyson (2009) pointed out that the m factor under the large-scale yielding (LSY) condition may be dependent on the specimen configuration and loading condition (e.g. bending or tension). This implies that the m-factor equations proposed for the SE(B) and C(T) specimens may not be adequate for the SE(T) specimen. The evaluation of the m factor for the clamped SE(T) specimen has been reported in the literature (Shen and Tyson, 2009; Moreira and Donato, 2010; DNV, 2010, 2012). For example, Moreira and Donato (2010) obtained values of $m_{(2)}$ for the clamped SE(T) specimens based on 2D FEA. Ruggieri (2012) evaluated the plastic geometry eta factors that are used to determine the plastic components of J and $CTOD$, from which $m_{(3)}$ can be evaluated. Shen and Tyson (2009) indicated that m is also dependent on the loading level (e.g. P/P_Y, with P_Y being the limit load) under the LSY condition. They carried out a series of 2D FEA of clamped SE(T) specimens with the daylight distance over width ratio (H/W) equal to 10 and proposed an empirical expression of $m_{(2)}$ as a function of P/P_Y in addition to a/W and n. More recently, Det Norske Veritas (DNV) (2012) proposed an equation for $m_{(1)}$ for the clamped SE(T) specimens with

H/W =10, whereby $m_{(1)}$ is a function of *CTOD*. The evaluation of the *m*-factors for the SE(T) specimens is the focus of the study reported in this chapter.

3.1.2 Literature Review of the *m* Factors for SE(T) Specimens

Previous versions of DNV-OS-F101 (2007, 2010) adopted the following *m*-factor equation proposed by Kirk and Wang (1995):

$$\begin{cases} m_{(2)} = 1.221 + 0.793\dfrac{a}{W} + 2.751N - 1.418N\dfrac{a}{W} \\ N = \dfrac{1}{n} = -3.965\left(\dfrac{\sigma_{YS}}{\sigma_{UTS}}\right)^3 + 8.326\left(\dfrac{\sigma_{YS}}{\sigma_{UTS}}\right)^2 - 6.098\left(\dfrac{\sigma_{YS}}{\sigma_{UTS}}\right) + 1.724 \end{cases} \qquad (3.4)$$

Note that Eq. (3.4) was originally proposed for the SE(B) specimen based on the results of 2D small-strain FEA that covered *a/W* ranging from 0.05 to 0.7, and four values of *n* (*n* = 4, 5, 10 and 50). Pisarski (2010) pointed out that Eq. (3.4) underestimates *CTOD* for the SE(T) specimen by approximately 25% based on the results of 2D FEA.

The current version of DNV-OS-F101 (2012) suggests that *CTOD* be estimated from *J* for both the clamped and pin-ended SE(T) specimens using Eq. (3.1) with $m_{(1)}$ given by

$$m_{(1)} = \begin{cases} 1.8\left(1 - v^2\right) & , \delta \leq 0.1\,\text{mm} \\ \left(1.9 - \delta\right)\left(1 - v^2\right) & , 0.1\,\text{mm} < \delta < 0.4\,\text{mm} \\ 1.5\left(1 - v^2\right) & , \delta \geq 0.4\,\text{mm} \end{cases} \qquad (3.5)$$

where *v* is Poisson's ratio. Equation (3.5) is applicable to plane-sided specimens with *a/W* ranging from 0.2 to 0.5 and *B/W* ranging from 2 to 5 according to DNV-OF-F101 (2012); however, how the equation is developed is unclear. The use of Eq. (3.5) to evaluate *CTOD* implies that an iterative procedure is required.

By carrying out 2D large-strain FEA of clamped SE(T) specimens with *a/W* equal to 0.2 and 0.5, and *n* equal to 5, 10, 15 and 20, Shen and Tyson (S&T) (2009) proposed the

following equation for $m_{(2)}$ to calculate *CTOD* from the corresponding *J* for the clamped SE(T) specimen:

$$m_{(2)} = \begin{cases} m_c & , P \leq P_Y \\ m_c - m_p \left(\dfrac{P}{P_Y} - 1 \right), & P > P_Y \end{cases} \tag{3.6a}$$

where $P_Y = B_N (W - a)\sigma_Y$, and P_Y and B_N are the limit load and net specimen thickness, respectively. The parameters m_c and m_p in the above equation are defined as

$$\begin{cases} m_c = A_1 \dfrac{a}{W} + A_2 \\ m_p = B_1 \dfrac{a}{W} + B_2 \\ A_1 = -0.1293 + 0.1152n - 0.00986n^2 + 0.000263n^3 \\ A_2 = 3.0867 - 0.297n + 0.0194n^2 - 0.000427n^3 \\ B_1 = 1.0169 - 0.0634n + 0.00567n^2 - 0.000200n^3 \\ B_2 = 0.6969 - 0.1216n + 0.01487n^2 - 0.000393n^3 \end{cases} \tag{3.6b}$$

Based on the results of three-dimensional (3D) FEA of clamped plane-sided and side-grooved SE(T) specimens with $a/W = 0.4, 0.5$ and 0.6, $B/W = 1$ and 2, and $n = 5, 10$ and 20, Wang et al. (2013) recently reported that the errors in the *CTOD* values predicted from the *m* factors given by Eq. (3.6) vary in the range of $5 - 42\%$, depending on a/W, B/W, n, the loading level and whether the specimen is plane-sided or side-grooved.

Moreira and Donato (M&D) (2010) investigated the *m* factors for clamped SE(T) specimens containing the base metal and weldment by carrying out 2D small-strain FEA. Their analyses covered a/W ranging from 0.1 to 0.7, and one value of *n* ($n = 10$). For evenmatched base metal and weldment, they proposed the following cubic polynomial expression for $m_{(2)}$ as a function of a/W:

$$m_{(2)} = -0.9111 \left(\frac{a}{W} \right)^3 + 0.6589 \left(\frac{a}{W} \right)^2 - 0.2093 \left(\frac{a}{W} \right) + 1.4724 \tag{3.7}$$

Moore and Pisarski (2012, 2013) reported that the *m* factors given by Eqs. (3.4), (3.5) and (3.7) generally lead to underestimated *CTOD* values compared with those determined from the double-clip gauge method for clamped SE(T) specimens with *a/W* = 0.3 and 0.5, whereas the *m* factors given by Eq. (3.6) lead to more accurate predictions of *CTOD* values for the same specimens.

Ruggieri (2012) evaluated the plastic geometry factors, η_δ and η_J, which respectively relate the *CMOD*-based plastic work to *CTOD* and *J*, based on 2D small-strain FEA of clamped SE(T) specimens with *a/W* ratios ranging from 0.2 to 0.7. The corresponding $m_{(3)}$ factor can be derived as follows:

$$m_{(3)} = \frac{J_{pl}}{\delta_{pl}\sigma_{YS}} = \frac{\eta_J}{\eta_\delta} = \frac{\sum\limits_{i=0}^{5} M_i \left(\dfrac{a}{W}\right)^i}{\sum\limits_{i=0}^{5} Q_i \left(\dfrac{a}{W}\right)^i} \tag{3.8}$$

where M_i and Q_i (i = 0, 1, ..., 5) are the fitting coefficients and tabulated in Table 3.1 for three different strain hardening exponents, i.e., *n* = 5, 10 and 20. The author further validated the developed equations for η_δ and η_J by carrying out 3D small-strain FEA of clamped SE(T) specimens with two *B/W* ratios (i.e. 0.5 and 2). For comparison, the basis of Eqs. (3.4) through (3.8) in terms of the type of FEA employed to develop the equations and ranges of the key parameters involved in FEA is summarized in Table 3.2.

3.1.3 Objective and Approach

The objective of the present study was to develop an empirical equation for the plastic constraint *m* factor for clamped SE(T) specimens with *H/W* equal to 10 based on 3D FEA. We carried out extensive 3D FEA of both plane-sided and side-grooved clamped SE(T) specimens with six crack lengths (*a/W* = 0.2, 0.3, 0.4, 0.5, 0.6 and 0.7), two thickness-to-width ratios (*B/W* = 1 and 2), and five strain hardening exponents (*n* = 5, 8.5, 10, 15 and 20). For each of the specimens, the value of *m* at a given loading level was calculated from Eq. (3.2) based on the corresponding *CTOD* and *J* values obtained from FEA. The least squares-based regression analysis was then performed to develop an empirical *m*-factor

equation as a function of a/W, B/W, σ_{YS}/σ_{UTS} and loading level characterized by the *CMOD* over crack length ratio (V/a). The rest of the chapter is structured as follows. Section 3.2 describes the configurations of the FE models, material properties and computational procedures. Section 3.3 shows the calculation results and development of the new *m*-factor equation as well as the validation of the proposed equation. Concluding remarks are presented in Section 3.4.

3.2 Numerical Analyses

The FEA code ADINA® (ADINA, 2012) was employed to analyze the three-dimensional models of both plane-sided (PS) and side-grooved (SG) SE(T) specimens with clamped ends. The analysis matrix includes specimens with six different a/W ratios (a/W = 0.2, 0.3, 0.4, 0.5, 0.6 and 0.7) and two B/W ratios (B/W = 1 and 2). A stationary crack was assumed in the analysis. For SG specimens, a side groove depth of $7.5\%B$ at each side of the specimen was adopted based on the recommendation in (Shen et al., 2010). All the specimens included in the analysis matrix have the same width (W = 20 mm) and daylight length (H/W = 10). The geometry, mesh configurations and materials properties of the FEA models adopted in the present study are the same as those presented in Chapter 2 (see Section 2.2) and are therefore not detailed in this chapter.

In the FEA, the load was applied based on the displacement control condition. Uniform displacements were applied on two lateral surfaces that are considered as the clamped surfaces with a length of $2W$ (see Fig. 2.3(a)). A final load line displacement of 1.3 – 1.8 mm for plane-sided specimens or 0.8 – 1.2 mm for side-grooved specimens was reached. Such displacements are sufficient to achieve the maximum loading level in FEA at around $1.25P_Y$, which is consistent with the typical maximum load level achieved in the fracture toughness testing of the SE(T) specimen (Dodds and Read, 1990; Pussegoda et al., 2013; Shen et al., 2009; Mathias et al., 2013).

The value of J in each layer along the thickness direction, i.e. the local J value, was calculated using the virtual crack extension method (ADINA, 2012). The average J (J_{ave}) value over the entire crack front was then calculated from the local J values using the weighted average method (ADINA, 2012). More details about the estimation procedure of

the local J values and J_{ave} in the FEA can be referred to Section 2.2. In this study, J_{ave} as opposed to the local J values was used to develop the J-$CTOD$ relationship because J values are commonly evaluated experimentally using the plastic geometry factor-based approach (Sumpter and Turner, 1976) and the plastic geometry factors specified in testing standards (e.g. ASTM, 2013; BSI, 1997) are typically corresponding to J_{ave}.

The numerically-simulated $CTOD$ (δ_{90}) was measured based on the 90° intercept method (Shih, 1981; Anderson, 2005) at the mid-thickness of the specimen as schematically shown in Fig. 3.1. A ±45° straight line originating at the deformed crack tip was intercepted by the deformed crack flanks. The position of the intersection point on each flank was calculated based on the locations of the two closest nodes by linear interpolation (Ruggieri, 2012). The distance between the two intersection points was considered as δ_{90} and only $\delta_{90}/2$ was computed in the FEA due to symmetry. Note that the initial value of δ_{90} equals twice the initial blunt tip radius (i.e., $2\rho_0 = 5$ μm). The values of δ_{90} and J_{ave} were evaluated from FEA for all the specimens at different loading levels. For a given specimen at a given loading level, the m factor was then calculated from Eq. (3.2) based on the corresponding values of δ_{90}, J_{ave} and σ_Y, where $\delta = \delta_{90}$ and $J = J_{ave}$ were assumed.

3.3 Determination of *J-CTOD* relationship for SE(T) Specimens

3.3.1 Results and Discussions

Figures (3.2) and (3.3) show variations of m values with the loading levels characterized by V/a for PS specimens with $B/W = 1$ and different a/W ratios and n values. Note that using V/a to characterize the loading levels is preferred over using P/P_Y because the former is less sensitive to the initial crack tip configuration of the FE model (i.e. ρ_0). Note also that in the present study, the loading levels of $V/a < 0.02$ were not considered as the corresponding J and $CTOD$ values are small compared with the typical fracture toughness values of pipeline steels. From these figures, it is observed that m depends on the loading level (V/a), a/W and n, which is consistent with the findings in the literature (Shen and Tyson, 2009; Moore and Pisarski, 2012). The m values generally increase with V/a within the range of $V/a = 0.02 – 0.05$, and then decrease as V/a further increases. At loading levels

of $V/a \geq 0.05$, the m-V/a relationship is approximately linear. Figures 3.2(a) through 3.2(e) suggest that for given n and the loading level, m increases with a/W within the range $V/a = 0.02 - 0.05$, whereas m decreases as a/W increases for $V/a \geq 0.05$. For high-hardening materials (i.e., $n = 5$), m is weakly dependent on the a/W ratio whereas this dependence is more significant for moderate- and low-hardening materials (i.e. larger n). This can be attributed to that the HRR solutions characterize the crack-tip stress and strain fields reasonably well for specimens with high-hardening materials; as a result, the relationship between J and $CTOD$ is weakly dependent on the specimen configuration. The impact of the strain hardening exponent on m is shown in Figs. 3.3(a) through 3.3(f). These figures indicate that for a given a/W ratio and the loading level, m decreases as n increases, which is consistent with the observation reported by Shih (1981).

Figures 3.4(a) through 3.4(f) depict the m values as a function of V/a for PS and SG specimens with $B/W = 1$ and 2, $n = 10$ and different a/W ratios. It is observed that the B/W ratio has a noticeable impact on m: m generally increases by 5% - 12% as B/W increases from 1 to 2, all the other conditions being the same. The influence of B/W on m is more significant as a/W decreases and/or V/a increases. Figures 3.4(a) through 3.4(f) also show the impact of the side-grooving on m. The values of m for the SG models are generally 10% higher than those for the PS models with the same a/W, B/W and n values. The above observations can be attributed to the fact that increasing the B/W ratio or introducing side-grooves in the specimens makes the plane-strain condition more prevalent along the crack front and that m corresponding to the plane-strain condition is higher than that corresponding to the plane-stress condition as reported in previous studies (Irwin, 1961; Shih, 1981). Note that the m-V/a relationships for the SG models are approximately parallel to those of the PS models.

3.3.2 Proposed New Equation for m

The following empirical equation was proposed to express m as a function of V/a, a/W and σ_{YS}/σ_{UTS} based on the values of m shown in Figs. (3.2) and (3.3):

$$\begin{cases} m_{(2)} = \lambda_0 \left[D_0 + D_1 (V/a) \right] \\ D_0 = \left[p_{00} + p_{01} \left(\dfrac{a}{W} \right) + p_{02} \left(\dfrac{a}{W} \right)^2 \right] + \left[p_{10} + p_{11} \left(\dfrac{a}{W} \right) + p_{12} \left(\dfrac{a}{W} \right)^2 \right] \left(\dfrac{\sigma_{YS}}{\sigma_{UTS}} \right) \\ D_1 = \left[q_{00} + q_{01} \left(\dfrac{a}{W} \right) + q_{02} \left(\dfrac{a}{W} \right)^2 \right] + \left[q_{10} + q_{11} \left(\dfrac{a}{W} \right) + q_{12} \left(\dfrac{a}{W} \right)^2 \right] \left(\dfrac{\sigma_{YS}}{\sigma_{UTS}} \right) \end{cases} \quad (3.9)$$

where λ_0 equals unity and 1.116 for PS and SG specimens, respectively, and the fitting coefficients p_{ij} and q_{ij} (i, j = 0, 1, 2) depend on B/W and are listed in Table 3.3. For comparison with Eqs. (3.4) - (3.8), key information about the FEA used to develop Eq. (3.9) is summarized in Table 2. The accuracy of Eq. (3.9) was examined by evaluating the error in *CTOD*, e_δ (%), computed from Eqs. (3.2) and (3.9) as follows:

$$e_\delta = \frac{\delta_{est} - \delta_{90}}{\delta_{90}} \times 100\% \quad (3.10)$$

where δ_{est} is *CTOD* computed through the use of Eqs. (3.2) and (3.9). Figure 3.5 depicts e_δ as a function of V/a ($0.02 \leq V/a \leq 0.2$) for the PS and SG specimens with $a/W = 0.2$ and $B/W = 1$ and 2. Figure 3.6 is similar to Fig. 3.5, except that the specimens in Fig. 3.6 have $a/W = 0.5$. These figures indicate that e_δ is in most cases between -2% and 4%. Negative and positive e_δ values correspond to δ_{est} underestimating and overestimating δ_{90}, respectively. The maximum values of $|e_\delta|$ occur at the relatively low loading levels (V/a around 0.02) and are about 10% and 8% for the specimens with $a/W = 0.2$ and 0.5, respectively. The values and variation of e_δ within the considered loading levels for specimens with $a/W = 0.3, 0.4, 0.6$ and 0.7 are similar to those shown in Figs. 3.5 and 3.6, and are not shown for the sake of brevity. The values of $|e_J|$ corresponding to $V/a > 0.02$ are less than 10% for all the analysis cases considered, except for the PS and SG specimens with $a/W = 0.2$ and $n = 5$ where maximum $|e_J|$ is approximately 15%.

To compare the accuracy of the proposed *m*-factor equation with those reported in the literature and reviewed in Section 3.1.2 (i.e. Eqs (3.4) – (3.8)), additional finite element analyses were carried out. The analysis included PS and SG specimens with $a/W = 0.25$,

0.35 and 0.45, $B/W = 1$ and $n = 10$. The values of e_δ corresponding to Eqs. (3.4) – (3.8) and (3.9) for these specimens were calculated and are plotted against V/a in Fig. 3.7. It is observed from Figs. 3.7(a) through 3.7(c) that for the PS specimens within the considered loading levels, Eq. (3.9) is the most accurate among all the equations considered. The accuracy of Eq. (3.6) is comparable to and marginally less than that of Eq. (3.9). The values of $|e_\delta|$ corresponding to these two equations are less than 10% within the considered loading levels. Equation (3.8) predicts *CTOD* values of the three PS specimens with acceptable accuracy: the values of $|e_\delta|$ are less than 15%. However, Eqs. (3.4), (3.5) and (3.7) are considered inadequate as they generally overestimate (or underestimate) *CTOD* by 10% - 45%. The results shown in Figs. 3.7(d) through 3.7(f) indicate that for the SG specimens, Eq. (3.9) is the most accurate among all the *m*-factor equations considered, with the corresponding errors in *CTOD* being less than 5%, followed by Eq. (3.4) with the maximum error in *CTOD* of about 10%, whereas Eqs (3.5) – (3.8) generally overestimate *CTOD* by 10% - 60%. It is noted that Eqs. (3.4) - (3.8) and (3.9) were also compared in terms of the accuracy of the predicted *CTOD* values for the specimens described in Section 3.1. As expected, the accuracy of Eq. (3.9) is the best among all the equations considered (the comparison is not shown for brevity). The relative orders of accuracy corresponding to different equations are similar to those shown in Fig. 3.7.

Finally, it is worth pointing out that the analyses carried out in the present study are with respect to specimens made of homogeneous materials. In the context of SBD of oil and gas pipelines, the SE(T) specimens tested in practice are likely made of non-homogeneous materials, i.e. consisting of both the weldment and base metal. Previous studies (Pisarski et al., 1995; Donato et al., 2009; Paredes and Ruggieri, 2012) on the plastic eta factor-based evaluations of *J* and *CTOD* for SE(B) and SE(T) specimens suggested that the eta factors developed for specimens with homogeneous materials can be applied to specimens with non-homogeneous materials without introducing significant errors (less than 10-15%), if the relative difference between the yield strengths of the weldment and base metal is within ±20%. We therefore remark that the *m*-factor equations developed in this study could be potentially applied to welded SE(T) specimens, if the strength mismatch is within ±20%. Detailed analyses are obviously needed to confirm the validity of such a suggestion.

3.4   Conclusions

Systematic three-dimensional finite element analyses with the large-displacement/large-strain formulation have been performed on clamped SE(T) specimens to evaluate the plastic constraint m factor that relates $CTOD$ to J. Both plane-sided and side-grooved SE(T) specimens with a range of configurations (a/W = 0.2 to 0.7 with an increment of 0.1, and B/W = 1 and 2) and strain hardening exponents (n = 5, 8.5, 10, 15 and 20) were considered in the analyses. A side groove depth of 7.5%B on each side was included in the SG specimens.

The analysis results suggest that the value of m depends on n, specimen configuration (i.e. a/W, B/W and side-grooving) as well as the loading level as represented by V/a. The findings are consistent with those reported in the literature. For loading levels that are of practical concern (i.e. $V/a \geq 0.02$), m is approximately a linear function of V/a. A new empirical m-factor equation for the clamped SE(T) specimen was proposed as a function of V/a, a/W, σ_{YS}/σ_{UTS} and B/W. Using the proposed equation can accurately predict $CTOD$ at loading levels $V/a \geq 0.02$ with the error being generally less than 10% for all the analysis cases considered (except for the PS and SG specimens with a/W = 0.2 and n = 5, where the maximum error is approximately 15%). The proposed m-factor equation was further compared with the equations adopted in the previous and current versions of DNV-OS-F101 (2007, 2012), as well as the equations developed by Shen and Tyson, Moreira and Donato and Ruggieri in terms of the accuracy of the predicted $CTOD$ values. It is observed that the proposed equation leads to the most accurate predictions of the $CTOD$ values for both the PS and SG SE(T) specimens among all the equations considered.

References

ADINA. (2012). Theory and Modeling Guide, ADINA R. & D. Inc., Watertown, USA.

Anderson, T. L. (2005). *Fracture Mechanics—Fundamentals and Applications*, Third edition. CRC Press, Boca Raton.

API. (2012). *API Specification 5L: Specification for Line Pipe*, Ed. 45, American Petroleum Institute, Washington, D.C.

ASTM (2002). *ASTM E1290-02: Standard Test Method for Crack-tip Opening Displacement (CTOD) Measurement. Annual Book of Standards*. America Society of Testing and Materials International, West Conshohocken, PA.

ASTM (2013). *ASTM E1820-13: Standard Test Method for Measurement of Fracture Toughness*. America Society of Testing and Materials International, West Conshohocken, PA.

BSI (1997). *BS 7448-4: Method for determination of fracture resistance curves and initiation values for stable crack extension in metallic materials,* British Standard Institution, London.

BSI (2005). *BS 7910: Guide to methods for assessing the acceptability of flaws in metallic structures*. British Standard Institution, London.

BSI (2014). *BS 8571: Method of Test for Determination of Fracture Toughness in Metallic Materials Using Single Edge Notched Tension (SENT) Specimens*, British Standards Institution, London.

Burdekin, F. M. and Dawes, M. G. (1971). Practical Use of Linear Elastic and Yielding Fracture Mechanics with Particular Reference to Pressure Vessels. *In proceedings, Institution of Mechanical Engineers Conference on Practical Application of Fracture Mechanics to Pressure Vessel Technology*, London, April 3-5, 28-37.

Chiesa, M., Nyhus, B., Skallerud, B. and Thaulow, C. (2001). Efficient fracture assessment of pipelines: A constraint-corrected SENT specimen approach. *Engineering Fracture Mechanics*, 68:527-547.

Cravero, S. and Ruggieri, C. (2007). Estimation Procedure of J Resistance Curves for SE (T) Fracture Specimens Using Unloading Compliance. *Engineering Fracture Mechanics*, 74(17):2735-2757.

Det Norske Veritas. (2010, 2012). Submarine pipeline systems. DNV-OS-F101. Norway: DNV.

Dieter, G. E. (1986). Mechanical metallurgy: McGraw-Hill.

Dodds, R, H. and Read, D. (1990). Experimental and numerical studies of the *J*-integral for a surface flaw. *International Journal of Fracture*, 43:47-67.

Dodds, R. H. (2009). WARP3D: Notes on solution & convergence parameters for a shallow-notch SE(B) model.

Donato, G. H., Magnabosco, R. and Ruggieri, C. (2009). Effects of weld strength mismatch on *J* and *CTOD* estimation procedure for SE(B) specimens. *International Journal of Fracture*, 159:1-20.

Fairchild, D. P., Kibey, S. A., Tang, H., Krishnan, V. R., Wang, X., Macia, M. L., and Cheng, W. (2012). Continued Advancements Regarding Capacity Prediction of Strain-based Pipelines. *Proceedings of 9th International Pipeline Conference (IPC2012)*, Calgary, Alberta, Canada, September 24–28.

Graba, M. and Galkiewicz, J. (2007). Influence of the crack tip model on results of the finite element method. *Journal of Theoretical and Applied Mechanics*, 45:225-237.

Hutchinson, J. W. (1968). Singular Behavior at the End of a Tensile Crack in a Hardening Material. *Journal of the Mechanics of Physics and Solids*, 16:13-31.

Irwin, G. R. (1961). Plastic zone near a crack and fracture toughness. *Sagamore Research Conference Proceedings*, 63-78.

ISO (2002). *ISO 12135: Metallic materials–Unified method of test for the determination of quasistatic fracture toughness*. International Organization for Standardization, Geneva.

Kirk, M. T. and Dodds, R. H. (1993). J and CTOD estimation equations for shallow cracks in single edge notch bend specimens. *Journal of Testing and Evaluation*, 21:228-238.

Kirk, M. T. and Wang, Y. Y. (1995). Wide Range CTOD Estimation Formulae for SE(B) Specimens. *Fatigue and Fracture Mechanics, ASTM STP 1256*, American Society for Testing and Materials, 26:126-141.

Kulka, R. and Sherry, A. (2012). Fracture toughness evaluation in C(T) specimens with reduced out-of-plane constraint. *ASME Pressure Vessels and Piping Conference*: American Society of Mechanical Engineers. p. 877-885.

Mathias, L. L., Sarzosa, D. F. and Ruggieri, C. (2013). Effects of specimen geometry and loading mode on crack growth resistance curves of a high-strength pipeline girth weld. *International Journal of Pressure Vessels and Piping*, 111:106-119.

Moore, P. and Pisarski, H. G. (2012). Validation of methods to determine *CTOD* from SENT specimens. *The 22nd International Ocean and Polar Engineering Conference*. Rodos Palace Hotel, Rhodes, Greece. ISOPE

Moore, P. and Pisarski, H. G. (2013). *CTOD* and pipelines: the past, present, and future. *The 6th International Pipeline Technology Conference (Rudi's Pipeline Conference)*, Ostend, Belgium. *Journal of Pipeline Engineering*; 6-9.

Moreira, F. C. and Donato, G. H. (2010). Estimation procedures for *J* and *CTOD* fracture parameters experimental evaluation using homogeneous and mismatched clamped SE(T) specimens. *ASME 2010 Pressure Vessels and Piping Division/K-PVP Conference*: American Society of Mechanical Engineers. p. 711-20.

Paredes, M, and Ruggieri, C. (2012). Further results in *J* and *CTOD* estimation procedures for SE(T) fracture specimens–Part II: Weld centerline cracks. *Engineering Fracture Mechanics*, 89:24-39.

Pisarski, H. G., Wang, Y-Y. and Gordon, R. (1995). The effect of yield strength mismatch on *CTOD* and *J* estimation procedures for weld metal fracture toughness determination. *Proceedings of the International Conference on Offshore Mechanics and Arctic Engineering*. p. 427-34.

Pisarski, H. G. (2010). Determination of pipe girth weld fracture toughness using SENT specimens. *The 8th International Pipeline Conference*: American Society of Mechanical Engineers. p. 217-224.

Pussegoda, L. N., Tiku, S., Tyson, W. R., Park, D-Y., Gianetto, J. A., Shen, G. and Pisarski, H.G. (2013). Comparison of resistance curves from multi-specimen and single-specimen SENT Tests. *Proceedings of Twenty-third International Offshore and Polar Engineering Conference*. Anchorage, Alaska, USA: The International Society of Offshore and Polar Engineers (ISOPE); p. 482-488.

Rice, J. R. and Rosengren, G. F. (1968). Plane Strain Deformation Near a Crack Tip in a Power Law Hardening Material. *Journal of the Mechanics of Physics and Solids*, 16:1-12.

Ruggieri, C. (2012). Further Results in J and CTOD Estimation Procedures for SE (T) Fracture Specimens–Part I: Homogeneous Materials. *Engineering Fracture Mechanics*, 79:245-265.

Shen, G., Bouchard, R., Gianetto, J. A. and Tyson, W. R. (2008). Fracture toughness evaluation of high strength steel pipe. *ASME Conference Proceedings*. 1275-1282.

Shen, G., and Tyson, W. R. (2009). Evaluation of CTOD from J-integral for SE(T) Specimens. *Pipeline Technology Conference*, Ostend, Belgium, October 12-14.

Shen, G., Tyson, W. R., Gianetto, J. A. and Park, D-Y. (2010). Effect of side grooves on compliance, *J*-Integral and constraint of a clamped SE(T) specimen. *ASME Conference Proceedings*, 81-89.

Shih, C. F. (1981). Relationships between the J-integral and the Crack Opening Displacement for Stationary and Extending Cracks. *Journal of the Mechanics and Physics of Solids*, 29(4):305-326.

Sumpter, J. D. G. and Turner, C. E. (1976). Method for Laboratory Determination of Jc (Contour Integral for Fracture Analysis). *Cracks and Fracture, ASTM STP 601*, ASTM, West Conshohocken, PA; 3-18.

Tang, H., Macia, M., Minnaar, K., Gioielli, P., Kibey, S. and Fairchild, D. (2010). Development of the SENT test for strain-based design of welded pipelines. *ASME Conference Proceedings*, 303-312.

Wang, E., Zhou, W. and Shen, G. (2013). Three-dimensional finite element analysis of crack-tip fields of clamped single-edge tension specimens – Part I: Crack-tip stress fields. *Engineering Fracture Mechanics*, 116:122-143.

Wang, Y., Liu, M., Song, Y. (2011). Second generation models for strain-based design. 3801 Kirby Drive, Suite 520, Houston, Texas, US 77098: Center for Reliable Energy Systems.

Table 3.1: Coefficients M_i and Q_i in Eq. (3.8).

	n	$i = 5$	$i = 4$	$i = 3$	$i = 2$	$i = 1$	$i = 0$
M_i	5	-12.6667	41.7774	-47.7238	23.2332	-5.4920	1.4324
	10	-1.1282	16.4779	-23.5153	10.9659	-2.3047	1.0823
	20	61.2821	-131.9872	108.4318	-43.2838	7.7140	0.4023
Q_i	5	81.5897	-180.7424	154.5238	-64.0121	12.5638	-0.5890
	10	33.4872	-70.1900	59.1272	-25.6393	5.3676	0.1254
	20	49.2308	-109.9534	97.1855	-43.1732	9.0697	-0.0157

Table 3.2: Summary of basis of Eqs. (3.4) – (3.9).

	DNV(07)	DNV(12)	S&T	M&D	Ruggieri	Present study
	Eq. (3.4)	Eq. (3.5)	Eq. (3.6)	Eq. (3.7)	Eq. (3.8)	Eq. (3.9)
2D or 3D	2D	/	2D	2D	2D*	3D
small strain or large strain	small strain	/	large strain	small strain	small strain	large strain
a/W	0.05 - 0.7	0.2 - 0.5	0.2 and 0.5	0.1 - 0.7	0.2 - 0.7	0.2 - 0.7
B/W	/	2 - 5	/	/	/	1 and 2
plane-sided (PS) or side-grooved (SG)	/	PS	/	/	/	PS and SG
n	4, 5, 10, 50	/	5, 10, 15, 20	10	5, 10, 20	5, 8.5, 10, 15, 20

* Equations for η_J and η_δ were validated by 3D FEA of PS SE(T) specimens with $B/W = 0.5$ and 2.

Table 3.3: Coefficients p_{ij} and q_{ij} in Eq. (3.11).

		B/W = 1			B/W = 2		
		$j = 0$	$j = 1$	$j = 2$	$j = 0$	$j = 1$	$j = 2$
p_{ij}	$i = 0$	2.201	1.106	-1.441	2.145	1.804	-2.241
	$i = 1$	-0.540	-1.303	2.280	-0.471	-1.622	2.616
q_{ij}	$i = 0$	7.036	-28.541	40.002	12.374	-45.815	55.681
	$i = 1$	-11.016	40.381	-64.389	-15.869	58.787	-82.230

Deformed crack flank

Nodes in the FEA

Initial crack flank

Crack tip node

$\delta_{90}/2$

45°

$\rho_0 = 2.5\ \mu m$
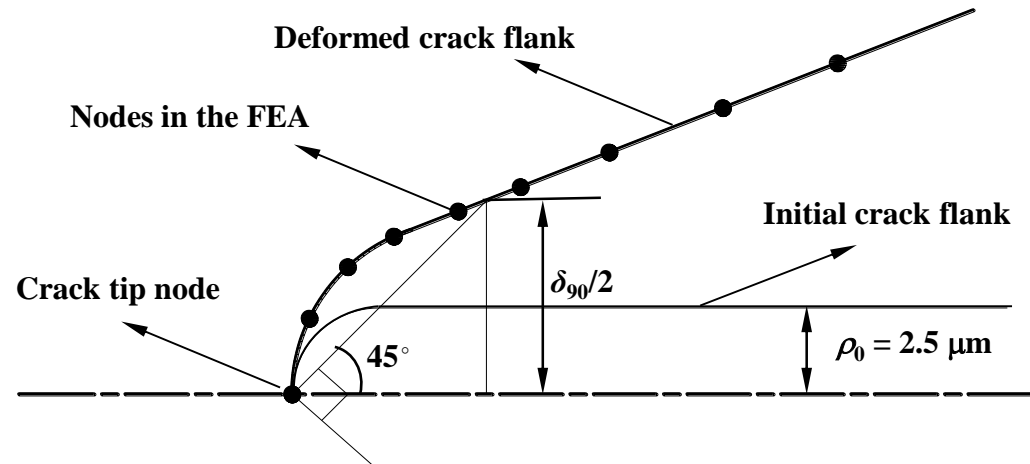
Figure 3.1. Schematic illustration of the determination of *CTOD* in FEA
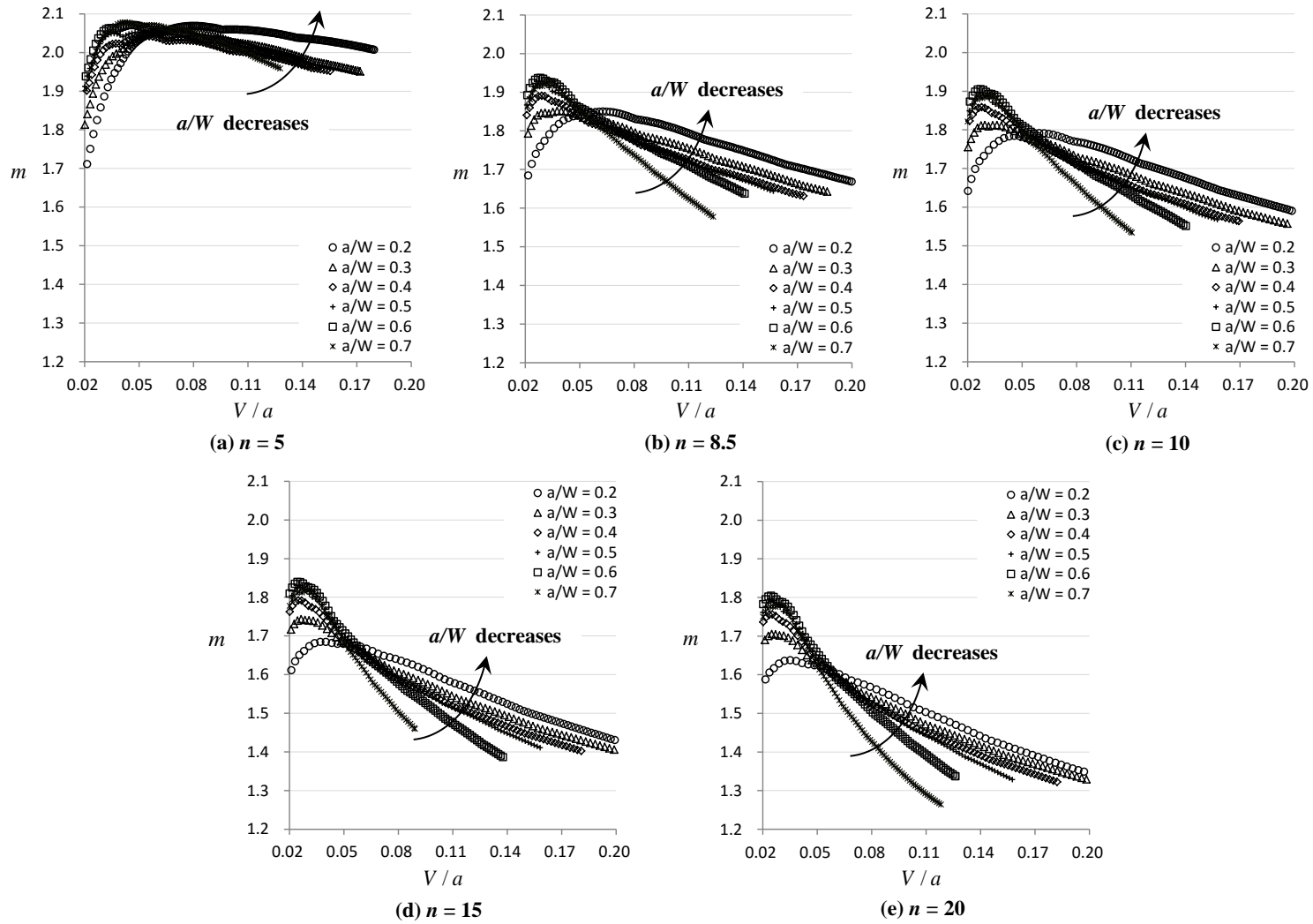
Figure 3.2. Variation of *m* with *V/a* for different *a/W* for plane-sided specimen with *B/W* = 1
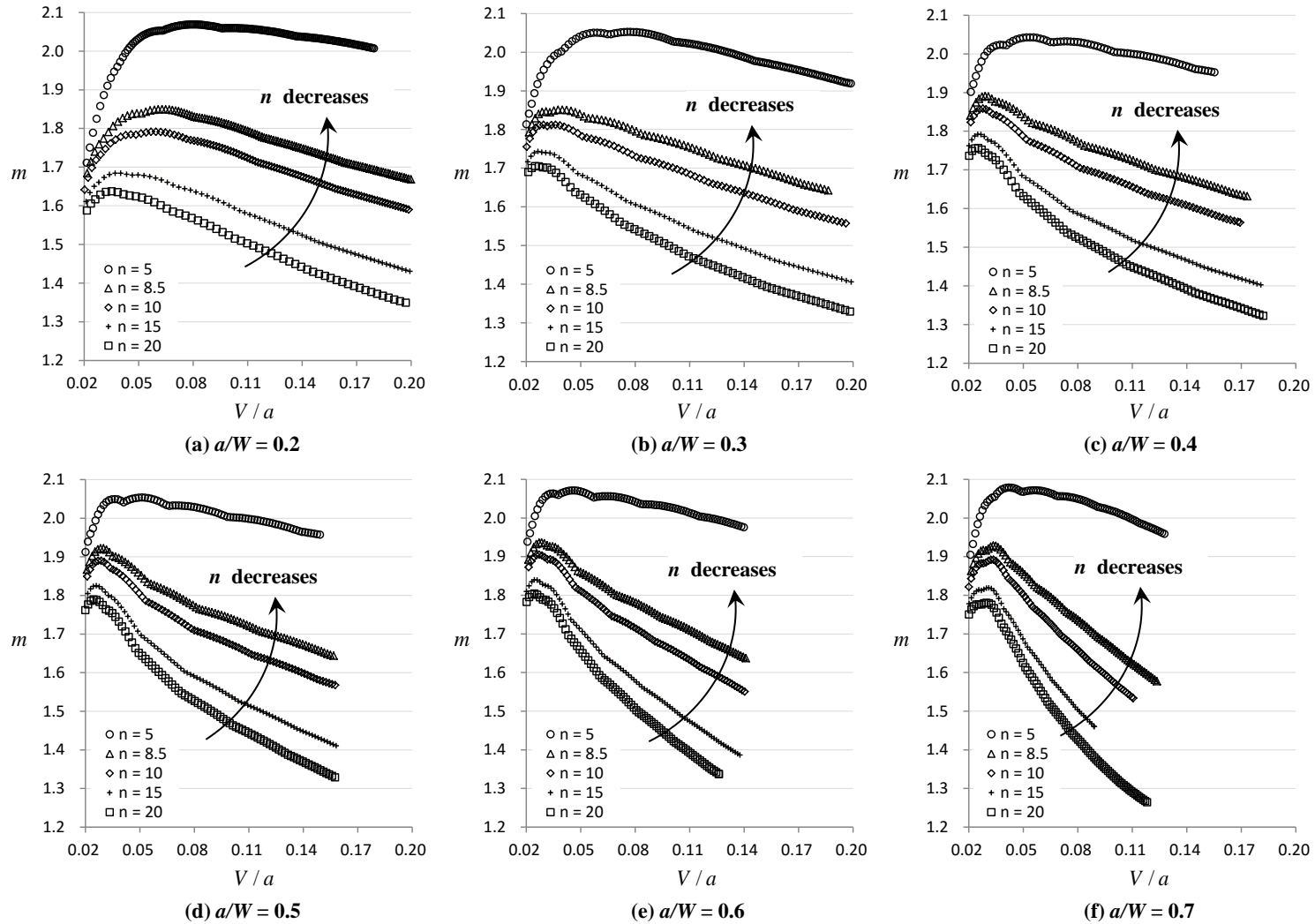
Figure 3.3. Variation of *m* with *V/a* for different *n* for plane-sided specimen with *B/W* = 1
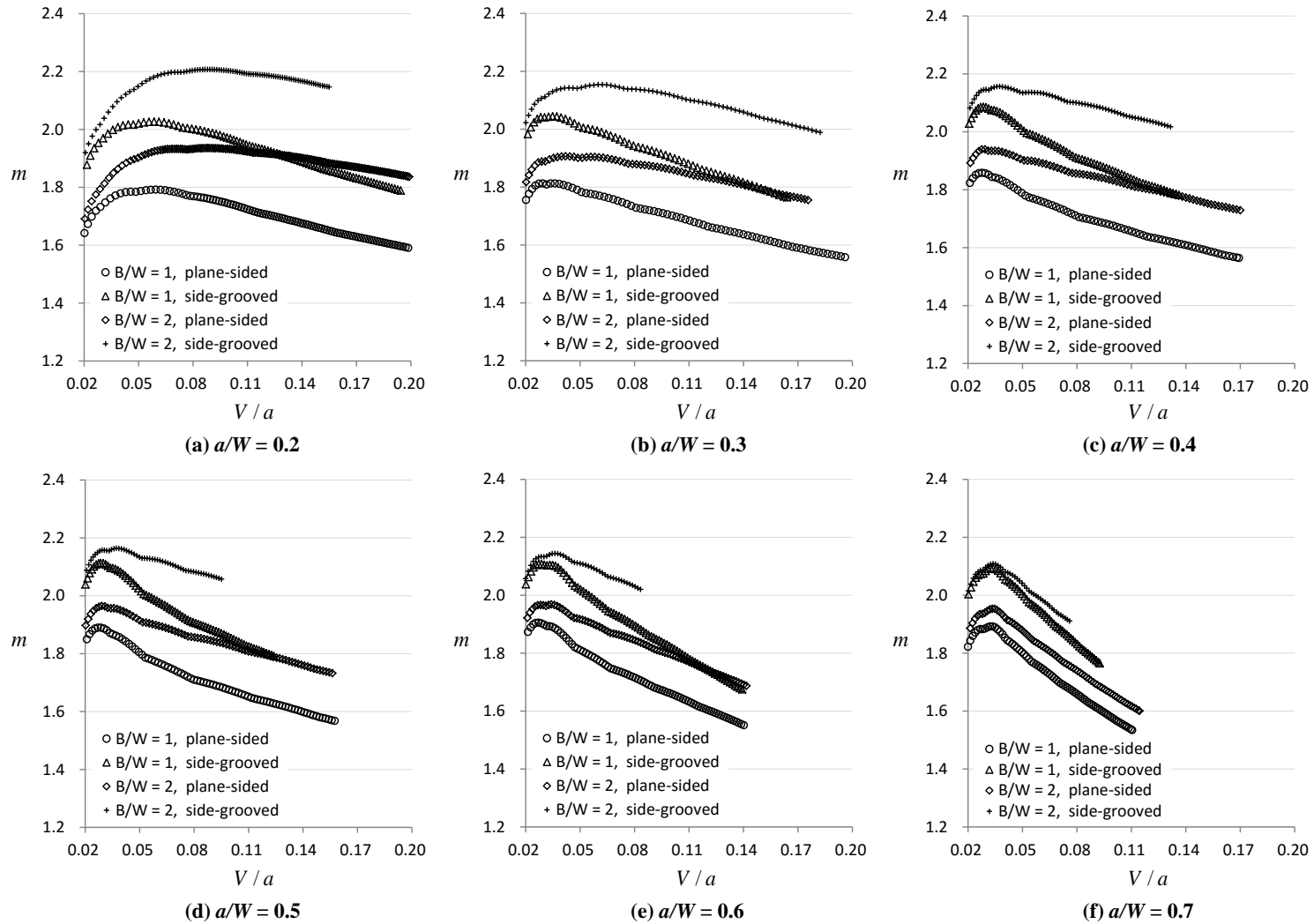
Figure 3.4. Variation of *m* with *V/a* for specimen with *n* = 10 and different *B/W*

Figure 3.5. Variation of e_δ with V/a for Eq. (3.9) for specimens with $a/W = 0.2$

(a) $a/W = 0.5$, $B/W = 1$, PS

(b) $a/W = 0.5$, $B/W = 2$, PS

(c) $a/W = 0.5$, $B/W = 1$, SG

(d) $a/W = 0.5$, $B/W = 2$, SG
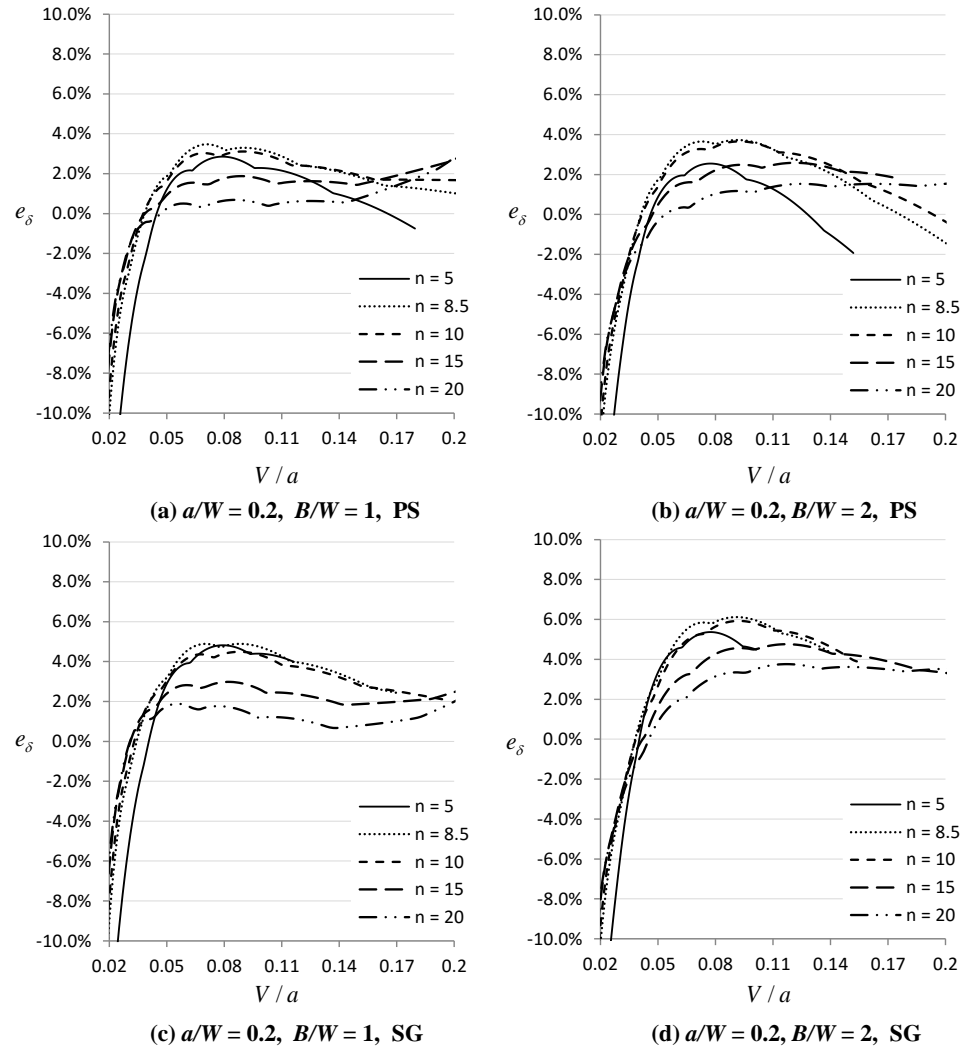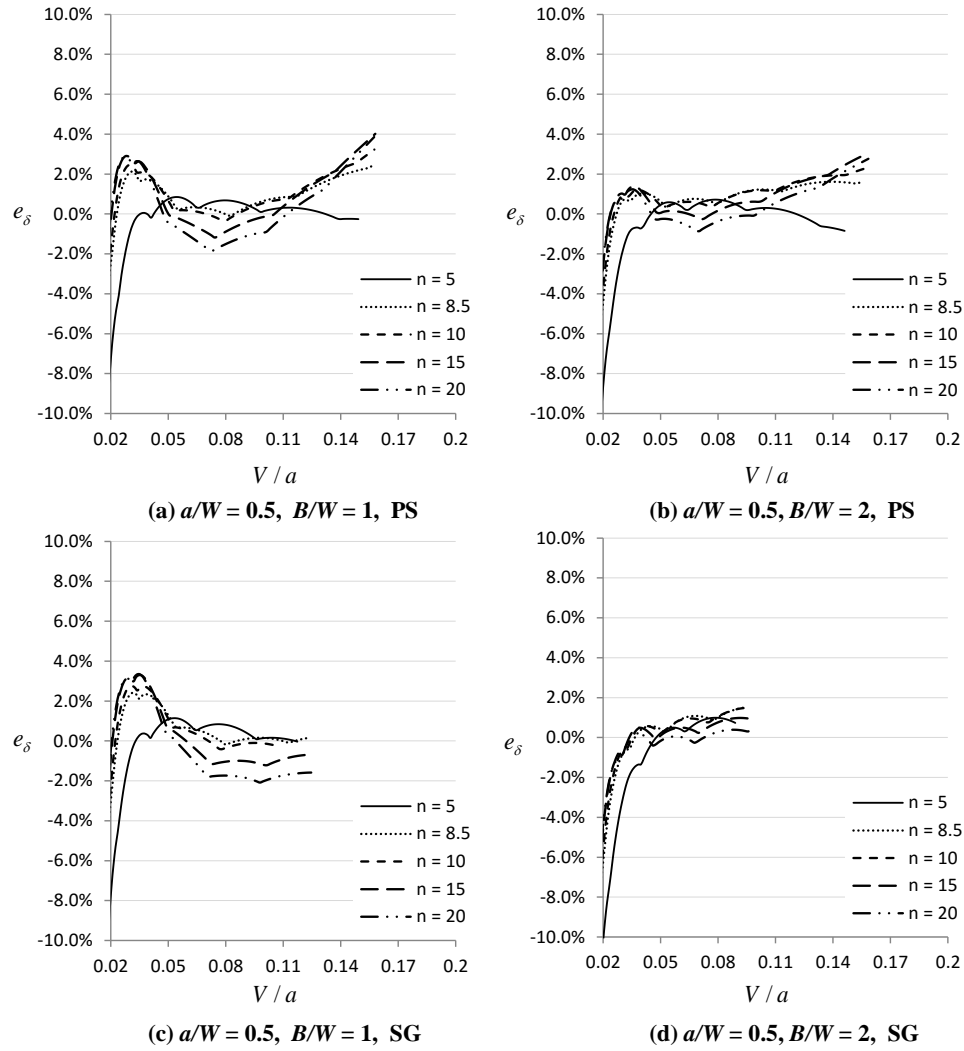
Figure 3.6. Variation of e_δ with V/a for Eq. (3.9) for specimens with $a/W = 0.5$
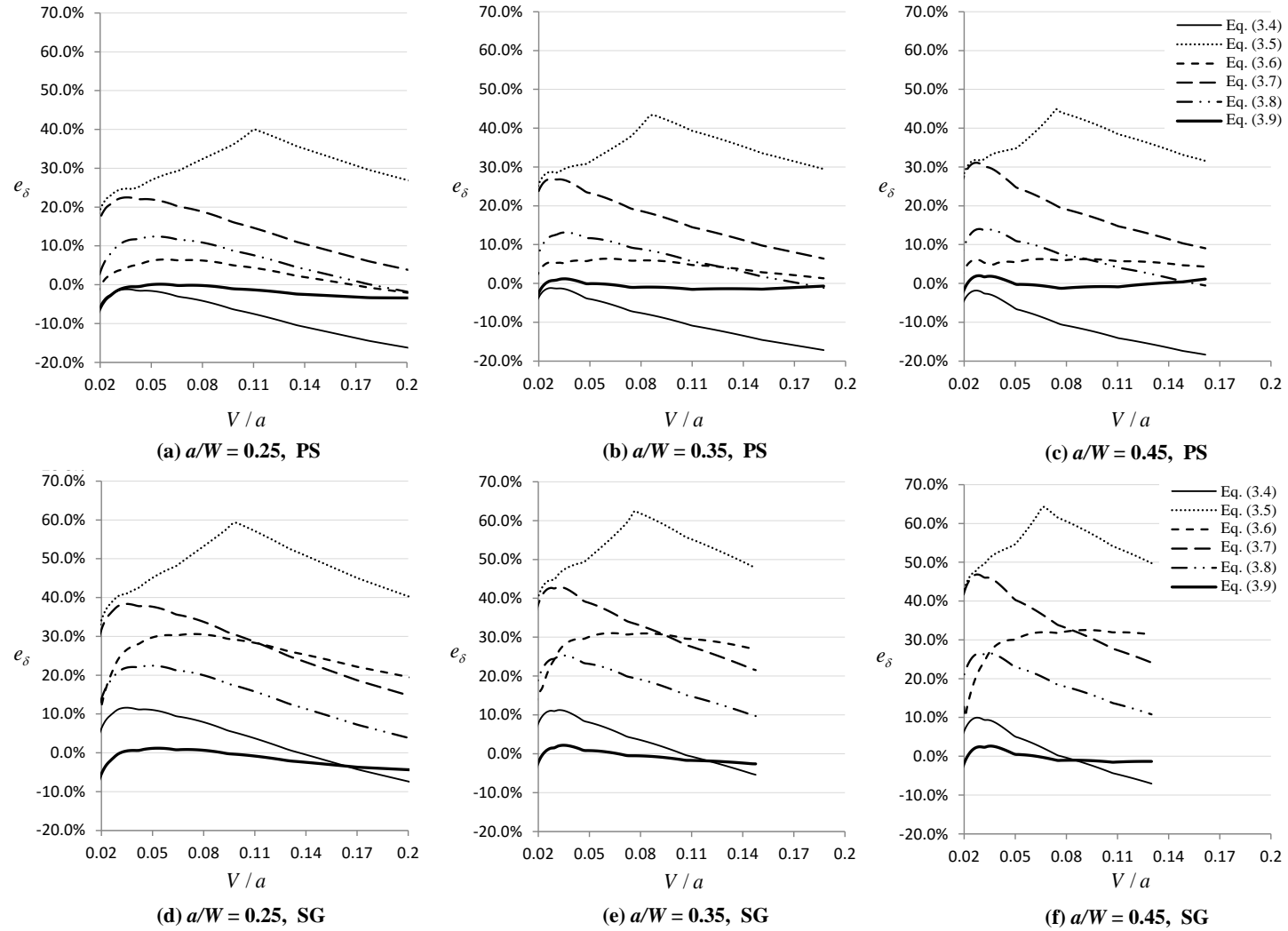
Figure 3.7. Variation of e_δ with V/a for specimens with $B/W = 1$ and $n = 1$

Chapter 4 Numerical Investigation of Compliance Equations Used in the *R*-Curve Testing for Clamped SE(T) Specimens

4.1 Background and Objective

4.1.1 Introduction

Simultaneous evaluations of the instantaneous *J*-integral (*J*) (or crack-tip opening displacement resistance (*CTOD*)) and crack length (*a*) are key to the widely-used single-specimen technique in the fracture toughness resistance (*R*) curve testing (Clarke et al., 1976). One of the common approaches to evaluate the crack length in the single-specimen technique is the elastic unloading compliance (UC) method (Clarke et al., 1976; Clarke and Landes, 1979). The UC method is based on a unique relationship between the crack length and elastic compliance (i.e. inverse of the stiffness, *C*) of the specimen, which is typically written as

$$\frac{a}{W} = f\left(BCE_{2\mathrm{D}}\right) \tag{4.1}$$

where *B* and *W* are the thickness and width of the specimen, respectively; $BCE_{2\mathrm{D}}$ is the non-dimensional normalized compliance, and $f(\bullet)$ represents the function that relate *a/W* to $BCE_{2\mathrm{D}}$. The value of elastic modulus in two-dimensional (2D) analysis, $E_{2\mathrm{D}}$, equals the Young's modulus (*E*) for plane-stress condition, and equals $E' = E/(1 - v^2)$ for plane-strain condition with *v* being Poisson's ratio.

By estimating the compliance of a specimen through the load-displacement data of a given unloading-reloading sequence in the test, the corresponding crack length can be determined. Figure 4.1 schematically shows the experimental measurement of the compliance based on the load vs. crack-mouth opening displacement (*P-CMOD*) curve for a specimen with a growing crack. The measured compliance usually increases with the crack length as shown in Fig. 4.1. It is noted that using the *CMOD* compliance to predict the relative crack length (*a/W*) is more advantageous than using the load line displacement

(*LLD*) compliance because *CMOD* can be more accurately and easily measured than *LLD* (Zhu et al., 2008).

As specified in test standards ASTM E1820-13 (ASTM, 2013) and BS7448-4 (BSI, 1997), experimental evaluation of *J* or *CTOD* in the *R*-curve test involves separating the total *CMOD* (*V*) into an elastic component, V_{el}, and a plastic component, V_{pl} (see Fig. 4.1):

$$V_{pl} = V - V_{el} = V - PC \tag{4.2}$$

where *P* is the applied load and *C* can be directly measured if the UC method is adopted. For test methods (such as the potential drop method) that directly measure the crack length instead of the compliance (Johnson, 1965; Schwalbe and Hellmann, 1981; Marschall et al., 1990), the following equation is needed to evaluate *C* in Eq. (4.2) based on the measured crack length:

$$BCE_{2D} = g\left(\frac{a}{W}\right) \tag{4.3}$$

where $g(\bullet)$ represents the function that relates BCE_{2D} to *a/W*. It follows that the accuracies of $f(BCE_{2D})$ and $g(a/W)$ directly impact the accuracy of the experimentally determined *R*-curve.

Recently, the use of the non-standard clamped single-edge tension (SE(T)) specimen (referred to as the SE(T) specimen hereafter for simplicity) to determine the *R*-curve has gained considerable research interests (Chiesa et al., 2001; Shen et al., 2008; Tamg et al., 2010; Wang et al., 2011) largely as a result of the development of the strain-based design and assessment methodologies in the energy pipeline industry. A great deal of studies are reported in the literature concerning the compliance equation for the SE(T) specimen (Tada et al. 1973; John et al., 1985; Jones, 1998; Cravero and Ruggieri, 2007; Shen et al., 2008, 2009; John and Rigling, 1998; Mathias et al., 2013; Fonzo et al., 2009; Donato and Moreira, 2013). For example, empirical *BCE'-a/W* equations for different types of specimens including SE(T) are well documented by Tada et al. (1973), while John et al. (1985) and Jones (1998) developed *BCE'-a/W* equations for SE(T) specimens with various *a/W* and

daylight-over-width ratios (H/W) based on the weight function analysis. Cravero and Ruggieri (2007) and Shen et al. (2008, 2009) respectively proposed the a/W-BCE_{2D} equations for the SE(T) specimen with $0.1 \leq a/W \leq 0.7$ and $0.05 \leq a/W \leq 0.95$ based on 2D plane-strain finite element analyses (FEA). By using 2D plane-stress FEA, John and Rigling (1998) developed a 6th-order polynomial a/W-BCE equation for the SE(T) specimen with $0.1 \leq a/W \leq 0.9$. Mathias et al. (2013) proposed an empirical a/W-BCE equation for the SE(T) specimen with $0.1 \leq a/W \leq 0.7$. Fonzo et al. (2009) proposed a/W-BCE' equations based on the results of 2D plane-strain FEA. Donato and Moreira (2013) carried out three-dimensional (3D) FEA of clamped plane-sided and side-grooved SE(T) specimens with $0.1 \leq a/W \leq 0.7$, $B/W = 1$ and $H/W = 6$. They developed an empirical a/W-BCE equation based on the FEA results and suggested that the equation be applied to both plane-sided and side-grooved SE(T) specimens with $0.25 \leq B/W \leq 1$.

Recently, Wang and Omiya (2015) examined the accuracy of the a/W-BCE_{2D} equations reported in (Cravero and Ruggieri, 2007; Shen et al., 2008, 2009; Mathias et al., 2013; Fonzo et al., 2009; Donato and Moreira, 2013) based on both 2D plane-strain and 3D FEA of SE(T) specimens with $H/W = 10$. Both plane-sided and side-grooved specimens were considered in the 3D FEA. Their analyses involved a/W ratios ranging from 0.05 to 0.7, two B/W ratios (i.e. $B/W = 1$ and 2) and three side-groove depths (i.e. $5\%B$, $7.5\%B$ and $10\%B$ on each side of the specimen). Based on the analysis results, Wang and Omiya developed the effective modulus, E_e, for the 3D condition to replace E_{2D} in Eq. (1) and showed that using E_e can markedly improve the accuracy of the predicted crack length for SE(T) specimens. The value of E_e was proposed to be evaluated as $E_e = \lambda_e E$, where λ_e is a dimensionless factor that is a function of BCE and B/W.

4.1.2 Objective and Approach

Despite the rich literature on the compliance of the SE(T) specimens, there are a few issues yet to be addressed. First, previous studies (Cravero and Ruggieri, 2007; Shen et al., 2008, 2009; John and Rigling, 1998; Mathias et al., 2013; Fonzo et al., 2009; Donato and Moreira, 2013; Wang and Omiya, 2015) focused on the accuracy of a/W-BCE_{2D} equations, whereas the accuracy of the BCE_{2D}-a/W equations has not been investigated

based on 3D FEA. Second, relatively thick specimens ($B/W > 2$) have been recommended in testing standards, e.g. DNV-RP-F108 (DNV, 2006), but the accuracy of the compliance equations for such specimens has not been well studied in the literature. Finally, although the use of E_e has been shown (Wang and Omiya, 2015) to markedly increase the accuracy of various a/W-BCE_{2D} equations, eight different empirical 4th-order polynomial equations were proposed in (Wang and Omiya, 2015) to evaluate the dimensionless factor λ_e that relates E_e to E, for different B/W ratios and depths of the side groove. These equations can be cumbersome to use in practice. Furthermore, E_e is developed based on the assumption that the BCE_{2D}-a/W equation employed in the development of E_e is perfectly accurate, which is not the case in reality. It can be inferred that the accuracy of the BCE_{2D}-a/W equations cannot be improved by replacing E_{2D} with E_e. Therefore, it is desirable to develop an easy-to-use approach to account for the impact of the 3D effects on both a/W-BCE_{2D} and BCE_{2D}-a/W equations.

The objective of the present study was to address the aforementioned issues. To this end, 3D linear-elastic FEA of plane-sided (PS) and side-grooved (SG) SE(T) specimens with a/W ranging from 0.1 to 0.9 and B/W ranging from 0.25 to 4 were carried out. The analysis was focused on specimens with $H/W = 10$ because the crack-tip stress fields of such a specimen correspond closely to those of the full-scale pipes containing circumferential cracks (Shen et al., 2008), which are of primiary concern to the strain-based design of pipelines. The FEA was carried out to investigate the accuracy of the existing a/W-BCE_{2D} and BCE_{2D}-a/W equations. Based on the FEA results, a simple approach was proposed to improve the accuracy of the compliance equations by introducing the crack length/compliance modification factors, $\rho_{(a/W)}$ and $\rho_{(BCE)}$. For a given compliance equation, the corresponding crack length (or compliance) modification factor can be evaluated from a single empirical equation for both plane-sided and side-grooved specimens with various B/W ratios. It should be noted that the present study is focused on the compliance of the SE(T) specimen in the undeformed position. For the compliance of the SE(T) specimen in the deformed position, Cravero and Ruggieri (2007) and Shen and Tyson (2009) have developed the compliance correction procedure to account for the effect of the geometry

change due to the rotational deformation of the specimen, which is detailed in Appendix C.

The rest of this chapter is structured as follows. A brief review of several compliance equations for the SE(T) specimen is included in Section 4.2; Section 4.3 describes the 3D finite element models and analysis procedures employed in this study for calculating the compliance; in Section 4.4, the accuracies of the compliance equations for the SE(T) specimens are examined based on the FEA results, and the 3D crack length/compliance modification factors for the SE(T) specimen are proposed and validated, followed by conclusions and recommendations in Section 4.5.

4.2   Review of Compliance Equations for Clamped SE(T) Specimen

4.2.1   *a*/*W* as a function of *BCE*$_{2D}$

Cravero and Ruggieri (2007) developed an *a/W-BCE*$_{2D}$ equation based on the 2D plane-strain FEA:

$$
\begin{cases}
\dfrac{a}{W} = 1.6485 - 9.1005u + 33.025u^2 - 78.467u^3 \\
\qquad + 97.344u^4 - 47.227u^5 \qquad\qquad ,0.1 \le a/W \le 0.7 \quad (a) \\
u = \dfrac{1}{1+\sqrt{BCE_{2D}}} \qquad\qquad\qquad\qquad\qquad (b)
\end{cases}
\tag{4.4}
$$

where *u* is a non-dimensional factor that used to construct the *a*/*W-BCE*$_{2D}$ relationship.

Similarly, Shen et al. (2008, 2009) proposed the following 9th- and 8th-order polynomial equations for the SE(T) specimen with *H/W* = 10 based on the results of 2D plane-strain FEA:

$$
\begin{cases}
\dfrac{a}{W} = 2.044 - 15.732u + 73.238u^2 - 182.898u^3 \\
\qquad + 175.653u^4 + 60.930u^5 - 113.997u^6 \qquad ,0.05 \le a/W \le 0.95 \quad (a) \\
\qquad - 113.031u^7 + 8.548u^8 + 142.840u^9 \\
\dfrac{a}{W} = 2.072 - 16.411u + 79.600u^2 - 211.670u^3 \\
\qquad + 236.857u^4 + 27.371u^5 - 179.740u^6 \qquad ,0.05 \le a/W \le 0.95 \quad (b) \\
\qquad - 86.2801u^7 + 171.764u^8
\end{cases}
\tag{4.5}
$$

Based on a series of 2D plane-stress FEA of SE(T) specimens, John and Rigling (1998) developed an empirical equation whereby a/W is a function of BCE and H/W for a wide range of specimen configurations (i.e. $0.1 \le a/W < 0.9$ and $2 \le H/W < 10$). For specimens with $H/W = 10$, the a/W-BCE relationship is presented as the following equation:

$$
\begin{aligned}
\frac{a}{W} &= -0.41881\left(\frac{1}{u}\right) + 0.485754\left(\frac{1}{u^2}\right) - 0.16556\left(\frac{1}{u^3}\right) \\
&\quad + 0.027639\left(\frac{1}{u^4}\right) - 0.00229\left(\frac{1}{u^5}\right) + 0.0000749\left(\frac{1}{u^6}\right) \\
&\qquad\qquad\qquad , \quad 0.1 \le a/W \le 0.9
\end{aligned}
\tag{4.6}
$$

Mathias et al. (2013) recently proposed an empirical compliance equation as follows by summarizing the FEA results reported in (Cravero and Ruggieri, 2007):

$$
\begin{aligned}
\frac{a}{W} &= 1.9215 - 13.2195u + 58.7080u^2 - 155.2823u^3 \\
&\quad + 207.3987u^4 - 107.9176u^5 \qquad\qquad ,0.1 \le a/W \le 0.7
\end{aligned}
\tag{4.7}
$$

Fonzo et al. (2009) developed the following 5th-order polynomial equations based on the 2D plane-strain FEA:

$$
\begin{aligned}
\frac{a}{W} &= 1.64461 - 8.7084u + 30.31342u^2 - 69.60922u^3 \\
&\quad + 83.52325u^4 - 39.11201u^5 \qquad\qquad ,0.1 \le a/W \le 0.7
\end{aligned}
\tag{4.8}
$$

Note that in the corresponding original publications (Cravero and Ruggieri, 2007; Shen et al., 2008, 2009; John and Rigling, 1998; Mathias et al., 2013; Fonzo et al., 2009), E_{2D}

was taken as the plane-stress elastic modulus (E) in Eqs. (4.5) – (4.7), and plane-strain elastic modulus (E') in Eqs. (4.4) and (4.8). Several studies (Shen et al., 2009; Wang and Omiya, 2015; Tyson et al., 2014) have revealed that using E instead of E' in Eqs. (4.4) and (4.8) can lead to more accurate predictions of a/W for specimens with $B/W = 1$. Based on this, E_{2D} was set to equal E in Eqs. (4.4) – (4.8) in the present study.

4.2.2 BCE_{2D} as a function of a/W

Tada et al. (1973) proposed the following equation to express BCE' as a function of a/W for the SE(T) specimen:

$$BCE' = \frac{4a}{W}\left[\frac{1.46 + 3.42\left(1 - \cos\dfrac{\pi a}{2W}\right)}{\left(\cos\dfrac{\pi a}{2W}\right)^2}\right] \quad ,0 \le a/W < 1 \tag{4.9}$$

Note that Eq. (4.9) is considered applicable for different H/W ratios as long as $H/W \ge 2$.

John and Rigling (1998) developed the following BCE-a/W equation for the SE(T) specimen with $H/W = 10$ based on the 2D plane-stress FEA from which Eq. (4.6) is developed:

$$BCE = \frac{\dfrac{2a}{W}\left[\begin{array}{c}2.9086 - 5.8808\left(\dfrac{a}{W}\right) + 20.3409\left(\dfrac{a}{W}\right)^2 - 53.8231\left(\dfrac{a}{W}\right)^3 \\[2mm] + 96.017\left(\dfrac{a}{W}\right)^4 - 101.172\left(\dfrac{a}{W}\right)^5 + 41.6725\left(\dfrac{a}{W}\right)^6\end{array}\right]}{\left(1 - \dfrac{a}{W}\right)^2} \tag{4.10}$$

The authors reported that Eq. (4.10) is accurate to within $\pm 0.7\%$ of the corresponding 2D FEA results.

Recently, Wang (2015) proposed the following BCE'-a/W equations, i.e. Eqs. (4.11a), (4.11b) and (4.11c), by fitting the inverse of Eqs. (4.4), (4.5a) and (4.5b), respectively:

$$
\begin{cases}
\begin{aligned}
BCE' = {} & 0.1341 + 3.4879\left(\dfrac{a}{W}\right) + 13.1816\left(\dfrac{a}{W}\right)^2 - 0.3217\left(\dfrac{a}{W}\right)^3 \\
& + 6.4377\left(\dfrac{a}{W}\right)^4 + 52.0490\left(\dfrac{a}{W}\right)^5
\end{aligned} & \text{(a)} \\[2em]
\begin{aligned}
BCE' = {} & -0.3570 + 25.5841\left(\dfrac{a}{W}\right) - 359.8746\left(\dfrac{a}{W}\right)^2 - 3186.5734\left(\dfrac{a}{W}\right)^3 \\
& - 15620.0237\left(\dfrac{a}{W}\right)^4 + 47001.2368\left(\dfrac{a}{W}\right)^5 - 88229.0334\left(\dfrac{a}{W}\right)^6 \\
& + 101299.6070\left(\dfrac{a}{W}\right)^7 - 64910.5190\left(\dfrac{a}{W}\right)^8 + 17743.9291\left(\dfrac{a}{W}\right)^9
\end{aligned} & \text{(b)} \\[2em]
\begin{aligned}
BCE' = {} & -0.0798 + 11.3975\left(\dfrac{a}{W}\right) - 97.1143\left(\dfrac{a}{W}\right)^2 + 752.0341\left(\dfrac{a}{W}\right)^3 \\
& - 2744.2227\left(\dfrac{a}{W}\right)^4 + 5720.0103\left(\dfrac{a}{W}\right)^5 - 6623.2211\left(\dfrac{a}{W}\right)^6 \\
& + 4163.4587\left(\dfrac{a}{W}\right)^7 - 1120.6101\left(\dfrac{a}{W}\right)^8
\end{aligned} & \text{(c)}
\end{cases}
$$

$$\tag{4.11}$$

The absolute fitting error of Eqs. (4.11a) through (4.11c) is reported in (Wang, 2015) to be less than 1% for $a/W \geq 0.1$. Note that the accuracies of Eqs. (4.9) – (4.11) have not been verified through 3D FEA of SE(T) specimens. Note also that for side-grooved specimens, the effective specimen thickness, $B_{e(1)}$, should be used to evaluate u (i.e. Eq. (4.4b)) for the a/W-BCE_{2D} equation and be used in Eqs. (4.9) – (4.11), where $B_{e(1)}$ is given by (ASTM, 2013; BSI, 1997):

$$
B_{e(1)} = B - \frac{\left(B - B_N\right)^2}{B} \tag{4.12}
$$

with B_N denoting the net specimen thickness.

4.3 Numerical Analyses

The commercial software ADINA 8.9.3 (ADINA, 2012) was used to carry out the FEA. Linear-elastic analyses of 63 PS and 63 SG SE(T) models were performed to evaluate the

CMOD compliance. Young's modulus and Poisson's ratio were set to be 207 GPa and 0.3, respectively. All the specimens included in this study have a width $W = 20$ mm and a daylight (*H*) of 10*W*. Seven *B/W* ratios (i.e. *B/W* = 1/4, 1/3, 1/2, 1, 2, 3 and 4), and nine *a/W* ratios (i.e. *a/W* = 0.1, 0.2, 0.3, 0.4, 0.5, 0.6, 0.7, 0.8 and 0.9) were included in the analyses. For the SG models, the side groove was modeled as a U-shape notch with a depths of 7.5%*B* on each side of the specimen (i.e. the net specimen thickness $B_N = 0.85B$) as suggested by Shen et al. (2010). The root radius (r_{sg}) of the side groove for models with *B/W* = 1/2, 1, 2, 3 and 4 was set to 0.5 mm as recommended in ASTM E1820 (ASTM, 2013) ($r_{sg} = 0.5 \pm 0.2$ mm). For models with *B/W* = 1/4 and 1/3, due to the thin specimen thickness, a smaller root radius (i.e. $r_{sg} = 0.3$ mm) was used. Results of sensitivity analyses (not reported here for the sake of brevity) indicate that the radius of the side groove has a negligible impact on the compliance of the SE(T) specimen for $r_{sg} \leq 1$ mm. Only a quarter of a given specimen was modeled in the FEA due to symmetry. The geometric configuration of a typical SG specimen in FEA is shown in Fig. 4.2(a) together with the fixation and loading conditions. A schematic of the side groove modeling is shown in Fig. 4.2(b).

The 20-node 3D brick elements with 3×3×3 integration were used in the analysis. Stationary cracks were assumed in all the FE models. A sharp crack tip was incorporated and the surfaces of the brick elements were collapsed to a line at the crack tip (see Fig. 4.2(c)) to simulate the singularity condition. A spider-web mesh around the crack tip was established with 45 concentric semicircles (i.e. rings) surrounding the crack tip. The model was divided into 12 layers over the half net thickness ($B_N/2$) and the groove (($B - B_N$)/2) was divided into 16 layers. The in-plane and out-of-plane size of the elements closest to the crack tip is about 1/2000*W* and 1/200*B*. The total number of elements is approximately 11,000 in a typical PS specimen, and 28,000 in a typical SG specimen. Convergence studies on mesh density were conducted by increasing the number of the layers along the half net tthickness from 12 to 17. Good convergence of the output compliance was observed.

Uniform displacements were applied on two lateral surfaces that are considered as the clamped surface with a length of 2*W*. Negligible differences (around 0.1%) of the analysis

results were observed when changing the length of the clamped surface from $2W$ to $4W$. Evaluation of the compliance requires computation of the load-displacement, i.e. *P-CMOD*, response in the FEA. The load (P) was calculated as the total reactions of the nodes on the clamped surface while *CMOD* (V) was recorded at the mid-thickness of the specimen. The values of P and V corresponding to an applied displacement of 2 μm were obtained, and the compliance was then calculated as *V/P*.

4.4 Results and Discussions

4.4.1 Prediction Error of the Compliance Equations

Let e_1 denote the error (%) associated with the value of *a/W* predicted from Eqs. (4.4) – (4.8), and e_2 denote the error (%) associated with the value of C predicted from Eq. (4.9) – (4.11); that is, e_1 and e_2 are given by

$$
\begin{cases}
e_1 = \dfrac{\left(\dfrac{a}{W}\right)_p - \left(\dfrac{a}{W}\right)_{FEA}}{\left(\dfrac{a}{W}\right)_{FEA}} & \text{(a)} \\[4ex]
e_2 = \dfrac{C_p - C_{FEA}}{C_{FEA}} & \text{(b)}
\end{cases}
\tag{4.13}
$$

where the subscripts "*p*" and "*FEA*" denote the values predicted from Eqs. (4.4) – (4.11) and values either incorporated in or obtained from the FEA models, respectively. Tables 4.1 and 4.2 list e_1 and e_2 for the PS and SG specimens considered in this study, respectively. Note that the positive (negative) values indicate overestimation (underestimation) of BCE_{2D} or *a/W* by a given equation. Tables 4.1 and 4.2 indicate that the error of prediction of a given equation depends on the *a/W* and *B/W* ratios. Table 4.1(a) suggests that Eqs. (4.4), (4.5a), (4.5b) and (4.6) lead to similar predictions of *a/W* for a given *BCE*. For a given *a/W*, the values of $|e_1|$ associated with Eqs. (4.4), (4.5a), (4.5b) and (4.6) in general increase as *B/W* increases; therefore, the highest error of prediction is typically for the thickest specimen (i.e. $B/W = 4$). For $a/W \geq 0.5$, the corresponding values of $|e_1|$ are always less than or equal to 2.5% regardless of *B/W*. For $a/W < 0.5$, the values of $|e_1|$ associated

with the four equations are in general less than 2% for relatively thin specimens (i.e. $B/W \le 0.5$); but for relatively thick specimens ($B/W \ge 1$), the corresponding values of $|e_2|$ can be significant. For example, the values of $|e_2|$ of Eq. (4.5a) and (4.6) are 10.4 and 9.4%, respectively, for $a/W = 0.1$ and $B/W = 4$. It is interesting to note that the trend in $|e_1|$ associated with Eqs. (4.7) and (4.8) is opposite to that in $|e_1|$ associated with Eqs. (4.4) through (4.6) in that for a given a/W $|e_1|$ associated with Eqs. (4.7) and (4.8) decreases as B/W increases, particularly for specimens with $a/W < 0.5$. For example, $|e_1|$ associated with Eq. (4.7) decreases from 9.2% to 0.9% as B/W increases from 0.25 to 4 for $a/W = 0.1$. The results in Table 4.1 further indicate that Eqs. (4.7) and (4.8) are accurate for relatively thick specimens regardless of a/W: the corresponding values of $|e_1|$ are generally less than 3.0% for $0.1 \le a/W \le 0.9$ and $1 \le B/W \le 4$.

As shown in Table 4.1(b), $|e_2|$ of Eq. (4.9) decreases from about 1400% to less than 15% as a/W decreases from 0.9 to 0.1. The results indicate that Eq. (4.9) is not adequate to characterize the $BCE'\text{-}a/W$ relationship for SE(T) specimens with $H/W = 10$. On the other hand, Eqs. (4.10), (4.11a), (4.11b) and (4.11c) lead to much more accurate predictions of C with values of $|e_2|$ generally being smaller than 10%. For a given a/W, the values of $|e_2|$ associated with Eqs. (4.10) in general increase as B/W increases whereas the opposite is the case for Eqs. (4.11a), (4.11b) and (4.11c). This can be explained by the fact that E and E' are employed in Eqs. (4.10) and (4.11), respectively. Eq. (4.10) is accurate for relatively thin specimens (i.e. $B/W \le 0.5$) with $a/W \ge 0.2$ with the error being less than 2%. The values of $|e_2|$ associated with Eqs. (4.11a), (4.11b) and (4.11c) for specimens with $a/W \le 0.3$ are in general less than 2% for specimens with $B/W \ge 2$, but the corresponding values of $|e_2|$ increase significantly as B/W decreases from 2 to 0.25 or a/W increases from 0.3 to 0.9.

The values of e_1 and e_2 for the SG specimens as shown in Table 4.2 are similar to those in Table 4.1. For specimens with $B/W \ge 1$, the predictions by Eqs. (4.4) through (4.8) for the SG specimens are generally more accurate than those for the PS specimens with the same a/W ratios; for specimens with $B/W < 1$, the predictions by the same equations for the SG specimens are slightly less accurate than those for the PS specimens. The predictions by Eqs. (4.7) and (4.8) for SG specimens are insensitive to B/W for $a/W \ge 0.5$; for a given

$a/W < 0.5$, the value of $|e_1|$ associated with Eqs. (4.7) and (4.8) in general decreases as B/W increases.

The results shown in Tables 4.1 and 4.2 indicate that a given compliance equation typically provides accurate predictions of a/W or C for certain ranges of a/W and B/W. For example, Eqs. (4.4), (4.5a), (4.5b) and (4.6) lead to accurate predictions of a/W for specimens with $a/W \geq 0.5$ and $0.25 \leq B/W \leq 4$, and for specimens with $0.1 < a/W < 0.5$ and $B/W \leq 0.5$; the predictions of a/W by Eqs. (4.7) and (4.8) are accurate for specimens with $a/W < 0.5$ and $B/W \geq 1$, and Eq. (4.10) leads to accurate predictions of C for specimens with $a/W > 0.2$ and $B/W \leq 0.5$. However, there is a lack of a single compliance equation that can accurately predict a/W (or C) for the entire ranges of a/W and B/W considered. Such an equation is desirable as it will facilitate practice as well as standardization of the SE(T) specimen-based J-R curve testing. Detailed procedure to construct such an equation is presented in Section 4.4.2.

4.4.2   Crack Length/Compliance Modification Factors for SE(T) Specimens

To develop a single equation that can accurately predict a/W for all the specimen configurations considered in this study, we introduce the crack length modification factor, $\rho_{(a/W)}$, as follows to account for the inaccuracies (e.g. due to the 3D effects) associated with a given a/W-BCE equation:

$$\frac{a}{W} = \rho_{(a/W)} f\left(BCE\right) \tag{4.14}$$

where $f(BCE)$ is the right hand side of Eq. (4.4), (4.5a), (4.5b), (4.6), (4.7) or (4.8). The modification factor can also be interpreted as the model error associated with $f(BCE)$. The values of $\rho_{(a/W)}$ corresponding to a given equation among Eqs. (4.4) through (4.8) for all the PS and SG specimens considered in the FEA were computed as

$$\rho_{(a/W)} = \frac{\left(\dfrac{a}{W}\right)_{FEA}}{\left(\dfrac{a}{W}\right)_{p}} \tag{4.15}$$

The values of $\rho_{(a/W)}$ associated with Eqs. (4.4) through (4.8) for all the specimens are plotted in Fig. 4.3(a) through 4.3(f) as a function of a non-dimensional factor, ω, which is defined as

$$\omega = \frac{1}{1+\sqrt{WCE}} \qquad (4.16)$$

It follows that ω increases as a/W decreases and/or B/W increases (i.e. C decreases). Figure 4.3 indicates that $\rho_{(a/W)}$ generally increases as ω increases for Eqs. (4.4) – (4.6), which implies that these 2D-based equations become less and less adequate under the 3D condition as the specimen thickness increases and/or the crack length decreases. The value of $\rho_{(a/W)}$ is relatively insensitive to ω for Eqs. (4.7) and (4.8). The advantage of plotting $\rho_{(a/W)}$ vs. ω instead of plotting $\rho_{(a/W)}$ vs. u (as defined in Eq. (4.4b)) is evident from Figure 4.3 in that a single equation can be developed to fit all the data points shown in the individual figure, which correspond to both PS and SG specimens with various a/W and B/W ratios. In contrast, a single empirical equation of $\rho_{(a/W)}$ in terms of u cannot incorporate all the B/W values because the value of $\rho_{(a/W)}$ is relatively sensitive to B/W for a given a/W but the value of u is insensitive to B/W for a given a/W (note that BC = const. for a given a/W under the 2D condition).

Based on Fig. 4.3, $\rho_{(a/W)}$ is expressed as the following quadratic function of ω with the corresponding fitting coefficients evaluated using the least squares method:

$$\rho_{(a/W)} = R_0 + R_1\omega + R_2\omega^2 \qquad (4.17)$$

where the coefficients R_i (i = 1, 2 or 3) associated with Eqs. (4.4) through (4.8) are listed in Table 4.3. Note that for Eqs. (4.7) and (4.8), a linear fit is considered adequate; therefore, R_2 is set to zero for these two equations. Equation (4.17) is depicted by the solid lines in Fig. 4.4(a) through 4.4(f), whereby the fitting error is less than 5% for all the data points. With Eq. (4.17), the advantage of using $\rho_{(a/W)}$ (as opposed to, say, using E_e) to improve the accuracy of the predicted a/W is clear in that a single quadratic (or linear) function is

sufficient to evaluate all the $\rho_{(a/W)}$ values corresponding to a wide range of B/W ratios for both the PS and SG specimens.

A similar approach was used to improve the accuracy of the *BCE-a/W* equation by introducing the compliance modification factor, $\rho_{(BCE)}$, as follows:

$$BCE = \rho_{(BCE)} g\left(\frac{a}{W}\right) \tag{4.18}$$

Note that only $g(a/W)$ associated with Eq. (4.10) is considered in the modification as Eq. (4.10) is in general more accurate than Eqs. (4.9) and (4.11) as shown in Tables 4.1 and 4.2. Similar to the interpretation of $\rho_{(a/W)}$, $\rho_{(BCE)}$ can be considered the model error associated with Eq. (4.10). The values of $\rho_{(BCE)}$ corresponding to Eq. (4.10) for all the specimens were computed by

$$\rho_{(BCE)} = \frac{C_{FEA}}{C_p} \tag{4.19}$$

It is envisioned that $\rho_{(BCE)}$ depends on a/W and B/W such that the 2D-based Eq. (4.10) multiplied by $\rho_{(BCE)}$ becomes adequate for the 3D condition. Figure 4.4 shows the variation of $\rho_{(BCE)}$ with a non-dimensional factor, γ, which is defined through trial and error as:

$$\gamma = \left(\frac{a}{W}\right)^{1/\left(1+\sqrt{\frac{B}{W}}\right)} \tag{4.20}$$

Note that for SG specimens, the parameter B on the right hand side of Eq. (4.20) is replaced by $B_{e(1)}$ as defined in Eq. (4.12). The following quadratic equation was developed to fit the data points shown in Fig. 4.4:

$$\rho_{(BCE)} = 1.00353 - 0.12740\gamma + 0.18021\gamma^2 \tag{4.21}$$

The above equation is depicted by the solid line in Fig. 4.4, whereby the fitting error is less than 4% for all the data points.

4.4.3 Numerical validations of the proposed $\rho(a/W)$ and $\rho(BCE)$

To validate Eqs. (4.17) and (4.21), Eqs. (4.13a) and (4.13b) were used to calculate the prediction errors of Eqs. (4.4) through (4.8), and (4.10), whereby the predictions of these equations were multiplied by the corresponding $\rho_{(a/W)}$ and $\rho_{(BCE)}$ evaluated from Eqs. (4.17) and (4.21) respectively. Tables 4.4 and 4.5 summarize the corresponding errors of prediction for PS and SG specimens with different configurations. Additional finite element analyses including PS and SG specimens with $a/W = 0.15$ and 0.25 and $B/W = 0.25 – 4$ were carried out, and the errors of prediction for these specimens are also shown in Tables 4.4 and 4.5 (see the shaded area). The results indicate that using $\rho_{(a/W)}$ and $\rho_{(BCE)}$ combined with Eqs. (4.4) – (4.8) and (4.10) lead to highly accurate predictions of a/W and C for both the PS and SG specimens with all the a/W and B/W ratios considered. The corresponding errors of predictions are less than 2% for most of the specimens, and the maximum errors of prediction error associated with Eqs. (4.4), (4.5a), (4.5b), (4.6), (4.7) or (4.8) and (4.10) are 3.7, 4.8, 4.2, 4.2, 6.3, 4.6 and 4.2%, respectively. It is noted that the highest errors of prediction for Eqs. (4.4) – (4.8) and (4.10) are corresponding to the SG specimens with $a/W < 0.2$, which can be attributed to the relatively poor fitting of the data by Eqs. (4.17) and (4.21) corresponding to large ω and small γ values (i.e. small a/W) as shown in Figs. 4.3 and 4.4. Among the five equations for predicting a/W considered in this study, we recommend Eq. (4.6) in conjunction with the corresponding modification factor for practice given that the equation is relatively simple (a 6th-order polynomial) and applicable for a/W values ($0.1 \leq a/W \leq 0.9$) that are of practical relevance.

4.5 Summary and Conclusions

Three-dimensional linear-elastic finite element analyses of clamped single-edge tension (SE(T)) specimens were carried out to investigate the accuracy of compliance equations that are used to evaluate the crack length (a/W) and compliance (C) in the R-curve test. A wide range of specimen configurations including nine a/W ratios ranging from 0.1 to 0.9, and seven B/W ratios ranging from 0.25 to 4 were considered in this study. Both plane-sided and side-grooved specimens were included in the analysis, with the side-groove depth set at 7.5%B on each side. Key observations and findings are summarized in the following.

1) To predict a/W from a given compliance, Eqs. (4.4), (4.5) and (4.6) proposed by Cravero and Ruggieri, Shen et al. and John and Rigling respectively lead to similar predictions and are accurate for specimens with $a/W \geq 0.5$ and $0.25 \leq B/W \leq 4$, and for specimens $a/W < 0.5$ and $B/W \leq 0.5$. Equations (4.7) and (4.8) developed by Mathias et al. and Fonzo et al., respectively, are accurate for specimens with $a/W < 0.5$ and $B/W \geq 1$. The errors of prediction associated with these equations for the mentioned a/W and B/W ranges are generally less than 2-3%.

2) To predict C from a given a/W, Eq. (4.9) developed by Tada et al. is not adequate for specimens with $H/W = 10$ because it leads to large errors of prediction. Equation (4.10) developed by John and Rigling is accurate for specimen with $a/W > 0.2$ and $B/W \leq 0.5$ with the error of prediction generally being less than 2%.

3) The crack length modification factor, $\rho_{(a/W)}$, and compliance modification factor, $\rho_{(BCE)}$, are introduced to improve the accuracy of the predicted a/W and C, respectively. For a given equation among Eqs. (4.4) through (4.8), a single empirical equation was developed to evaluate the corresponding $\rho_{(a/W)}$ from a non-dimensional factor ω that is a function of WCE for both PS and SG specimens with all the a/W and B/W ratios considered in this study. Similarly, a single empirical equation was developed to evaluate $\rho_{(BCE)}$ associated with Eq. (4.10) from a non-dimensional factor γ that is a function of a/W and B/W. The single-equation evaluation of $\rho_{(a/W)}$ and $\rho_{(BCE)}$ greatly facilitates their application in practice.

4) Using the proposed modification factors in Eqs. (4.4) through (4.8) and (4.10) leads to consistently highly accurate predictions of a/W and C for all the specimen configurations considered in this study, with the errors of predictions being less than 2% in most cases. For practice, Eq. (4.6) along with the corresponding modification factor is recommended for predicting a/W considering its relative simplicity and wide range of applicability in terms of the a/W ratio.

References

ADINA (2012). *Theory and Modeling Guide*. ADINA R & D Inc., Watertown, MA.

ASTM (2013). *ASTM E1820-13: Standard Test Method for Measurement of Fracture Toughness*. America Society of Testing and Materials International, West Conshohocken, PA.

BSI (1997). *BS 7448-4: Method for determination of fracture resistance curves and initiation values for stable crack extension in metallic materials,* British Standard Institution, London.

Chiesa, M., Nyhus, B., Skallerud, B. and Thaulow, C. (2001). Efficient fracture assessment of pipelines: A constraint-corrected SENT specimen approach. *Engineering Fracture Mechanics*, 68:527-547.

Clarke, G. A., Andrews, W. R., Paris, P. C., Schmidt, D. W. (1976). Single Specimen Tests for J_{IC} Determination. *Mechanics of Crack Growth*, *ASTM STP 590. Philadelphia:* America Society of Testing and Materials International, 590, 27-42.

Clarke, G. A., Landes, J. D. (1979). Evaluation of the *J* integral for the Compact Specimen. *ASTM Journal of Testing and Eval*uation, 7:264-269.

Cravero, S. and Ruggieri, C. (2007). Estimation Procedure of J Resistance Curves for SE (T) Fracture Specimens Using Unloading Compliance. *Engineering Fracture Mechanics*, 74(17):2735-2757.

Det Norske Veritas. (2012). Submarine pipeline systems. DNV-OS-F101. Norway: DNV.

Donato, G. H. B. and Moreira, F. C. (2013). Effects of Side-Grooves and 3-D Geometries on Compliance Solutions and Crack Size Estimations Applicable to C(T), SE(B) and Clamped SE(T) Specimens. *ASME 2013 Pressure Vessels and Piping Conference: American Society of Mechanical Engineers*;. p. V06ATA019-V06AT06A.

Fonzo, A., Melis, G., Di, Vito L., Mannucci, G., Darcis, P., Richard, G., Quintanilla, H. and Armengol, M. (2009). Techniques for fracture toughness testing of offshore pipelines. *ASME 2009 28th International Conference on Ocean*, *Offshore and Arctic Engineering*: American Society of Mechanical Engineers. p. 249-257.

John, R., Kaldon, S. G., Johnson, D. A. and Coker, D. (1985). Weight function for a single edge cracked geometry with clamped ends. *International Journal of Fracture*, 72:145-158.

John, R. and Rigling, B. (1998). Effect of height to width ratio on *K* and *CMOD* solutions for a single edge cracked geometry with clamped ends. *Engineering fracture mechanics*, 60(2):147-156.

Johnson, H. (1965). Calibrating the electric potential method for studying slow crack growth(Calibration of electric potential technique to study slow or steady crack growth in high strength materials). *Materials Research and Standards*, 5:442-445.

Jones, I. (1998). A wide range weight function for a single edge cracked geometry with clamped ends. *International Journal of Fracture*, 89:1-18.

Marschall, C., Held, P., Landow, M. and Mincer, P. (1990). Use of the direct-current electric potential method to monitor large amounts of crack growth in highly ductile metals. *ASTM special technical publication*, 581-593.

Mathias, L. L., Sarzosa, D. F. and Ruggieri, C. (2013). Effects of specimen geometry and loading mode on crack growth resistance curves of a high-strength pipeline girth weld. *International Journal of Pressure Vessels and Piping*, 111:106-119.

Schwalbe, K-H. and Hellmann, D. (1981). Application of the electrical potential method to crack length measurements using Johnson's formula. *ASTM Journal of Testing and Eval*uation, 9:218-220.

Shen, G., Bouchard, R., Gianetto, J. A. and Tyson, W. R. (2008). Fracture toughness evaluation of high strength steel pipe. *ASME Conference Proceedings*, 1275-82.

Shen, G., Gianetto, J. A, and Tyson, W. R. (2008). Report 2008-18(TR): Development of procedure for low-constraint toughness testing using a single-specimen technique. Ottawa, Canada: CANMET-MTL.

Shen, G. and Tyson, W. R. (2009). Crack size evaluation using unloading compliance in single-specimen single-edge-notched tension fracture toughness testing. *ASTM Journal of Testing and Evaluation*, 37:347-357.

Shen, G., Tyson, W. R., Gianetto, J. A. and Park, D-Y. (2010). Effect of side grooves on compliance, *J*-Integral and constraint of a clamped SE(T) specimen. *ASME Conference Proceedings*. 81-9.

Tada, H., Paris, P. C. and Irwin, G. R. (1973). *The Stress Analysis of Cracks Handbook.* Del Research Corporation, Hellertown, PA.

Tang, H., Macia, M., Minnaar, K., Gioielli, P., Kibey, S. and Fairchild, D. (2010). Development of the SENT test for strain-based design of welded pipelines. *ASME Conference Proceedings*, 303-312.

Tyson, B., Ding, P. and Wang, X. (2014). Elastic compliance of single-edge-notched tension SE(T) (or SENT) specimens. *Fracture and Structural Integrity*, 95-100.

Wang, E. (2015). A study on CMOD-based compliance calibration functions for clamped single-edge tension specimens. *ASTM Journal of Testing and Eval*uation, 43(3):711-715.

Wang, E. and Omiya, M. (2015). Finite element analysis of crack mouth opening displacement compliance in crack length evaluation for clamped single edge tension specimens. *Fatigue and Fracture of Engineering Materials and Structures*, 38(3):315-329.

Wang, Y., Liu, M., Song, Y. (2011). Second generation models for strain-based design. 3801 Kirby Drive, Suite 520, Houston, Texas, US 77098: Center for Reliable Energy Systems.

Zhu, X. K., Leis, B. N. and Joyce, J. A. (2008). Experimental Estimation of J-R Curves From Load-CMOD Record for SE(B) Specimens. *Journal of ASTM International*, 5:231–245.

Table 4.1: Prediction errors of different compliance equations for plane-sided specimens.

(a) e_1 (%) for Eqs. (4.4) – (4.8)

a/W	B/W	C&R Eq. (4.4)	S&T Eq. (4.5a)	Eq. (4.5b)	J&R Eq. (4.6)	Mathias al. Eq. (4.7)	Fonzo al. Eq. (4.8)	a/W	B/W	C&R Eq. (4.4)	S&T Eq. (4.5a)	Eq. (4.5b)	J&R Eq. (4.6)	Mathias al. Eq. (4.7)	Fonzo al. Eq. (4.8)
	1/4	-1.5	-0.3	-0.3	-0.4	2.1	0.4		1/4	0.2	-0.3	-0.3	-0.4	4.7	3.6
	1/3	-1.6	-0.3	-0.3	-0.4	2.1	0.3		1/3	-0.4	-0.9	-0.9	-1.0	4.1	3.1
	1/2	-1.6	-0.4	-0.4	-0.5	2.1	0.3		1/2	-0.2	-0.7	-0.7	-0.8	4.3	3.3
0.9	1	-1.6	-0.4	-0.4	-0.5	2.0	0.3	0.4	1	-1.2	-1.7	-1.7	-1.8	3.3	2.6
	2	-1.7	-0.5	-0.5	-0.6	2.0	0.2		2	-2.5	-3.0	-3.0	-3.1	2.0	1.7
	3	-1.8	-0.7	-0.7	-0.8	1.8	0.1		3	-2.9	-3.5	-3.4	-3.6	1.5	1.4
	4	-2.0	-0.8	-0.8	-0.9	1.7	-0.1		4	-3.1	-3.6	-3.6	-3.7	1.3	1.2
	1/4	-0.1	-0.2	-0.2	0.1	3.0	2.1		1/4	0.1	-1.1	-1.0	-0.7	5.1	5.3
	1/3	-0.1	-0.3	-0.3	0.1	2.9	2.0		1/3	-0.7	-1.8	-1.8	-1.5	4.3	4.5
	1/2	-0.2	-0.4	-0.4	0.0	2.8	1.9		1/2	-0.4	-1.6	-1.5	-1.2	4.6	4.8
0.8	1	-0.4	-0.6	-0.6	-0.2	2.6	1.8	0.3	1	-2.0	-3.2	-3.1	-2.8	3.0	3.2
	2	-0.5	-0.7	-0.7	-0.3	2.5	1.7		2	-3.7	-4.9	-4.8	-4.5	1.2	1.4
	3	-0.7	-0.9	-0.9	-0.5	2.3	1.5		3	-4.2	-5.4	-5.3	-5.0	0.7	0.9
	4	-0.8	-1.0	-1.0	-0.6	2.2	1.4		4	-4.4	-5.5	-5.5	-5.1	0.5	0.8
	1/4	0.3	-0.6	-0.6	-0.6	3.1	2.8		1/4	-0.3	-0.7	-0.8	-0.4	6.5	6.3
	1/3	0.2	-0.7	-0.7	-0.6	3.0	2.7		1/3	-1.3	-1.7	-1.8	-1.4	5.4	5.2
	1/2	0.1	-0.8	-0.8	-0.8	2.8	2.6		1/2	-1.4	-1.7	-1.9	-1.4	5.4	5.2
0.7	1	-0.2	-1.2	-1.2	-1.1	2.5	2.3	0.2	1	-3.8	-4.0	-4.2	-3.8	3.0	2.7
	2	-0.5	-1.5	-1.4	-1.4	2.2	2.0		2	-5.7	-5.8	-5.9	-5.6	1.2	0.7
	3	-0.7	-1.6	-1.6	-1.6	2.0	1.8		3	-6.0	-6.1	-6.3	-6.0	0.8	0.4
	4	-0.8	-1.8	-1.8	-1.8	1.9	1.7		4	-6.1	-6.2	-6.4	-6.1	0.7	0.3
	1/4	0.3	-0.5	-0.5	-0.5	3.4	3.2		1/4	-1.6	-2.9	-2.4	-2.6	9.2	6.9
	1/3	0.2	-0.6	-0.6	-0.6	3.3	3.1		1/3	-3.6	-5.2	-4.6	-4.7	6.8	4.8
	1/2	0.0	-0.8	-0.8	-0.8	3.1	2.9		1/2	-4.5	-6.1	-5.5	-5.5	5.7	4.0
0.6	1	-0.5	-1.3	-1.3	-1.3	2.6	2.4	0.1	1	-7.1	-9.1	-8.3	-8.3	2.3	1.3
	2	-1.0	-1.8	-1.8	-1.8	2.1	1.9		2	-8.2	-10.4	-9.5	-9.4	0.9	0.1
	3	-1.3	-2.1	-2.0	-2.0	1.8	1.6		3	-8.3	-10.6	-9.7	-9.6	0.7	0.0
	4	-1.4	-2.2	-2.2	-2.2	1.7	1.5		4	-8.2	-10.4	-9.5	-9.4	0.9	0.1
	1/4	0.2	-0.2	-0.2	-0.2	4.0	3.6								
	1/3	0.1	-0.3	-0.3	-0.3	3.9	3.5								
	1/2	-0.1	-0.5	-0.5	-0.5	3.7	3.3								
0.5	1	-0.8	-1.2	-1.2	-1.2	3.0	2.6								
	2	-1.6	-2.0	-2.0	-2.1	2.2	1.7								
	3	-2.0	-2.4	-2.4	-2.4	1.8	1.4								
	4	-2.1	-2.5	-2.5	-2.6	1.7	1.2								

(b) e_2 (%) for Eqs. (4.9) – (4.11)

a/W	B/W	Tada al. Eq. (4.9)	J&R Eq. (4.10)	Eq. (4.11a)	Wang Eq. (4.11b)	Eq. (4.11c)	a/W	B/W	Tada al. Eq. (4.9)	J&R Eq. (4.10)	Eq. (4.11a)	Wang Eq. (4.11b)	Eq. (4.11c)
	1/4	1402.3	-1.0	-5.3	6.9	-10.5		1/4	31.2	0.6	-9.2	-8.4	-8.5
	1/3	1403.9	-0.9	-5.2	7.0	-10.4		1/3	31.6	0.9	-9.0	-8.2	-8.3
	1/2	1405.7	-0.8	-5.1	7.1	-10.3		1/2	32.2	1.4	-8.5	-7.7	-7.8
0.9	1	1408.1	-0.6	-4.9	7.3	-10.1	0.4	1	35.0	3.5	-6.6	-5.8	-5.9
	2	1413.0	-0.3	-4.6	7.7	-9.8		2	38.6	6.3	-4.1	-3.3	-3.3
	3	1421.0	0.2	-4.1	8.2	-9.3		3	39.9	7.3	-3.2	-2.4	-2.4
	4	1430.1	0.8	-3.5	8.9	-8.8		4	40.4	7.7	-2.9	-2.0	-2.1
	1/4	355.3	-1.0	-9.1	-7.5	-8.4		1/4	20.0	0.6	-9.0	-7.3	-7.3
	1/3	356.5	-0.7	-8.9	-7.2	-8.2		1/3	20.3	0.8	-8.8	-7.1	-7.1
	1/2	358.3	-0.3	-8.5	-6.8	-7.8		1/2	21.0	1.5	-8.2	-6.5	-6.5
0.8	1	360.9	0.2	-8.0	-6.3	-7.3	0.3	1	24.2	4.1	-5.8	-4.1	-4.1
	2	363.2	0.7	-7.5	-5.9	-6.8		2	27.9	7.2	-3.0	-1.2	-1.2
	3	365.5	1.2	-7.1	-5.4	-6.4		3	29.0	8.1	-2.2	-0.4	-0.4
	4	368.0	1.8	-6.6	-4.9	-5.9		4	29.3	8.4	-2.0	-0.2	-0.1
	1/4	155.7	0.1	-10.0	-7.2	-7.2		1/4	12.9	2.1	-9.2	-8.2	-8.2
	1/3	156.5	0.4	-9.7	-6.9	-7.0		1/3	14.2	3.2	-8.8	-7.8	-7.9
	1/2	157.9	1.0	-9.2	-6.4	-6.5		1/2	16.4	5.2	-7.8	-6.8	-6.9
0.7	1	160.7	2.1	-8.2	-5.4	-5.4	0.2	1	19.7	8.3	-4.8	-3.7	-3.8
	2	163.3	3.1	-7.3	-4.5	-4.5		2	21.2	9.6	-2.3	-1.2	-1.3
	3	164.8	3.7	-6.8	-3.9	-3.9		3	21.4	9.7	-1.8	-0.7	-0.8
	4	166.1	4.2	-6.3	-3.4	-3.5		4	21.2	9.6	-1.7	-0.6	-0.7
	1/4	84.1	0.7	-9.9	-7.5	-7.5		1/4	12.6	1.1	-6.6	-6.1	-6.3
	1/3	84.6	1.0	-9.6	-7.2	-7.3		1/3	16.8	1.0	-5.5	-5.1	-5.2
	1/2	85.7	1.6	-9.1	-6.7	-6.8		1/2	15.1	3.3	-3.7	-3.2	-3.4
0.6	1	88.4	3.1	-7.8	-5.3	-5.4	0.1	1	19.0	6.8	-0.9	-0.4	-0.6
	2	91.4	4.7	-6.3	-3.8	-3.9		2	21.4	9.0	0.3	0.8	0.6
	3	92.8	5.5	-5.6	-3.1	-3.2		3	21.8	9.4	0.4	0.9	0.7
	4	93.7	5.9	-5.2	-2.7	-2.8		4	21.8	9.3	0.3	0.8	0.6
	1/4	50.1	0.8	-9.6	-8.5	-8.6							
	1/3	50.5	1.0	-9.3	-8.2	-8.3							
	1/2	51.3	1.6	-8.9	-7.8	-7.8							
0.5	1	54.0	3.4	-7.3	-6.1	-6.2							
	2	57.3	5.6	-5.2	-4.1	-4.2							
	3	58.7	6.5	-4.4	-3.3	-3.3							
	4	59.3	7.0	-4.0	-2.9	-2.9							

Table 4.2: Prediction errors of different compliance equations for side-grooved specimens.

(a) e_1 (%) for Eqs. (4.4) – (4.8)

		e_1								e_1				
a/W	B/W	C&R	S&T		J&R	Mathias al.	Fonzo al.	a/W	B/W	C&R	S&T		J&R	Mathias al.	Fonzo al.
		Eq. (4.4)	Eq. (4.5a)	Eq. (4.5b)	Eq. (4.6)	Eq. (4.7)	Eq. (4.8)			Eq. (4.4)	Eq. (4.5a)	Eq. (4.5b)	Eq. (4.6)	Eq. (4.7)	Eq. (4.8)
	1/4	-1.7	-0.6	-0.6	-0.7	1.9	0.1		1/4	0.0	-0.6	-0.5	-0.7	4.4	4.1
	1/3	-1.7	-0.6	-0.6	-0.7	1.9	0.2		1/3	0.0	-0.6	-0.5	-0.7	4.5	4.1
	1/2	-1.7	-0.5	-0.5	-0.6	2.0	0.2		1/2	0.0	-0.5	-0.5	-0.6	4.5	4.1
0.9	1	-1.6	-0.4	-0.4	-0.5	2.0	0.3	0.4	1	-0.6	-1.2	-1.2	-1.3	3.8	3.5
	2	-1.6	-0.4	-0.4	-0.5	2.1	0.3		2	-1.4	-2.0	-1.9	-2.1	3.0	2.7
	3	-1.7	-0.5	-0.5	-0.6	2.0	0.2		3	-1.6	-2.2	-2.1	-2.2	2.8	2.5
	4	-1.8	-0.6	-0.6	-0.7	1.9	0.1		4	-1.7	-2.3	-2.2	-2.4	2.7	2.4
	1/4	-0.3	-0.5	-0.5	-0.1	2.7	1.9		1/4	-0.2	-1.3	-1.3	-1.0	4.8	5.0
	1/3	-0.3	-0.5	-0.5	-0.1	2.7	1.9		1/3	-0.2	-1.3	-1.3	-1.0	4.8	5.0
	1/2	-0.3	-0.5	-0.5	-0.1	2.7	1.9		1/2	-0.3	-1.4	-1.4	-1.1	4.7	4.9
0.8	1	-0.2	-0.4	-0.4	0.0	2.8	2.0	0.3	1	-1.6	-2.8	-2.7	-2.4	3.4	3.6
	2	-0.1	-0.3	-0.3	0.1	2.9	2.1		2	-2.9	-4.1	-4.1	-3.7	2.0	2.2
	3	-0.2	-0.3	-0.3	0.1	2.9	2.0		3	-3.2	-4.4	-4.3	-4.0	1.7	1.9
	4	-0.2	-0.4	-0.4	0.0	2.8	1.9		4	-3.3	-4.5	-4.4	-4.1	1.6	1.8
	1/4	0.1	-0.8	-0.8	-0.8	2.9	2.6		1/4	-0.5	-0.9	-1.0	-0.5	6.3	6.1
	1/3	0.1	-0.8	-0.8	-0.8	2.8	2.6		1/3	-0.7	-1.0	-1.2	-0.7	6.1	5.9
	1/2	0.1	-0.8	-0.8	-0.8	2.8	2.6		1/2	-1.3	-1.6	-1.8	-1.3	5.5	5.3
0.7	1	0.1	-0.9	-0.8	-0.8	2.8	2.6	0.2	1	-3.8	-4.0	-4.2	-3.8	3.0	2.6
	2	0.1	-0.8	-0.8	-0.8	2.9	2.6		2	-5.5	-5.6	-5.8	-5.4	1.4	1.0
	3	0.1	-0.8	-0.8	-0.8	2.9	2.6		3	-5.6	-5.7	-5.8	-5.5	1.3	0.9
	4	0.1	-0.9	-0.9	-0.8	2.8	2.6		4	-5.6	-5.7	-5.9	-5.5	1.2	0.8
	1/4	0.1	-0.8	-0.7	-0.8	3.2	3.0		1/4	-1.9	-3.3	-2.7	-2.9	8.8	6.6
	1/3	0.1	-0.8	-0.7	-0.8	3.2	2.9		1/3	-3.2	-4.7	-4.1	-4.2	7.3	5.3
	1/2	0.1	-0.7	-0.7	-0.7	3.2	3.0		1/2	-5.3	-7.1	-6.4	-6.4	4.6	3.1
0.6	1	0.0	-0.9	-0.8	-0.9	3.1	2.8	0.1	1	-8.6	-10.9	-10.0	-9.8	0.3	-0.3
	2	-0.1	-0.9	-0.9	-0.9	3.0	2.8		2	-9.1	-11.5	-10.6	-10.4	-0.4	-0.8
	3	-0.1	-1.0	-0.9	-1.0	3.0	2.7		3	-8.8	-11.1	-10.2	-10.1	0.1	-0.5
	4	-0.2	-1.0	-1.0	-1.0	2.9	2.7		4	-8.5	-10.8	-9.9	-9.8	0.4	-0.2
	1/4	0.0	-0.4	-0.4	-0.4	3.8	3.4								
	1/3	0.0	-0.4	-0.4	-0.4	3.8	3.4								
	1/2	0.1	-0.4	-0.4	-0.4	3.9	3.4								
0.5	1	-0.2	-0.7	-0.7	-0.7	3.6	3.1								
	2	-0.6	-1.0	-1.0	-1.0	3.2	2.8								
	3	-0.7	-1.1	-1.1	-1.1	3.1	2.7								
	4	-0.8	-1.2	-1.2	-1.2	3.0	2.6								

(b) e_2 (%) for Eqs. (4.9) – (4.11)

a/W	B/W	e_2 Tada al. Eq. (4.9)	J&R Eq. (4.10)	Wang Eq. (4.11a)	Eq. (4.11b)	Eq. (4.11c)
	1/4	1416.3	-0.1	-4.4	7.9	-9.6
	1/3	1415.7	-0.1	-4.4	7.8	-9.7
	1/2	1413.2	-0.3	-4.6	7.7	-9.8
0.9	1	1408.9	-0.6	-4.9	7.4	-10.1
	2	1407.1	-0.7	-5.0	7.2	-10.2
	3	1411.2	-0.4	-4.7	7.5	-9.9
	4	1417.3	0.0	-4.3	8.0	-9.6
	1/4	358.8	-0.2	-8.4	-6.7	-7.7
	1/3	359.0	-0.2	-8.4	-6.7	-7.7
	1/2	358.7	-0.2	-8.4	-6.8	-7.7
0.8	1	357.6	-0.5	-8.6	-7.0	-8.0
	2	356.2	-0.8	-8.9	-7.3	-8.2
	3	356.9	-0.7	-8.8	-7.1	-8.1
	4	358.4	-0.3	-8.5	-6.8	-7.8
	1/4	157.8	0.9	-9.2	-6.4	-6.5
	1/3	157.9	1.0	-9.2	-6.4	-6.5
	1/2	157.9	1.0	-9.2	-6.4	-6.5
0.7	1	158.0	1.0	-9.2	-6.4	-6.4
	2	157.5	0.8	-9.4	-6.6	-6.6
	3	157.6	0.8	-9.3	-6.5	-6.6
	4	158.1	1.1	-9.1	-6.3	-6.4
	1/4	85.3	1.4	-9.3	-6.9	-6.9
	1/3	85.3	1.4	-9.3	-6.9	-6.9
	1/2	85.2	1.3	-9.3	-6.9	-7.0
0.6	1	86.0	1.7	-9.0	-6.5	-6.6
	2	86.3	1.9	-8.8	-6.4	-6.4
	3	86.5	2.0	-8.7	-6.3	-6.4
	4	86.8	2.2	-8.6	-6.1	-6.2
	1/4	51.0	1.3	-9.1	-8.0	-8.1
	1/3	50.9	1.3	-9.1	-8.0	-8.1
	1/2	50.8	1.2	-9.2	-8.1	-8.2
0.5	1	52.0	2.0	-8.5	-7.4	-7.4
	2	53.2	2.9	-7.7	-6.6	-6.7
	3	53.6	3.1	-7.5	-6.4	-6.4
	4	53.9	3.3	-7.3	-6.2	-6.2

a/W	B/W	e_2 Tada al. Eq. (4.9)	J&R Eq. (4.10)	Wang Eq. (4.11a)	Eq. (4.11b)	Eq. (4.11c)
	1/4	31.9	1.1	-8.8	-8.0	-8.0
	1/3	31.8	1.1	-8.8	-8.0	-8.1
	1/2	31.8	1.0	-8.8	-8.1	-8.1
0.4	1	33.5	2.4	-7.6	-6.8	-6.9
	2	35.7	4.0	-6.1	-5.3	-5.4
	3	36.2	4.5	-5.8	-5.0	-5.0
	4	36.5	4.7	-5.6	-4.8	-4.8
	1/4	20.5	1.0	-8.6	-6.9	-6.9
	1/3	20.5	1.0	-8.6	-6.9	-6.9
	1/2	20.7	1.2	-8.5	-6.8	-6.8
0.3	1	23.4	3.5	-6.4	-4.7	-4.7
	2	26.2	5.8	-4.3	-2.5	-2.5
	3	26.8	6.3	-3.9	-2.1	-2.1
	4	27.0	6.5	-3.7	-1.9	-1.9
	1/4	13.3	2.4	-9.0	-7.9	-8.0
	1/3	14.8	3.8	-8.7	-7.7	-7.8
	1/2	17.4	6.2	-8.0	-6.9	-7.0
0.2	1	21.7	10.1	-4.7	-3.7	-3.7
	2	22.4	10.7	-2.6	-1.5	-1.6
	3	22.0	10.3	-2.5	-1.4	-1.4
	4	21.6	10.0	-2.4	-1.3	-1.4
	1/4	12.9	1.3	-6.3	-5.8	-6.0
	1/3	17.0	1.2	-5.0	-4.6	-4.7
	1/2	15.4	3.6	-2.8	-2.3	-2.5
0.1	1	20.0	7.7	0.7	1.2	1.0
	2	22.0	9.5	1.3	1.8	1.6
	3	21.9	9.4	1.0	1.5	1.3
	4	21.7	9.3	0.7	1.1	1.0

Table 4.3: Fitting coefficients R_i in Eq. (4.17).

	Eq. (4.4)	Eq. (4.5a)	Eq. (4.5b)	Eq. (4.6)	Eq. (4.7)	Eq. (4.8)
R_0	1.01593	1.01353	1.01178	1.01105	0.96352	0.97098
R_1	-0.13845	-0.11444	-0.09813	-0.09618	0.02381	0.01728
R_2	0.36030	0.36850	0.33481	0.32747	0	0

Table 4.4: Prediction error (%) of Eqs. (4.4) – (4.8) and (4.10) for plane-sided specimen using $\rho_{(a/W)}$ and $\rho_{(BCE)}$.

				e_1				e_2					e_1				e_2
a/W	B/W	C&R	S&T		J&R	Mathias al.	Fonzo al.	J&R	a/W	B/W	C&R	S&T		J&R	Mathias al.	Fonzo al.	J&R
		Eq. (4.4)	Eq. (4.5a)	Eq. (4.5b)	Eq. (4.6)	Eq. (4.7)	Eq. (4.8)	Eq. (4.10)			Eq. (4.4)	Eq. (4.5a)	Eq. (4.5b)	Eq. (4.6)	Eq. (4.7)	Eq. (4.8)	Eq. (4.10)
0.9	1/4	-0.7	0.4	0.4	0.2	-1.4	-2.4	2.5	0.3	1/4	0.4	-0.4	-0.3	-0.1	1.9	2.7	-1.7
	1/3	-0.8	0.3	0.3	0.1	-1.4	-2.4	2.0		1/3	0.4	-0.3	-0.2	0.0	1.8	2.6	-2.0
	1/2	-1.0	0.2	0.2	0.0	-1.4	-2.4	1.3		1/2	0.3	-0.3	-0.2	0.0	1.5	2.3	-2.2
	1	-1.2	0.1	0.0	-0.1	-1.4	-2.4	0.1		1	-0.3	-0.7	-0.7	-0.5	0.2	0.9	-0.8
	2	-1.4	0.0	0.0	-0.2	-1.3	-2.4	-1.0		2	-0.6	-0.8	-0.9	-0.7	-1.4	-0.7	1.0
	3	-1.6	-0.1	-0.1	-0.3	-1.4	-2.5	-1.2		3	0.0	-0.1	-0.2	0.0	-1.7	-1.1	1.3
	4	-1.7	-0.2	-0.1	-0.3	-1.5	-2.6	-1.2		4	0.7	0.8	0.5	0.7	-1.8	-1.2	1.2
0.8	1/4	0.6	0.4	0.4	0.7	-0.6	-0.7	1.2	0.25	1/4	0.4	-0.4	-0.3	0.2	2.2	3.2	-1.7
	1/3	0.5	0.3	0.2	0.6	-0.6	-0.8	0.9		1/3	-0.3	-0.9	-0.9	-0.4	1.5	2.4	-2.0
	1/2	0.2	0.1	0.1	0.4	-0.7	-0.8	0.6		1/2	0.2	-0.3	-0.3	0.2	1.7	2.6	-2.0
	1	-0.1	-0.1	-0.1	0.2	-0.8	-0.9	-0.1		1	-0.6	-0.8	-0.9	-0.4	0.0	0.8	-0.4
	2	-0.3	-0.2	-0.2	0.2	-0.8	-0.9	-0.8		2	-0.8	-0.8	-1.0	-0.5	-1.7	-0.9	1.3
	3	-0.3	-0.2	-0.1	0.2	-0.8	-1.0	-1.0		3	-0.1	0.1	-0.2	0.3	-2.0	-1.3	1.4
	4	-0.3	-0.1	-0.1	0.2	-0.9	-1.1	-1.0		4	0.7	1.1	0.7	1.1	-2.0	-1.4	1.2
0.7	1/4	0.9	0.0	-0.1	-0.1	-0.4	0.0	1.0	0.2	1/4	0.4	0.5	0.4	0.8	3.3	3.8	-1.5
	1/3	0.7	-0.2	-0.2	-0.2	-0.5	0.0	0.8		1/3	0.3	0.6	0.5	0.8	3.1	3.5	-1.8
	1/2	0.4	-0.4	-0.4	-0.4	-0.6	-0.1	0.7		1/2	0.1	0.5	0.3	0.7	2.5	2.8	-1.6
	1	0.0	-0.7	-0.6	-0.7	-0.8	-0.4	0.7		1	-1.0	-0.1	-0.5	-0.2	0.4	0.5	0.3
	2	-0.2	-0.7	-0.7	-0.7	-0.9	-0.6	0.6		2	-1.0	0.2	-0.3	-0.1	-1.2	-1.2	1.6
	3	-0.1	-0.6	-0.5	-0.6	-1.0	-0.7	0.5		3	0.0	1.3	0.7	0.9	-1.4	-1.5	1.5
	4	0.0	-0.4	-0.4	-0.4	-1.0	-0.7	0.5		4	0.9	2.3	1.6	1.8	-1.4	-1.5	1.2
0.6	1/4	0.7	-0.1	0.0	-0.1	-0.1	0.4	0.6	0.15	1/4	0.7	2.4	2.0	1.6	6.1	4.6	-1.3
	1/3	0.6	-0.2	-0.2	-0.2	-0.1	0.3	0.3		1/3	0.6	2.4	1.9	1.5	5.6	4.1	-1.3
	1/2	0.3	-0.4	-0.3	-0.4	-0.2	0.2	0.3		1/2	0.0	2.0	1.5	1.0	4.6	2.9	-0.8
	1	-0.2	-0.7	-0.6	-0.7	-0.6	-0.2	0.7		1	-1.0	1.3	0.6	0.0	2.2	0.3	1.0
	2	-0.4	-0.7	-0.6	-0.7	-0.9	-0.6	1.2		2	-0.5	2.1	1.2	0.5	0.8	-1.2	1.7
	3	-0.2	-0.4	-0.4	-0.5	-1.1	-0.7	1.4		3	0.5	3.3	2.4	1.6	0.7	-1.4	1.3
	4	0.0	0.0	0.0	-0.2	-1.1	-0.8	1.4		4	1.6	4.5	3.5	2.7	0.8	-1.3	0.8
0.5	1/4	0.6	0.3	0.3	0.2	0.6	0.9	-0.3	0.1	1/4	0.0	-0.4	0.0	-0.3	6.3	4.5	-0.1
	1/3	0.4	0.2	0.2	0.1	0.6	0.8	-0.6		1/3	-0.5	-1.0	-0.5	-0.8	5.1	3.5	0.3
	1/2	0.2	0.1	0.1	0.0	0.5	0.7	-0.7		1/2	-1.3	-2.0	-1.5	-1.7	3.0	1.8	1.2
	1	-0.3	-0.2	-0.2	-0.3	-0.1	0.1	0.0		1	-2.0	-2.9	-2.4	-2.5	0.0	-0.7	2.4
	2	-0.5	-0.2	-0.2	-0.4	-0.7	-0.6	1.2		2	-0.9	-1.8	-1.3	-1.4	-1.2	-1.6	2.1
	3	-0.2	0.2	0.2	0.0	-0.9	-0.9	1.5		3	0.4	-0.4	-0.1	-0.2	-1.3	-1.7	1.4
	4	0.2	0.7	0.6	0.5	-1.0	-0.9	1.6		4	1.6	0.8	1.1	1.0	-1.0	-1.5	0.7
0.4	1/4	0.5	0.2	0.2	0.0	1.4	1.6	-1.2									
	1/3	0.4	0.2	0.2	0.0	1.3	1.6	-1.5									
	1/2	0.2	0.1	0.2	0.0	1.1	1.4	-1.7									
	1	-0.2	-0.2	-0.2	-0.4	0.3	0.5	-0.7									
	2	-0.5	-0.2	-0.3	-0.5	-0.7	-0.6	1.0									
	3	-0.1	0.3	0.2	0.0	-1.1	-0.9	1.4									
	4	0.5	1.0	0.8	0.6	-1.2	-1.0	1.4									

Table 4.5: Prediction error (%) of Eqs. (4.4) – (4.8) and (4.10) for side-grooved specimen using $\rho_{(a/W)}$ and $\rho_{(BCE)}$.

				e_1				e_2
a/W	B/W	C&R	S&T		J&R	Mathias al.	Fonzo al.	J&R
		Eq. (4.4)	Eq. (4.5a)	Eq. (4.5b)	Eq. (4.6)	Eq. (4.7)	Eq. (4.8)	Eq. (4.10)
	1/4	-0.9	0.2	0.1	-0.1	-1.6	-2.6	3.5
	1/3	-1.0	0.1	0.1	-0.1	-1.6	-2.6	2.8
	1/2	-1.1	0.1	0.0	-0.1	-1.5	-2.6	1.8
0.9	1	-1.2	0.1	0.0	-0.1	-1.4	-2.4	0.2
	2	-1.3	0.1	0.1	-0.1	-1.2	-2.3	-1.3
	3	-1.4	0.1	0.1	-0.1	-1.2	-2.3	-1.8
	4	-1.5	0.1	0.1	-0.1	-1.3	-2.4	-2.0
	1/4	0.4	0.2	0.1	0.5	-0.8	-0.9	2.0
	1/3	0.3	0.1	0.1	0.4	-0.8	-0.9	1.5
	1/2	0.2	0.1	0.0	0.4	-0.7	-0.8	0.7
0.8	1	0.1	0.1	0.1	0.4	-0.6	-0.7	-0.8
	2	0.1	0.2	0.3	0.6	-0.4	-0.5	-2.3
	3	0.2	0.4	0.4	0.7	-0.3	-0.5	-2.8
	4	0.2	0.5	0.5	0.8	-0.3	-0.6	-3.0
	1/4	0.7	-0.3	-0.3	-0.3	-0.7	-0.2	1.9
	1/3	0.6	-0.3	-0.3	-0.4	-0.6	-0.2	1.4
	1/2	0.5	-0.4	-0.4	-0.4	-0.6	-0.1	0.7
0.7	1	0.3	-0.4	-0.3	-0.4	-0.5	-0.1	-0.3
	2	0.5	-0.1	0.0	-0.1	-0.3	0.1	-1.6
	3	0.7	0.2	0.3	0.2	-0.2	0.1	-2.2
	4	0.8	0.5	0.5	0.4	-0.2	0.1	-2.4
	1/4	0.5	-0.3	-0.3	-0.3	-0.3	0.2	1.3
	1/3	0.4	-0.3	-0.3	-0.4	-0.2	0.2	0.8
	1/2	0.4	-0.3	-0.2	-0.3	-0.2	0.3	0.1
0.6	1	0.3	-0.2	-0.2	-0.3	-0.2	0.2	-0.6
	2	0.5	0.2	0.2	0.1	-0.1	0.3	-1.4
	3	0.9	0.6	0.7	0.6	0.0	0.4	-1.9
	4	1.2	1.1	1.1	0.9	0.0	0.4	-2.1
	1/4	0.3	0.0	0.1	0.0	0.4	0.7	0.3
	1/3	0.3	0.1	0.1	0.0	0.5	0.7	-0.2
	1/2	0.3	0.2	0.2	0.1	0.6	0.8	-1.0
0.5	1	0.2	0.3	0.3	0.2	0.4	0.6	-1.3
	2	0.5	0.8	0.8	0.6	0.3	0.4	-1.4
	3	1.0	1.4	1.4	1.2	0.3	0.4	-1.7
	4	1.5	2.0	1.9	1.7	0.3	0.4	-1.8
	1/4	0.2	-0.1	0.0	-0.2	1.1	1.4	-0.7
	1/3	0.3	0.0	0.1	-0.1	1.2	1.5	-1.2
	1/2	0.4	0.3	0.3	0.1	1.3	1.5	-2.0
0.4	1	0.3	0.3	0.3	0.1	0.9	1.0	-1.8
	2	0.5	0.8	0.7	0.5	0.3	0.4	-1.1
	3	1.1	1.6	1.5	1.2	0.2	0.3	-1.3
	4	1.7	2.3	2.1	1.9	0.2	0.3	-1.4

				e_1				e_2
a/W	B/W	C&R	S&T		J&R	Mathias al.	Fonzo al.	J&R
		Eq. (4.4)	Eq. (4.5a)	Eq. (4.5b)	Eq. (4.6)	Eq. (4.7)	Eq. (4.8)	Eq. (4.10)
	1/4	0.2	-0.6	-0.5	-0.3	1.6	2.4	-1.3
	1/3	0.3	-0.4	-0.4	-0.1	1.7	2.5	-1.8
	1/2	0.5	-0.2	-0.1	0.1	1.7	2.4	-2.4
0.3	1	0.0	-0.4	-0.4	-0.2	0.5	1.3	-1.4
	2	0.1	-0.1	-0.2	0.0	-0.6	0.1	-0.3
	3	0.9	0.9	0.7	0.9	-0.7	-0.1	-0.4
	4	1.7	1.7	1.5	1.7	-0.8	-0.1	-0.5
	1/4	0.1	-0.6	-0.6	-0.1	2.0	3.0	-1.3
	1/3	0.3	-0.4	-0.3	0.2	2.0	3.0	-1.8
	1/2	0.4	-0.1	-0.1	0.4	1.9	2.8	-2.3
0.25	1	-0.4	-0.6	-0.7	-0.2	0.2	1.1	-0.8
	2	-0.3	-0.3	-0.5	0.0	-1.1	-0.4	0.5
	3	0.7	0.9	0.6	1.0	-1.2	-0.5	0.2
	4	1.5	1.8	1.4	1.8	-1.2	-0.5	0.0
	1/4	0.2	0.3	0.2	0.6	3.2	3.6	-1.2
	1/3	0.3	0.5	0.4	0.7	3.1	3.5	-1.6
	1/2	0.1	0.6	0.4	0.7	2.6	2.9	-1.6
0.2	1	-1.1	-0.2	-0.6	-0.3	0.3	0.5	0.4
	2	-0.8	0.3	-0.1	0.0	-1.0	-1.0	1.4
	3	0.4	1.7	1.1	1.3	-1.0	-1.0	0.9
	4	1.3	2.8	2.1	2.2	-0.9	-1.0	0.5
	1/4	0.5	2.2	1.8	1.4	5.9	4.4	-1.0
	1/3	0.3	2.2	1.7	1.3	5.4	3.9	-1.1
	1/2	-0.3	1.7	1.2	0.7	4.3	2.6	-0.4
0.15	1	-1.8	0.5	-0.1	-0.7	1.5	-0.4	2.0
	2	-1.0	1.6	0.8	0.0	0.5	-1.6	2.2
	3	0.4	3.2	2.2	1.5	0.6	-1.5	1.4
	4	1.6	4.5	3.4	2.6	0.8	-1.3	0.8
	1/4	-0.3	-0.8	-0.4	-0.7	5.9	4.2	0.3
	1/3	-1.0	-1.6	-1.1	-1.4	4.5	3.0	0.9
	1/2	-2.2	-3.1	-2.5	-2.7	2.0	1.0	2.2
0.1	1	-3.7	-4.8	-4.2	-4.2	-2.0	-2.2	4.2
	2	-2.0	-3.0	-2.5	-2.5	-2.5	-2.6	3.2
	3	-0.2	-1.1	-0.7	-0.8	-1.9	-2.2	2.0
	4	1.1	0.3	0.6	0.5	-1.5	-1.9	1.1

Figure 4.1: Typical *P-CMOD* curve with unloading-reloading sequences

(a) Configuration of a typical side-grooved FE model with *a/W* = 0.5 and *B/W* = 1

(b) Configuration of the U-shape side groove

(c) Sharp crack tip for linear-elastic analyses
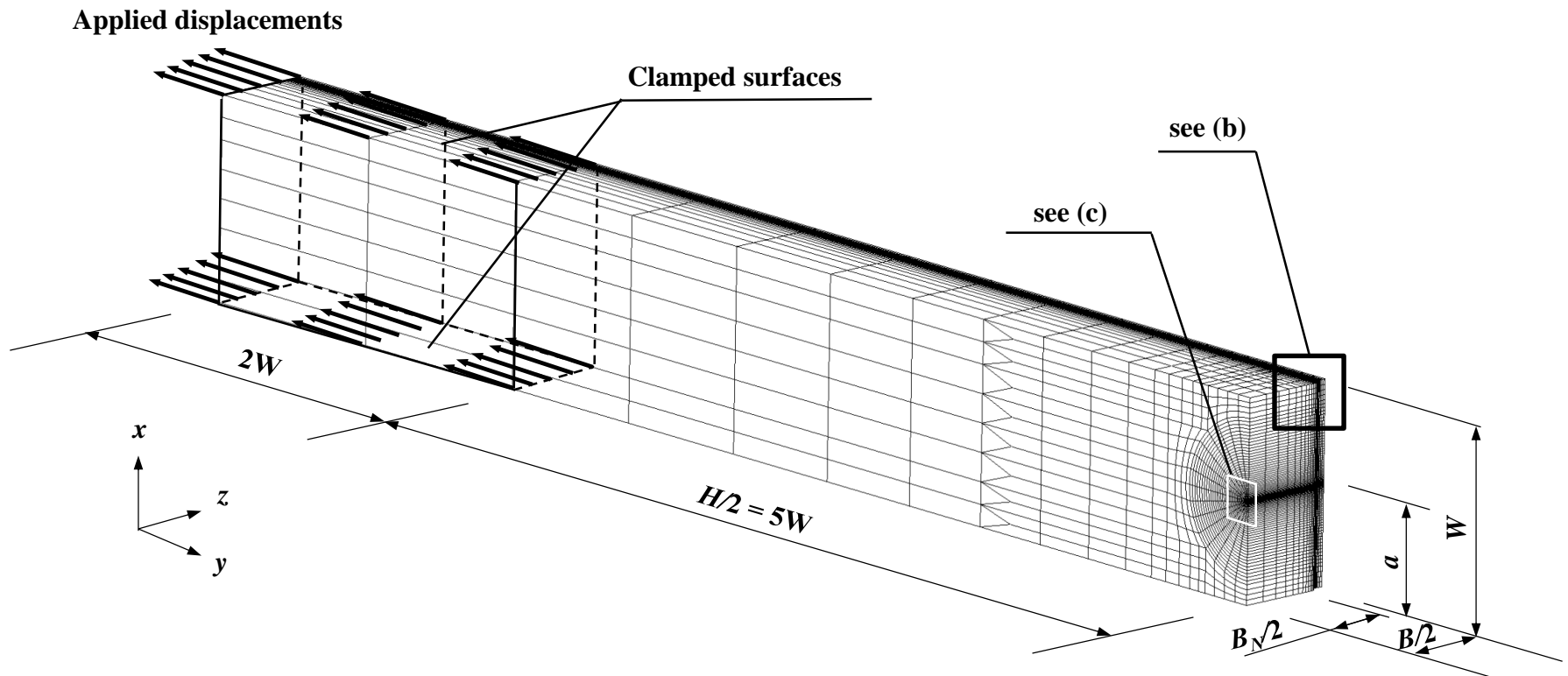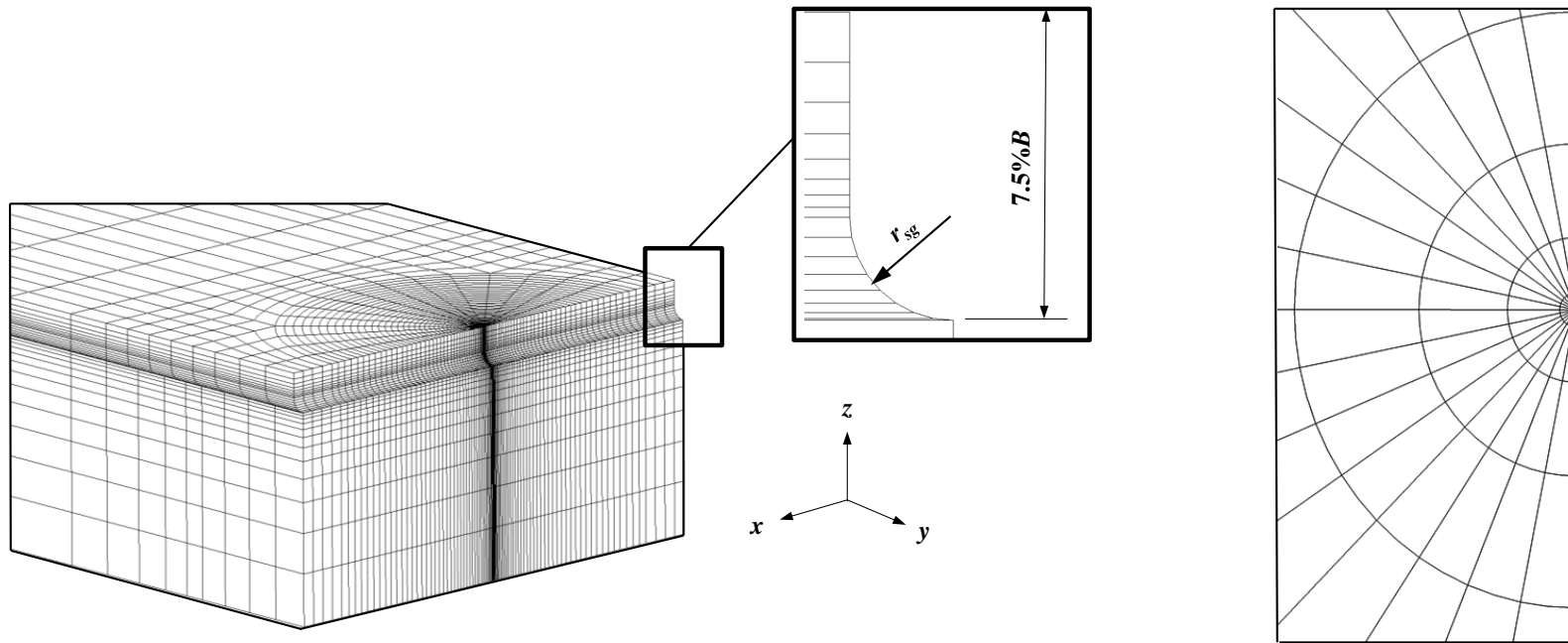
Figure 4.2: Configuration and meshing of a typical finite element model
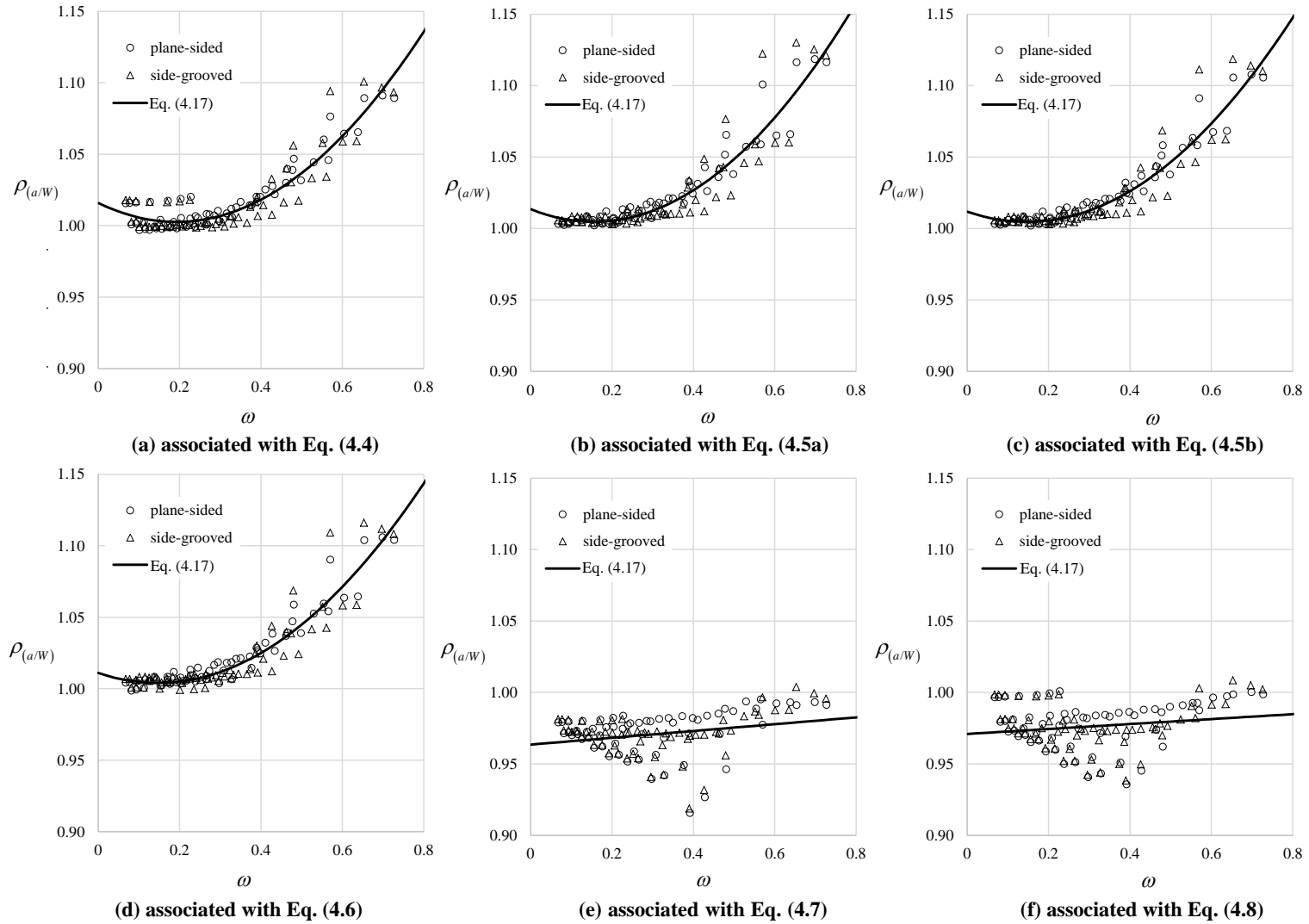
Figure 4.3: $\rho_{(a/W)}$ as functions of ω for plane-sided and side-grooved clamped SE(T) specimens

Figure 4.4: $\rho_{(BCE)}$ associated with Eq. (4.10) as functions of γ for plane-sided and side-grooved clamped SE(T) specimens

Chapter 5 Effects of Crack Front Curvature on *J-R* Curve Testing Using Clamped SE(T) Specimens of Homogeneous Materials

5.1 Background and Objective

5.1.1 Introduction

Testing on plane-sided (PS) SE(B) and C(T) specimens made of homogeneous materials generally leads to a thumbnail-shaped crack front and shear failur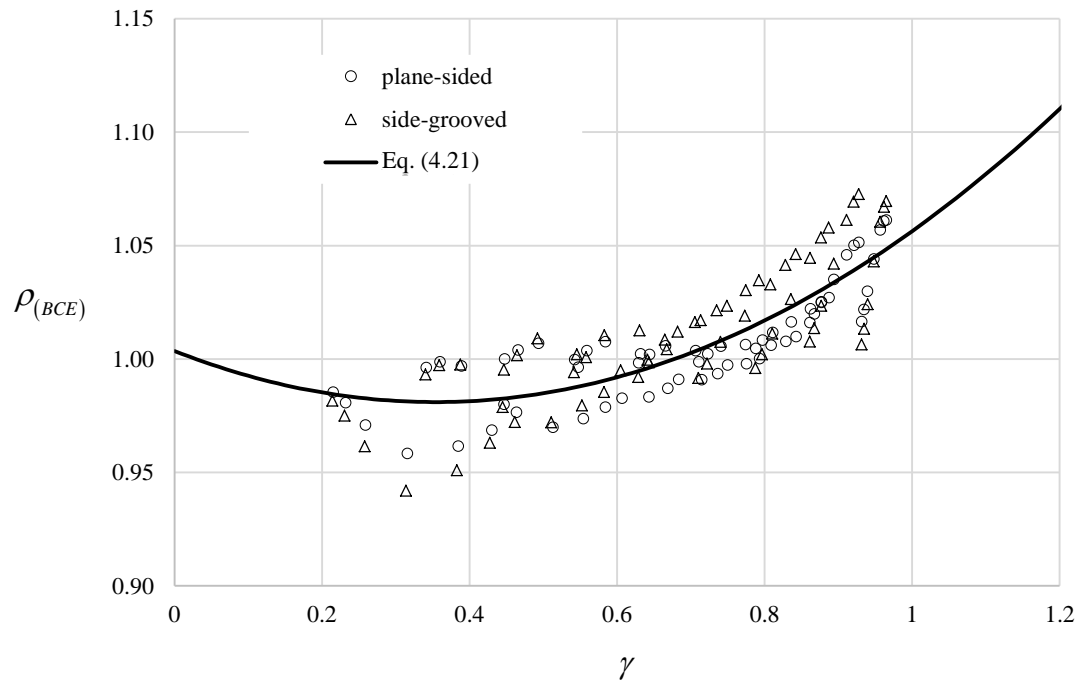e of the trailing edge (Shih et al., 1977). These phenomena are caused by the difference in the states of stress along the crack front. At the region near the center of the PS specimen, the stress state is close to the plane-strain condition with high stress triaxiality, which promotes a relatively fast crack growth. On the other hand, the stress state near the side surface is close to the plane-stress condition with low stress triaxiality, therefore causing relatively slow crack growth and the shear lips near the free surface (Anderson, 2005). Numerical and experimental studies concerning the impact of the crack front curvature on the elastic compliance and crack driving forces (i.e. the *J*-integral (*J*) and the crack tip opening displacement (*CTOD*)) associated with the SE(B) and C(T) specimens are well reported in the literature (e.g. Steenkamp, 1988; Crouch, 1991; Nikishkov et al., 1999; Zhou and Soboyejo, 2002; Zuo et al., 2008; Hutchison and Pisarski, 2013; Yan and Zhou, 2014, 2015). These studies reveal that the compliance, *J* and *CTOD* values evaluated by assuming a straight crack front in the SE(B) and C(T) specimens may involve large errors if the actual crack front is curved. To ensure the accuracy of the experimentally determined *J*(*CTOD*)-*R* curve, testing standards (e.g. ASTM, 2013; BSI, 1997b) usually specify acceptable levels of the crack front curvature for both the fatigue pre-crack and final crack fronts for the SE(B) and C(T) specimens.

5.1.2 Review of the Standard Requirements on Crack Front Curvature for SE(B) and C(T) Specimens

In this section, the crack front straightness criteria for the SE(B) and C(T) specimens prescribed in BS 7448: Part I (BSI, 1991), Part II (BSI, 1997a), Part III (BSI, 2005) and

Part IV (BSI, 1997b), ISO 12135 (ISO, 2002) and 15653 (ISO, 2010) and ASTM E1820-13 (ASTM, 2013) are reviewed. BS 7448: Part I provides a method for determining the plane-strain fracture toughness (K_{IC}), critical J and critical $CTOD$ for specimens made of the base metal (BM); Part II is applicable to fracture toughness testing for specimens containing the weld metal (WM) and heat-affected zone (HAZ); Part III deals with the dynamic fracture toughness for specimens containing BM or WM, and Part IV provides a test method for evaluating the R-curve for specimens containing BM or WM. ISO 12135 (ISO, 2002) has a similar scope as the ASTM E1820 but is only applicable to specimens made of homogeneous materials. In 2010, BS 7448: Part II was withdrawn and replaced by ISO 15653 (ISO, 2010), which deals with the testing method for specimens containing WM and HAZ and complements ISO 12135. ASTM E1820-13 (ASTM, 2013) covers testing methods for determining the critical J, critical $CTOD$ and R-curve, and is considered applicable to specimens of homogeneous materials. A brief summary of the applicability of the aforementioned standards is given in Table 5.1.

Figure 5.1 shows a cross section of a typical test specimen with a straight machined notch and two curved crack fronts caused by fatigue pre-cracking and stable tearing. The aforementioned standards (BSI, 1991, 1997a, 1997b, 2005; ISO, 2002, 2010; ASTM, 2013) adopt the nine-point measurement approach to determine the initial and final average crack length, a_{ave9}. The nine points (see Fig. 5.1) are equally spaced along the specimen thickness (z direction) with the two end points (i.e. points (1) and (9)) being a certain distance (Λ) away from the specimen side surfaces. BS 7448 and the two ISO standards (BSI, 1991, 1997a, 1997b, 2005; ISO, 2002, 2010) specify the two end points at $0.01B$ from the side surfaces, whereas ASTM E1820-13 (ASTM, 2013) specifies the two end points at $0.005W$ from the side surfaces. In all of the seven standards reviewed, a_{ave9} is defined by

$$a_{ave9} = \frac{1}{8}\left(\frac{a_{(1)} + a_{(9)}}{2} + \sum_{i=2}^{8} a_{(i)}\right) \qquad (5.1)$$

where $a_{(i)}$ ($i = 1, 2, \ldots, 9$) denote the crack lengths corresponding to the nine measurement points.

The straightness requirements for the fatigue pre-crack front in the above-mentioned standards are reviewed first. BS 7448: Part I specifies the following crack front straightness requirement:

$$a_{\max 9} - a_{\min 9} \leq 0.1 a_{ave9} \tag{5.2}$$

where a_{max9} and a_{min9} are the maximum and minimum values of the crack lengths at the nine measurement points. For simplicity of the discussions presented in the following sections, a crack front shape parameter β_9 is defined here as $\beta_9 = (a_{max9} - a_{min9})/W$. It follows that Eq. (5.2) can be expressed as $\beta_9 \leq 0.1 a_{ave9}/W$.

The crack front straightness criterion in BS 7448: Part II is given by

$$a_{\max 7} - a_{\min 7} \leq 0.2 a_{ave9} \tag{5.3}$$

where a_{max7} and a_{min7} are the maximum and minimum values of crack lengths measured at the seven inner points along the specimen thickness (i.e. points (2) through (8) in Fig. 5.1). By introducing a shape parameter $\beta_7 = (a_{max7} - a_{min7})/W$, Eq. (5.3) is recast as $\beta_7 \leq 0.2 a_{ave9}/W$.

BS 7448: Part III specifies Eq. (5.2) as the crack front straightness criterion for specimens of BM, and the following equation for specimens containing WM and HAZ:

$$\beta_9 \leq 0.2 \frac{a_{ave9}}{W} \tag{5.4}$$

BS 7448: Part IV specifies that the difference between a_{ave9} and any of the nine crack length measurements not exceed $0.1 a_{ave9}$ for specimens made of BM, and $0.2 a_{ave9}$ for specimens containing WM and HAZ; that is,

$$\begin{cases} \mathrm{Max}\left[a_{\max 9} - a_{ave9}, a_{ave9} - a_{\min 9}\right] \leq 0.1 a_{ave9} & \text{, for BM} \qquad \text{(a)} \\ \mathrm{Max}\left[a_{\max 9} - a_{ave9}, a_{ave9} - a_{\min 9}\right] \leq 0.2 a_{ave9} & \text{, for WM and HAZ} \quad \text{(b)} \end{cases} \tag{5.5}$$

Let $\lambda_{9(\mathrm{BS})} = \mathrm{Max}[a_{max9} - a_{ave9}, a_{ave9} - a_{min9}]/W$. The above criteria are then $\lambda_{9(\mathrm{BS})} \leq 0.1 a_{ave9}/W$ for BM and $\lambda_{9(\mathrm{BS})} \leq 0.2 a_{ave9}/W$ for WM and HAZ.

ISO 12135 requires that the difference between a_{ave9} and any of the inner seven crack length measurements not exceed $0.1a_{ave9}$ for specimens made of BM, whereas ISO 15653 suggests that the fatigue pre-crack front straightness requirement defined in ISO 12135 be relaxed to $0.2a_{ave9}$ for the *CTOD* and *J* tests using SE(B) specimens. By introducing a shape parameter $\lambda_7 = \text{Max}[a_{max7} - a_{ave9}, a_{ave9} - a_{min7}]/W$ these two criteria are given by

$$
\begin{cases}
\lambda_7 \leq 0.1 \dfrac{a_{ave9}}{W} & \text{, for BM} \qquad\qquad (a) \\[2ex]
\lambda_7 \leq 0.2 \dfrac{a_{ave9}}{W} & \text{, for WM and HAZ} \quad (b)
\end{cases}
\qquad (5.6)
$$

The crack front straightness criterion specified in ASTM E1820-13 is different from those in the other standards considered in this study in that the former is expressed in terms of the specimen thickness (B) as opposed to the average crack length a_{ave9}. Letting $\lambda_{9(ASTM)}$ be defined as $\lambda_{9(ASTM)} = \text{Max}[a_{max9} - a_{ave9}, a_{ave9} - a_{min9}]/W$, the ASTM crack front straightness criterion is expressed as

$$
\lambda_{9(ASTM)} \leq 0.05 \frac{B}{W} \qquad (5.7)
$$

Note that although the expressions for $\lambda_{9(BS)}$ and $\lambda_{9(ASTM)}$ are the same, these two parameters are different because the locations of the nine measurement points are defined differently in BS 7448 and ASTM E1820. The crack front straightness criteria given by Eqs. (5.2) through (5.7) are summarized in Table 5.1.

For the *R*-curve measurement, additional requirements need to be satisfied for the final crack front straightness and/or uniformity of the crack extension. BS 7448: Part IV specifies that the difference between maximum and minimum values of crack extension measured at the nine points shall not exceed 20% of the mean crack extension or 0.15 mm, whichever is greater; ISO 12135 requires that the shape of the final crack front should also satisfy Eq. (5.6a); ASTM E1820 adopts Eq. (5.7) to control the final crack front straightness and requires none of the nine measurements of the crack extension shall be less than 50% of the average crack extension. Because the numerical analyses carried out in the present study do not involve growing crack, we focused on the straightness

requirement for both initial and final crack fronts. The uniformity of the crack extension is beyond the scope of this study.

5.1.3 Requirements on Crack Front Curvature for SE(T) Specimens

Malpas et al. (2012) conducted three-dimensional (3D) finite element analyses (FEA) to investigate the impact of the crack front curvature on the estimated J and $CTOD$ for SE(T) specimens with the average crack length (a_{ave}) over specimen width (W) ratio equal to 0.3 and the thickness-over-width ratio (B/W) equal to 2. Five crack front curvatures corresponding to five fatigue pre-crack straightness requirements for SE(B) and C(T) specimens specified in BS7448 (Parts I, II and IV) (BSI, 1991, 1997a, 1997b), ISO12135 (ISO, 2002) and ASTM E1820 (ASTM, 2013) were considered in their study. Based on the FEA results, the authors suggested that the crack front straightness requirements defined in BS 7448 Part IV be used for SE(T) specimens made of homogeneous (i.e. base metal only) or inhomogeneous (i.e. base metal and weld) materials, albeit with the allowable curvature increased to 20% from 10% as specified in BS 7448 Part IV. This criterion was considered the optimal choice because it led to the acceptance of over 70% of the welded specimens and over 90% of the base metal specimens based on the authors' experimental data, while the predictive errors for $CTOD$ and J caused by the crack front curvature were less than 10 and 13%, respectively.

5.1.4 Objective and Approach

It is noted that study by Malpas et al. (2012) is focused on SE(T) specimens with a_{ave}/W = 0.3 and B/W = 2. For specimens with other values of a_{ave}/W and B/W, the impact of the crack front curvature on the evaluation of J and $CTOD$ is unclear. Furthermore, to our knowledge, the impact of the crack front curvature on the compliance of the SE(T) specimen and rotation correction factor (see Appendix C) for the compliance measured from the UC method have not been studied. Motivated by these observations, a 3D FEA-based investigation of the impact of the crack front curvature on J, the compliance and rotation correction factor for SE(T) specimens with wide ranges of a_{ave}/W and B/W were carried out. The focus of the present study is the clamped SE(T) specimen with H/W = 10

because the crack-tip stress fields of such a specimen correspond closely to those of the full-scale pipes containing circumferential cracks (Shen et al., 2008), which are of primary concern to the strain-based design of pipelines. Only specimens made of the base metal are considered in the present study. We carried out both linear-elastic and elastic-plastic 3D finite element analyses of plane-sided clamped SE(T) specimens with a_{ave}/W ranging from 0.2 to 0.7 and B/W ranging from 0.5 to 2. Based on the results of the investigation, a set of crack front straightness criteria were proposed to strike a balance between the accuracy of the R curve testing and specimen acceptance rate.

The rest of this chapter is structured as follows. Section 5.2 describes the characterization of the curved crack front employed in this study. Section 5.3 describes the configurations of the FE models, material properties and computational procedures involved in the present study. In Section 5.4, the impact of the crack front curvature on the compliance, J and the rotation correction factor are investigated. The proposed crack front straightness criteria for the SE(T) specimen are presented in Section 5.5, followed by conclusions in Section 5.6.

5.2   Characteristics of Curved Crack Front

Previous studies (Nikishkov, 1999; Yan and Zhou, 2015) indicated that curved crack fronts in specimens made of homogeneous materials are typically symmetric about the mid-plane. Therefore, a symmetric curved crack front was assumed in the present study, and the power-law function suggested by Nikishkov et al. (Nikishkov, 1999) was adopted to characterize both initial and final crack fronts:

$$\begin{cases} a_z = a_{z=0} - \beta W \left(\dfrac{2|z|}{B} \right)^p \\ \beta = \dfrac{a_{z=0} - a_{z=\pm B/2}}{W} \end{cases} \tag{5.8}$$

where z ($-B/2 \leq z \leq B/2$) is the coordinate in the specimen thickness direction; a_z is the crack length at the location of coordinate z; $a_{z=0}$ and $a_{z=\pm B/2}$ denote the crack lengths at the mid-plane and free surfaces of the specimen, respectively, and β and p ($p > 1$) are

parameters characterizing the curvature of the crack front. By examining the fatigue pre-crack fronts of a series of plane-sided C(T), SE(B) and SE(T) specimens, Nikishkov et al. (1999) and Yan and Zhou (2015) showed that the parameter p in Eq. (5.8) can be adequately set to a fixed value of 3.0 for different curved crack fronts. For the present study, it is more convenient to express Eq. (5.8) in terms of the average crack length, a_{ave}, instead of $a_{z=0}$. The relationship between a_{ave} and $a_{z=0}$ can be derived as follows:

$$a_{ave} = \frac{\int_0^{\frac{B}{2}} a_z dz}{\left(\frac{B}{2}\right)} = a_{z=0} - \frac{\int_0^{\frac{B}{2}} \beta W \left(\frac{2z}{B}\right)^p dz}{\left(\frac{B}{2}\right)} = a_{z=0} - \frac{\beta W}{p+1} \qquad (5.9)$$

Let $\lambda = \dfrac{a_{ave} - a_{z=\pm B/2}}{W}$. Note that $\lambda = 0$ corresponds to a straight crack front. The relationship between λ and β is then given by

$$\lambda = \frac{a_{ave} - a_{z=\pm B/2}}{W} = \frac{1}{W}\left(a_{z=0} - \frac{\beta W}{p+1} - a_{z=\pm B/2}\right) = \frac{1}{W}\left(\beta W - \frac{\beta W}{p+1}\right) = \frac{\beta p}{p+1} \quad (5.10)$$

For the crack front characterized by Eq. (5.8), it follows that

$$\begin{cases} a_{ave9} = a_{ave} + q_1 \lambda W & \text{(a)} \\[2mm] q_1 = \dfrac{1}{p} - \dfrac{p+1}{p}\left(0.25 - \dfrac{\Lambda}{2B}\right)^p \left[\dfrac{1}{8}\sum_{i=1}^{8}\left[abs\left(i-5\right)^p\right]\right] & \text{(b)} \end{cases} \qquad (5.11)$$

where $\Lambda = 0.005W$ and $0.01B$ for the ASTM and BS (ISO) standards, respectively. The shape parameters associated with Eqs. (5.2) through (5.7) can be expressed in terms of λ as follows:

$$\begin{cases} \beta_7 = \dfrac{p+1}{p}(0.735)^p \, \lambda & \text{(a)} \\[2mm] \beta_9 = \dfrac{p+1}{p}(0.98)^p \, \lambda & \text{(b)} \\[2mm] \lambda_7 = \dfrac{p+1}{p}(0.245)^p \left[\dfrac{1}{8}\sum_{i=1}^{8}\left[abs(i-5)^p \right] \right] \lambda & \text{(c)} \\[2mm] \lambda_{9(BS)} = \dfrac{p+1}{p}(0.245)^p \left[4^p - \dfrac{1}{8}\sum_{i=1}^{8}\left[abs(i-5)^p \right] \right] \lambda & \text{(d)} \\[2mm] \lambda_{9(ASTM)} = \dfrac{p+1}{p}\left(0.25 - \dfrac{0.005W}{2B} \right)^p \left[4^p - \dfrac{1}{8}\sum_{i=1}^{8}\left[abs(i-5)^p \right] \right] \lambda & \text{(e)} \end{cases} \qquad (5.12)$$

Detailed derivations of Eqs. (5.11) and (5.12) are provided in Appendix D. Equation (5.12) can be written in a generic form: $\kappa = q_2\lambda$, where κ equals either β_7, β_9, λ_7, $\lambda_{9(BS)}$ or $\lambda_{9(ASTM)}$, and q_2 represents the right hand side of Eqs. (5.12a), (5.12b), (5.12c), (5.12d) or (5.12e) but without λ. The values of q_1 in Eq. (5.11a) and q_2 corresponding to different p values are listed in Table 5.2. The table indicates that for $p = 2.5 - 3.5$, a_{ave9}/W is very close to a_{ave}/W, with the maximum difference equal to $1.8\%\lambda$. For parameters β_7, β_9 and λ_7, q_2 is sensitive to p as the maximum difference between q_2 corresponding to different p is about $10 - 32\%$. On the other hand, q_2 is insensitive to p for $\lambda_{9(BS)}$, $\lambda_{9(ASTM)}$ as the difference of q_2 corresponding to different p is within 2.5%. For a crack front with $p = 3.0$, Eqs. (5.11) and (5.12) are then simplified as the following:

$$\begin{cases} a_{ave9} = \begin{cases} a_{ave} - \left(5.5\times10^{-6}\right)\lambda W & \text{, for BS and ISO standards} \\[2mm] a_{ave} + \lambda W\left(\dfrac{1}{3}\right)\left[1 - 68\left(0.25 - \dfrac{0.005W}{2B} \right)^3 \right] & \text{, for ASTM standard} \end{cases} & \text{(a)} \\[4mm] \beta_7 = 0.5294\lambda & \text{(b)} \\ \beta_9 = 1.2549\lambda & \text{(c)} \\ \lambda_7 = 0.3333\lambda & \text{(d)} \\ \lambda_{9(BS)} = 0.9216\lambda & \text{(e)} \\[2mm] \lambda_{9(ASTM)} = 62.6667\left(0.25 - \dfrac{0.005W}{2B} \right)^3 \lambda & \text{(f)} \end{cases}$$

$$(5.13)$$

Given Eq. (5.13), the crack front straightness criteria specified in the BS, ISO and ASTM standards can be recast in terms of λ and a_{ave}:

$$
\begin{cases}
\lambda \leq 0.0797 \dfrac{a_{ave}}{W} & \text{,for BS7448-I (BM)} & \text{(a)} \\[2mm]
\lambda \leq 0.3778 \dfrac{a_{ave}}{W} & \text{,for BS7448-II (WM and HAZ)} & \text{(b)} \\[2mm]
\lambda \leq 0.1594 \dfrac{a_{ave}}{W} & \text{,for BS7448-III (WM and HAZ)} & \text{(c)} \\[2mm]
\lambda \leq 0.1085 \dfrac{a_{ave}}{W} & \text{,for BS7448-IV (BM)} & \text{(d)} \\[2mm]
\lambda \leq 0.2170 \dfrac{a_{ave}}{W} & \text{,for BS7448-IV (WM and HAZ)} & \text{(e)} \\[2mm]
\lambda \leq 0.3000 \dfrac{a_{ave}}{W} & \text{,for ISO12135 (BM)} & \text{(f)} \\[2mm]
\lambda \leq 0.6000 \dfrac{a_{ave}}{W} & \text{,for ISO15653 (WM and HAZ)} & \text{(g)} \\[2mm]
\lambda \leq \begin{cases} 0.0271 & \text{,for } B/W = 0.5 \\ 0.0526 & \text{,for } B/W = 1 \\ 0.1037 & \text{,for } B/W = 2 \end{cases} \text{,for ASTM E1820 (BM)} & & \text{(h)}
\end{cases}
\tag{5.14}
$$

Note that the allowable λ suggested in the BS 7448 and ISO standards depends only on a_{ave}/W with Eqs. (5.14a) and (5.14g) giving the most and least stringent crack front straightness criteria, respectively. On the other hand, the allowable λ defined in the ASTM standard is a function of B/W and increases with B/W.

5.3 Numerical Analyses

Three groups of FE models, namely Groups 1 to 3, were analyzed to evaluate the crack mouth opening displacement (*CMOD*) compliance (C_0), J and rotation correction factors (F_r), respectively. Detailed information about these FE models is summarized in Table 5.3. Linear-elastic analyses of 198 SE(T) models in Group 1 were performed to evaluate C_0, whereas the elastic-plastic analyses of 198 models in Group 2 and 36 models in Group 3 were carried out to evaluate J and F_r, respectively. For Group 2 (3), the J_2 incremental theory of plasticity and small- (large-) displacement small- (large-) strain formulation (ADINA, 2012) was employed in FEA. The true stress (σ) and true strain (ε) relationship

employed in the elastic-plastic FEA follows the Ramberg-Osgood law (i.e. Eq. (1.18)) where σ_0 is the reference stress and typically set equal to the yield strength (σ_{YS}); ε_0 ($\varepsilon_0 = \sigma_{YS}/E$) denotes the yield strain, and α and n are parameters of the Ramberg-Osgood relationship with n commonly known as the strain hardening exponent. In this study, materials with $\sigma_{YS} = 576$ MPa, $E = 207$ GPa, $v = 0.3$, $\alpha = 0.704$ and $n = 13.3$ were selected to simulate the X80 (API, 2012) grade pipeline steel (Leis et al., 2009). The corresponding ultimate tensile strength σ_{UTS} equals 675 MPa. The limit load for the SE(T) specimen, P_Y, is defined as $B(W - a_{ave})(\sigma_{YS} + \sigma_{UTS})/2$ (Shen et al., 2008; Shen and Tyson, 2009).

Three-dimensional models of plane-sided SE(T) specimens with clamped ends were prepared for FEA. As listed in Table 5.3, the analysis matrices in both Group 1 (G1) and Group 2 (G2) include specimens with six different a_{ave}/W ratios ($a_{ave}/W = 0.2, 0.3, 0.4, 0.5, 0.6$ and 0.7), three B/W ratios ($B/W = 0.5, 1$ and 2) and eleven λ values ($\lambda = 0, 0.01, 0.02, 0.03, 0.04, 0.05, 0.06, 0.07, 0.08, 0.09$ and 0.1); Group 3 (G3) is the same as G1 and G2 except that only two λ values ($\lambda = 0$ and 0.1) are considered. Stationary cracks were assumed in all the analyses. All the specimens have the same width ($W = 20$ mm) and daylight length ($H/W = 10$). Only a quarter of the specimen with appropriate constraints imposed on the remaining ligament was modelled due to symmetry. A typical FE model with $a_{ave}/W = 0.5$, $\lambda = 0.1$ and $B/W = 1$ is schematically shown in Fig. 5.2(a) together with the fixation and loading conditions.

The FEA code ADINA® (ADINA, 2012) was employed to analyze all the models. A typical quarter-symmetric 3D model has 10 layers over the half thickness ($B/2$). The thickness of each layer was arranged such that the corresponding mesh density increases from the mid-plane to the free surface to capture the high stress gradient at these locations (see Fig. 5.2(b)). The 20-node 3D brick elements with $3\times3\times3$ integration were adopted in the linear-elastic analysis, whereas the 8-node 3D brick elements with $2\times2\times2$ integration were adopted in the elastic-plastic analysis to improve the computational efficiency; the accuracy of using such elements to calculate J has been shown to be adequate (Kulka and Sherry, 2012).

For models in Groups 1 and 2, a sharp crack tip was incorporated, and the surfaces of the brick elements were collapsed to a line at the crack tip (see Fig. 5.2(c)) to simulate the singularity condition. For models in Group 3 (i.e. large-strain analysis), a blunt crack tip with a radius (ρ_0) of 2.5 μm (see Fig. 5.2(d)) was incorporated in the FE model to facilitate convergence (Hutchinson, 1983). It is reported in (Shen et al., 2008; Shen and Tyson, 2009) that a blunt crack tip with a radius of such size has no impact on the evaluated compliance. A spider-web mesh around the crack tip was established with 45 concentric semicircles (i.e. rings) surrounding the crack tip. All of the FE models have 45 focused rings around the crack tip with 16 elements in each ring. The minimum in-plane dimension of the first ring (i.e. closest to the crack tip) is about $0.1\rho_0$ (Graba and Galkiewicz, 2007), whereas the corresponding in-plane dimension of the elements in the 45th ring is about 2,000 times that of the element in the first ring (Gullerud et al., 2001). The total number of elements is approximately 12,000 in a typical specimen.

The load was applied based on the displacement-controlled condition. Uniform displacements (h) were applied on two lateral surfaces that are considered as the clamped surfaces with a length of $2W$ (see Fig. 5.2(a)). Evaluation of the compliance requires computation of the load-displacement, i.e. P-$CMOD$, response in the FEA. The load P was calculated as the total reactions of the nodes on the clamped surface while $CMOD$ (V) was recorded at the mid-plane of the specimen. The compliance of the undeformed specimen (C_0) is calculated as V/P from one loading step that corresponds to an applied displacement of 2 μm.

A final applied displacement corresponding to $h/a_{ave} = 0.3$ for models in Group 2 was reached in 500 increments for specimens with $a_{ave}/W > 0.2$. For specimens with $a_{ave}/W = 0.2$, the final applied displacement was set to $h/a_{ave} = 0.5$. The maximum applied displacement corresponds approximately to a loading level of $1.3P_Y$. The values of J in each layer along the thickness direction, i.e. the local J values, were calculated using the virtual crack extension method (Anderson, 2005; ADINA, 2012). A brief description of this method is included in Appendix B. The weighted average J value over the entire crack front, J_{ave}, is then calculated based on the trapezoidal rule as detailed in Section 2.2.3. To ensure the path-independence of the calculated J values, the two outermost semicircular

rings surrounding the crack tip were used to define the virtual shifts (Anderson, 2005; ADINA, 2012). For a representative specimen with $a/W = 0.5$, $B/W = 1$ and $\lambda = 0.1$, the difference between J_{ave} corresponding to the 20th and 45th ring is about 3.6%, and the difference between J_{ave} corresponding to the 40th and 45th rings is about 0.7% at the loading level of $P/P_Y = 1.3$.

For models in Group 3, the final applied displacements corresponding to loading levels of $1.2 - 1.3P_Y$ were reached with $6 - 18$ loading-unloading-reloading sequences. Within each sequence, the magnitude of the unloading is 0.01 mm (approximately corresponding to $0.05P_Y$). The compliance of the deformed specimen (C_i) was determined by linear regression of the unloading-reloading ΔP vs. ΔV data, and the corresponding rotation correction factor ($F_{r(FEA)}$) was calculated as

$$F_{r(FEA)} = \frac{C_0}{C_i} \tag{5.15}$$

5.4   Effects of Crack Front Curvature on *J-R* Curve

5.4.1   Effect of Crack Front Curvature on Compliance

For specimens with the same a_{ave}/W and B/W ratios, the *CMOD* compliance corresponding to a curved crack front, C_0, was compared with that corresponding to a straight crack front, $C_{0(\lambda=0)}$. The difference between C_0 and $C_{0(\lambda=0)}$ is quantified by the parameter e_C defined as

$$e_C = \frac{C_0 - C_{0(\lambda=0)}}{C_{0(\lambda=0)}} \times 100\% \tag{5.16}$$

The values of e_C corresponding to various λ are listed in Tables 5.4(a) through 5.4(c). Positive and negative values of e_C mean that C_0 is larger than and smaller than $C_{0(\lambda=0)}$, respectively.

Table 5.4 suggests that λ has a relatively small impact on C_0 for specimens with a_{ave}/W ≥ 0.3 and various B/W ratios as the maximum absolute value of e_C is about 6%; however,

λ can have a large impact on C_0 for specimens with $a_{ave}/W < 0.3$ as the corresponding maximum absolute value of e_C is as high as 12%. Tables 5.4 also indicates that both a_{ave}/W and B/W influence e_C. For example, for specimens with the same B/W and λ values, e_C decreases as a_{ave}/W increases. For specimens with the same a_{ave}/W and λ values, e_C tends to increase as B/W increases.

5.4.2 Effect of Crack Front Curvature on Rotation Correction Factor

Let e_F evaluated from the following equation denote the error (%) associated with the value of F_r predicted from Eq. (C.2), $F_{r(EST)}$:

$$e_F = \frac{F_{r(EST)} - F_{r(FEA)}}{F_{r(FEA)}} \times 100\% \tag{5.17}$$

where $F_{r(FEA)}$ is the value of F_r output from the FEA through Eq. (5.15). Figures 5.3(a) through 5.3(f) show e_F values plotted against P/P_Y for specimens with $\lambda = 0$ and 0.1. Only values of e_F corresponding to $P/P_Y \le 1.25$ are shown in these figures because $P = 1.25 - 1.3P_Y$ is typically the maximum loading level in the SE(T)-based J-R curve test (Shen et al., 2009; Mathias et al., 2013; Dodds and Read, 1990; Pussegoda, 2013). Due to the convergence issue of the large-strain FEA, only data corresponding to $P/P_Y \le 0.9 - 1.0$ are available for specimens with $\lambda = 0.1$ and $B/W = 0.5$. It is observed from Figs. 5.3(a) through 5.3(e) that the F_r values evaluated from Eq. (C.2) agree well with those obtained from FEA with the difference generally being less than 5% for $P/P_Y \le 1.0$. The values of e_F decrease rapidly as P/P_Y further increases to 1.2 especially for specimens with $B/W = 0.5$. This is due to the relatively poor fitting of Eq. (C.2) to the FEA results corresponding to $P/P_Y > 1$, where F_r is dependent on the strain hardening, and $F_{r(EST)}$ underestimates and overestimates F_r for $n = 10$ and $n = 15$ materials, respectively, as reported by Shen and Tyson (2009). For specimens with $a_{ave}/W = 0.7$ as shown in Fig. 5.3(f), the values of e_F increase rapidly as P/P_Y increases from 1.0 to 1.2. It is explained by Shen and Tyson (2009) that for high loading levels (e.g. $P/P_Y \ge 1.1$) in the large-strain analysis, the ligament of the specimen is shortened (by $3 - 6\%$ based on the present FEA results) due to the large plastic deformation. This phenomenon, causing larger compliance and smaller $F_{r(FEA)}$ values, is more significant

for specimens with deep cracks and higher *n* values. Figures 5.3(a) through 5.3(f) also suggest that λ has little impact on F_r; therefore, Equation (C.2) is considered sufficiently accurate for specimens with $0.2 \leq a_{ave}/W \leq 0.7$, $B/W = 0.5$, 1 and 2 and $\lambda \leq 0.1$, although the results for specimens with $B/W = 0.5$ and $\lambda = 0.1$ are obtained for $P/P_Y \leq 0.9 - 1.0$ only.

5.4.3   Effect of Crack Front Curvature on *J*

At each loading level characterized by h/a_{ave}, the difference between the average *J* obtained from a specimen with a curved crack front (J_{ave}) and the average *J* obtained from the specimen with a straight crack front and the same a_{ave}/W and B/W ratios ($J_{ave(\lambda=0)}$) is defined as

$$e_{J(\lambda)} = \frac{J_{ave} - J_{ave(\lambda=0)}}{J_{ave(\lambda=0)}} \times 100\% \tag{5.18}$$

Figures (5.4) through (5.6) show $e_{J(\lambda)}$ values plotted against h/a_{ave} for specimens with different a_{ave}/W, B/W and λ values. Loading levels corresponding to $P = 1.0P_Y$ and $P = 1.3P_Y$ are also indicated in the figures. The eleven dashed lines in the same subfigure correspond to specimens with the same B/W and a_{ave}/W but different crack front curvatures characterized by λ varying from 0.01 to 0.1, whereas the solid line in the subfigure corresponds to the specimen with a straight crack front. These figures suggest that $e_{J(\lambda)}$ strongly depends on B/W and the loading level, and mildly depends on a_{ave}/W. For example, the absolute values of $e_{J(\lambda)}$ corresponding to $P/P_Y = 1.0 - 1.3$ for specimens with $B/W = 2$ are less than 5% whereas these values are generally around 10% – 15% for specimens with $B/W = 0.5$. For a specimen with a given configuration, $|e_{J(\lambda)}|$ generally decreases as the loading increases from 0 to $0.7P_Y$ and increases as the loading further increases. Given a_{ave}/W, B/W and h/a_{ave}, $|e_{J(\lambda)}|$ consistently increases as λ increases from 0 to 0.1.

5.5   Recommended Crack Front Straightness Criteria

Based on the analysis results shown in Table 5.4 and Figs. (5.4) through (5.6), crack front straightness criteria for the SE(T) specimen are suggested by limiting $|e_C|$ and $|e_{J(\lambda)}|$ (for $P/P_Y = 1.0 - 1.3$) to be less than 5% simultaneously. The values of allowable λ based on the proposed criteria are summarized in Table 5.5. For practical application, the allowable λ is expressed as functions of a_{ave} for specimens with different B/W ratios:

$$\lambda \le \begin{cases} \text{Min}\left[0.06-0.1\dfrac{a_{ave}}{W},\ 0.03\right] & ,\text{for } \dfrac{B}{W}=0.5, \quad 0.2 \le \dfrac{a_{ave}}{W} \le 0.7 \\[2ex] \text{Min}\left[0.03+0.2\dfrac{a_{ave}}{W},\ 0.08\right] & ,\text{for } \dfrac{B}{W}=1, \quad 0.2 \le \dfrac{a_{ave}}{W} \le 0.7 \\[2ex] \text{Min}\left[-0.06+0.5\dfrac{a_{ave}}{W},\ 0.3\dfrac{a_{ave}}{W}\right] & ,\text{for } \dfrac{B}{W}=2, \quad 0.2 \le \dfrac{a_{ave}}{W} \le 0.7 \end{cases} \qquad (5.19)$$

Note that for specimens with $B/W = 2$ and $a_{ave}/W > 0.3$, the allowable λ may be further increased and Eq. (5.19) for such specimen configurations is equivalent to Eq. (5.14f). Equation (5.19) is shown in Fig. 5.7 together with the crack front straightness criteria specified in the seven testing standards considered in this study (i.e. Eq. 5.14(a) through 5.14(h)). The figure indicates that the allowable λ is dependent on a_{ave}/W if $a_{ave}/W \le 0.3$ and is generally independent of a_{ave}/W for $a_{ave}/W > 0.3$. Furthermore, the B/W ratio has a significant impact on the allowable λ. Neither the BS7448-ISO nor ASTM crack front straightness criteria take into account the influences of both a_{ave}/W and B/W. From the standpoint of controlling the difference between the specimens with curved and straight crack fronts in terms of J and the compliance, these criteria are not optimal. For example, the criterion given by Eq. (5.14d) is generally too liberal (i.e. resulting in more than 5% difference in the J (compliance) values corresponding to specimens with straight and curved crack fronts) for specimens with $B/W = 0.5$, but overly restrictive for specimens with $B/W = 1$ and 2. For specimens with $B/W = 2$, the crack front straightness criterion in ASTM E1820 (Eq. (5.14h)) is overly restrictive for specimens with $a_{ave}/W > 0.3$, but too liberal for specimens with $a_{ave}/W \le 0.3$.

To facilitate the practical application of Eq. (5.19) in the context of the nine-point measurement approach specified in the BS (ISO) and ASTM standards, Eq. (5.19) is slightly revised as follows:

$$\kappa \leq \begin{cases} q_2\text{Min}\left[0.06-0.1\dfrac{a_{ave9}}{W},\ 0.03\right] & ,\text{for } \dfrac{B}{W}=0.5,\ \ 0.2 \leq \dfrac{a_{ave9}}{W} \leq 0.7 \\[2mm] q_2\text{Min}\left[0.03+0.2\dfrac{a_{ave9}}{W},\ 0.08\right] & ,\text{for } \dfrac{B}{W}=1,\ \ \ 0.2 \leq \dfrac{a_{ave9}}{W} \leq 0.7 \\[2mm] q_2\text{Min}\left[-0.06+0.5\dfrac{a_{ave9}}{W},\ 0.3\dfrac{a_{ave9}}{W}\right] & ,\text{for } \dfrac{B}{W}=2,\ 0.2 \leq \dfrac{a_{ave9}}{W} \leq 0.7 \end{cases} \qquad (5.20)$$

where a_{ave}/W in Eq. (5.19) is replaced by a_{ave9}/W in Eq. (5.20) given that these two quantities are very close as shown in Table 5.2, and λ in Eq. (5.19) is replaced by κ/q_2 (see Eq. (5.12)) in Eq. (5.20) with the values of q_2 associated with $p = 3.0$ given in Table 5.2. It is recommended that κ be chosen as either $\lambda_{9(BS)}$ or $\lambda_{9(ASTM)}$ since the corresponding q_2 is insensitive to p. Note that the proposed crack front straightness requirement is considered applicable to both the fatigue pre-crack front and final crack front.

To examine the validity of Eqs. (5.19) and (5.20) for specimens containing curved crack fronts with the shape parameter p equal to values other than 3.0, additional finite element analyses for specimens with $a_{ave}/W = 0.2, 0.4$ and 0.7, $B/W = 1$, and three allowable λ values given by Eq. (5.19) (i.e. $\lambda = 0.07$ for $a_{ave}/W = 0.2$, and $\lambda = 0.08$ for $a_{ave}/W = 0.4$ and 0.7) were carried out. The value of p was selected to 2.5 for the additional analyses. The rationale for selecting $p = 2.5$, as opposed to, say, $p = 3.5$, in the analysis is that for a given λ, β increases as p decreases (see Eq. (5.10)), causing the central portion of the crack front, which has the largest contribution to J_{ave}, to become more curved (Yan and Zhou, 2015). The values of e_C and $e_{J(\lambda)}$ for these specimens are shown in Table 5.4(b) (see values in the brackets) and Fig. 5.8, respectively. The results indicate that decreasing p from 3.0 to 2.5 but maintaining a_{ave}/W and λ has small impacts on the compliance and J_{ave}; therefore, Eqs. (5.19) and (5.20) are also applicable for curved crack fronts with $p = 2.5$.

5.6 Conclusions

Three-dimensional FEA was performed to investigate the impact of the crack front curvature on the undeformed compliance (C_0), rotation correction factor (F_r) and average J over the crack front (J_{ave}) for plane-sided clamped SE(T) specimens made of homogeneous materials. Symmetric bowed crack fronts characterized by a power-law expression were considered in the analysis. Three specimen thicknesses ($B/W = 0.5$, 1 and 2), six average crack lengths ($a_{ave}/W = 0.2$ to 0.7) and eleven crack front curvatures ($\lambda = 0$ to 0.1) were included in this study. Three groups of FE models with the use of linear-elastic, small-strain and large-strain elastic-plastic formulations were analyzed to estimate C_0, J_{ave} and F_r, respectively. Given a_{ave}/W and B/W, C_0 and J_{ave} corresponding to the straight crack front and curved crack fronts with different curvatures were compared. The rotation correction factors F_r corresponding to specimens with straight and curved crack fronts are compared with those estimated from the empirical equation proposed by Shen et al. In addition to FEA, the crack front straightness criteria for the SE(B) and C(T) specimens specified in BS7448 (Parts I, II, III and IV), ISO12135, ISO15653 and ASTM E1820 were reviewed.

The numerical results suggest that λ has little impact on C_0 for specimens with $a_{ave}/W \geq 0.3$ as the maximum absolute value of e_C is about 6%, whereas e_C strongly depends on λ for specimens with $a_{ave}/W < 0.3$ as the corresponding maximum absolute value of e_C is as high as 12%. The value of $|e_{J(\lambda)}|$ strongly depends on B/W and h/a_{ave}, and mildly depends on a_{ave}/W. On the other hand, λ has little impact on F_r and the empirical equation proposed by Shen et al. is considered sufficiently accurate for specimens with $0.2 \leq a_{ave}/W \leq 0.7$, $B/W = 0.5$, 1 and 2 and $\lambda \leq 0.1$. Based on the analysis results and the criterion that $|e_C|$ and $|e_{J(\lambda)}|$ should be no more than 5%, crack front straightness criteria for the SE(T) specimen were recommended. To facilitate the practical application, the proposed crack front straightness criteria were further expressed in terms of the nine-point measurement approach specified in the BS and ASTM standards. The proposed criteria are more advantageous than those specified in the BS, ISO and ASTM standards in that the former ensure the differences in J and the compliance between the specimens with curved and straight crack fronts to be within a reasonably small range, i.e. no more than 5%.

References

ADINA (2012). *Theory and Modeling Guide*. ADINA R & D Inc., Watertown, MA.

Anderson, T. L. (2005). *Fracture Mechanics-Fundamentals and Applications, Third edition*. CRC Press, Boca Raton.

API. (2012). *API Specification 5L: Specification for Line Pipe*, Ed. 45, American Petroleum Institute, Washington, D.C.

ASTM (2013). *ASTM E1820-13: Standard Test Method for Measurement of Fracture Toughness*. America Society of Testing and Materials International, West Conshohocken, PA.

BSI (1991). *BS 7448: Part I. Method for determination of K_{Ic}, critical CTOD and critical J values of metallic materials*. British Standard Institution, London.

BSI (1997a). *BS 7448: Part II. Method for determination of K_{Ic}, critical CTOD and critical J values of welds in metallic materials.* British Standard Institution, London.

BSI (2005). *BS 7448: Part III. Method for determination of fracture toughness of metallic materials at rates of increase in stress intensity factor greater than 3.0 MPa $m^{0.5}s^{-1}$.* British Standard Institution, London.

BSI (1997b). *BS 7448 IV: Method for determination of fracture resistance curves and initiation values for stable crack extension in metallic materials,* British Standard Institution, London.

Chiesa, M., Nyhus, B., Skallerud, B. and Thaulow, C. (2001). Efficient fracture assessment of pipelines: A constraint-corrected SENT specimen approach. *Engineering Fracture Mechanics*, 68:527-547.

Cravero, S. and Ruggieri, C. (2007). Estimation Procedure of J Resistance Curves for SE (T) Fracture Specimens Using Unloading Compliance. *Engineering Fracture Mechanics*, 74(17):2735-2757.

Crouch, B. A. (1991). The Effect of Crack Front Curvature and Side-Grooving on Three Point Bend Specimen Fracture Toughness Measurements. *International Journal of Fracture*, 52:275–292.

Dodds, R, H. and Read, D. (1990). Experimental and numerical studies of the *J*-integral for a surface flaw. *International Journal of Fracture*, 43:47-67.

Graba, M. and Galkiewicz, J. (2007). Influence of the crack tip model on results of the finite element method. *Journal of Theoretical and Applied Mechanics*, 45:225-237.

Gullerud, A. S., Koppenhoefer, K. C., Arun, R. Y., Roychowdhury, S. and Dodds, R. H. (2001). WARP3D–Release 13.15 Manual. Civil engineering, Report no. UILU-ENG-95-2012, University of Illinois.

Hutchinson, J. W. (1983). Fundamentals of the Phenomenological Theory of Nonlinear Fracture Mechanics. *Journal of Applied Mechanics*, 50:1042-1051.

Hutchison, E. K. and Pisarski, H. G. (2013). Effects of crack front curvature on J and CTOD determination in fracture toughness specimens by FEA. *ASME 2013 32nd International Conference on Ocean, Offshore and Arctic Engineering*. Nantes, France, ASME, Paper No. OMAE2013-11447.

ISO (2002). *ISO 12135: Metallic materials–Unified method of test for the determination of quasistatic fracture toughness*. International Organization for Standardization, Geneva.

ISO (2010). *ISO 15653: Metallic materials-method of test for the determination of quasistatic fracture toughness of welds*. International Organization for Standardization, Geneva.

Kulka, R. S. and Sherry, A. H. (2012). Fracture Toughness Evaluation in C(T) Specimens with Reduced Out-of-plane Constraint. *Proceedings of the 2012 ASME Pressure Vessel*

and Piping Division Conference, Toronto, Ontario, Canada, July 15–19, ASME, New York.

Leis, B., Zhu, X., Shen, G. and Tyson, W. (2009). Effective experimental measurement and constraint quantification of J-R curves for X80 pipeline steel. Proceedings of the 12th International Conference on Fracture, Ottawa, Canada,.

Malpas, A. R., Moore, P. L. and Pisarski, H. G. (2012). Crack front straightness qualification in SENT specimens. The 22nd International Ocean and Polar Engineering Conference Rodos Palace Hotel, Rhodes, Greece: ISOPE, p.613-18

Mathias, L. L., Sarzosa, D. F. and Ruggieri, C. (2013). Effects of specimen geometry and loading mode on crack growth resistance curves of a high-strength pipeline girth weld. *International Journal of Pressure Vessels and Piping*, 111:106-119.

Nikishkov, G. P., Heerens, J. and Hellmann, D. (1999). Effect of Crack Front Curvature and Side Grooving on CTOD δ5 and J-Integral in CT and 3PB Specimens. *Journal of Testing and Evaluation*, 27(5):312–319.

Pussegoda, L. N., Tiku, S., Tyson, W. R., Park, D-Y., Gianetto, J. A., Shen, G. and Pisarski, H.G. (2013). Comparison of resistance curves from multi-specimen and single-specimen SENT Tests. *Proceedings of Twenty-third International Offshore and Polar Engineering Conference*. Anchorage, Alaska, USA: The International Society of Offshore and Polar Engineers (ISOPE); p. 482-8.

Shen, G., Bouchard, R., Gianetto, J. A. and Tyson, W. R. (2008). Fracture toughness evaluation of high strength steel pipe. *ASME Conference Proceedings*. 1275-82.

Shen, G., Gianetto, J. A, and Tyson, W. R. (2008). Report 2008-18(TR): Development of procedure for low-constraint toughness testing using a single-specimen technique. Ottawa, Canada: CANMET-MTL.

Shen, G. and Tyson, W. R. (2009). Crack size evaluation using unloading compliance in single-specimen single-edge-notched tension fracture toughness testing. *ASTM Journal of Testing and Evaluation*, 37:347-357.

Shen, G., Gianetto, J. A., and Tyson, W. R. (2009). Measurement of J-R Curves Using Single-Specimen Technique on Clamped SE(T) Specimens. *Proceedings of Nineteenth International Offshore and Polar Engineering Conference*, the International Society of Offshore and Polar Engineers (ISOPE), Osaka, Japan, 92-99.

Shih, C. F., Lorenzi, H. G. and Andrews, W. R. (1977). Elastic compliances and stress-intensity factors for side-grooved compact specimens. *International Journal of Fracture*, 13:544-548.

Steenkamp P. (1988). J^R-curve Testing of Three-point Bend Specimen by the Unloading Compliance Method. *Fracture Mechanics 18th Symposium*, ASTM STP 945, 583-610.

Yan, Z. and Zhou, (2014). Effect of crack front curvature on CMOD compliance and crack length evaluation for single-edge bend specimens. *2014 Proceedings of The Canadian Society for Mechanical Engineering International Congress*. Toronto, Ontario, Canada: CSME.

Yan, Z. and Zhou, W. (2015). Effect of crack front curvature on experimental evaluation of J-integral for single-edge bend specimens. *ASTM Journal of Testing and Evaluation*, 43(5).

Zhou, J. and Soboyejo, W. O. (2002). An Investigation of the Effects of Crack Front Curvature on the Crack-Tip Opening Displacement of A707 Steel. *International Journal of Fracture*, 115(3):287-305.

Zuo, J., Cheng, C-S., Deng, X. and Sutton, M. A. (2008). Three-dimensional crack growth in ductile materials: effect of stress constraint on crack tunneling. *Journal of Pressure Vessel Technology*, 130:031401.

Table 5.1: Summary of crack front straightness criteria for SE(B) and C(T) specimens

Standards	Material	Scope	Criteria for any crack fronts	Criteria for crack front described by Eq. (5.8) with $p = 3$
Part I	BM [1]	K_{IC}, critical J and $CTOD$	$\beta_9 \leq 0.1 a_{ave9}/W$ [4]	$\lambda \leq 0.0797 a_{ave}/W$ [6]
Part II	WM [2] and HAZ [3]	K_{IC}, critical J and $CTOD$	$\beta_7 \leq 0.2 a_{ave9}/W$	$\lambda \leq 0.3778 a_{ave}/W$
BS 7448 Part III	WM and HAZ	Dynamic fracture toughness	$\beta_9 \leq 0.2 a_{ave9}/W$	$\lambda \leq 0.1594 a_{ave}/W$
Part IV	BM	R-curves	$\lambda_{9(BS)} \leq 0.1 a_{ave9}/W$	$\lambda \leq 0.1085 a_{ave}/W$
Part IV	WM and HAZ	R-curves	$\lambda_{9(BS)} \leq 0.2 a_{ave9}/W$	$\lambda \leq 0.2170 a_{ave}/W$
ISO 12135	BM	K_{IC}, critical J and $CTOD$ and R-curves	$\lambda_7 \leq 0.1 a_{ave9}/W$	$\lambda \leq 0.3000 a_{ave}/W$
ISO 15653	WM and HAZ	K_{IC}, critical J and $CTOD$ and R-curves	$\lambda_7 \leq 0.2 a_{ave9}/W$ [5]	$\lambda \leq 0.6000 a_{ave}/W$
ASTM E1820	BM	K_{IC}, critical J and $CTOD$ and R-curves	$\lambda_{9(ASTM)} \leq 0.05 B/W$	$\lambda \leq 0.0271$, for $B/W = 0.5$ $\lambda \leq 0.0526$, for $B/W = 1$ $\lambda \leq 0.1037$, for $B/W = 2$

Notes:
1. BM: base material.
2. WM: weld material.
3. HAZ: heat-affected zone.
4. Curvature parameters based on the nine points measurement: $\beta_9 = (a_{max9} - a_{min9})/W$; $\beta_7 = (a_{max7} - a_{min7})/W$; $\lambda_7 = \text{Max}[a_{max7} - a_{ave9}, a_{ave9} - a_{min7}]/W$; $\lambda_9 = \text{Max}[a_{max9} - a_{ave9}, a_{ave9} - a_{min9}]/W$ (subscripts "(BS)" and "(ASTM)" denote the measurement methods specified in the corresponding standards).
5. Only applicable for J and $CTOD$ test using SE(B) specimens.
6. Curvature parameter for the crack front characterized by Eq. (5.8): $\lambda = (a_{ave} - a_{z = \pm B/2})/W$.

Table 5.2: Values of q_1 and q_2 corresponding to different p values

| p | BS (ISO) standards | q_1 ASTM standard | | | q_2 | | | | $\lambda_{9(ASTM)}$ | | |
		$B/W = 0.5$	$B/W = 1$	$B/W = 2$	β_7	β_9	λ_7	$\lambda_{9(BS)}$	$B/W = 0.5$	$B/W = 1$	$B/W = 2$
2.5	2.29E-03	2.29E-03	-7.93E-03	-1.31E-02	0.6484	1.3310	0.3977	0.9333	0.9333	0.9573	0.9695
2.6	1.83E-03	1.83E-03	-8.41E-03	-1.36E-02	0.6218	1.3138	0.3828	0.9310	0.9310	0.9559	0.9685
2.7	1.37E-03	1.37E-03	-8.89E-03	-1.41E-02	0.5968	1.2976	0.3690	0.9286	0.9286	0.9544	0.9675
2.8	9.07E-04	9.07E-04	-9.37E-03	-1.46E-02	0.5731	1.2825	0.3562	0.9263	0.9263	0.9530	0.9665
2.9	4.50E-04	4.50E-04	-9.84E-03	-1.51E-02	0.5507	1.2683	0.3444	0.9239	0.9239	0.9515	0.9655
3	-5.50E-06	-5.50E-06	-1.03E-02	-1.55E-02	0.5294	1.2549	0.3333	0.9216	0.9216	0.9501	0.9646
3.1	-4.59E-04	-4.59E-04	-1.08E-02	-1.60E-02	0.5092	1.2423	0.3230	0.9193	0.9193	0.9486	0.9636
3.2	-9.11E-04	-9.11E-04	-1.13E-02	-1.65E-02	0.4900	1.2303	0.3134	0.9169	0.9169	0.9472	0.9626
3.3	-1.36E-03	-1.36E-03	-1.17E-02	-1.70E-02	0.4717	1.2190	0.3044	0.9146	0.9146	0.9458	0.9616
3.4	-1.81E-03	-1.81E-03	-1.22E-02	-1.75E-02	0.4543	1.2082	0.2959	0.9123	0.9123	0.9443	0.9606
3.5	-2.26E-03	-2.26E-03	-1.27E-02	-1.80E-02	0.4377	1.1979	0.2880	0.9100	0.9100	0.9429	0.9597

Table 5.3: Summary of information of FE models

Group #	Formulation	a_{ave}/W	λ	B/W
1	Linear-elastic	0.2, 0.3, 0.4, 0.5, 0.6, 0.7	0, 0.01, 0.02, 0.03, 0.04, 0.05, 0.06, 0.07, 0.08, 0.09, 0.1	0.5, 1, 2
2	Elastic-plastic Small strain/small displacement	0.2, 0.3, 0.4, 0.5, 0.6, 0.7	0, 0.01, 0.02, 0.03, 0.04, 0.05, 0.06, 0.07, 0.08, 0.09, 0.1	0.5, 1, 2
3	Elastic-plastic Large strain/large displacement	0.2, 0.3, 0.4, 0.5, 0.6, 0.7	0, 0.1	0.5, 1, 2

Table 5.4: Variation of e_C (%) with λ for specimens with various a_{ave}/W ratios

(a) B/W = 0.5

						λ						
		0	0.01	0.02	0.03	0.04	0.05	0.06	0.07	0.08	0.09	0.1
	0.7	0.0	0.1	0.0	-0.2	-0.5	-1.0	-1.7	-2.5	-3.5	-4.6	-5.8
	0.6	0.0	0.0	0.0	-0.2	-0.6	-1.0	-1.7	-2.4	-3.4	-4.4	-5.6
a_{ave}/W	0.5	0.0	0.2	0.1	-0.1	-0.4	-0.8	-1.4	-2.2	-3.0	-4.0	-5.1
	0.4	0.0	0.2	0.1	0.0	-0.3	-0.7	-1.3	-2.0	-2.8	-3.8	-4.8
	0.3	0.0	0.1	0.2	0.1	-0.1	-0.5	-1.0	-1.6	-2.4	-3.3	-4.4
	0.2	0.0	0.7	0.9	1.0	1.0	0.7	0.3	-0.2	-0.9	-1.7	-2.7

(b) B/W = 1

						λ						
		0	0.01	0.02	0.03	0.04	0.05	0.06	0.07	0.08	0.09	0.1
	0.7	0.0	0.1	0.1	0.1	-0.1	-0.3	-0.6	-1.0	-1.0 (-1.8)	-2.1	-2.8
	0.6	0.0	0.1	0.1	0.1	0.0	-0.1	-0.4	-0.7	-1.2	-1.7	-2.2
a_{ave}/W	0.5	0.0	0.2	0.3	0.4	0.3	0.2	0.0	-0.2	-0.6	-1.0	-1.5
	0.4	0.0	0.3	0.5	0.6	0.6	0.6	0.5	0.3	0.1 (0.0)	-0.2	-0.6
	0.3	0.0	0.4	0.7	1.0	1.2	1.3	1.4	1.4	1.4	1.3	1.1
	0.2	0.0	1.1	1.9	2.6	3.2	3.8	4.3	4.8 (5.2)	5.2	5.5	5.8

(c) B/W = 2

						λ						
		0	0.01	0.02	0.03	0.04	0.05	0.06	0.07	0.08	0.09	0.1
	0.7	0.0	0.2	0.2	0.2	0.2	0.1	0.0	-0.2	-0.4	-0.7	-1.1
	0.6	0.0	0.1	0.3	0.4	0.4	0.4	0.4	0.3	0.2	0.0	-0.2
a_{ave}/W	0.5	0.0	0.3	0.6	0.8	0.9	1.0	1.1	1.2	1.2	1.1	1.1
	0.4	0.0	0.5	0.8	1.2	1.5	1.8	2.0	2.3	2.5	2.6	2.7
	0.3	0.0	0.6	1.3	1.9	2.5	3.1	3.7	4.2	4.7	5.2	5.7
	0.2	0.0	1.6	2.8	4.0	5.2	6.4	7.6	8.8	9.9	11.0	12.1

Notes: values in the brackets are e_C corresponding to crack fronts with $p = 2.5$.

Table 5.5: Maximum allowable λ corresponding to $|e_C|$ and $|e_{J(\lambda)}|$ being no more than 5%

B/W	a_{ave}/W					
	0.2	0.3	0.4	0.5	0.6	0.7
0.5	0.04	0.03	0.03	0.03	0.04	0.04
1	0.07	0.09	0.08	0.08	0.08	0.08
2	0.04	0.09	0.1[1]	0.1[1]	0.1[1]	0.1[1]

Notes:

1.   Maximum λ considered in this study. The value of maximum allowable λ may be further increased without violating the corresponding controlling criteria.
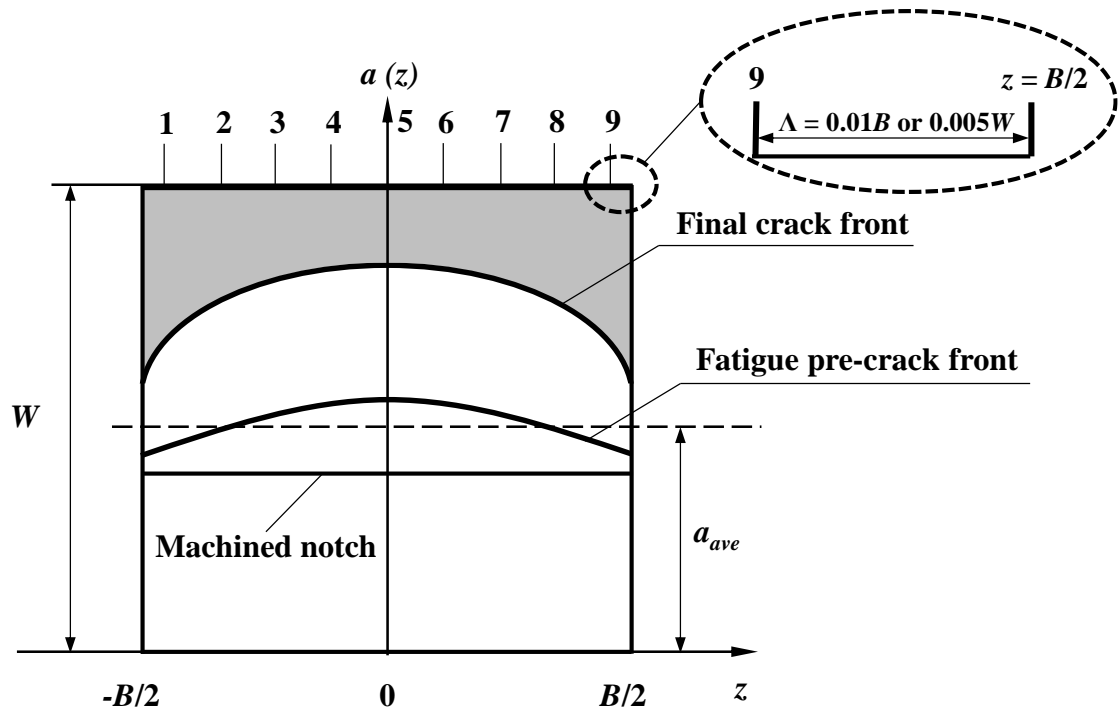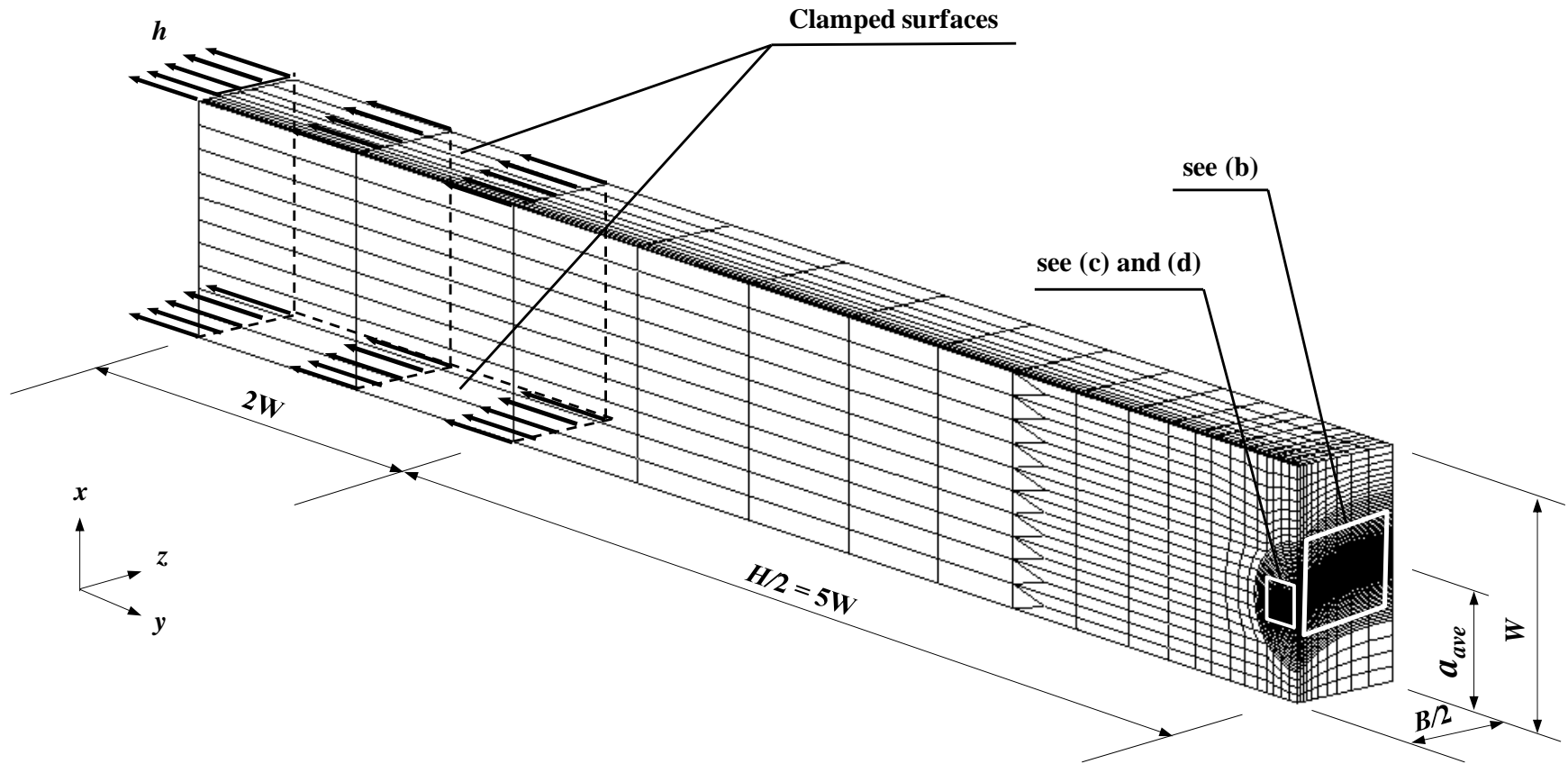
Figure 5.1. Determination of the crack front curvature through the nine-point measurement specified in BS7448 and ASTM E1820.

(a) Configuration of a typical FE model with $a_{ave}/W = 0.5$, $\lambda = 0.1$ and $B/W = 1$
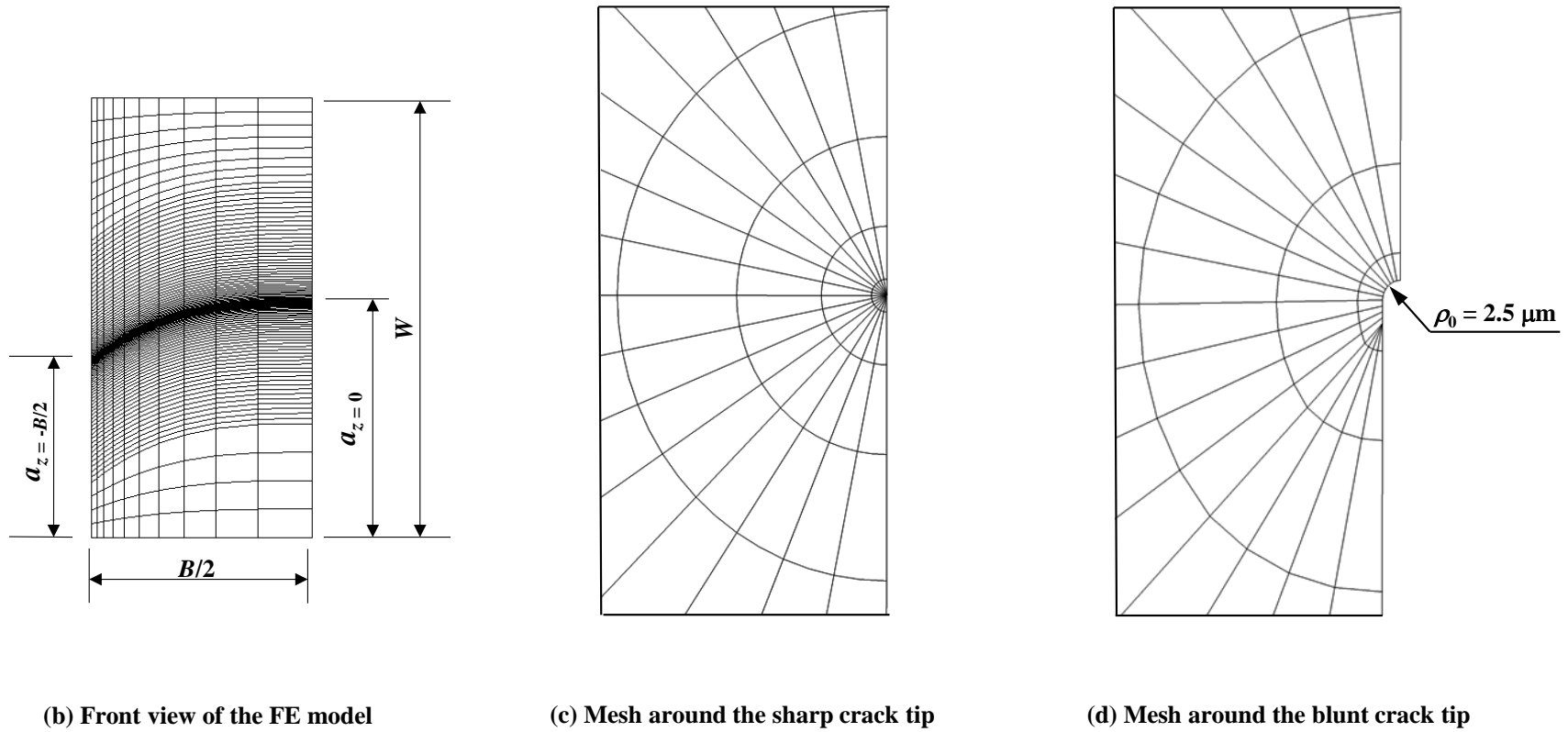
(b) Front view of the FE model **(c) Mesh around the sharp crack tip** **(d) Mesh around the blunt crack tip**

Figure 5.2. Configuration and meshing of a typical finite element model.
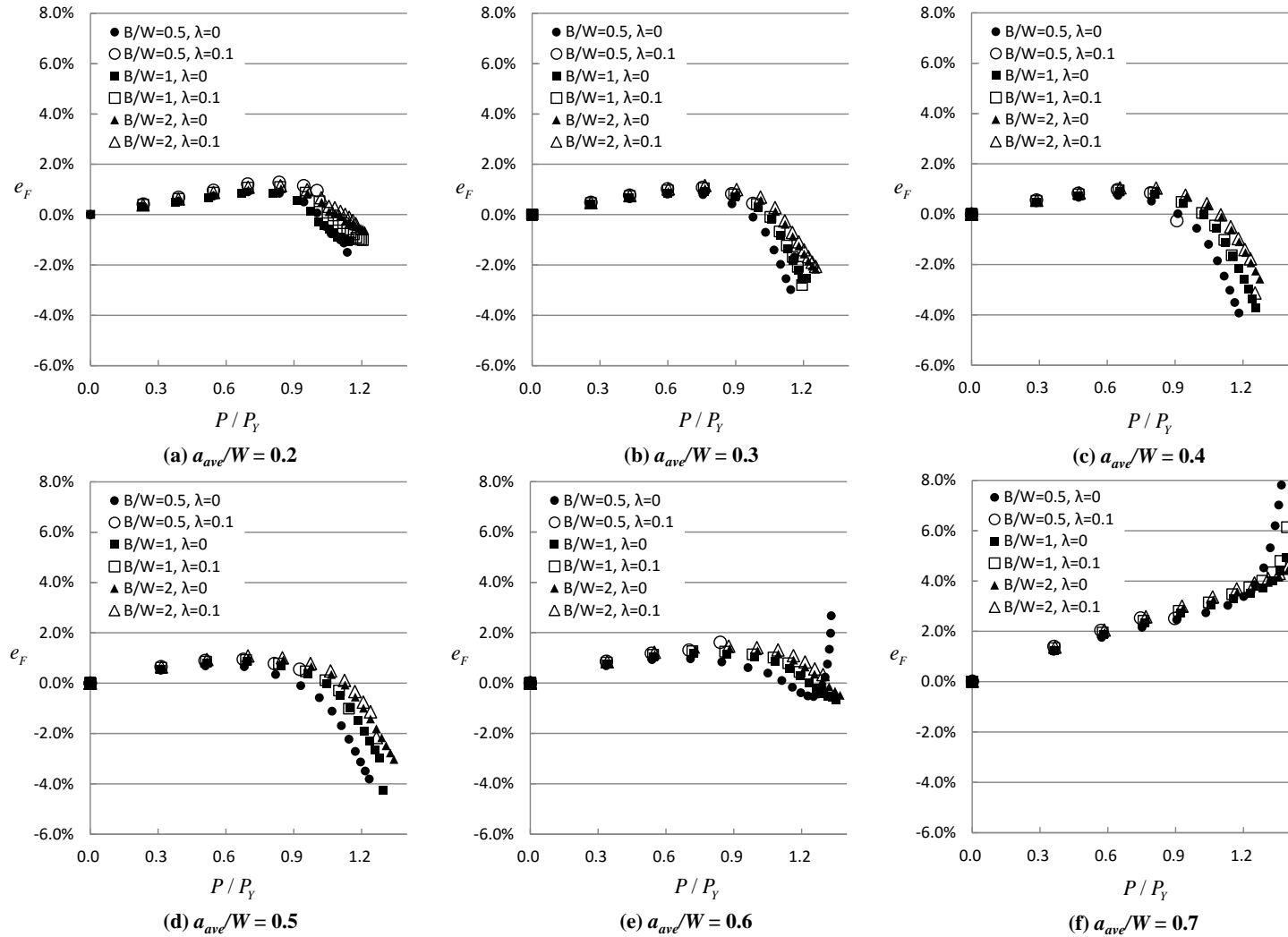
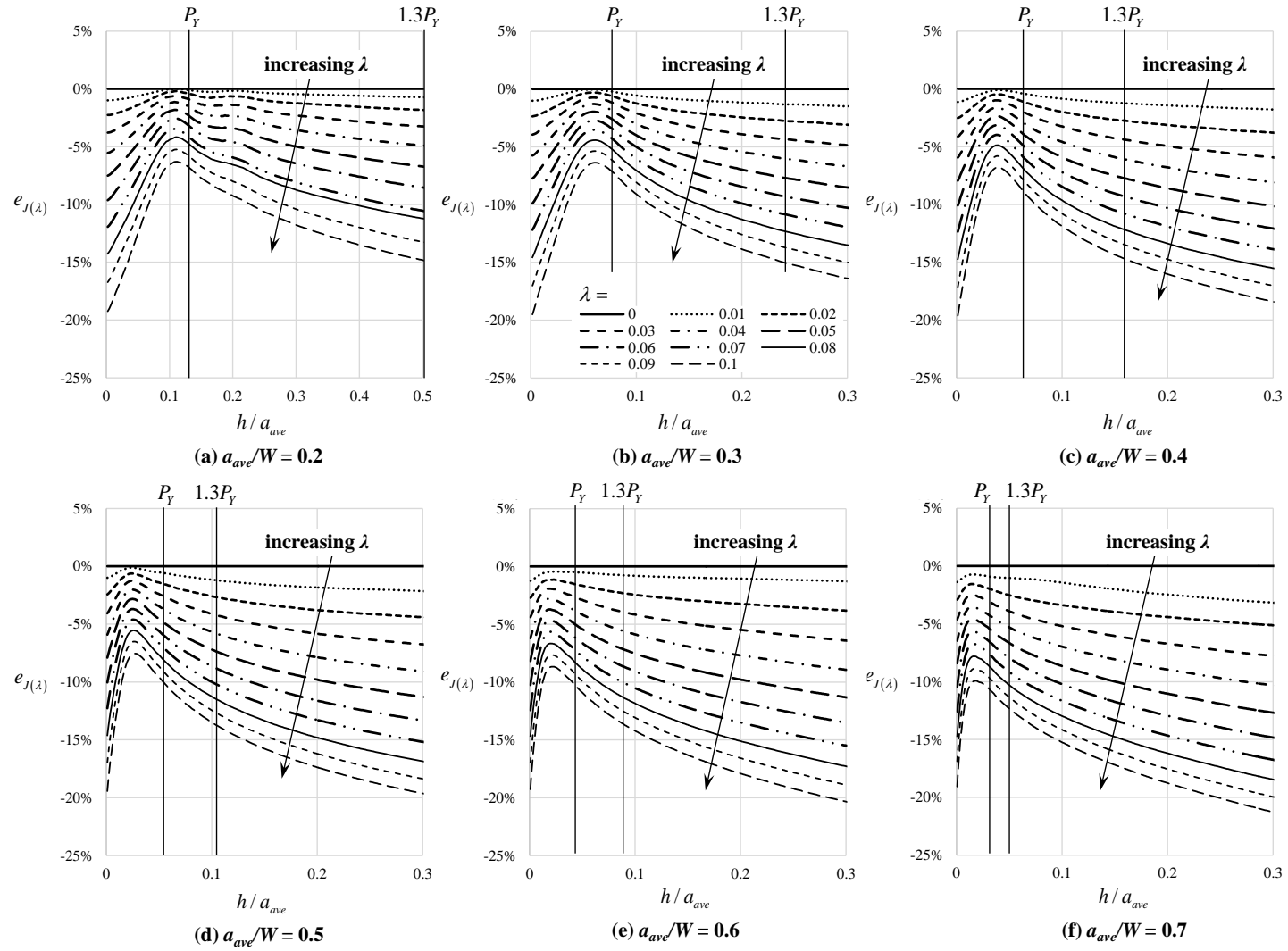Figure 5.3. Variation of e_F with P/P_Y for specimens with various a_{ave}/W, B/W and λ values.

Figure 5.4. Variation of $e_{J(\lambda)}$ with h/a_{ave} and λ for specimens with $B/W = 0.5$ and various a_{ave}/W ratios.
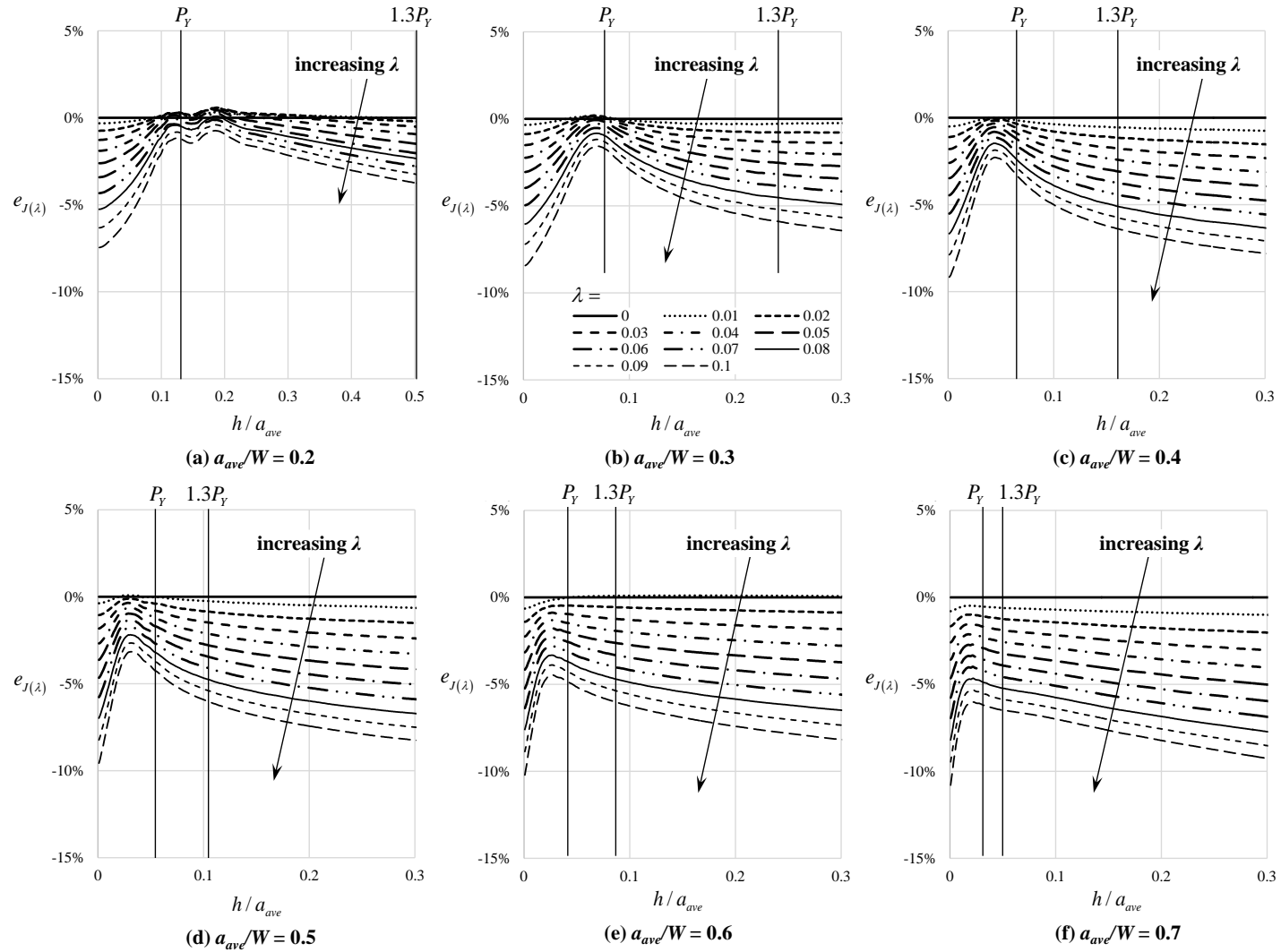
158

Figure 5.5. Variation of $e_{J(\lambda)}$ with h/a_{ave} and λ for specimens with $B/W = 1$ and various a_{ave}/W ratios.
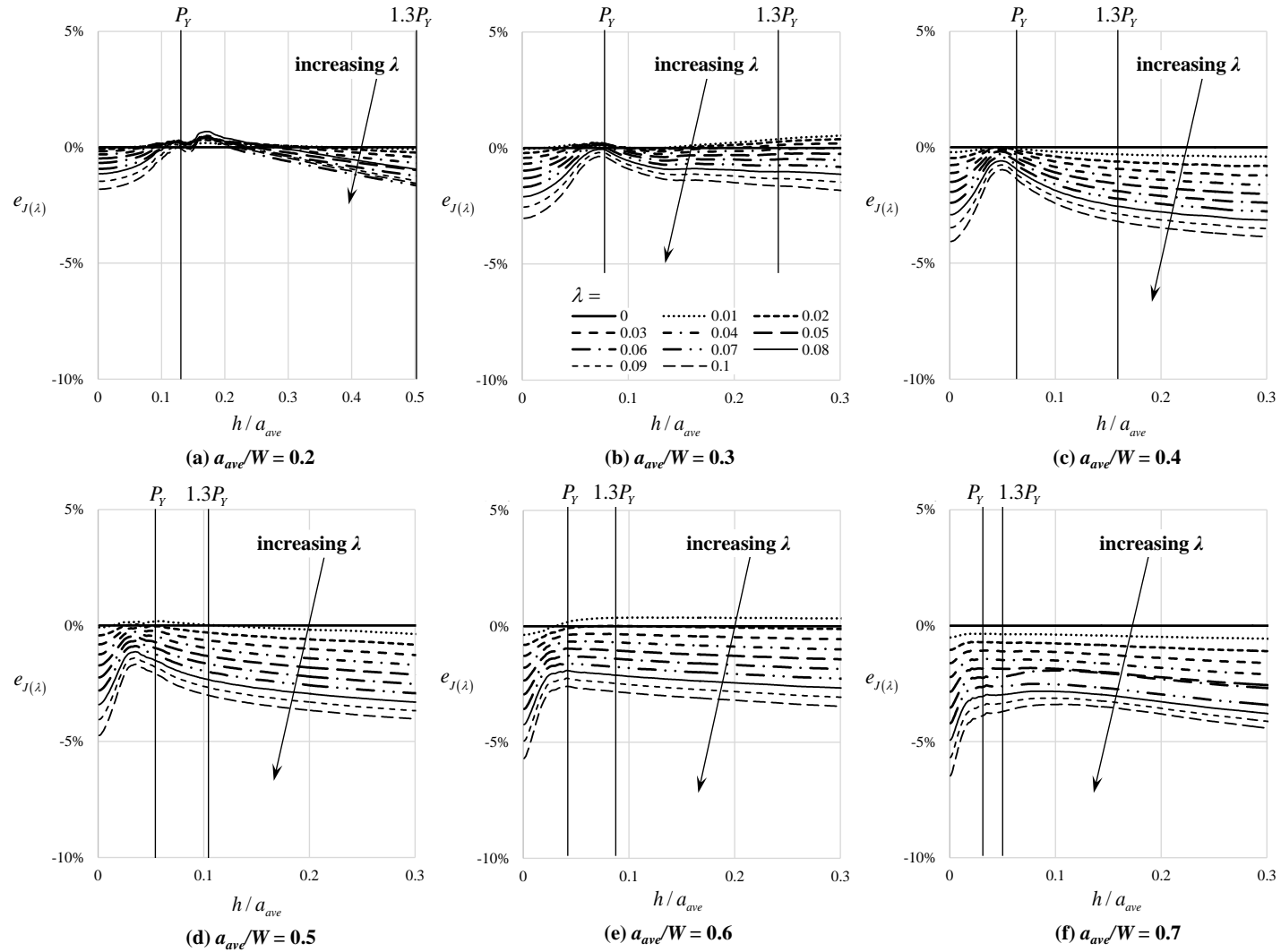
Figure 5.6. Variation of $e_{J(\lambda)}$ with h/a_{ave} and λ for specimens with $B/W = 2$ and various a_{ave}/W ratios.
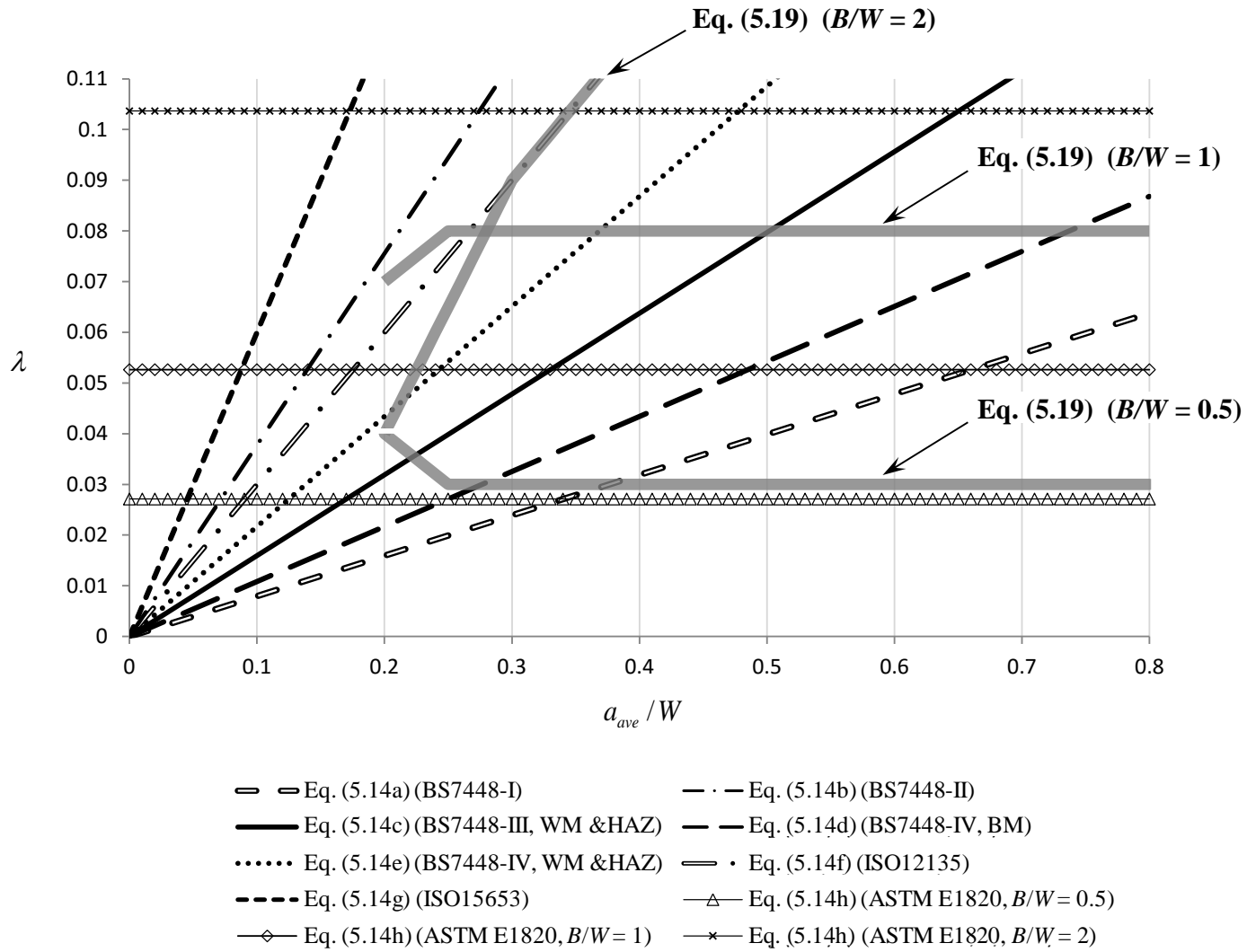
Figure 5.7. Comparison of the proposed crack front straightness criteria and those specified in BS, ISO and ASTM standards.
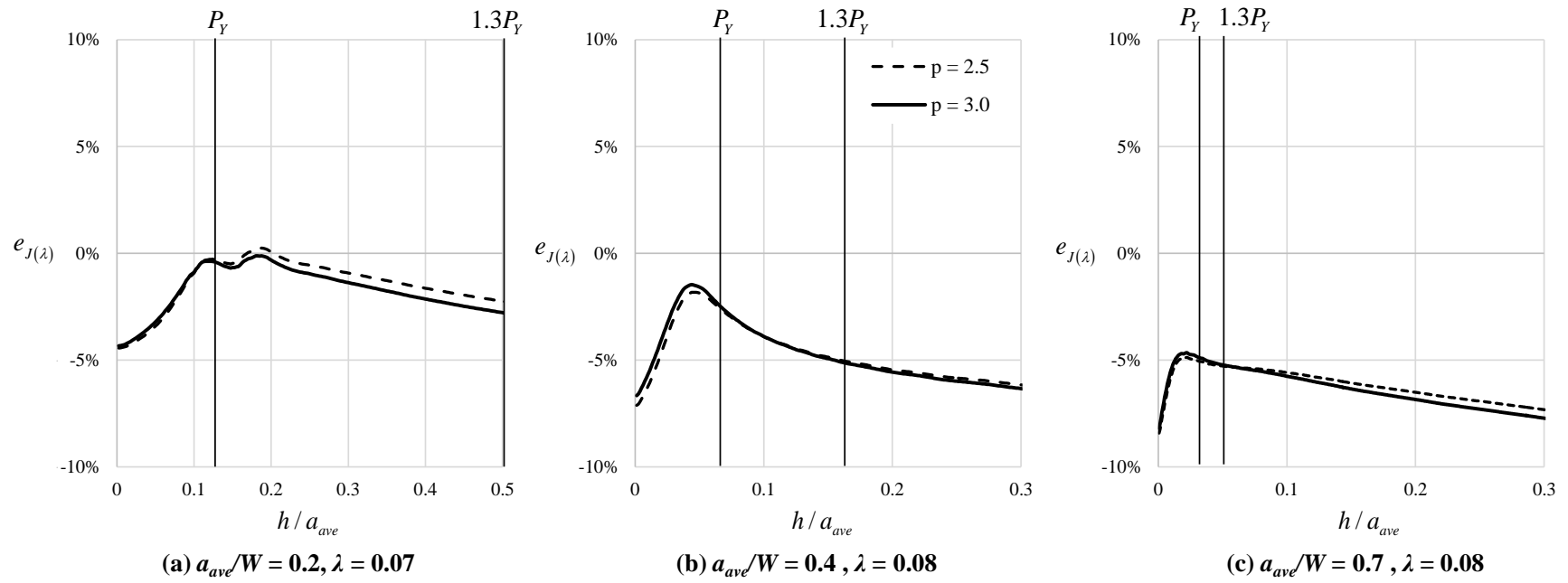
Figure 5.8. Variation of $e_{J(\lambda)}$ with h/a_{ave} for crack fronts with $p = 2.5$ and 3.0.

Chapter 6 Effective Thickness of Side-grooved Clamped SE(T) Specimens for *J-R* Curve Testing

6.1 Background and Objective

6.1.1 Effective Thickness for Side-grooved Specimens

The fracture toughness resistance (R) curve, such as the *J*-integral-resistance (*J-R*) or crack-tip opening displacement-resistance (*CTOD-R*) curve, is generally obtained from the small-scale fracture test specimens such as the single-edge notched three-point bend (SE(3PB) or SE(B)) and compact tension (C(T)) specimens. The test procedures for such specimens have been standardized in standards such as ASTM E1820-13 (ASTM, 2013), BS7448-4 (BSI, 1997) and ISO 12135 (ISO, 2002). Testing on the plane-sided (PS) SE(B) and C(T) specimens made of homogeneous materials generally leads to a curved crack front caused by the difference in the states of stress along the crack front (Shih et al., 1977; Anderson, 2005). The side-grooved (SG) specimens are used in the *R*-curve testing to achieve relatively straight crack fronts. Figure 6.1 schematically shows the configurations of a side groove in a typical SE(B) or C(T) specimen. As illustrated in the figure, one groove is machined into each lateral side of the specimen. The side groove has a depth (d_{sg}), a root radius (r_{sg}) and a machined angle (θ_{sg}). The specimen has a gross thickness (B), whereas the net thickness between the side grooves (B_N) can be calculated as $B_N = B - 2d_{sg}$. ASTM E1820-13 (ASTM, 2013) suggests machining the side groove with a radius $r_{sg} = 0.5\pm0.2$ mm, a machined angle $0 \leq \theta_{sg} \leq 90$ degrees and a ratio $d_{sg}/B \leq 12.5\%$, whereas BS7448-4 (BSI, 1997) and ISO 12135 (ISO, 2002) specify a radius $r_{sg} = 0.4\pm0.2$ mm, a machined angle $30 \leq \theta_{sg} \leq 90$ degrees and a ratio $d_{sg}/B = 10\%$.

It is reported that the *J-R* curves obtained from the SG specimens are generally lower than those obtained from the PS specimens (Andrews and Shih, 1979; Wang et al., 2012; Park et al., 2010). Previous studies revealed that both r_{sg} and θ_{sg} have a negligible impact on the *J-R* curve (Park et al., 2010; Lucon and Scibetta, 2009; Yasufumi and Tomokazu, 1984. On the other hand, d_{sg} significantly influences the normalized compliance (C_N), the stress intensity factor (K) and the plastic component of J (J_{pl}) of the specimen, which are

important variables in the *J-R* curve testing. The so-called "effective thickness" (B_e) is introduced to account for the impact of the side grooves (more specifically, d_{sg}) on these variables. In the evaluations of C_N, K and J_{pl} (i.e., Eqs (4.1) and (4.3), (2.22a) and (2.8)), the specimen gross thickness B is replaced by the corresponding B_e, which is a function of B and B_N (or d_{sg}). The present *R*-curve test standards (ASTM, 2013; BSI, 1997; ISO, 2002) specify the following three effective thickness expressions ($B_{e(1)}$, $B_{e(2)}$ and $B_{e(3)}$) for SE(B) and C(T) specimens:

$$\begin{cases} B_{e(1)} = B - \dfrac{\left(B - B_N\right)^2}{B} & \text{, for normalized compliance } \left(C_N\right) \quad \text{(a)} \\[2mm] B_{e(2)} = \sqrt{BB_N} & \text{, for stress intensity factor } \left(K\right) \quad \text{(b)} \\[2mm] B_{e(3)} = B_N & \text{, for plastic component of } J \left(J_{pl}\right) \quad \text{(c)} \end{cases} \qquad (6.1)$$

The use of the clamped single-edge tension (SE(T) or SENT) specimen to determine the *R*-curve has recently gained significant interests (Donato and Moreira, 2014) in the energy pipeline industry. The crack-tip stress and strain fields of the SE(T) specimen are similar to those of the full-scale pipe containing surface cracks under longitudinal tension and/or internal pressure (Chiesa et al., 2001; Shen et al., 2008a); therefore, the *J-R* curve determined from the SE(T) specimen can lead to more accurate design and assessment of pipelines with respect to cracks. Several research groups have put forward *J-R* curve test methods involving SG SE(T) specimens with various d_{sg}/B ratio (e.g. Shen et al., 2008a; Cravero and Ruggieri, 2007; Tang et al., 2010; Pisarski et al., 2013). For example, Cravero and Ruggieri (2007) developed a test method using SG SE(T) specimens with $d_{sg}/B = 10\%$; Shen et al. (2008a) suggested using SG SE(T) specimens with $d_{sg}/B = 7.5\%$, and the ExxonMobil research group (2010) and TWI research group (2013) focus on SG specimens with $d_{sg}/B = 5\%$, which is also suggested in the recently published standard BS 8571 (BSI, 2014).

All of the above groups recommend using Eqs. (6.1a) – (6.1c) for the SG SE(T) specimen in the *J-R* curve testing. Shen et al. (2010) reported that, for SE(T) specimens, the difference between the normalized compliance C_N obtained from two dimensional (2D)

plane-stress finite element analyses (FEA) and that from three-dimensional (3D) FEA is less than 4% if Eq. (6.1a) is used in the calculation. Specimens with the daylight length (distance between grips, H) equal to $10W$, $B/W = 1$, relative crack lengths (a/W) equal to 0.2 and 0.5, and $d_{sg}/B = 0\%$, 5%, and 10% were investigated in their study. Donato and Moreira (2013) carried out 3D FEA of SG SE(T) specimens with $H/W = 6$, $B/W = 0.5$, a/W ratio from 0.1 to 0.7 and $d_{sg}/B = 0\%$, 2.5%, 5%, and 10%. For a given a/W, they calculated $B_{e(1)}$ by forcing the normalized compliance, C_N, obtained from SG specimens equal to those obtained from PS specimens. Based on their results, the error of Eq. (6.1a) is reported to be about 1.5%. Note that SE(T) specimens with $H/W = 10$ and $B/W \geq 1$ are generally preferred because the corresponding crack-tip stress fields are close to those of the full-scale pipes containing cracks Shen et al. (2008b). The adequacy of Eqs. (6.1b) and (6.1c) for the SG SE(T) specimen has not been investigated.

6.1.2 Literature Review of $B_{e(2)}$ and $B_{e(3)}$

The experimental evaluation of J includes separate calculations of its elastic and plastic components, J_{el} and J_{pl} (see Eq. (2.4)). J_{el} can be determined from the stress intensity factor, K, through Eq. (2.5) and J_{pl} can be evaluated using Eq. (2.8). K can be estimated using Eq. (2.22) where the non-dimensional function $F(a/W)$ for SE(T) specimens has been well documented by Ahmad et al. (1991), John and Rigling (J&R) (1998) (for $H/W = 10$), Cravero and Ruggieri (C&R) (2007) and Shen et al. (2008a) (see Fig. 2.5). Note that for SG specimens, Eqs. (2.22a) and (2.8) need to be revised by replacing B with the corresponding effective specimen thickness, $B_{e(2)}$ and $B_{e(3)}$, respectively.

The origin of Eq (6.1b) is found in a study by Freed and Krafft (1966), who proposed $B_{e(2)}$ for the four-point bend SE(B) specimen (SE(4PB)) to be given by

$$B_{e(2)} = B\left(\frac{B_N}{B}\right)^{\tau} \qquad (6.2)$$

where τ is a coefficient between 0.5 and unity depending on the material isotropy and d_{sg}/B. In the experimental work carried out by Rolfe and Novak (1970), Eq. (6.2) with τ equal to 0.5 and 0.7 for $d_{sg}/B \leqslant 5\%$ and $d_{sg}/B = 30\%$, respectively, was employed to determine the

critical stress intensity factor (K_{IC}) for SE(4PB) specimens made of isotropic materials. Note that Eq. (6.2) with $\tau = 0.5$ is equivalent to Eq. (6.1b).

Zhang and Shi (1992) proposed the following $B_{e(3)}$ equation for the SE(B) specimen:

$$B_{e(3)} = B_N \left[1 + 0.67 \left(\frac{B_N}{B} \right) \left(1 - \frac{B_N}{B} \right) \right] \qquad (6.3)$$

Machida (1997) developed the following $B_{e(3)}$ equation for C(T) and CC(T) specimens:

$$B_{e(3)} = \mu \sqrt{BB_N} \qquad (6.4)$$

where $\mu = 0.95$ for the C(T) specimen, and μ ranges from 0.85 to 1 for the CC(T) specimen depending on the specimen thickness.

The recently published R-curve test standard BS 8571 (BSI, 2014) adopts Eqs. (6.1a) – (6.1c) for SG SE(T) specimens with $B/W < 1$. For specimens with $B/W \geq 1$, Eq. (6.1c) is replaced by Eq. (6.4) with $\mu = 1$, which is the same as Eq. (6.1b). A thickness correction factor, $\psi_{(i)}$, is introduced in this study to relate the specimen effective thickness to the gross thickness, i.e. $B_{e(i)} = \psi_{(i)}B$ ($i = 2$ and 3). Equations (2.22a) and (2.8) can then be written for both the PS and SG specimens as follows:

$$\begin{cases} K = \dfrac{P}{\psi_{(2)}B\sqrt{W}} F\left(\dfrac{a}{W} \right) & \text{(a)} \\[4mm] J_{pl} = \dfrac{\eta_{pl}^{CMOD} A_{pl}^{CMOD}}{\psi_{(3)}B(W - a)} & \text{(b)} \end{cases} \qquad (6.5)$$

where η_{pl}^{CMOD} and A_{pl}^{CMOD} are the crack mouth opening displacement- (*CMOD*-) based plastic geometry factor and plastic work. Note that for PS specimen, $\psi_{(i)} = 1$. Let $\chi = B_N/B$ denote the ratio between the net and gross specimen thicknesses. The expressions for $\psi_{(i)}$ corresponding to the effective thickness expressions given in Eq. (6.1) are therefore

$$\begin{cases} \psi_{(2)} = \chi^{0.5} & \text{, for stress intensity factor } (K) \qquad \text{(a)} \\ \psi_{(3)} = \chi & \text{, for plastic component of } J \left(J_{pl} \right) \qquad \text{(b)} \end{cases} \qquad (6.6)$$

Similarly, Eqs. (6.2), (6.3) and (6.4) can be recast as Eqs. (6.7a), (6.7b) and (6.7c), respectively as follows:

$$\begin{cases} \psi_{(2)} = \chi^{\tau} & \text{, for } K \quad \text{(Freed and Krafft, 1966)} \qquad \text{(a)} \\ \psi_{(3)} = \chi \left(1 + 0.67\chi - 0.67\chi^2 \right) & \text{, for } J_{pl} \quad \text{(Zhang and Shi, 1966)} \qquad \text{(b)} \\ \psi_{(3)} = \mu\chi^{0.5} & \text{, for } J_{pl} \quad \text{(Machida, 1966)} \qquad \text{(c)} \end{cases} \qquad (6.7)$$

6.1.3 Objective and Approach

The objective of the study reported in this chapter is to carry out a 3D FEA-based investigation of the effective thickness for the stress intensity factor and the plastic component of J, J_{pl}, for SE(T) specimens with wide ranges of a/W and d_{sg}/B. The focus of the present study is the clamped SE(T) specimen with $H/W = 10$. Only specimens with $B/W = 1$ are investigated as previous studies (DNV, 2006; Malpas et al., 2012) suggest that the crack fronts in SE(T) specimens with $B/W > 1$ are likely to remain relatively straight without side grooving. Based on the analysis of the obtained results, the adequacy of Eqs. (6.1b) and (6.1c) is examined, and new effective thickness expressions for the evaluation of the stress intensity factor and of J_{pl} are proposed for the SE(T) specimen.

This chapter is organized as follows. Section 6.2 describes the finite element models and analysis procedures. The thickness correction factors for the stress intensity factor and for the J_{pl} for the SE(T) specimen are obtained and discussed in Section 6.3, and the proposed expressions and values are validated in Section 6.4. Finally, summary and conclusions are presented in Section 6.5.

6.2 Numerical Analysis

6.2.1 Finite Element Model

The commercial software ADINA® 9.0.1 (ADINA, 2012) is used to carry out FEA. Due to symmetry, only a quarter of a given specimen is modeled in the FEA. The geometric configuration of a typical SE(T) specimen in the FEA is shown in Fig. 6.2(a) together with the fixation and loading conditions. All the specimens included in this study have a width $W = 20$ mm, a daylight (H) of $10W$ and a thickness $B = W = 20$ mm. Both PS and SG specimens were modeled and parameters (e.g., $F(a/W)$ and η_{pl}) obtained from the PS specimens are used as the reference to evaluate $\psi_{(i)}$. The analyses matrix consists of six crack lengths (i.e. $a/W = 0.2, 0.3, 0.4, 0.5, 0.6$ and 0.7) and eleven side groove depths (i.e. $d_{sg}/B = 0\%, 3\%, 4\%, 5\%, 6\%, 7\%, 7.5\%, 8\%, 9\%, 10\%$, and 12.5%) with the corresponding thickness reduction ratios $\chi = 1, 0.94, 0.92, 0.9, 0.88, 0.86, 0.85, 0.84, 0.82, 0.8$ and 0.75, respectively. The side groove is modeled as a U-notch (i.e. $\theta_{sg} = 0$) with a fixed root radius $r_{sg} = 0.5$ mm as recommended in ASTM E1820 (ASTM, 2013). Schematics of U-notched side grooves are shown in Figs. 6.2(b). The 8-node 3D brick elements with $2\times2\times2$ integration are used.

Stationary cracks are incorporated in the FE model. A sharp crack tip is assumed and the surfaces of the brick elements are collapsed to a line at the crack tip to ensure the simulation of the singularity (see Fig. 6.2(c)). A spider-web mesh around the crack tip was established with 45 concentric semicircles (i.e. rings) surrounding the crack tip. The in-plane and out-of-plane lengths of the elements closest to the crack tip are about $1/2000W$ and $1/200B$, respectively. The model is divided into 10 layers over the half net thickness ($B_N/2$). For the SG model, the side groove ($(B - B_N)/2$) was divided into 12 layers. The mesh density increases from the mid plane to the free surface (or root of the side groove) to capture the high stress gradients near the free surface. The total number of elements is approximately 15,000 in a typical PS specimen, and 28,000 in a typical SG specimen.

6.2.2 Material Model

An elastic-plastic constitutive model based on the J_2 incremental theory of plasticity as well as the small-displacement small-strain formulation (ADINA, 2012) is adopted in FEA. The true stress (σ) and true strain (ε) relationship of the material is characterized by Eq. (2.19) where σ_{YS} is the yield strength; $\varepsilon_0 = \sigma_{YS}/E$, and n is the strain hardening exponent. In this study, a material with $\sigma_{YS} = 510$ MPa, $E = 207$ GPa, $v = 0.3$, and $n = 13$ is selected to simulate the X80 (API, 2012) grade pipeline steel. The flow stress (σ_Y) that is used to determine the limit load ($P_Y = B_N(W - a)\sigma_Y$) (Shen et al., 2008, 2009) for the SE(T) specimen is calculated as ($\sigma_{YS} + \sigma_{UTS}$)/2. The quantity σ_{UTS} is the ultimate tensile strength and can be estimated from Eq. (2.20) where ε_u is the (true) strain corresponding to σ_{UTS} and assumed to equal $1/n$ (Dieter, 1986). For the material considered in this study, σ_{UTS} is estimated to be 615 MPa ($\sigma_{YS}/\sigma_{UTS} = 0.829$) and $\sigma_Y = 563$ MPa.

6.2.3 Computational Procedure

The load is applied based on the displacement-controlled condition. Uniform displacements (h) are applied on the two clamped surfaces with a length of $2W$ (see Fig. 6.2(a)). Evaluations of $F(a/W)$ and η_{pl}^{CMOD} require computation of the load-displacement, i.e. P-$CMOD$, response in the FEA. The load P is calculated as the total reactions of the nodes on the clamped surface while $CMOD$ (V) is recorded at the mid-plane of the specimen.

The values of J in each layer along the thickness direction, i.e. the local J values, were calculated using the virtual crack extension method (Anderson, 2005; ADINA, 2012). A brief description of this method is included in Appendix B. The weighted average J value over the entire crack front, J_{ave}, is then calculated based on the trapezoidal rule as detailed in Section 2.2.3. To ensure the path-independence of the calculated J values, the two outermost semicircular rings surrounding the crack tip were used to define the virtual shifts. For a representative specimen with $a/W = 0.5$, $B/W = 1$ and $\chi = 0.85$, the difference between J_{ave} corresponding to the 20th and 45th ring is about 3.6%, and the difference between J_{ave} corresponding to the 40th and 45th rings is about 0.7% at the loading level of $P/P_Y = 1.3$.

These results demonstrate that the J_{ave} values determined from rings remote from the crack tip are indeed path independent.

At small loading levels (i.e. $P/P_Y = 0.02$ to 0.05), J is equivalent to the linear-elastic energy release rate and the average stress intensity factors (K_{ave}) can be calculated through the following equations:

$$K_{ave} = \sqrt{\frac{J_{ave}E}{1-v^2}} \qquad (6.8)$$

The values of K_{ave} determined from FEA for PS specimens are first used to evaluate the values of the non-dimensional function $F(a/W)$ in Eq. (2.22a) by equating Eqs. (2.22a) and (6.8). The value of $\psi_{(2)}$ for an SG specimen with a given a/W is then evaluated as follows based on K_{ave} determined from FEA for the SG specimen and the value of $F(a/W)$ determined for the PS specimen with the same a/W:

$$\psi_{(2)} = \frac{PF\left(\dfrac{a}{W}\right)}{K_{ave}B\sqrt{W}} \qquad (6.9)$$

To evaluate the value of $\psi_{(3)}$ for an SG specimen with a given a/W, the following procedure is employed. The value of η_{pl}^{CMOD} for the PS specimen with the same a/W is determined first. This requires computation of the plastic component of J (J_{pl}) and plastic work (A_{pl}^{CMOD}) for the specimen. At a given loading level (i.e. h/a), J_{pl} is calculated as the difference between J_{ave} and J_{el} as indicated in Eqs. (2.4) and (2.5). The calculation of A_{pl}^{CMOD} follows Eq. (2.23), which is consistent with Fig. 2.2. A single value of η_{pl}^{CMOD} for the PS specimen is determined from the regression analysis of a set of data within a certain range of loading levels. In general, the η_{pl}^{CMOD} factor is approximately independent of the loading level at $P \geq P_Y$ (see Section 2.3.1) and the maximum loading level in typical tests is about 1.1 to $1.3P_Y$ for clamped SE(T) specimens (Shen et al., 2008b; Dodds and Read, 1990; Pussegoda et al., 2013). In this study, the regression analysis is carried out to obtain η_{pl}^{CMOD} within the loading range $P_Y \leq P \leq 1.3P_Y$ by minimizing the sum of relative errors of the estimated J values (e_{ac}) as defined in Eq. (2.25) where J_η is the J value estimated from

Eqs. (2.4), (2.5), (2.8), (2.22a) and (2.23) based on a given η_{pl}^{CMOD} at a specific loading level, and the summation is carried over all the loading levels between P_Y and $1.3P_Y$. Once η_{pl}^{CMOD} for the PS specimen is determined, the value of $\psi_{(3)}$ for the SG specimen is evaluated by minimizing the sum of e_ψ as defined in Eq. (6.10a):

$$
\begin{cases}
\sum_P |e_\psi| = \sum_P \left| \dfrac{J_\psi - J_{pl}}{J_{pl}} \right| & \text{(a)} \\[3ex]
J_\psi = \dfrac{\eta_{pl}^{CMOD} A_{pl}^{CMOD}}{\psi_{(3)} B(W-a)} & \text{(b)}
\end{cases}
\qquad (6.10)
$$

where J_ψ is the plastic component of J estimated from Eq. (6.10b) based on a given $\psi_{(3)}$ at a specific loading level; $J_{pl} = J_{ave} - J_{el}$ is the plastic component of J evaluated from FEA at the same loading level; A_{pl}^{CMOD} is the plastic work for the SG specimen, and the summation in Eq. (6.10a) is over all the loading levels between P_Y and $1.3P_Y$.

6.3   Results and Discussions

6.3.1   Effective Thickness for Stress Intensity Factor

The values of $\psi_{(2)}$ for SG specimens with different χ are listed in Table 6.1 and plotted in Fig. 6.3. For comparisons, the values of $\psi_{(2)}$ obtained from Eq. (6.6a) and Eq. (6.7a) with $\tau = 0.7$, respectively (Eq. (6.6a) is equivalent to Eq. (6.7a) with $\tau = 0.5$), are also shown in Fig. 6.3. The figure indicates that the $\psi_{(2)}$ values obtained in this study are not sensitive to a/W and generally lie between those from Eq. (6.6a) and Eq. (6.7a) with $\tau = 0.7$. The following equation for $\psi_{(2)}$ as a power-law function of χ is proposed based on the $\psi_{(2)}$ values given in Table 1:

$$
\psi_{(2)} = \chi^{0.58} \qquad \left(0.75 \le \chi \le 1, \ \ 0.2 \le \frac{a}{W} \le 0.7 \right) \qquad (6.11)
$$

The maximum fitting error of Eq. (6.11) is about 2%. Equation (6.11) corresponds to Eq. (6.7a) with $\tau = 0.58$.

6.3.2 Effective Thickness for Plastic Component of J

The values of $\psi_{(3)}$ for the SG specimens with different χ are listed in Table 6.2 and plotted in Fig. 6.4, together with Eqs. (6.6b), (6.7b) and (6.7c) with $\mu = 0.95$ and 1. The $\psi_{(3)}$ values obtained from Eq. (6.6b) are close to (the difference being less than 4%) those obtained in this study for specimens with $a/W = 0.7$ and $\chi \leq 0.88$, and specimens with $0.2 \leq a/W \leq 0.6$ and $\chi \geq 0.88$. On the other hand, the values of $\psi_{(3)}$ obtained from Eqs. (6.7b) and (6.7c) with $\mu = 1$ are generally greater than those obtained in this study by 2 to 35%; Eq. (6.7c) with $\mu = 0.95$ is adequate to calculate $\psi_{(3)}$ only for $0.88 \leq \chi \leq 0.92$; therefore, Eqs. (6.7b) and (6.7c) are considered unsuitable for the SE(T) specimens. Because $\psi_{(3)}$ obtained in this study show high dependency on a/W when $\chi \leq 0.9$. It is recommend using the $\psi_{(3)}$ listed in Table 6.2 and interpolating values for other a/W ratios once χ is given.

6.4 Validation of Proposed Thickness Correction Factors

6.4.1 Accuracy of the Proposed $\psi_{(2)}$

To investigate the adequacy of the proposed equation for $\psi_{(2)}$, Eq. (6.11), the K values estimated from Eq. (6.5a) corresponding to a given $F(a/W)$, K_F, are compared with the corresponding K_{ave} values obtained from FEA. The prediction error for K_F, e_K, is then calculated as

$$e_K = \frac{K_F - K_{ave}}{K_{ave}} \times 100\% \qquad (6.12)$$

For comparison, $\psi_{(2)}$ values evaluated from Eqs. (6.6a) are also used to compute K_F. The solution of $F(a/W)$ proposed by Shen et al. (2008a) (i.e. Eq. (2.22b)) is selected because this solution is practically identical to the solutions reported in three other independent studies (Ahmad et al., 1991; John and Rigling, 1998; Cravero and Ruggieri, 2007) and therefore considered accurate. A comparison of these solutions is shown in Fig. 2.5. Table 6.3 lists values of e_K for specimens with various a/W and χ. The table indicates that $|e_K|$ ranges from 0% to 5.8% if Eqs. (6.6a) is used to evaluate $\psi_{(2)}$. On the other hand, $|e_K|$

ranges from 0% to 3.6% if Eq. (6.11) is used to evaluate $\psi_{(2)}$. Furthermore, the use of Eq. (6.11) makes e_K less dependent on χ.)

6.4.2   Accuracy of the Proposed $\psi_{(3)}$

The validation of the proposed $\psi_{(3)}$ values, listed in Table 6.2, was conducted based on the FEA results (*P-CMOD* curve and J_{ave}) for SG SE(T) specimens with $B/W = 1$, $a/W = 0.2$, 0.25, 0.3, 0.35, 0.4, 0.45 and 0.5, $d_{sg}/B = 7.5\%$ (i.e. $\chi = 0.85$),the strain hardening exponent $n = 8.5$, 10, 15 and 20 from a separate study reported in Chapter 3. The range of n values between 8.5 and 20 is considered representative of typical pipeline steels. Note that the FEA results in Chapter 3 are based on large-strain/large displacement formulation.

The prediction error of J_η, e_J, as defined in Eq. (2.25) is estimated with J_η evaluated from Eqs. (2.4), (2.5), (2.22b), (6.5a) and (6.5b) based on the given η_{pl}^{CMOD}. The values of η_{pl}^{CMOD} used in the error analyses are developed in Chapter 2 based on the large-strain FEA results of PS SE(T) specimens and are listed in Table 2.3(a). $\psi_{(2)}$ is determined using Eq. (6.11), whereas two different $\psi_{(3)}$ values evaluated from Table 6.2 and Eq. (6.6b), respectively, are used to calculate e_J.   Figure 6.5 depicts e_J as a function of the loading level characterized by P/P_Y. Only values of e_J corresponding to $0.8 \leq P/P_Y \leq 1.3$ (or J_{ave} approximately between 100 and 400 kN/m) are shown in the figure. Figure 6.5 indicates that the η_{pl}^{CMOD} values in Table 2.3 together with $\psi_{(3)}$ values in Table 6.2 generally lead to underestimated J values (i.e. $e_J < 0$) for $0.8 \leq P/P_Y \leq 1.2$, but overestimated J values (i.e. $e_J > 0$) for $P > 1.2P_Y$, for specimens with a/W ratios from 0.2 to 0.5 and $8.5 \leq n \leq 20$. On the other hand, J_η associated with Eq. (6.6b) continually underestimates J_{ave} throughout the considered loading level. The values and variation of e_J within the considered loading levels for specimens with $a/W = 0.25$, 0.35 and 0.45 are similar to those shown in Fig. 6.5, and are not shown for the sake of brevity. Table 6.4 summarize the maximum values of $|e_J|$ for 1.0 $\leq P/P_Y \leq 1.3$ for all the validation cases considered. The results in Table 6.4 indicate that $|e_J|$ corresponding to $\psi_{(3)}$ values in Table 6.2 are generally controlled within 7% and 10 to 20% lower than $|e_J|$ associated with Eq. (6.6b). The maximum values of $|e_J|$ within the considered loading levels for SG specimens are similar to those obtained from PS

specimens reported in Section 2.4.2, which are between 4 and 8%. Therefore, the proposed $\psi_{(3)}$ values are considered effective for these specimen configurations and materials.

6.5 Conclusions

Three-dimensional finite element analyses are carried out to investigate the effective thickness for the stress intensity factor and η_{pl}-based J evaluation of the clamped SE(T) specimen. Specimens with $H/W = 10$, $B/W = 1$, a/W ratios from 0.2 to 0.7 and χ values from 1 to 0.75 are analyzed. The thickness correction factors corresponding to K and J_{pl} are evaluated and compared with those reported in the literature. Based on the FEA results, a new expression for $\psi_{(2)}$ is proposed as functions of χ. Validation analyses show that the maximum prediction error in K is 3.6% by using the proposed expression for $\psi_{(2)}$, whereas the maximum prediction error in K is 5.8% by using the expression for $\psi_{(2)}$ adopted in ASTM E1820, BS 7448 and ISO 12135. By using the proposed $\psi_{(3)}$ values, the maximum errors in the η_{pl}-based J values for the SG specimens are generally 4% to 8%, whereas such errors are 5% to 10% by using the expression for $\psi_{(3)}$ adopted in ASTM E1820, BS 7448 and ISO 12135. The research outcome will facilitate the evaluation of J-R curves using SG SE(T) specimens.

References

ADINA. (2012). Theory and Modeling Guide, ADINA R. & D. Inc., Watertown, USA.

Ahmad, J., Papaspyropoulos, V. and Hopper, A. T. (1991). Elastic-plastic analysis of edge-notched panels subjected to fixed grip loading. *Engineering fracture mechanics*, 38(4):283-294.

Anderson, T. L. (2005). *Fracture Mechanics—Fundamentals and Applications, Third edition*. CRC Press, Boca Raton.

Andrews, W. R., and Shih, C. F. (1979). Thickness and Side-groove Effects on J- and δ-resistance Curves for A533-B Steel at 93°C, *Elastic-Plastic Fracture*, *ASTM STP 668*,

Landes, J. D., Begley, J. A., and Clarke, G.A., Eds., ASTM International, West Conshohocken, PA, pp. 426-450.

API. (2012). *API Specification 5L: Specification for Line Pipe*, Ed. 45, American Petroleum Institute, Washington, D.C.

ASTM (2013). *ASTM E1820-13: Standard Test Method for Measurement of Fracture Toughness*. America Society of Testing and Materials International, West Conshohocken, PA.

BSI (1997). *BS 7448-4: Method for determination of fracture resistance curves and initiation values for stable crack extension in metallic materials,* British Standard Institution, London.

BSI (2014). *BS 8571: Method of Test for Determination of Fracture Toughness in Metallic Materials Using Single Edge Notched Tension (SENT) Specimens*, British Standards Institution, London.

Chiesa, M., Nyhus, B., Skallerud, B. and Thaulow, C. (2001). Efficient fracture assessment of pipelines: A constraint-corrected SENT specimen approach. *Engineering Fracture Mechanics*, 68:527-547.

Cravero, S. and Ruggieri, C. (2007). Estimation Procedure of J Resistance Curves for SE (T) Fracture Specimens Using Unloading Compliance. *Engineering Fracture Mechanics*, 74(17):2735-2757.

Det Norske Veritas. (2006). Fracture control for pipeline installation methods introducing cyclic plastic strain. DNV-RP-F108. Norway: DNV.

Dieter, G. E. (1986). Mechanical metallurgy: McGraw-Hill.

Dodds, R, H. and Read, D. (1990). Experimental and numerical studies of the *J*-integral for a surface flaw. *International Journal of Fracture*, 43:47-67.

Donato, G. H. B. and Moreira, F. C. (2013). Effects of Side-Grooves and 3-D Geometries on Compliance Solutions and Crack Size Estimations Applicable to C(T), SE(B) and Clamped SE(T) Specimens. *ASME 2013 Pressure Vessels and Piping Conference: American Society of Mechanical Engineers*;. p. V06ATA019-V06AT06A.

Donato G.H.B. and Moreira F.C. (2014). Improved compliance solutions for C(T), SE(B) and clamped SE(T) specimens including side-grooves, varying thicknesses and 3-D effects, *ASME 2014 International Mechanical Engineering Congress and Exposition*, Montreal, Canada, November 14–20.

Freed, C. N. and Krafft, J. M. (1966). Effect of Side Grooving on Measurements of Plane-strain Fracture Toughness, *Journal of Materials*, 1(4):770-790.

Huang, Y., Zhou, W. and Yan, Z. (2013). Evaluation of plastic geometry factor for SE(B) specimens based on three-dimensional finite element analyses. *International Journal of Pressure Vessels and Piping*, 123:99-110.

ISO (2002). *ISO 12135: Metallic materials–Unified method of test for the determination of quasistatic fracture toughness*. International Organization for Standardization, Geneva.

John, R. and Rigling, B. (1998). Effect of height to width ratio on *K* and *CMOD* solutions for a single edge cracked geometry with clamped ends. *Engineering fracture mechanics*, 60(2):147-156.

Lucon, E., Scibetta, M. (2009). *SCK•CEN-BLG-1064: Influence of Side-groove Root Radius on the Ductile Fracture Toughness of Miniature C(T) Specimens*, Belgian Nuclear Research Center SCK-CEN, Belgium.

Machida, K. (1997). J_{IC} Evaluation and Effective Thickness of Thin Specimens with and without Side-grooves, *International Journal of Pressure Vessels and Piping*, 71(2):181-188.

Malpas, A. R., Moore, P. L. and Pisarski, H. G. (2012). Crack front straightness qualification in SENT specimens. The 22nd International Ocean and Polar Engineering Conference Rodos Palace Hotel, Rhodes, Greece: ISOPE, p.613-618

Park, D-Y., Tyson, W. R., Gianetto, J. A., Shen, G. and Eagleson, R. S. (2010). Evaluation of Fracture Toughness of X100 Pipe Steel Using SE(B) and Clamped SE (T) Single Specimens, *Proceedings of the eighth ASME International Pipeline Conference*, Calgary, Alberta, Canada, September 27 - October 1, pp. 101-108.

Pisarski, H. G., Moore, P. L., Hutchison, E. and Horn, A. (2013). Development of a British Standard Single Edge Notch Tension (SENT) Test Method (BS 8571), *Proceedings of the Sixth International Pipeline Technology Conference*, Ostend, Belgium, October 6-9, 2013, Paper S07-5.

Pussegoda, L. N., Tiku, S., Tyson, W. R., Park, D-Y., Gianetto, J. A., Shen, G. and Pisarski, H.G. (2013). Comparison of resistance curves from multi-specimen and single-specimen SENT Tests. *Proceedings of Twenty-third International Offshore and Polar Engineering Conference*. Anchorage, Alaska, USA: The International Society of Offshore and Polar Engineers (ISOPE); p. 482-488.

Rolfe, S. T. and Novak, S. R. (1970). Slow bend K_{IC} Testing of Medium Strength, High Toughness Steels, *Review of Developments in Plane Strain Fracture Toughness Testing*, *ASTM STP 463*, Brown, W. F., Ed., ASTM International, West Conshohocken, PA, pp. 124-159.

Shen, G., Gianetto, J. A, and Tyson, W. R. (2008a). Report 2008-18(TR): Development of procedure for low-constraint toughness testing using a single-specimen technique. Ottawa, Canada: CANMET-MTL.

Shen, G., Bouchard, R., Gianetto, J. A. and Tyson, W. R. (2008b). Fracture toughness evaluation of high strength steel pipe. *ASME Conference Proceedings*, 1275-1282.

Shen, G., Tyson, W. R., Gianetto, J. A. and Park, D-Y. (2010). Effect of side grooves on compliance, *J*-Integral and constraint of a clamped SE(T) specimen. *ASME Conference Proceedings*, 81-89.

Shih, C. F., Lorenzi, H. G. and Andrews, W. R. (1977). Elastic compliances and stress-intensity factors for side-grooved compact specimens. *International Journal of Fracture*, 13:544-548.

Tang, H., Macia, M., Minnaar, K., Gioielli, P., Kibey, S. and Fairchild, D. (2010). Development of the SENT test for strain-based design of welded pipelines. *ASME Conference Proceedings*, 303-312.

Wang, E., Zhou, W., Shen, G. and Duan, D. (2012). An Experimental Study on J(CTOD)-R Curves of Single Edge Tension Specimens for X80 Steel, *International Pipeline Conference*, Calgary, Alberta, Canada, September 24–28, 2012, Paper Number: IPC2012-90323.

Wang, E., Zhou, W. and Shen, G. (2013). Three-dimensional finite element analysis of crack-tip fields of clamped single-edge tension specimens – Part I: Crack-tip stress fields. *Engineering Fracture Mechanics*, 116:122-143.

Yasufumi, I. and Tomokazu, M. (1984). Effect of Side Grooves for Three-point Bending Fracture Toughness Specimens - Three-Dimensional Elastic-Plastic Finite Element Analysis, *Bulletin of Japan Society of Mechanical Engineers*, 27(227):909-916.

Zhang, X. P. and Shi, Y. W. (1992). Constraint of Side-groove and Its Influence on Fracture Toughness Parameter in Charpy-size Specimens, *Engineering Fracture Mechanics*, 43(5):863-867.

Zhu, X. K., Leis, B. N., and Joyce, J. A. (2008). Experimental estimation of *J-R* curves from load-*CMOD* record for SE(B) specimens. *Journal of ASTM International*, 5:66-86.

Table 6.1: Thickness correction factors ($\psi_{(2)}$) for stress intensity factor.

a/W	F(a/W)	χ										
		1.00	0.94	0.92	0.90	0.88	0.86	0.85	0.84	0.82	0.80	0.75
0.2	1.06	1.0000	0.9683	0.9561	0.9431	0.9294	0.9152	0.9079	0.9005	0.8853	0.8697	0.8290
0.3	1.51	1.0000	0.9705	0.9582	0.9452	0.9316	0.9174	0.9101	0.9026	0.8875	0.8719	0.8314
0.4	2.07	1.0000	0.9703	0.9580	0.9450	0.9313	0.9171	0.9098	0.9025	0.8874	0.8719	0.8318
0.5	2.78	1.0000	0.9700	0.9576	0.9447	0.9312	0.9171	0.9100	0.9027	0.8879	0.8728	0.8337
0.6	3.69	1.0000	0.9700	0.9578	0.9451	0.9318	0.9182	0.9112	0.9042	0.8899	0.8754	0.8381
0.7	4.81	1.0000	0.9702	0.9585	0.9462	0.9336	0.9207	0.9142	0.9076	0.8943	0.8808	0.8463

Table 6.2: Thickness correction factors ($\psi_{(3)}$) for plastic component of J (J_{pl}).

a/W	η_{pl}	χ										
		1.00	0.94	0.92	0.90	0.88	0.86	0.85	0.84	0.82	0.80	0.75
0.2	0.88	1.0000	0.9431	0.9199	0.8941	0.8647	0.8327	0.8145	0.7936	0.7518	0.7164	0.6171
0.3	0.83	1.0000	0.9362	0.9098	0.8791	0.8469	0.8126	0.7937	0.7736	0.7344	0.6914	0.6066
0.4	0.77	1.0000	0.9279	0.8983	0.8666	0.8336	0.8008	0.7815	0.7614	0.7282	0.6937	0.6126
0.5	0.71	1.0000	0.9314	0.9024	0.8718	0.8410	0.8084	0.7899	0.7742	0.7423	0.7100	0.6374
0.6	0.61	1.0000	0.9412	0.9166	0.8884	0.8601	0.8308	0.8157	0.8004	0.7717	0.7409	0.6709
0.7	0.51	1.0000	0.9807	0.9567	0.9324	0.9065	0.8794	0.8666	0.8517	0.8241	0.7995	0.7375

Table 6.3: Variation of e_K (%) with χ.

a/W	$\psi_{(2)}$	χ										
		1.00	0.94	0.92	0.90	0.88	0.86	0.85	0.84	0.82	0.80	0.75
0.2	Eq. (6.6a)	-1.6	-1.7	-1.9	-2.2	-2.5	-2.9	-3.1	-3.3	-3.8	-4.3	-5.8
	Eq. (6.11)	-1.6	-1.3	-1.3	-1.4	-1.5	-1.7	-1.8	-2.0	-2.3	-2.6	-3.6
0.3	Eq. (6.6a)	-1.2	-1.1	-1.3	-1.5	-1.8	-2.2	-2.4	-2.7	-3.1	-3.6	-5.1
	Eq. (6.11)	-1.2	-0.6	-0.6	-0.7	-0.8	-1.0	-1.2	-1.3	-1.6	-1.9	-2.9
0.4	Eq. (6.6a)	-1.5	-1.4	-1.6	-1.9	-2.2	-2.6	-2.8	-3.0	-3.5	-4.0	-5.4
	Eq. (6.11)	-1.5	-1.0	-1.0	-1.1	-1.2	-1.4	-1.5	-1.7	-2.0	-2.3	-3.2
0.5	Eq. (6.6a)	-1.1	-1.0	-1.2	-1.5	-1.8	-2.1	-2.3	-2.5	-3.0	-3.5	-4.8
	Eq. (6.11)	-1.1	-0.5	-0.6	-0.6	-0.8	-1.0	-1.1	-1.2	-1.4	-1.7	-2.5
0.6	Eq. (6.6a)	0.4	0.4	0.2	0.0	-0.3	-0.6	-0.8	-1.0	-1.4	-1.8	-2.9
	Eq. (6.11)	0.4	0.9	0.9	0.8	0.7	0.6	0.5	0.4	0.2	0.0	-0.6
0.7	Eq. (6.6a)	0.7	0.8	0.7	0.5	0.3	0.0	-0.1	-0.2	-0.5	-0.8	-1.5
	Eq. (6.11)	0.7	1.3	1.3	1.3	1.3	1.2	1.2	1.2	1.1	1.0	0.7

Table 6.4: Maximum absolute values of e_J (%) corresponding to η_{pl}^{CMOD} over $P/P_Y = 1.0$ to 1.3

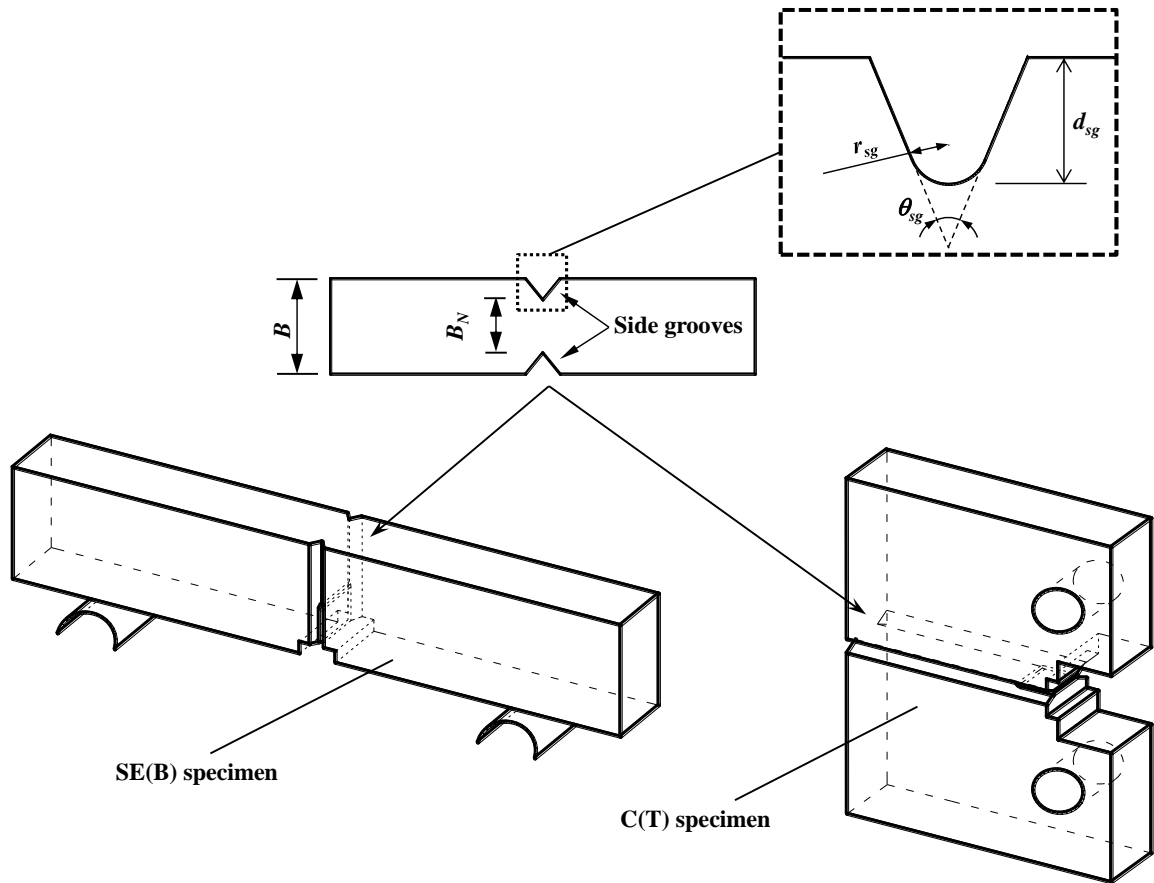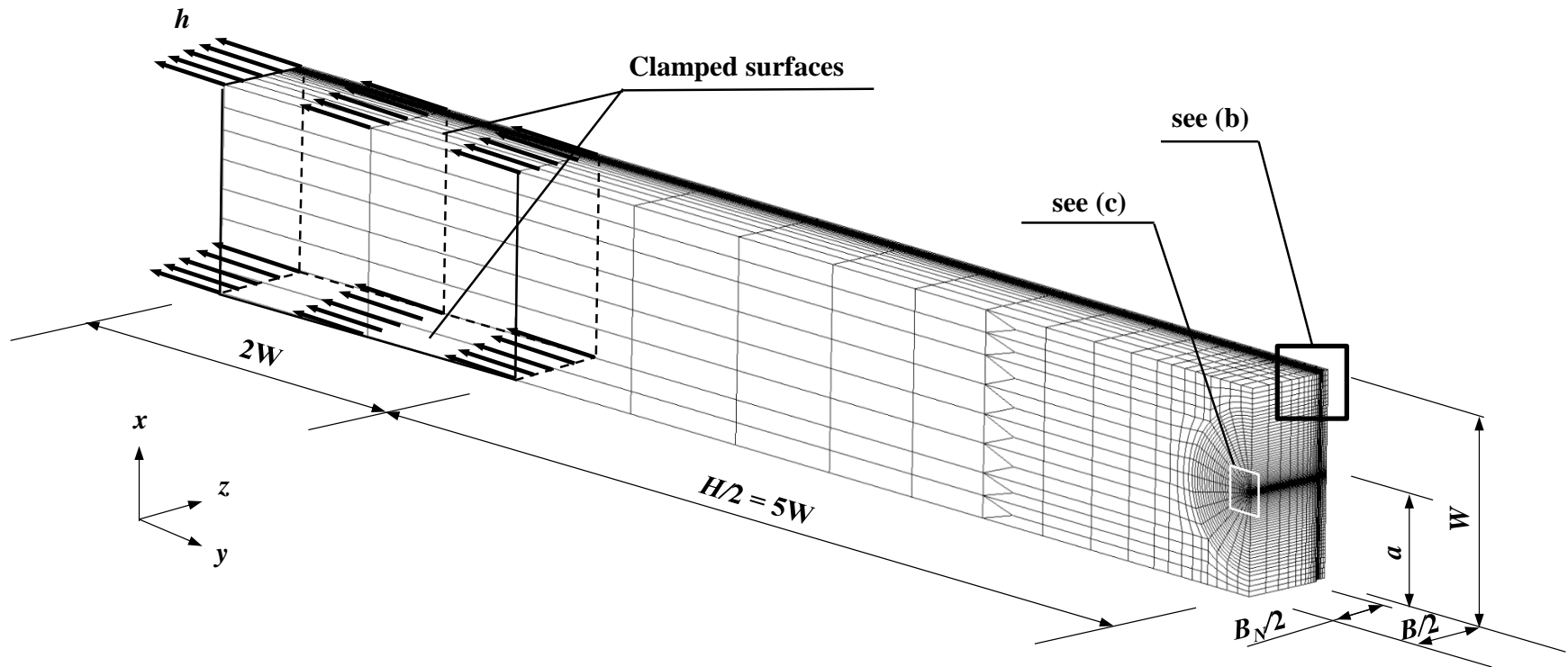| n	a/W													
	0.2		0.25		0.3		0.35		0.4		0.45		0.5	
	Table 6.2	Eq. (6.6b)	Table 6.2	Eq. (6.6b)	Table 6.2	Eq. (6.6b)	Table 6.2	Eq. (6.6b)	Table 6.2	Eq. (6.6b)	Table 6.2	Eq. (6.6b)	Table 6.2	Eq. (6.6b)
8.5	5.7	7.3	-	-	4.0	6.6	-	-	6.5	5.5	-	-	4.5	4.6
10	6.7	8.1	4.6	6.1	4.3	6.6	5.4	6.2	4.7	6.3	4.4	5.7	4.8	4.3
15	8.0	9.2	-	-	5.1	7.3	-	-	3.9	6.8	-	-	3.8	4.8
20	9.0	10.0	-	-	5.8	7.8	-	-	4.6	7.4	-	-	3.4	5.0

Figure 6.1. Schematics of the side-grooved single-edge and compact tension specimens

(a) Configuration of a typical side-grooved FE model with $a/W = 0.5$
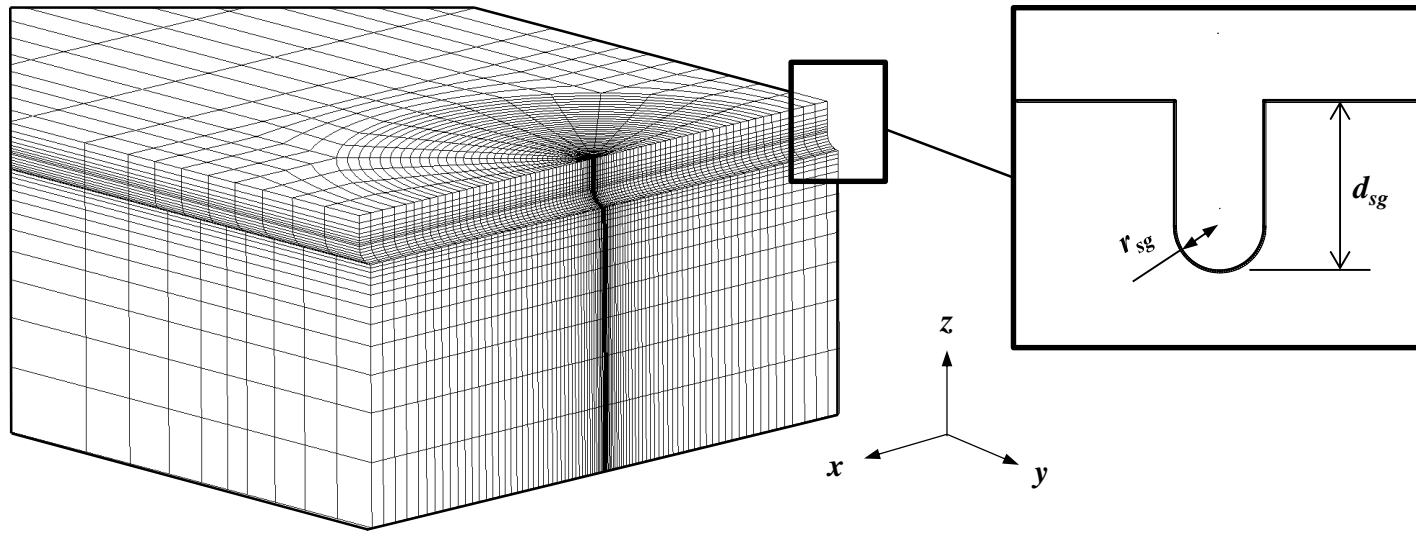
(b) Configuration of the U-shape side groove
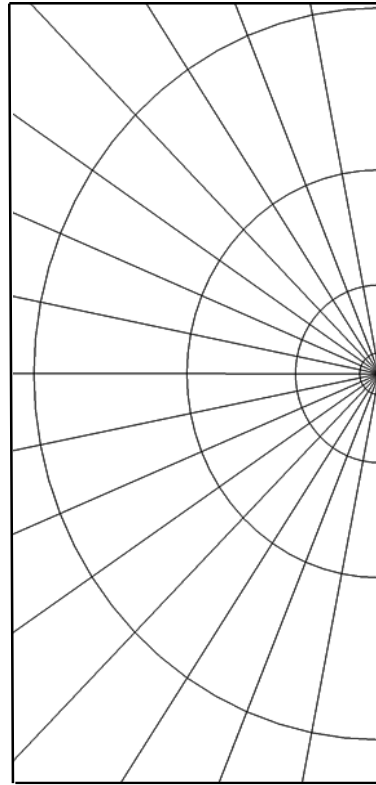
(c) Mesh around the sharp crack tip

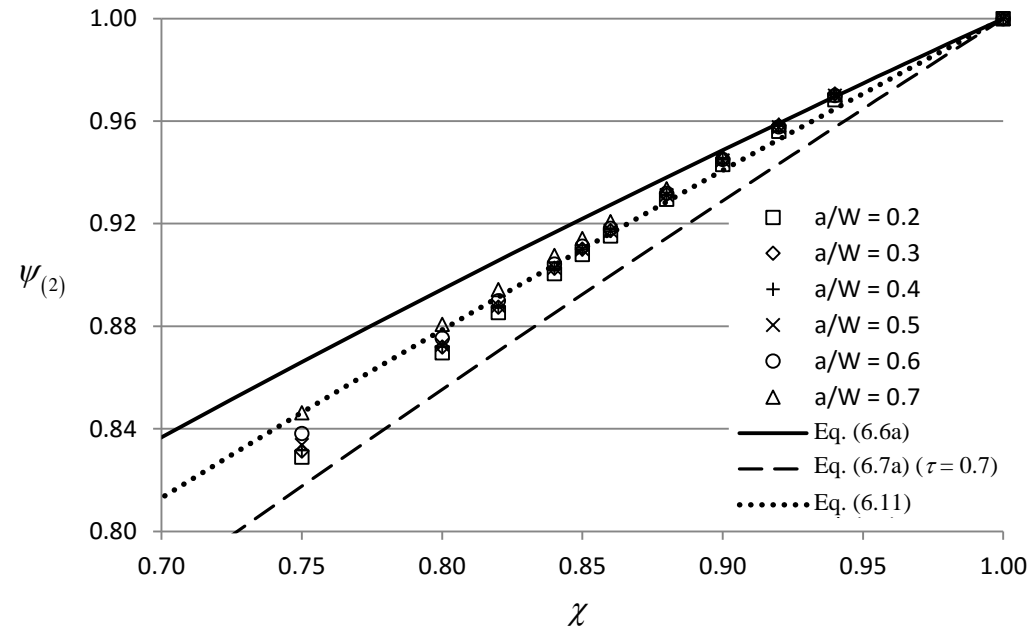Figure 6.2. Configuration of a typical finite element model with a blunt crack tip
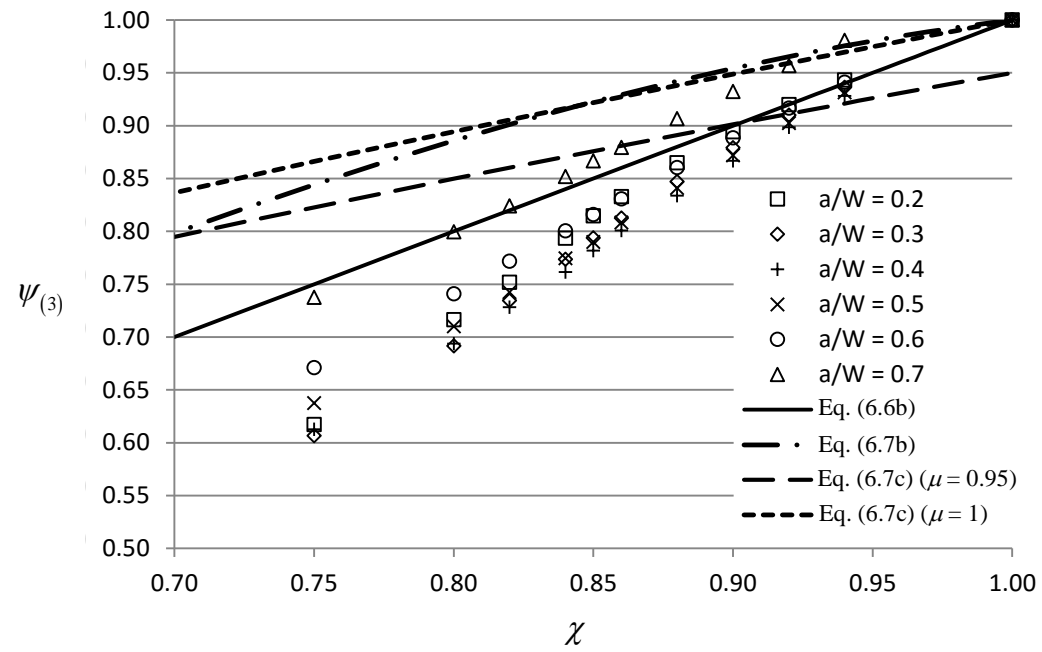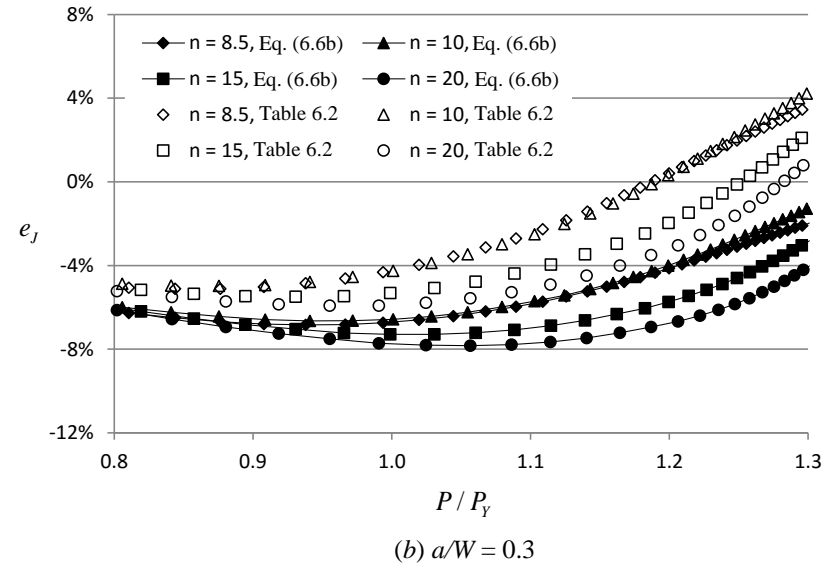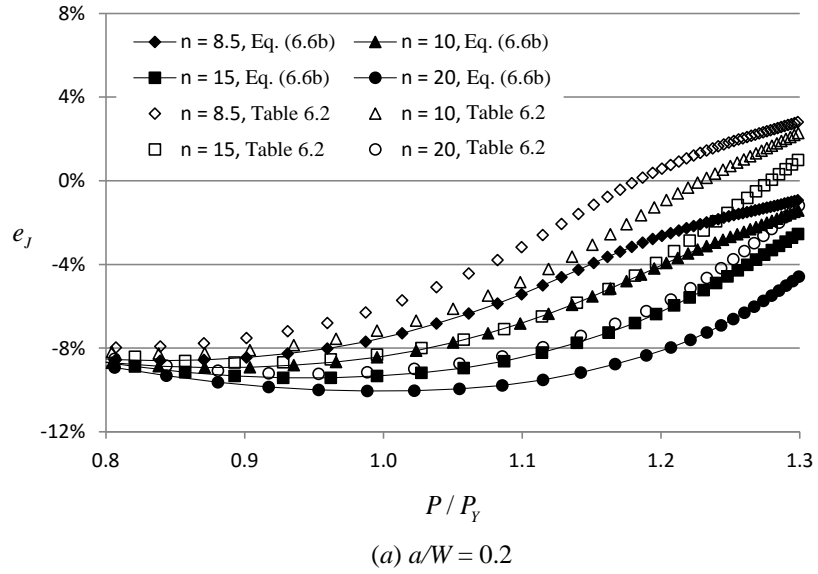
Figure 6.3. Variation of $\psi_{(2)}$ with various χ and a/W

Figure 6.4. Variation of $\psi_{(3)}$ with various χ and a/W

(*a*) *a/W* = 0.2

(*b*) *a/W* = 0.3
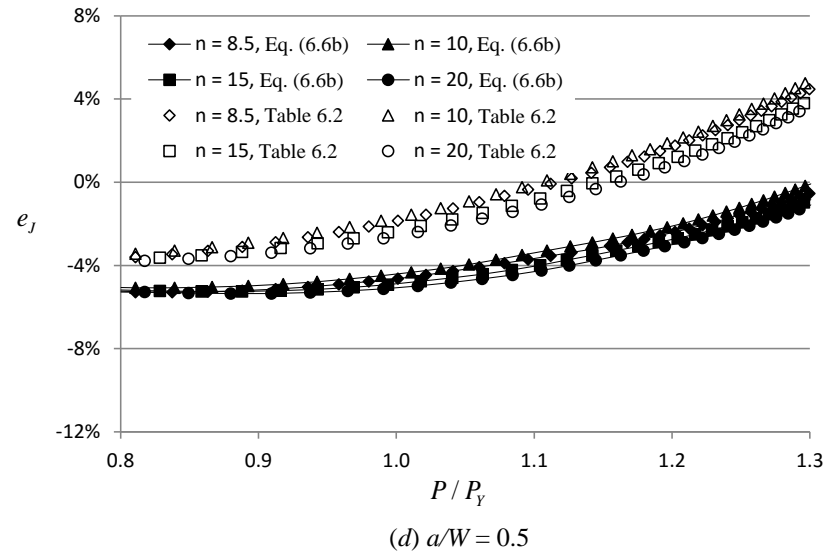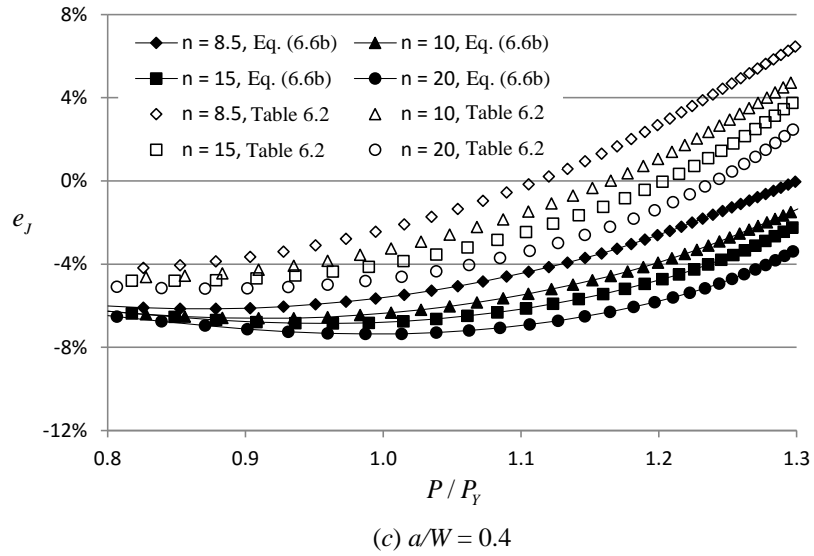
(c) $a/W = 0.4$

(d) $a/W = 0.5$

Figure 6.5. Error in J values evaluated using the $\psi_{(3)}$ associated with Eq. (6.6b) and Table 6.2 for the specimens with different a/W and n

Chapter 7 Summary, Conclusions and Recommendations for Future Study

7.1 General

The fracture toughness of the pipe steel and weldments is a key input to the structural integrity assessment and strain-based design of energy pipelines with respect to planar defects. For ductile materials such as the modern pipe steels, the fracture process is often accompanied by relatively large plastic deformation at the crack tip and considerable crack extension. In this case, the fracture toughness is typically characterized by the fracture toughness resistance curve (e.g. J-integral (J) or crack tip opening displacement ($CTOD$) resistance curve). The newly-developed clamped single-edge notched tension (SE(T) or SENT) specimen is increasingly used to determine the fracture toughness resistance curve in the pipeline industry. There are two main components of the toughness resistance curves, namely the crack growth, Δa, and the toughness value (J or $CTOD$) corresponding to this particular crack growth. The work reported in this thesis is focused on improving the current SE(T) test method regarding the evaluations of J, $CTOD$ and Δa. The research outcome can increase the accuracy of measured fracture toughness resistance curve using SE(T) specimen and therefore facilitates the development and application of strain-based design methodology used in the pipeline industry.

7.2 Estimation of J and $CTOD$ for SE(T) Specimens

Three-dimensional (3D) finite element analyses (FEA) were carried out to perform a systematic investigation of the plastic η factor (η_{pl}) and plastic constraint factor (m) for SE(T) specimens. The incremental-plasticity together with the large-displacement/large-strain formulation was used in the analysis. The von Mises yield criterion with isotropic hardening was adopted. The analysis covered both plane-sided and side-grooved SE(T) specimens with a range of specimen configurations, i.e. six crack depth-over-specimen width ratios (a/W = 0.2 to 0.7) and two thickness-over-width ratios (B/W = 1 and 2), and five strain hardening exponents (n =5, 8.5, 10, 15 and 20).were analyzed.

The load-line displacement (*LLD*)- and crack mouth opening displacement (*CMOD*)-based η_{pl} factors corresponding to the average *J* value over the crack front were evaluated and tabulated. The *CTOD* values at the mid-plane were also outputted to evaluate the *m* factors. The impacts of *a/W*, *B/W*, side-grooves and strain hardening characteristics on η_{pl} and *m* factors were investigated. Based on the analysis results, a set of expressions for η_{pl} are proposed. A new empirical *m*-factor equation is proposed as a function of *a/W*, *B/W*, the yield-to-tensile strength ratio and loading level. The proposed η_{pl}-factor and *m*-factor equations will improve the accuracy of the *J*(*CTOD*)-*R* curve obtained from the experiment and facilitate the evaluation of *J*(*CTOD*)-*R* curves using SE(T) specimens.

7.3   Estimation of Crack Size/Compliance for SE(T) Specimens

The elastic unloading compliance method is widely used to estimate the crack length of the specimen in the fracture toughness testing. In this method, the crack length can be estimated from the measured compliance based on the compliance equations. On the other hand, the compliance equations are required to estimate the compliance if the crack length can be directly measured.

Three-dimensional linear-elastic finite element analyses of clamped SE(T) specimens were carried out to investigate the accuracy of compliance equations that are used to evaluate *a/W* and compliance (*C*) in the *R*-curve test. A wide range of specimen configurations including nine *a/W* ratios ranging from 0.1 to 0.9, and seven *B/W* ratios ranging from 0.25 to 4 were considered in this study. Both plane-sided and side-grooved specimens were included in the analysis, with the side-groove depth set at 7.5%*B* on each side.

It is observed that equations proposed by Cravero and Ruggieri, Shen et al. and John and Rigling respectively lead to similar predictions and are accurate to predict *a/W* from a given compliance for specimens with $a/W \geq 0.5$ and $0.25 \leq B/W \leq 4$, and for specimens $a/W <$ 0.5 and $B/W \leq 0.5$. Equations developed by Mathias et al. and Fonzo et al., are accurate for specimens with $a/W < 0.5$ and $B/W \geq 1$. To predict *C* from a given *a/W*, equation developed by John and Rigling is accurate for specimen with $a/W > 0.2$ and $B/W \leq 0.5$ with the error of prediction generally being less than 2%. Two modification factors, $\rho_{(a/W)}$ and

$\rho_{(BCE)}$), are introduced to improve the accuracy of the predicted a/W and C, respectively. Using the proposed modification factors in Eqs. (4.4) through (4.8) and (4.10) leads to consistently highly accurate predictions of a/W and C for all the specimen configurations considered in this study, with the errors of predictions being less than 2% in most cases.

7.4 Influences of Crack Front Curvature and Side Grooves on *J-R* Curve for SE(T) Specimens

Two groups of 3D FEA were carried out to perform investigations on the effects of crack front curvature and side grooves, respectively, on *J-R* curve testing. The impact of the crack front curvature on the undeformed compliance (C_0), rotation correction factor (F_r) and average J over the crack front for plane-sided clamped SE(T) specimens were investigated. Symmetric bowed crack fronts characterized by a power-law expression were considered in the analysis. Three specimen thicknesses ($B/W = 0.5$, 1 and 2), six average crack lengths ($a_{ave}/W = 0.2$ to 0.7) and eleven crack front curvatures ($\lambda = 0$ to 0.1) were included in this study. The numerical results suggest that λ has little impact on C_0 for specimens with $a_{ave}/W \geq 0.3$ and relatively large impact on $C0$ for specimens with $a_{ave}/W < 0.3$. On the other hand, λ has little impact on F_r and the empirical equation proposed by Shen et al. is considered sufficiently accurate for specimens with $0.2 \leq a_{ave}/W \leq 0.7$, $B/W = 0.5$, 1 and 2 and $\lambda \leq 0.1$. Based on the analysis results, new crack front straightness criteria were proposed to ensure the differences in J and the compliance between the specimens with curved and straight crack fronts to be within a reasonably small range, i.e. no more than 5%.

Three-dimensional finite element models of side-grooved (SG) SE(T) specimens were analysed to investigate the effective thickness for the stress intensity factor and *CMOD*-based η_{pl} factors. Specimens with $H/W = 10$, $B/W = 1$, a/W ratios from 0.2 to 0.7 and ratio between the net and gross specimen thicknesses (χ) from 1 to 0.75 are analyzed. The thickness correction factors corresponding to K and J_{pl} are evaluated and compared with those reported in the literature. Based on the FEA results, new thickness correction factors are suggested. The research outcome will facilitate the evaluation of *J-R* curves using SG SE(T) specimens.

7.5   Recommendations for Future Work

Recommendations for future work are as follows:

1. Investigate the impact of the crack front curvature on the $J(CTOD)$-R curve for SE(T) specimens by employing appropriate crack growth models, such as the Gurson-Tvergaard-Needleman (GTN) model, in the FEA.

2. Develop the crack front straightness criteria for side-grooved SE(T) specimens and specimens made of nonhomogeneous materials, i.e. containing the weldment and heat-affected zone.

3. Investigate the influences of anisotropy, residual stresses, and plastic wake of pre-cracking on the estimation of J.

4. Analyze the crack-tip fields of full-scale pipes containing surface cracks subjected to internal pressure and/or longitudinal tensile force, and compare the results with the crack-tip fields of SE(T) specimens.

Appendix A Evaluation of J_{pl} for growing cracks

Based on the deformation theory of plasticity, J is independent of the load path leading to the current *LLD* (or *CMOD*) and crack length a, given that the J-controlled crack growth conditions are satisfied (Sumpter and Turner, 1976). Accordingly, J is a function of two independent variables, a and Δ. Ernst et al. (1981) developed an incremental method to estimate J for growing cracks by deriving the total differential of J_{pl} as

$$dJ_{pl} = \frac{\eta_{pl}P}{bB}d\Delta_{pl} - \frac{\gamma_{pl}}{b}J_{pl}da \tag{A.1}$$

with

$$\gamma_{pl} = \left(\eta_{pl} - 1 - \frac{b}{W}\frac{1}{\eta_{pl}}\frac{\partial \eta_{pl}}{\partial(a/W)} \right) \tag{A.2}$$

Integrating both sides of Eq. (A.1) yields

$$J_{pl} = \int_0^{\Delta_{pl}} \frac{\eta_{pl}P}{bB}d\Delta_{pl} - \int_{a_0}^{a} \frac{\gamma_{pl}}{b}J_{pl}da \tag{A.3}$$

where a_0 is the initial crack length. Equation (A.3) can be applied to any loading path leading to the current values of Δ_{pl} and a. Figure A.1 shows a schematic of the estimation of J_{pl} for growing cracks. The figure includes a typical P-Δ_{pl} curve for a growing crack, and three deformation paths for the initial crack length, a_0, and two arbitrary crack lengths a_i and a_{i+1} respectively. The actual loading path AC in the figure can be replaced by the fictitious loading paths AB and BC. Integrating both sides of Eq. (A.3) along the loading path AB results in

$$J_{pl}^{B} = J_{pl}^{i} + \frac{\eta_{pl}^{i}}{b_i B} A_{pl}^{i,i+1} \tag{A.4}$$

where J_{pl}^{i} is the value of J_{pl} at A or step i; J_{pl}^{B} is the value of J_{pl} at B or the intermediate value of J_{pl} between step i and step $i+1$; $b_i = W - a_i$, and $A_{pl}^{i,i+1}$ equals the area of $AB\Delta_{pl}^{i}\Delta_{pl}^{i+1}$

but can be adequately approximated by the area under the actual loading path between Δ^i_{pl} and Δ^{i+1}_{pl} (i.e. the shaded area in Fig. A.1), if $\Delta^{i+1}_{pl} - \Delta^i_{pl}$ is sufficiently small; $A^{i,i+1}_{pl}$ can be evaluated using the trapezoidal rule as $A^{i,i+1}_{pl} \cong \frac{1}{2}(P^i + P^{i+1})(\Delta^{i+1}_{pl} - \Delta^i_{pl})$. Integrating both sides of Eq. (A.3) again along the loading path BC results in

$$J^{i+1}_{pl} = J^B_{pl}\left[1 - \frac{\gamma^i_{pl}}{b_i}(a_{i+1} - a_i)\right] \tag{A.5}$$

where J^{i+1}_{pl} is the value of J_{pl} at C or step $i+1$. Combining Eqs. (A.4) and (A.5) leads to the following general incremental expression for calculating J_{pl}:

$$J^{i+1}_{pl} = \left(J^i_{pl} + \frac{\eta^i_{pl}}{b_i B}A^{i,i+1}_{pl}\right)\left[1 - \frac{\gamma^i_{pl}}{b_i}(a_{i+1} - a_i)\right] \tag{A.6}$$

Equation (A.6) is adopted by ASTM E1820-11E2 (ASTM, 2013) as the main procedure to experimentally evaluate the *J-R* curve. The crack length corresponding to each loading step can be determined using the unloading compliance method, which is described in Chapter 4.

References

ASTM (2013). *ASTM E1820-13: Standard Test Method for Measurement of Fracture Toughness*. America Society of Testing and Materials International, West Conshohocken, PA.

Ernst, H. A., Paris, P. C. and Landes, J. D. (1981). Estimation on *J*-integral and tearing modulus *T* from a single specimen test record. *Fracture mechanics: Thirteenth conference*, ASTM STP 743. Baltimore, MD: American Society for Testing and Materials; p. 476-502.

Sumpter, J. D. G., Turner, C. E. (1976). Method for laboratory determination of J_c. In: Kaufman JG, editor. Cracks and Fracture, *ASTM STP 601*. Baltimore, MD; p. 3-18.
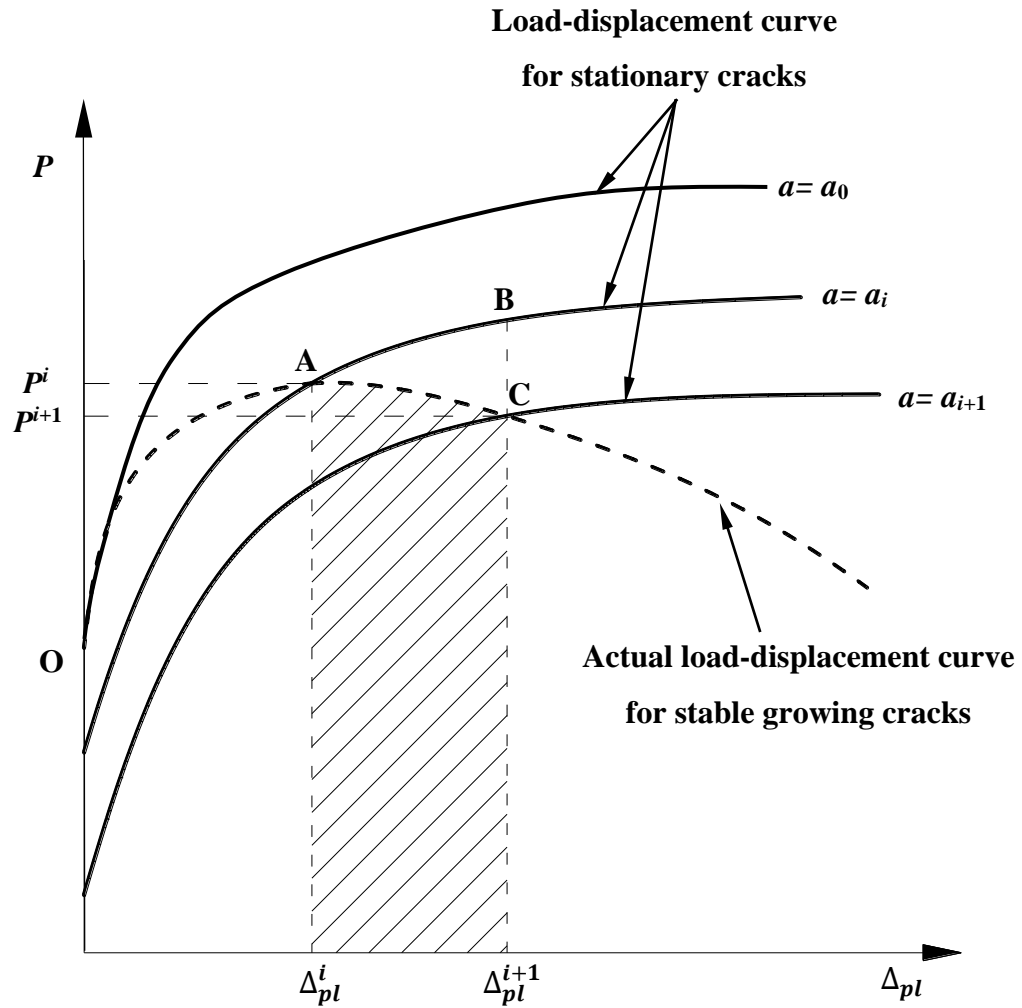

Figure A.1: Schematic of the estimation of J_{pl} for growing cracks

Appendix B Computation of *J*-integral using Virtual Crack Extension Method

Parks (1974) and Hellen (1975) first developed the virtual crack extension approach based on the finite element method to calculate the energy release rate in elastic bodies (Anderson, 2005). deLorenzi (1982, 1985) improved the virtual crack extension method, which is used in the FEA reported in this thesis and is briefly described here.

Figure B.1 schematically shows the virtual crack extension method in two-dimensional analysis. The crack front is surrounded by three zones of material divided by two contours. During the crack advance, material points in zone I are rigidly translated in the x_1 direction by an amount Δx_1, while points in zone III remain fixed, causing a distortion in the material in zone II. Since zone I contains the crack front, the crack length is increased by an amount Δa. This virtual translation of the material points is defined as the "virtual shift" in ADINA (ADINA, 2012). For a material that obeys the deformation plasticity theory, deLorenzi (1982, 1985) showed that the energy release rate in a two-dimensional body can be expressed as:

$$J = \frac{1}{\Delta a} \int_{A_C} \left(\sigma_{ij} \frac{\partial u_j}{\partial x_1} - w\delta_{i1} \right) \frac{\partial \Delta x_1}{\partial x_i} dA_C \tag{B.1}$$

where u_i is components of the displacement ($i = 1$ or 2); w is the strain energy density; A_C is area of the cracked body, and δ_{ij} is the Kronecker delta.

In the virtual crack extension method adopted in ADINA (ADINA, 2012), a more general form of Eq. (B.1) is used to calculate *J* considering 3D cracked body (deLorenzi, 1982 and 1985):

$$J = \frac{1}{\Delta A_C} \int_{V_C} \left(\sigma_{ij} \frac{\partial u_i}{\partial x_k} - w\delta_{ik} \right) \frac{\partial \Delta x_k}{\partial x_j} dV_C \tag{B.2}$$

where V_C is volume of the cracked body; Δx_k is components of the virtual crack extension vector ($k = 1$, 2 or 3), and ΔA_C is the increase in crack area corresponding to Δx_k.

The calculation of ΔA_C is discussed here. For a 2D cracked body, $\Delta A_C = b\sqrt{\Delta x_1^2 + \Delta x_2^2}$ where b is the thickness at the crack tip. Figure B.2 schematically shows the virtual shift in 3D analysis. For a 3D cracked body, $\Delta A_C = \int \sqrt{\Delta x_i' \Delta x_i'}\, ds$ where $\Delta x_i' = \Delta x_i - (\sum_{j=1}^{3} t_j \Delta x_j) t_i$, t_i ($i = 1$, 2 or 3) is the component or directional cosine of the unit tangent vector along the crack front and ds is the differential length along the crack front (see Fig. B.2). The definition of $\Delta x_i'$ ensures that it is perpendicular to t_i. In a 3D problem, J typically varies along the crack front. Defining ΔA_C in the above way would result in a local measure of J (Anderson, 2005).

The virtual crack extension formulation of J requires an area integration and a volume integration for 2D and 3D analysis, respectively. Such an approach is easier to implement numerically and is more accurate than contour and surface integrations for 2D and 3D problems, respectively (Anderson, 2005). Note that Eq. (B.2) is the basic expression of J and does not consider the impacts of hoop stress and pressure, thermal effect, and dynamic effect (ADINA, 2012). Additional information about the virtual crack extension approach can be found in the relevant literature (e.g. ADINA, 2012; Anderson, 2005; deLorenzi, 1982 and 1985; Hellen, 1975).

References

ADINA. (2012). Theory and Modeling Guide, ADINA R. & D. Inc., Watertown, USA.

Anderson, T. L. (2005). *Fracture Mechanics—Fundamentals and Applications, Third edition*. CRC Press, Boca Raton.

deLorenzi, H. G. (1982). On the Energy Release Rate and the *J*-Integral of 3-D Crack Configurations. *International Journal of Fracture*, 19:183-93.

deLorenzi, H. G. (1985). Energy Release Rate Calculation by the Finite Element Method. *Engineering Fracture Mechanics*, 21:129-143.

Hellen, T. K. (1975). On the Method of Virtual Crack Extension. *International Journal for Numerical Methods in Engineering*; 9:187-207.

Parks, D. M. (1974). A Stiffness Derivative Finite Element Technique for Determination of Crack Tip Stress Intensity Factors. *International Journal of Fracture*; 10:487-502.

I: zone rigidly shifted by virtual shift

II: zone distorted by virtual shift

III: zone unchanged by virtual shift

(a) Before the virtual shift   **(b) After the virtual shift**
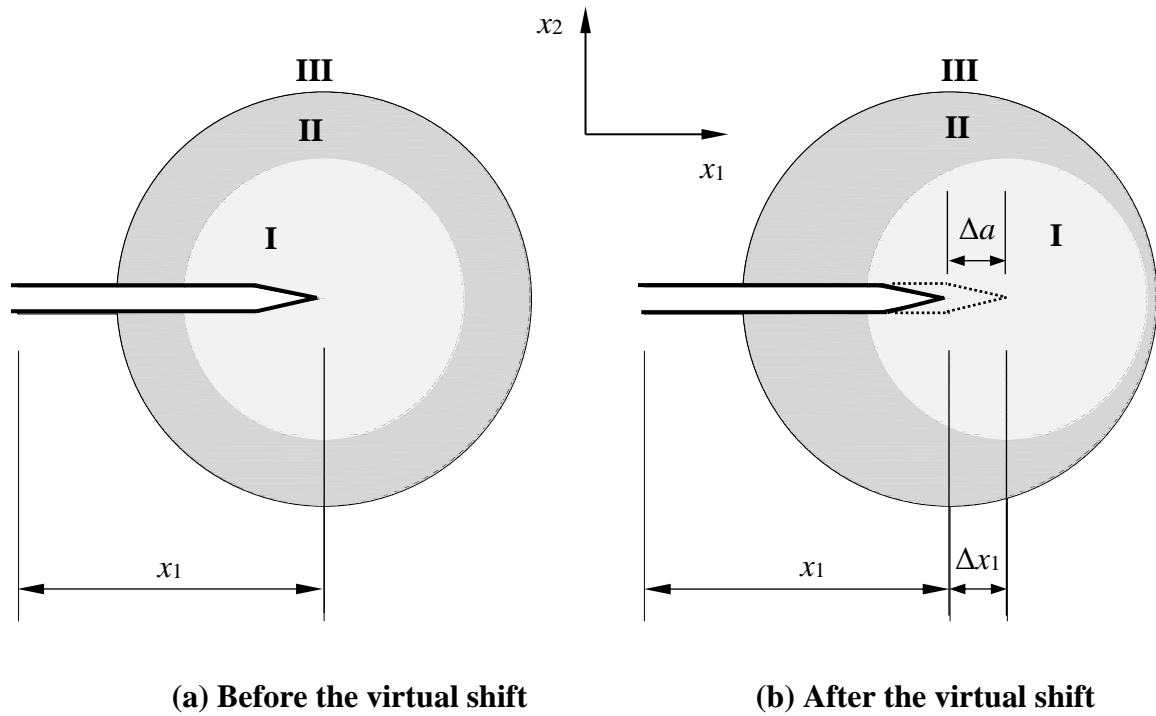
Figure B.1: The virtual crack extension method in two-dimensional analysis

x_2

x_1

x_3

Virtual increase of crack area

Crack front

(a) Before virtual shift

(b) After virtual shift

$\Delta x'$

Δx

t

ds

ΔA_C

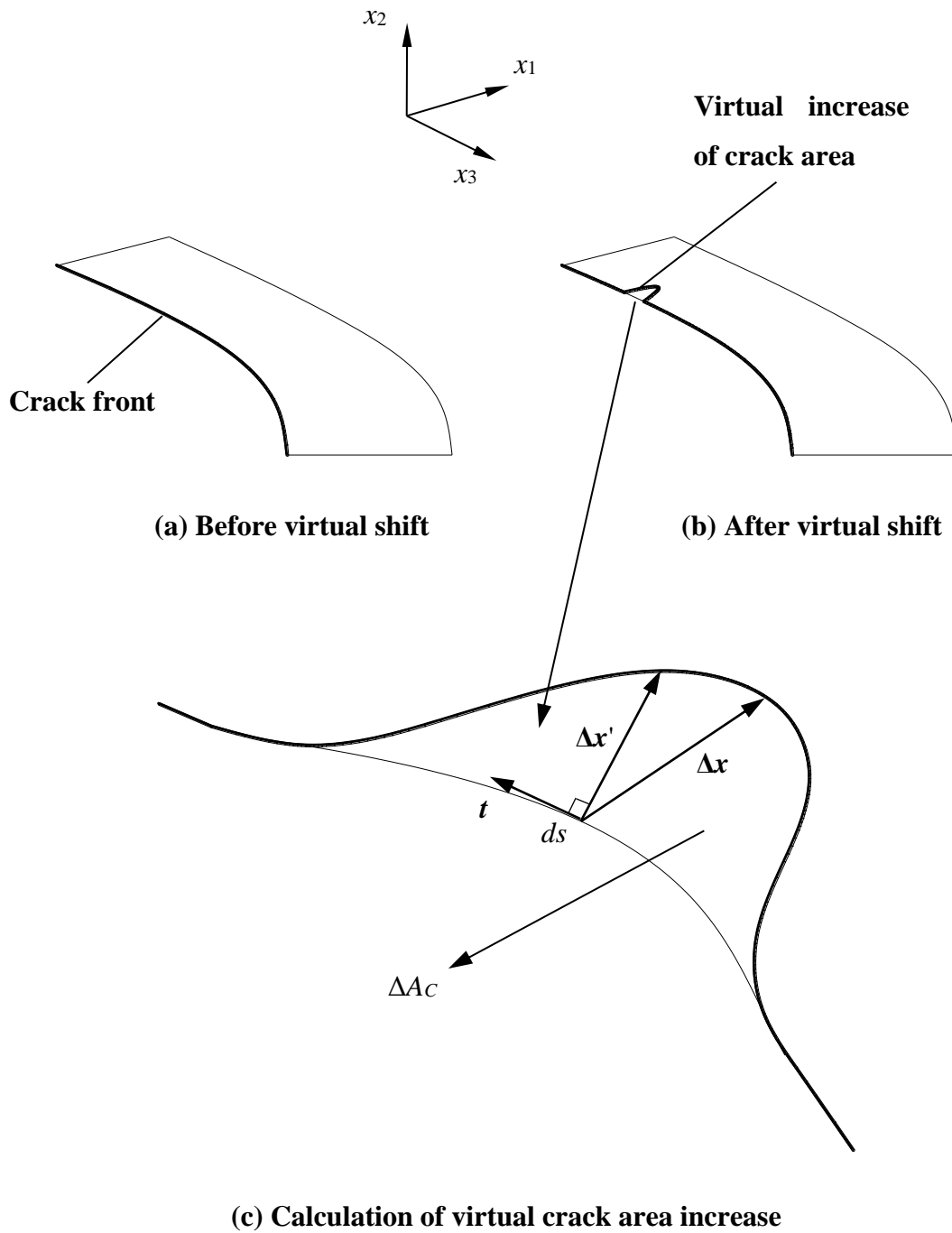**(c) Calculation of virtual crack area increase**

Figure B.2: The virtual shift in three-dimensional analysis

Appendix C Rotation Correction in the Unloading Compliance Method for Evaluating the Crack Length

The elastic unloading compliance method (Clarke et al., 1976) is widely used to evaluate the immediate crack length and plastic work done in the specimen as introduced in section 4.1. In the *J*(*CTOD*)-*R* curve test, the specimen compliance (inverse of the stiffness) is estimated as the slope of the load vs. crack-mouth opening displacement (*P-CMOD*) curve from each loading-unloading sequence. For SE(B) specimen, there is an unique relationship between the normalized compliance and the specimen crack length. Any increase of the compliance contributes the growth of the crack length and vice verce.

Previous studies (Shen et al., 2008, 2009; Cravero and Ruggieri, 2007) suggested that the compliance of the undeformed SE(T) specimen generally increases as the crack grows, whereas the compliance of a specimen with a stationary crack in the deformed position decreases, as the rotational deformation increases and the load-line eccentricity decreases. To estimate the crack length for the SE(T) specimen using the one-to-one crack length-compliance relationship, the measured compliance (i.e. compliance of the deformed specimen, C_i) needs to be first converted to the compliance of the undeformed specimen (C_0). This process is known as the rotation correction of the compliance and can be generally expressed as the following equation:

$$C_0 = F_r C_i \qquad\qquad (C.1)$$

where F_r is the rotation correction factor. Several studies (Shen et al., 2008, 2009; Cravero and Ruggieri, 2007) have been carried out to evaluate the rotation correction factor for SE(T) specimens with straight crack fronts. Based on the finite element analyses (FEA) results of (two-dimensional) 2D plane-strain SE(T) models with crack depth-over-specimen width ratios $a/W = 0.2$, 0.35 and 0.5, and a three-dimensional (3D) SE(T) model with $a/W = 0.5$ and thickness-over-width ratios $B/W = 1$, Shen et al. (2008, 2009) developed the following empirical expression for F_r:

$$F_r = \frac{1}{1 - 0.165\dfrac{a}{W}\left(\dfrac{P}{P_Y}\right)} \tag{C.2}$$

where P is the applied load, and P_Y is the limit load for the SE(T) specimen. The adequacy of Eq. (C.2) for specimens containing curved crack fronts was investigated in the Chapter 5.

References

Clarke, G. A., Andrews, W. R., Paris, P. C., Schmidt, D. W. (1976). Single Specimen Tests for J_{IC} Determination. *Mechanics of Crack Growth, ASTM STP 590. Philadelphia: America Society of Testing and Materials International*, 590:27-42.

Cravero, S. and Ruggieri, C. (2007). Estimation Procedure of J Resistance Curves for SE (T) Fracture Specimens Using Unloading Compliance. *Engineering Fracture Mechanics*, 74(17):2735-2757.

Shen, G., Bouchard, R., Gianetto, J. A. and Tyson, W. R. (2008). Fracture toughness evaluation of high strength steel pipe. *ASME Conference Proceedings*, 1275-1282.

Shen, G. and Tyson, W. R. (2009). Crack size evaluation using unloading compliance in single-specimen single-edge-notched tension fracture toughness testing. *ASTM Journal of Testing and Evaluation*, 37:347-357.

Appendix D Derivation of the Relationship Between β_7, β_9, λ_7, $\lambda_{9(BS)}$, $\lambda_{9(ASTM)}$ and λ for Symmetric Bowed Crack Fronts

For specimens with symmetric bowed crack fronts characterized by Eq. (5.8), crack lengths corresponding to the nine measurement points $a_{(i)}$ can be expressed as:

$$a_{(i)} = a_{z=0} - \beta W \left[abs\left(i-5\right)\left(0.25 - \frac{\Lambda}{2B}\right) \right]^p \quad (i = 1, 2, ..., 9) \tag{D.1}$$

where $\Lambda = 0.005W$ and $0.01B$ for ASTM and BS (ISO) standards, respectively. Combining Eqs. (5.9), (5.10) and (D.1), the average crack length from nine-point measurement is recast as:

$$\begin{aligned}
a_{ave9} &= a_{z=0} - \beta W \left(0.25 - \frac{\Lambda}{2B}\right)^p \left[\frac{1}{8}\sum_{i=1}^{8}\left[abs\left(i-5\right)^p \right] \right] \\
&= a_{ave} + \beta W \left\{ \frac{1}{p+1} - \left(0.25 - \frac{\Lambda}{2B}\right)^p \left[\frac{1}{8}\sum_{i=1}^{8}\left[abs\left(i-5\right)^p \right] \right] \right\} \\
&= a_{ave} + \lambda W \left\{ \frac{1}{p} - \frac{p+1}{p}\left(0.25 - \frac{\Lambda}{2B}\right)^p \left[\frac{1}{8}\sum_{i=1}^{8}\left[abs\left(i-5\right)^p \right] \right] \right\}
\end{aligned} \tag{D.2}$$

The maximum crack lengths from the nine- and seven-point measurement equal the crack length corresponding to the specimen mid plane:

$$a_{\max 9} = a_{\max 7} = a_{z=0} \tag{D.3}$$

Given Eq. (D.1), the minimum crack lengths from the nine- and seven-point measurement are calculated as the following:

$$\begin{aligned}
a_{\min 9} = a_{(1)} = a_{(9)} &= a_{z=0} - \beta W \left[4\left(0.25 - \frac{\Lambda}{2B}\right) \right]^p \\
&= a_{z=0} - \frac{p+1}{p}\lambda W \left[4\left(0.25 - \frac{0.01B}{2B}\right) \right]^p \\
&= a_{\max 9} - \frac{p+1}{p}\lambda W \left(0.98\right)^p
\end{aligned} \tag{D.4}$$

and

$$a_{\min 7} = a_{(2)} = a_{(8)} = a_{z=0} - \beta W \left[3 \left(0.25 - \frac{\Lambda}{2B} \right) \right]^p$$

$$= a_{z=0} - \frac{p+1}{p} \lambda W \left[3 \left(0.25 - \frac{0.01B}{2B} \right) \right]^p \qquad \text{(D.5)}$$

$$= a_{\max 7} - \frac{p+1}{p} \lambda W (0.735)^p$$

Combining (D.3), (D.4) and (D.5) lead to the following equation:

$$\begin{cases} \beta_9 = \dfrac{1}{W} \left(a_{\max 9} - a_{\min 9} \right) = \dfrac{p+1}{p} (0.98)^p \lambda & \text{(a)} \\[4mm] \beta_7 = \dfrac{1}{W} \left(a_{\max 7} - a_{\min 7} \right) = \dfrac{p+1}{p} (0.735)^p \lambda & \text{(b)} \end{cases} \qquad \text{(D.6)}$$

The following equations can be derived from Eqs. (D.2) through (D.5):

$$\begin{cases} \left(a_{\max 9} - a_{ave 9} \right) - \left(a_{ave 9} - a_{\min 9} \right) = \dfrac{p+1}{2p} \lambda W \left(0.25 - \dfrac{\Lambda}{2B} \right)^p \left(1 + 2^p + 3^p - \dfrac{3}{2} 4^p \right) & \text{(a)} \\[4mm] \left(a_{\max 7} - a_{ave 9} \right) - \left(a_{ave 9} - a_{\min 7} \right) = \dfrac{p+1}{2p} \lambda W \left(0.25 - \dfrac{\Lambda}{2B} \right)^p \left(1 + 2^p - 3^p + \dfrac{1}{2} 4^p \right) & \text{(b)} \end{cases}$$

$$\text{(D.7)}$$

For $p > 1$, the derivative of the right hand sides of Eqs. (D.7a) and (D.7b) with respect to p are always negative and positive, i.e., $(a_{max9} - a_{ave9}) - (a_{ave9} - a_{min9}) < 0 < (a_{max7} - a_{ave9}) - (a_{ave9} - a_{min7})$.

Therefore for $p > 1$, it follows that

$$
\left\{
\begin{aligned}
\lambda_7 &= \frac{1}{W} \mathrm{Max}\left[a_{\max 7} - a_{ave9}, a_{ave9} - a_{\min 7}\right] = \frac{1}{W}\left(a_{\max 7} - a_{ave9}\right) \\
&= \frac{p+1}{p}\lambda\left(0.245\right)^p\left[\frac{1}{8}\sum_{i=1}^{8}\left[abs\left(i-5\right)^p\right]\right] \qquad\qquad \text{(a)} \\
\lambda_{9(BS)} &= \frac{1}{W}\mathrm{Max}\left[a_{\max 9} - a_{ave9}, a_{ave9} - a_{\min 9}\right] = \frac{1}{W}\left(a_{ave9} - a_{\min 9}\right) \\
&= \frac{p+1}{p}\lambda\left(0.245\right)^p\left[4^p - \frac{1}{8}\sum_{i=1}^{8}\left[abs\left(i-5\right)^p\right]\right] \qquad \text{(b)} \\
\lambda_{9(ASTM)} &= \frac{1}{W}\mathrm{Max}\left[a_{\max 9} - a_{ave9}, a_{ave9} - a_{\min 9}\right] = \frac{1}{W}\left(a_{ave9} - a_{\min 9}\right) \\
&= \frac{p+1}{p}\lambda\left(0.25 - \frac{0.005W}{2B}\right)^p\left[4^p - \frac{1}{8}\sum_{i=1}^{8}\left[abs\left(i-5\right)^p\right]\right] \qquad \text{(c)}
\end{aligned}
\right. \qquad (D.8)
$$

Equations (D.6) and (D.8) define relationships between shape parameters associated with the nine-point measturement to λ for specimens with symmetric bowed crack fronts.

Appendix E Copyright Permission

Permission to include the following articles has been requested and granted with the condition that this thesis would not be published commercially or on a website:

Huang, Y. and Zhou, W. (2014). "Investigation of plastic eta factors for clamped SE(T) specimens based on three-dimensional finite element analyses." *Engineering Fracture Mechanics*. 2014;132:120-35.

Huang, Y. and Zhou, W. (2014). "J-CTOD relationship for clamped SE(T) specimens based on three-dimensional finite element analyses." *Engineering Fracture Mechanics*. 2014;131:643-55.

Huang, Y. and Zhou, W. (2015). "Numerical investigation of compliance equations used in the R-curve testing for clamped SE(T) specimens." *Fatigue and Fracture of Engineering Materials and Structures*. 2015;38:1137-54.

Huang, Y. and Zhou, W. (2015). "Effects of crack front curvature on J-R curve testing using clamped SE(T) specimens of homogeneous materials." *International Journal of Pressure Vessels and Piping.* 2015;134:112-27.

Huang, Y. and Zhou, W. (2016). "Effective thickness of side-grooved clamped SE(T) specimens for J-R curve testing." *ASTM Journal of Testing and Evaluation*. http://dx.doi.org/10.1520/JTE20150274. ISSN 0090-3973.

RE: Copyright waiver of journal papers for thesis submission

July 7th, 2016

Elsevier Permissions Helpdesk (permissionshelpdesk@elsevier.com)

Dear Sir/Madam:

I am a graduate student at the University of Western Ontario and am completing a PhD thesis which includes materials that were originally published in three Elsevier articles.

I am requesting that you send an official copyright waiver for the following articles:

1. Huang, Y. and Zhou, W. (2014). "Investigation of plastic eta factors for clamped SE(T) specimens based on three-dimensional finite element analyses." Engineering Fracture Mechanics. 2014;132:120-35.

2. Huang, Y. and Zhou, W. (2014). "J-CTOD relationship for clamped SE(T) specimens based on three-dimensional finite element analyses." Engineering Fracture Mechanics. 2014;131:643-55.

3. Huang, Y. and Zhou, W. (2015). "Effects of crack front curvature on J-R curve testing using clamped SE(T) specimens of homogeneous materials." International Journal of Pressure Vessels and Piping. 2015;134:112-27.

Thank you for your time and consideration in the processing of this information for me, I greatly appreciate it If you require further information from me please contact me immediately at yhuan95@uwo.ca.

Regards,

Yifan Huang

FW: Copyright waiver of journal papers for thesis submission

Dear Yifan:

As an Elsevier journal author, you retain the right to **include the article in a thesis or dissertation (provided that this is not to be published commercially)** whether in part or *in toto*, subject to proper acknowledgment; see

http://www.elsevier.com/about/company-information/policies/copyright/personal-use

for more information. As this is a retained right, no written permission from Elsevier is necessary.

If I may be of further assistance, please let me know.

Best of luck with your PhD thesis and best regards,
Hop

Hop Wechsler
Permissions Helpdesk Manager
Elsevier
1600 JFK Boulevard
Suite 1800
Philadelphia, PA 19103-2899
Tel: +1-215-239-3520
Fax: +1-215-239-3805
Email: h.wechsler@elsevier.com
Contact the Permissions Helpdesk:
 +1-800-523-4069 x 3808   permissionshelpdesk@elsevier.com

8/2016

Elsevier Copyright Policy

Copyright

Describes the rights related to the publication and distribution of research. It governs how authors (as well as their employers or funders), publishers and the wider general public can use, publish and distribute articles or books.

Journal author rights

In order for Elsevier to publish and disseminate research articles, we need publishing rights. This is determined by a publishing agreement between the author and Elsevier. This agreement deals with the transfer or license of the copyright to Elsevier and authors retain significant rights to use and share their own published articles. Elsevier supports the need for authors to share, disseminate and maximize the impact of their research and these rights, in Elsevier proprietary journals* are defined below:Authors can use their articles, in full or in part, for a wide range of scholarly, non-commercial purposes as outlined below:

For subscription articles

Authors transfer copyright to the publisher as part of a journal publishing agreement, but have the right to:

- Share their article for <u>Personal Use</u>, <u>Internal Institutional Use</u> and <u>Scholarly Sharing</u> purposes, with a DOI link to the version of record on ScienceDirect (and with the Creative Commons <u>CC-BY-NC- ND license</u> for author manuscript versions)
- Retain patent, trademark and other intellectual property rights (including raw research data).
- Proper attribution and credit for the published work.

Personal use

Authors can use their articles, in full or in part, for a wide range of scholarly, non-commercial purposes as outlined below:

- Use by an author in the author's classroom teaching (including distribution of copies, paper or electronic)
- Distribution of copies (including through e-mail) to known research colleagues for their personal use (but not for Commercial Use)

- **Inclusion in a thesis or dissertation (provided that this is not to be published commercially)**
- Use in a subsequent compilation of the author's works
- Extending the Article to book-length form
- Preparation of other derivative works (but not for Commercial Use)
- Otherwise using or re-using portions or excerpts in other works

These rights apply for all Elsevier authors who publish their article as either a subscription article or an open access article. In all cases we require that all Elsevier authors always include a full acknowledgement and, if appropriate, a link to the final published version hosted on Science Direct.

RE: Copyright waiver of journal papers for thesis submission

July 8th, 2016

Wiley Global Permissions (permissions@wiley.com)

Dear Sir/Madam:

I am a graduate student at the University of Western Ontario and am completing a PhD thesis which includes materials that were originally published in a Fatigue & Fracture of Engineering Materials & Structure article.

I am requesting that you send an official copyright waiver for the following article:

Huang, Y. and Zhou, W. (2015). "Numerical investigation of compliance equations used in the R-curve testing for clamped SE(T) specimens." Fatigue and Fracture of Engineering Materials and Structures. 2015;38:1137-54.

Thank you for your time and consideration in the processing of this information for me, I greatly appreciate it If you require further information from me please contact me immediately at yhuan95@uwo.ca.

Regards,

Yifan Huang

FW: Copyright waiver of journal papers for thesis submission

Dear Yifan Huang

Thank you for your request.

Permission is granted for you to use the material requested for your thesis/dissertation subject to the usual acknowledgements (author, title of material, title of book/journal, ourselves as publisher) and on the understanding that you will reapply for permission if you wish to distribute or publish your thesis/dissertation commercially. You must also duplicate the copyright notice that appears in the Wiley publication in your use of the Material; this can be found on the copyright page if the material is a book or within the article if it is a journal.

Permission is granted solely for use in conjunction with the thesis, and the material may not be posted online separately.

Any third party material is expressly excluded from this permission. If any of the material you wish to use appears within our work with credit to another source, authorisation from that source must be obtained.

Best wishes,

Aimee Masheter
Permissions Assistant
John Wiley & Sons Ltd
The Atrium
Southern Gate, Chichester
West Sussex, PO19 8SQ
UK

RE: Copyright waiver of journal papers for thesis submission

August 3rd, 2016

ASTM INTERNATIONAL (khooper@astm.org)

Dear Sir/Madam:

I am a graduate student at the University of Western Ontario and am completing a PhD thesis which includes materials that were originally published in an ASTM Journal of Testing and Evaluation article.

I am requesting that you send an official copyright waiver for the following article:

Huang, Y. and Zhou, W. (2016). "Effective thickness of side-grooved clamped SE(T) specimens for J-R curve testing." ASTM Journal of Testing and Evaluation. http://dx.doi.org/10.1520/JTE20150274. ISSN 0090-3973.

Thank you for your time and consideration in the processing of this information for me, I greatly appreciate it If you require further information from me please contact me immediately at yhuan95@uwo.ca.

Regards,

Yifan Huang

FW: Copyright waiver of journal papers for thesis submission

Dear Yifan Huang,

Thank you for your email today.

The ASTM Author Agreement allows authors to the right to include their article, in full or in part, in a thesis or dissertation provided that this is not to be published commercially. Please ensure the following credit line appears on the article: "Reprinted, with permission, from the Journal of Testing and Evaluation, http://dx.doi.org/10.1520/JTE20150274, copyright ASTM International, 100 Barr Harbor Drive, West Conshohocken, PA 19428."

Thank you for your contribution to ASTM's publications program.

Kind regards,
Kathe

Kathe Hooper
Manager, Rights and Permissions
—
ASTM INTERNATIONAL
Helping our world work better
—
100 Barr Harbor Drive, PO Box C700
West Conshohocken, PA 19428-2959, USA
tel +1.610.832.9634 fax +1.610.834.7018
www.astm.org

8/2013

<div align="center">

ASTM International
Author/Copyright Owner Agreement

</div>

Paper/Chapter Title as submitted (the "Work")

For U.S. and foreign government employees *who have prepared this Work as a part of their official duties, it is understood that copyright is not available for assignment. This agreement must be accepted so as to agree to and acknowledge all other terms of this agreement.*

"You" means the Author(s) (and Copyright Owner(s), if different))

Author's Obligations. You have submitted the Work to ASTM for publication. You represent that the Work submitted has not been previously published. You promise that the Work is not currently under consideration by another publication. You warrant that the Work is original material (except for any material from copyrighted sources reproduced with the written permission of the copyright holder sufficient to permit ASTM to use the Work as contemplated), and is in no way a violation or an infringement of any copyright belonging to any third party; that the materials contained in the Work are accurate; and that the Work contains no defamatory or otherwise illegal materials.

You grant the following rights to ASTM: the worldwide and perpetual right to (a) print and/or electronically publish and distribute the Work (or portions thereof) in all versions of ASTM publications (in any language and with the right to translate), websites and/or newsletters and right to print and/or electronically publish and distribute the Work to other sites under license or contract with ASTM; (b) include the Work in advertising and promotion; (c) include the Work in print and non-print products anywhere in the world.

Corresponding Author: The corresponding author is the person with whom ASTM communicates. He/She is responsible for updating all co-authors regarding the status of the Work. The corresponding author is responsible for transferring copyright and has communicated the terms of ASTM copyright with co-authors prior to publication.

Electronically accepting this Agreement represents and warrants that you (and any co-authors) are the sole copyright holder(s) of the Work and that you have identified all co-authors to ASTM. You also represent that each of the co-author(s) have also granted permission to ASTM to use their name(s) in connection with any past, present, or future promotional activity by ASTM, including, but not limited to, promotions for upcoming issues or publications, circulation solicitations, advertising, or other publications in connection with the publication.

Compensation. You will not receive or be entitled to any royalty, fee, commission, payment or other compensation.

Copyright Assignment. It is ASTM's policy to require authors/copyright owners to assign the copyright in the submitted works, in order that ASTM may disseminate the Work to the fullest extent. You hereby assign all rights, including the copyright, in the Work to ASTM, prior to publication, by executing this Agreement. including but not limited to any and all copyright(s) therein held by each Author, together with any rights of each to secure renewals, reissues and extensions of copyright that may be secured under the laws now or hereafter in force and effect in the United States or in any other country, and any and all rights to enforce such copyright(s) or bring other claim in connection with such copyright.

The Work becomes the copyrighted property of ASTM and shall not be published anywhere without the prior written consent of ASTM. ***ASTM reserves the right of first publication of all papers offered for publication.***

The author(s), if different from the copyright owner(s) also represents that he/she/they prepared the Work within the scope of their employment, as a work-for-hire.

Peer Review Policy. All papers are subject to review by two anonymous peer reviewers, as the process is described in ASTM's peer review process (copy will be provided upon request). Submission of Work does not in any way guarantee that ASTM will publish the Work.

Limited Right of Use by Author(s)' Employer. ASTM grants the authors' employer the limited and non-exclusive license to make a limited number of photocopies (hardcopy paper copies, specifically excluding any electronic copies) and circulate these copies within its company for internal purposes. Author(s)' employer acknowledges and will retain ASTM's copyright notice on each hardcopy it makes.

As the Author, ASTM permits you certain uses that do not require permission from ASTM. These include:

- The right to make copies of the Work for your own personal use, including for your own classroom teaching use;
- The right to make copies and distribute copies of the Work to research colleagues, for the personal use by such colleagues(but not commercially or systematically, e.g. via an email list or list serve);
- The right to post the pre-print version of the Work on your website or your employer's website with reference to the publication by ASTM as the copyright holder. This preprint will be sent to you by the copyeditor. This version does not include the final edits. Such preprints may be posted as electronic files on the Author's own website for personal or professional use, or on the Author's internal university or corporate networks/intranet, or secure external website at the Author's institution, but not for commercial sale or for any systematic external distribution by a third party (eg: a list server or database connected to a public access server). Prior to publication, the Author must include the following notice on the preprint: "This is a preprint of an article accepted for publication in

Publication (journal or book) Title, Copyright @ (year), ASTM International, West Conshohocken, PA, doi10/1520_____". NOTE: Directing researchers to the doi will ensure the authors get appropriate citations from CrossRef.

- After publication of the Work by ASTM International, the preprint notice should be amended to read as follows: "This is a preprint of an article published in Publication (journal or book) Title, Copyright @ (year), ASTM International, West Conshohocken, PA, doi10/1520_____, page numbers, www.astm.org". The Author agrees not to update the preprint or replace it with the published version of the Work;

- A PFD of the final version will be supplied to each author and co-author, with a Watermark on the last page that states: "Copyright ASTM International. All rights reserved, date, time. Downloaded by (author's name, affiliation, pursuant to Author/Copyright Owner Agreement. No further reproduction authorized." This version can be given to your employer or funding agency. Continue to direct researchers to the doi for proper CrossRef attribution.

- The right to present the Work at a meeting or conference and to distribute copies of such Work to the delegate attending the meeting after the Work is published by ASTM with appropriate citation to the published article;

- For the author's employer, if the Work is a "work for hire", made within the scope of the author's employment, the right to use all or part of the information in (any version of) the Work for other intra-company use (e.g., training);

- You retain any patent and trademark rights and rights to any process or procedure described in the Work ;

- **The right to include the Work in full or in part in a thesis or dissertation (provided that this is not to be published commercially);**

- The right to use the Work or any part thereof in a printed compilation of works of the author, such as collected writings or lecture notes (subsequent to publication of the Work by ASTM); and

- The right to prepare other derivative works, to the extent the Work is not book-length form, or to otherwise re-use portions or excerpts in other publications, with full acknowledgement of its original publication by ASTM.

Other uses by authors must be authorized in writing by ASTM.

By electronically accepting this Agreement, you agree to all the above terms and limitations.

N:Author_Agreements_Journals_Current/UniversalAuthorCopyright HolderAgreementElectronic(tbo).doc

Curriculum Vitae

Name:	Yifan HUANG
Post-secondary Education and Degrees:	China University of Mining and Technology Xuzhou, Jiangsu, China 2007-2011, B.E.Sc. (Civil Engineering) The University of Western Ontario London, Ontario, Canada 2011-2013, M.E.Sc. (Structural Engineering) The University of Western Ontario London, Ontario, Canada 2014-2016, Ph.D. (Structural Engineering)
Honours and Awards:	Scholarship of Excellent Student, CUMT 2007-2010 Western Graduate Research Scholarship, UWO 2011-2016 Dr. Robert Addie Graduate Scholarship, UWO 2015-2016 Chinese Government Award for Outstanding Self-Financed Students Abroad, The China Scholarship Council 2015-2016
Related Work Experience	Research Assistant The University of Western Ontario 2011 - 2016 Teaching Assistant The University of Western Ontario 2011 - 2016

Publications:

Articles in Refereed Journals

[1] **Huang, Y.** Zhou, W. and Wang, E. (2014). "Constraint-corrected J–R curve based on three-dimensional finite element analyses." *Fatigue and Fracture of Engineering Materials and Structures*. 2014;37:1101-15.

[2] **Huang, Y.** Zhou, W. and Yan, Z. (2014). "Evaluation of plastic geometry factors for SE(B) specimens based on three-dimensional finite element." *International Journal of Pressure Vessels and Piping*. 2014;123:99-110.

[3] **Huang, Y.** and Zhou, W. (2014). "Investigation of plastic eta factors for clamped SE(T) specimens based on three-dimensional finite element analyses." *Engineering Fracture Mechanics*. 2014;132:120-35.

[4] **Huang, Y.** and Zhou, W. (2014). "J-CTOD relationship for clamped SE(T) specimens based on three-dimensional finite element analyses." *Engineering Fracture Mechanics*. 2014;131:643-55.

[5] **Huang, Y.** and Zhou, W. (2015). "Numerical investigation of compliance equations used in the R-curve testing for clamped SE(T) specimens." *Fatigue and Fracture of Engineering Materials and Structures*. 2015;38:1137-54.

[6] **Huang, Y.** and Zhou, W. (2015). "Effects of crack front curvature on J-R curve testing using clamped SE(T) specimens of homogeneous materials." *International Journal of Pressure Vessels and Piping*. 2015;134:112-27.

[7] **Huang, Y.** and Zhou, W. (2016). "Effective thickness of side-grooved clamped SE(T) specimens for J-R curve testing." *ASTM Journal of Testing and Evaluation*. http://dx.doi.org/10.1520/JTE20150274. ISSN 0090-3973.

[8] **Huang, Y.** and Zhou, W. (2015). "Residual stress state in single-edge notched tension specimen caused by the local compression technique." *Archive of Mechanical Engineering*. (submitted in October 2015, AME-S-15-00089)

[9] **Huang, Y.** and Zhou, W. (2016). "Impacts of residual stresses on J-integral for clamped SE(T) specimens with weld centerline cracks." *International Journal of Pressure Vessels and Piping*. (submitted in August 2016, IPVP_2016_213)

Conference Papers *(all are oral presentations* with * denoting presenter)*

[10] **Huang, Y.***, Zhou, W, Wang, E, Shen, G (2013). "Evaluation of plastic η factors for SE(B) specimens based on three-dimensional finite element analysis." Proc. 23rd Int. Offshore and Polar Eng Conf, June 30 - July 5, Anchorage, ISOPE. p.591-7. ISBN 978-1-880653-99–9 (Set); ISSN 1098-6189 (Set)

[11] Yan, Z.*, **Huang, Y.** and Zhou, W. (2014). "Accuracy of the double-clip on gauge method for evaluating CTOD of SE(T) specimens." Proceedings of the 2014 10th International Pipeline Conference (IPC2014), September 29 - October 3, 2014, Calgary, Alberta, Canada. DOI: 10.1115/IPC2014-33219

[12] **Huang, Y.*** and Zhou, W. (2015). "Residual stress state in single-edge notched tension specimen caused by the local compression technique." Proceedings of the 25th CANCAM London, Ontario, Canada, May 31 – June 4, 2015. pp. 0037

[13] **Huang, Y.*** and Zhou, W. (2016). "Impacts of residual stresses on J-integral for clamped SE(T) specimens." 24th International Congress of Theoretical and Applied Mechanics (ICTAM), Montréal, Quebec, Canada, August 21 – 26, 2016.